Title

KINETICS AND MECHANISM OF METAL-CARBONYL-CATALYZED HYDROGENATION OF AROMATIC HYDROCARBON MODELS FOR COAL CONSTITUENTS

Author

Derencsenyi, Tibor T.

Publication Date

1979-09-01

LBL-9777 C.2

Lawrence Berkeley Laboratory
UNIVERSITY OF CALIFORNIA

ENERGY & ENVIRONMENT DIVISION

KINETICS AND MECHANISM OF METAL-CARBONYL-CATALYZED HYDROGENATION OF AROMATIC HYDROCARBON MODELS FOR COAL CONSTITUENTS

Tibor T. Derencsenyi and Theodore Vermeulen
(Ph.D. thesis)

September 1979

Prepared for the U.S. Department of Energy under Contract W-7405-ENG-48

DISCLAIMER

KINETICS AND MECHANISM OF METAL-CARBONYL-CATALYZED HYDROGENATION OF AROMATIC HYDROCARBON MODELS FOR COAL CONSTITUENTS

Tibor T. Derencsenyi and Theodore Vermeulen

Energy and Environment Division
Lawrence Berkeley Laboratory
Chemical Engineering Department
University of California
Berkeley, CA 94720

ABSTRACT

Transition-metal carbonyls have been investigated as potential co-catalysts for use in non-pyrolytic coal liquefaction process employing massive amounts of molten zinc chloride as both an acidic cracking catalyst and vehicle for the products. Upon substitution with alkyl phosphine and other ligands, transition-metal carbonyls become more stable than the parent compound and are viable homogeneous catalyst for hydrogenating aromatic model compounds of coal such as anthracene and quinoline.

Homogeneous catalytic hydrogenation of anthracene by $Mn_2(CO)_8(PBu_3)_2$ and cyclohexene by $RhCl(PPh_3)_3$ were studied, and mechanisms for both reactions are presented. The manganese operates by two competing steps, the formation of a trihydride and an anthracene-manganese complex reacting to produce 9,10-dihydroanthracene, whereas the rhodium forms a dihydride-olefine-rhodium complex whose decomposition is the rate determining step.

Substitution of the phosphine ligands on $Mn_2(CO)_8(PBu_3)_2$ show that the rate of anthracene hydrogenation is dependent on the

nature of the ligand. The rate did not correlate with the basicity of the phosphine, but additivity effects were noted which led to an excellent correlation of the rate with ^{31}P NMR shift of the phosphine oxide. This correlation has been shown to be a novel linear free-energy relationship that may be extended to other metal complexes for the purposes of describing catalytic activity and the mechanistic details of reactions such as oxidative addition of hydrogen, cis-trans equilibrium, and ligand exchange.

KINETICS AND MECHANISM OF METAL-CARBONYL-CATALYZED HYDROGENATION OF AROMATIC HYDROCARBON MODELS FOR COAL CONSTITUENTS

Contents

I. INTRODUCTION

A. Transition-Metal Carbonyls as Hydrogenation Catalysis

Even by 1920 the knowledge that transition-metal surfaces catalyze hydrogenation of unsaturated compounds had led to important commercial applications (T1). Fifteen years further work brought forth the discovery that transition metals in the form of liquid-soluble ligand-complexes can also catalyze hydrogenation (C1). The advent of homogeneous hydrogenation made possible new synthesis routes, and improved the selectivities for a variety of reactions on the laboratory level.

The most active catalysts are noble-metal complexes such as $RhCl(Ph_3P)_3$ (Wilkinson's catalyst) and $Ir(CO)Cl(Ph_3P)_2$, but activity is not limited to this group. Efficient catalysts are also formed from the other transition metals, notably $H_3Co(Ph_3P)_3$, $Co(CN)_5^{-3}$ $Co_2(CO)_8$ and $Fe(CO)_5$.

A type of homogeneous hydrogenation catalyst that may prove useful in coal liquefaction was developed through research on the Fischer-Tropsch synthesis, involving reactions of both CO and H_2. Certain Fischer-Tropsch catalysts possess the ability to add H and CHO across an olefinic bond, so as to produce aldehydes and subsequently alcohols. This reaction, called hydroformylation from its two reactive groups, has been commercialized as he "Oxo" process. The catalyst originally used for hydroformylation was metallic cobalt on a porous-pellet support (B1). The true nature of the catalytic process was discovered by Otto Roelen (R1) to be homogeneous, not

heterogeneous, with the solid serving only as a source for cobalt. The cobalt reacts in situ with carbon monoxide to form a liquid or gaseous cobalt carbonyl, which behaves as a true homogeneous catalyst. Since Roelen's work, other transition metal carbonyls have also been found to catalyze hydroformylation. In addition to hydroformylation, transition metal carbonyls catalyze simple hydrogenation as a competitive step.

Homogeneous hydrogenation catalysts also afford the possibility of hydrogenating insoluble substrates, which are not amenable to heterogeneous catalysis. Unlike solid catalysts which can only make point contact with a solid substrate, a soluble catalyst can wet the solid and involve its accessible components in chemical reaction. For the catalyst to be most effective, the reacted (hydrogenated) form of the substrate should be soluble, so that it can diffuse out and expose more unreacted substrate to the catalyst.

As a sparingly soluble solid hydrocarbon, coal potentially can be hydrogenated by homogeneous (i.e., liquid) catalysts. The solid state of coal is gradually converted to liquid or extractable fragments through the combined action of hydrogen and catalysts. To date heterogeneous hydrogenation catalysts of metal-ligand form have been ineffective in producing such fragments. Nevertheless, other homogeneous catalysts (notably metal halide melts such as zinc chloride) have shown useful results, and metal-ligand complexes may become important as additives.

1. Hydroformylation with Metal Carbonyls

Transition metal carbonyls are a family of volatile compounds in which a metal atom (Fe, Ni, Co, Mn . . .) is surrounded by a certain number of carbon monoxide moieties. Nickel carbonyl was the first such compound to be discovered (M1). Soon after the report that metallic nickel combines with carbon monoxide, the carbonyls of iron and cobalt were identified (M2). Only these three metals react directly with carbon monoxide.

Some time later, alternate routes to other transition metal carbonyls were devised. In particular, carbonyls can be prepared by reduction of suitable salts or complexes of the metallic element in the presence of CO. All of the metals in groups VI, VII, and VIII of the Periodic Table are now known to form carbonyls (C7).

The carbonyls are valued for their utility as precursors or catalysts in synthesis routes. Metal carbonyls catalyze reactions in the areas of hydrogenation, hydrogenolysis, hydroformylation, hydrosilation, isomerization, carboxylation, carbonylation, and polymerization. Only the first three areas, which are the most significant for coal liquefaction, will be reviewed here. Among these, hydroformylation is of the least direct interest, but it is accompanied by unwanted hydrogenation and hydrogenolysis. Hence the literature on the Oxo process provides a valuable data base.

The Oxo reaction usually employs temperatures of 100-120^{o}C and pressures of 200 to 300 atmospheres of "synthesis gas" (a 1:1 to 1:1.3 mixture of H_2 and CO) in the presence of a catalyst. Hydrogen and

carbon monoxide add to an olefin, in the liquid phase, to produce aldehydes:

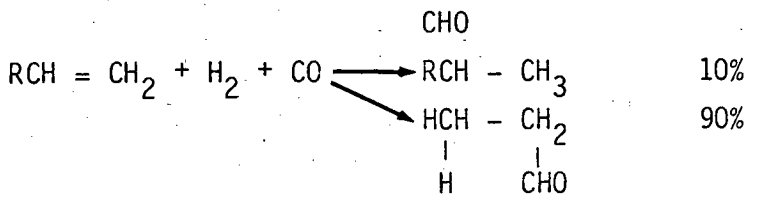

In his studies of this reaction Otto Roelen (R1) suggested that the active catalytic species, forming from the solid, was homogeneous $HCo(CO)_4$. This suggestion was verified when $HCo(CO)_4$ was prepared and tested. Further work has yielded considerable kinetic data, and mechanisms for the reaction have been proposed. $HCo(CO)_4$ has been successfully modified to give other cobalt carbonyl structures with greater activity and better selectivity. Based on earlier studies by Natta (N1,N2), the definitive kinetic experiments on hydroformylation have been carried out with dicobalt octacarbonyl as the source of cobalt (W2). Batch autoclave experiments showed that the hydroformylation rate is:

(a) doubled for a temperature rise of 7-8^{o}C

(b) independent of pressure between 100 and 400 atm

(c) first-order with respect to olefin concentration

(d) approximately porportional to amount of cobalt present

(e) increases with increasing hydrogen pressure at constant CO pressure

(f) decreases with increasing CO pressure at constant H_2 pressure

Because the last condition excludes the direct addition of carbon monoxide to the olefin, the reaction must surely proceed through an intermediate complex. Dicobalt octacarbonyl activates molecular hydrogen to form the true catalyst (cobalt hydrotetracarbonyl) by the reaction:

$$Co_2(CO)_8 + H_2 \rightleftharpoons 2\ HCo(CO)_4$$

The best mechanism to explain the kinetic data has been summarized by Orchin and Rupilius (03). In a somewhat modified form, the mechanism becomes:

(a) First-order dissociation accompanied by olefinic complex formation (pi-bonded complex).

$$RCH = CH_2 + HCo(CO)_4 \rightleftharpoons RCH \underset{\downarrow}{=} CH_2 + CO$$
$$\qquad\qquad\qquad\qquad\qquad\qquad\qquad\quad HCo(CO)_3$$

(b) Addition of H to the double bond

$$HCH \underset{\downarrow}{=} CH_2 \rightleftharpoons RCo(CO)_3 \text{ with } R = R'CH_2CH_2$$
$$\quad HCo(CO)_3$$

(c) CO addition, alkyl migration, then further CO addition

$$RCo(CO)_3 \overset{+CO}{\rightleftharpoons} RCo(CO)_4 \rightleftharpoons RCOCo(CO)_3 \overset{+CO}{\rightleftharpoons} RCOCo(CO)_4$$

(d) Product release with catalyst recovery

$$RCOCo(CO)_4 \overset{H_2}{\rightleftharpoons} RCHO + RCo(CO)_4$$

Although the alkyl intermediates have not been identified, they are analogous to compounds made from other transition metal carbonyls.

2. Hydrogenation with Metal Carbonyls

The ability of dicobalt octacarbonyl to activate hydrogen bonds suggests that it could be used as a hydrogenation catalyst. The hydrogenation of an olefin is thermodynamically favored over its hydroformylation. For example, with ethylene, the standard-state free energy change at 25°C for the two reactions (W2) differs by 8 kcal:

$$CH_2CH_2 + H_2 \rightarrow CH_3CH_3 \qquad \Delta G = -22{,}608 \text{ cal/g-mole}$$

$$CH_2CH_2 + CO + H_2 \rightarrow CH_3CH_2CHO \qquad \Delta G = -14{,}460 \text{ cal/g-mole}$$

Saturated hydrocarbons have been produced occasionally during the Oxo reaction. For example, C_8 and higher olefins, treated in acetic acid solution at 250°C at 700 atm of 1 H_2:1 CO, yielded as much as 30% saturated hydrocarbon. The hydrogenation reaction is especially favored when the olefin is branched, conjugated, or has electroegative

substituents (J1). Nevertheless, at low temperatures (119-140°C) simple olefins treated with dicobalt octacarbonyl yield virtually no saturated hydrocarbons.

As mentioned earlier, hydrogenation of aldehydes to alcohols occurs in the Oxo reaction at the upper end of its effective temperature range (170-200°C), for prolonged contact times. Butyraldehyde has been hydrogenated in good yield to butanol at 180°C. Kinetic studies show that hydrogenation is fastest at low CO pressures down to the point of catalyst decomposition (P_{CO} = 32 atm), the rate equation being (L1):

$$\frac{d(ROH)}{dt} = \frac{k(RCHO)\ P_{H_2}}{P_{CO}^2}$$

Although introduction of two formyl groups by hydroformylation of a diolefin would yield monomeric reactions for manufacturing new polymers, unfortunately one bond is hydroformylated while the other is hydrogenated. Extensive experiments have supported the generalization that the more the double bond is involved in conjugation, as in an aromatic ring, the larger is the tendency toward hydrogenation rather than hydroformylation (W2). This result led to efforts to hydrogenate polynuclear aromatics like the isomeric $C_{14}H_{10}$ compounds phenantrene and anthracene. in such tests Friedman and co-workers at the U. S. Bureau of Mines (F1) found that anthracene is quantitatively reduced to 9,10-dihydroanthracene at 135°C, but phenanthrene was only slightly reduced. Amplification of this work has indicated that several polycyclic hydrocarbons can be partially hydrogenated with

high selectivity, but that isolated benzene rings and phenanthroid systems are generally resistant to reduction (see Table 1). The thiophene ring system is also reduced under these conditions with less susceptibility of the catalyst to sulfur poisoning than with heterogeneous catalyst (L2). Nitrogen compounds such as indoles (S1) and pyridine (P1) may also be reduced.

Wender and co-workers (W3) first reported that hydroformation of alcohols to give the next higher alcohol yielded some hydrogenolysis products particularly for aromatic compounds. An example of the reaction is formation of toluene and water from benyzl alcohol and hydrogen. The yield was especially high for para or meta electron donors, substituted into the $-CH_2OH$ group. An example of the reaction is the formation of toluene and 2-phenylethanol (2:1) from benzyl alcohol. The rates were especially high for benzyl alcohol substituted with para or meta electron donors $p\text{-}OCH_3 >> p\text{-}CH_3 > m\text{-}CH_3$, p-, t-butyl > H > p-Cl > $m\text{-}OCH_3 > m\text{-}CF_3$. The rate trend above is expected for a carbonium ion intermediate. For example a p-methoxy group would stabilize the benzyl carbonium ion produced by the acid $HCo(CO)_4$

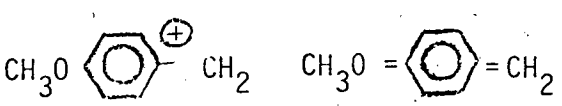

Most research on hydroformylation has been conducted with $CO_2(CO)_8$ as catalyst, although many other carbonyls catalyze the reaction at lower rates. Rhodium carbonyl has recently replaced cobalt in several plants (Z1). For saturating fatty acids, iron

Table 1. Aromatic compounds hydrogenated by $Co_2(CO)_8$ (Ref. L1).

Substrate	Products
Naphthalenes	Tetralins
Anthracene	9,10-Dihydroanthracene
Phenanthrene	9,10-Dihydrophenanthrene
Acenaphthene	2a,3,4,5-Tetrahydroacenaphthene
Fluoranthene	1,2,3,10b-Tetrahydrofluoranthene
Pyrene	4,5-Dihydropyrene
Naphthacene	5,12-Dihydronaphthacene
Chrysene	5,6-Dihydrochrysene
Perylene	1,2,3,10,11,12-hexahydroperylene
Thiophene(s)	Thiolane(s)
Pyridine	N-Formyl-and N-methylpiperidines

carbonyl is perferred. Reaction with $Fe(CO)_5$ is slower than with $CO_2(CO)_8$, but cobalt stops at the monoene stage, whereas iron continues to full saturation.

The faster rate of hydrogenation by cobalt has been attributed to its different mechanism of hydride formation, cleaving the weak Co-Co bond in $CO_2(CO)_8$ to give a homolytic split of molecular hydrogen. For nickel and iron, hydride formation must follow an initial CO dissociation, a much slower process (B1).

The hydrogenation of polynuclear aromatics by Friedman et al. (F1) is the study most pertinent to coal liquefaction due to the high aromaticity of coal. Unfortunately, the apparent applicability of metal carbonyls as catalysts for liquefaction is limited by their tendency to decompose to the insoluble parent metal if insufficient CO pressure is present. Friedman's work utilized a 1:1 ratio of H_2 to CO at 5300 psi total pressure to prevent precipitation at 200°C. These pressures are prohibitive for a full-scale coal liquefaction process. Consequently for a metal carbonyl to be a viable catalyst in a commercial process, it must somehow be stabilized to require lower CO pressures. The method to achieve this goal is reported in Chapter III.

B. The Mechanism of Metal-Carbonyl Catalysis

Extensive research has been conducted on hydrogenation by metal carbonyls much of which resulted from investigations of hydroformylation. Complete reviews are given in several books and

articles (J1,B1,K1,03,C2). The present discussion focuses on the general characteristics of metal complexes that seem to be required for catalytic activity. This section considers the reactions that a metal atom must go through to hydrogenate a substrate, namely hydrogen activation and substrate activation, and then describes the effect of the surrounding chemical groups or ligands which facilitate the hydride-activation and substrate activation steps.

1. Hydrogen Activation by Metal Carbonyle

The primary function of all hydrogenating catalysts, either heterogeneous or homogeneous, is the ability to complex molecular hydrogen, split the hydrogen-hydrogen bond, and supply a hydride ion to react with the substrate. This function is termed hydrogen activation. The best known and most important activators are solids, especially transition metals or their oxides. This is exemplified by the apparent activation energy of 50 kcal/mole for the hydrogenation of ethylene in the gas phase but only 10 kcal/mole on a nickel or palladium surface where monatomic hydrogen appears to be generated as the molecular hydrogen is absorbed onto the metal (H1).

Numerous metal ions and complexes have been found to activate hydrogen in solution (H1,K1). The first discovered was hydrogen reduction of either cupric acetate (to cuprous acetate) or benzoquinone (to hydroquinone) using as catalyst cuprous acetate in quinoline solution at 100^{o}C (C1). Since this discovery, it has been found that ions of copper, mercury, the silver can activate hydrogen

in aqueous solutions (H2-H6). Metals known to be complexed as coordination compounds ($RhCl(Ph_3P)_3$, $Co(CN)_5^{3-}$, or $Co_2(CO)_8$ and other metal carbonyls) activate hydrogen by drawing the hydrogen molecule into the coordination sphere as a ligand.

The solid metals which are good heterogeneous catalysts--ruthenium, cobalt, nickel, palladium, and platinum--have the same number of electrons in their valence shell as the catalytically active metal ions—palladium(II), copper(II), copper(I), silver(I), and mercury(II), respectively. Both heterogeneous and homogeneous hydrogenation activation seem to arise from particular d-electron configurations.

Only ions with d^5 to d^{10} electronic configurations have been found to activate hydrogen, but many such ions including manganese(II), cobalt(II), nickel(II), and iron(III) fail to do so.

The interation of molecular hydrogen with a metal may occur by three types of reactions—heterolytic splitting, homolytic splitting, and oxidative addition.

Heterolytic splitting (as in the examples of Cu^{2+}, Hg_2^{2+}, or $RuCl_6^{3-}$) can be represented by the steps:

$$MX_i^{n+} + H_2 \rightarrow HMX_{i-1}^{(n-1)+} + H^+ + X$$

$$HMX_{i-1}^{(n-1)+} + X + S \rightarrow SH^- + MX_i^{n+}$$

where S is the substrate, M is a metal atom, and X is a ligand. Homolytic splitting, characterized best by Hg^{+}, is believed to occur as follows:

$$H_2 + 2\ Ag^{+}\ (\text{or } Ag_2^{++}) \rightarrow 2\ AgH^{+}$$

$$2\ AgH^{+} + S \rightarrow SH_2 + 2\ Ag^{+}$$

Oxidative addition, the conversion of both atoms of a hydrogen molecule into hydride ions, is most directly related to metal-carbonyl catalysis. Oxidative addition has been reported for four- or five-coordinate d^8 complexes of cobalt(I), rhodium(I), iridium(I), ruthenium(I), and osmium(0) (K1). In such cases cis-dihydro metal complexes are formed with concurrent oxidation of the metal ion by two units, e.g.,

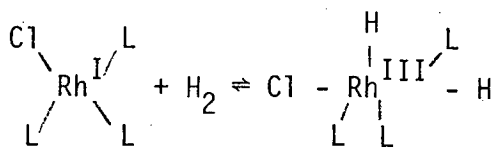

The tendency for oxidative addition to d^8 complexes increases with atomic weight in a group, and from left to right in a triad, Os(0) > Ru(0) > Fe(0) or Fe(0) > CO(I) > Ni(II) (C3). Polarizable ligands which form only σ-bonds with the metal, called soft σ-donors, tend to favor oxidative addition. For $IrX(CO)(Ph_3P)_3$ the

propensity for hydrogen activation decreases in the order I^- > Br^- > Cl^- due to the decreasing electron density on the metal (C4). π-acid or π-aceptor ligands, such as CO or Ph_3P, bind to a metal by donating electrons to form a σ-bond, and concurrently they acept metal d-electrons into an appropriate empty orbital to form a π-bond. Stronger π-acceptor properties diminish the ease of dihydride formation; replacing CO by Ph_3P increases dihydride formation. Ligand effects are discussed more fully in a later section.

Crystal field theory (07) has been found useful for describing the stability of metal-complex hydrides in terms of energy-level spacing. A metal M^{m+} that requires the electrons of six ligands to attain the next noble-gas configuration has a coordination number of six, and usually possesses an octahedral configuration as shown in Fig. 1. The ligands, viewed as point charges, cause a splitting of energy levels of the five equivalent d-orbitals of the free metal ion.

An electron added to the d shell of the metal is unlikely to occupy one of the two orbitals that are spacially coincident with the original negatively charged ligands, due to electronic repulsion. It would instead occupy one of the last three orbitals in Fig. 2, which are situated between the perpendicular bonding directions of the ligands. The nonequivalence of the orbitals can be represented by an energy-level diagram as in Fig. 3, in which the energy-level splitting caused by the octahedral set of ligands is denoted by Δ_o.

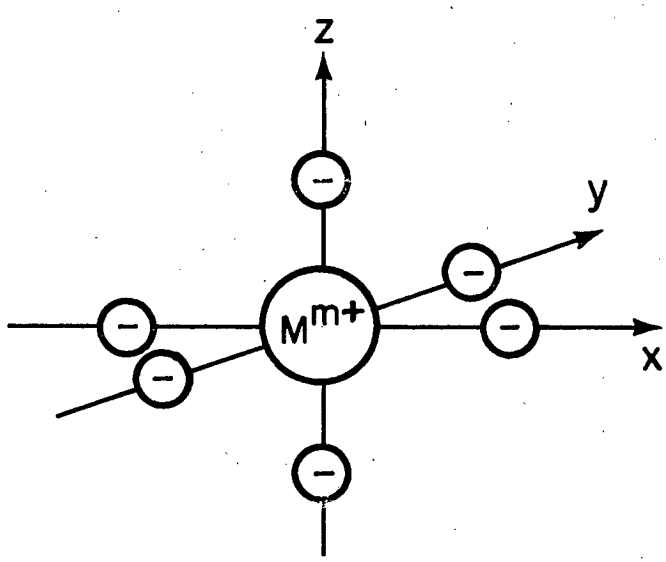

XBL 794-9345

Fig. 1. Sketch showing six negative charges arranged octahedrally around a central M^{m+} ion with a set of Cartesian axes for reference (C7).

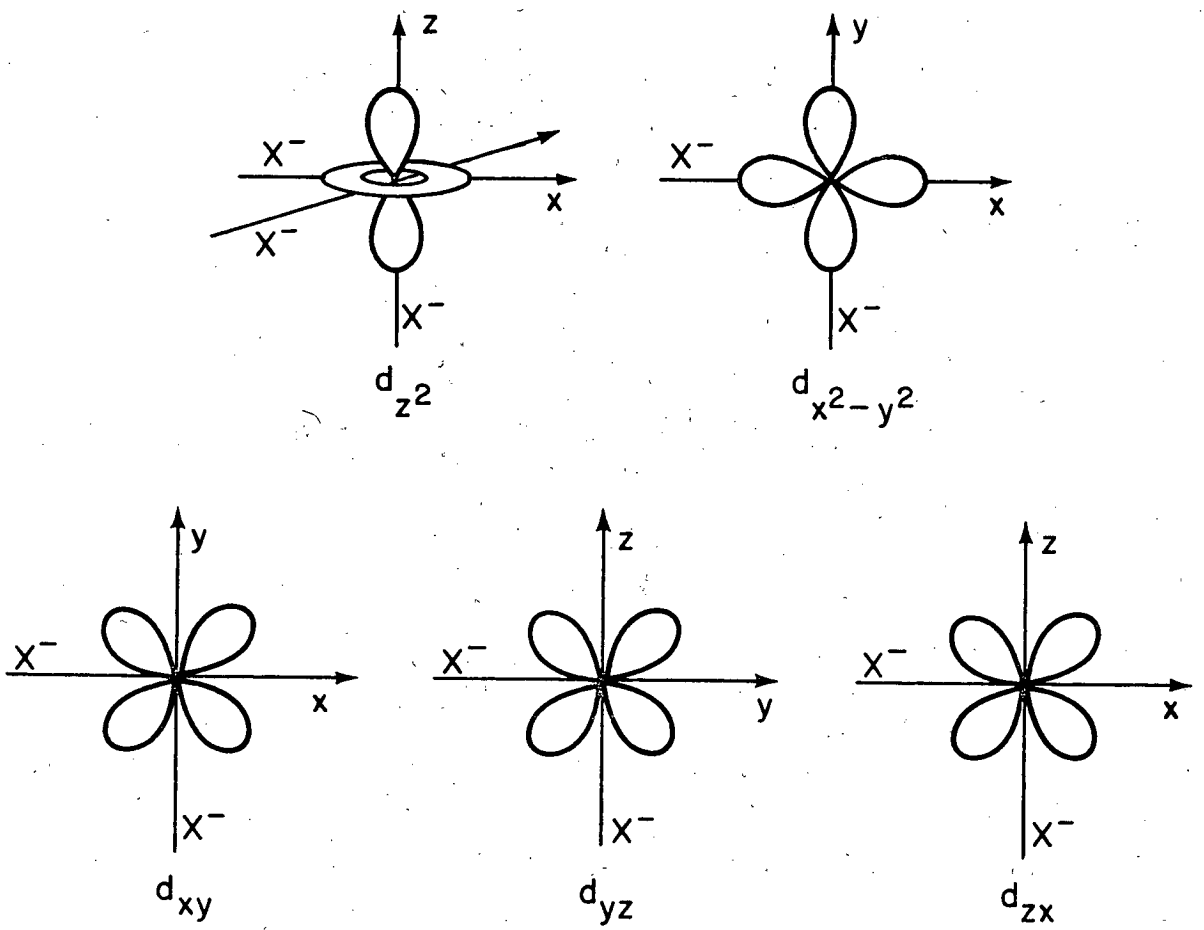

Fig. 2. Sketches showing the distribution of electron density in the five d orbitals with respect to a set of a six octahedrally arranged negative charges (C7).

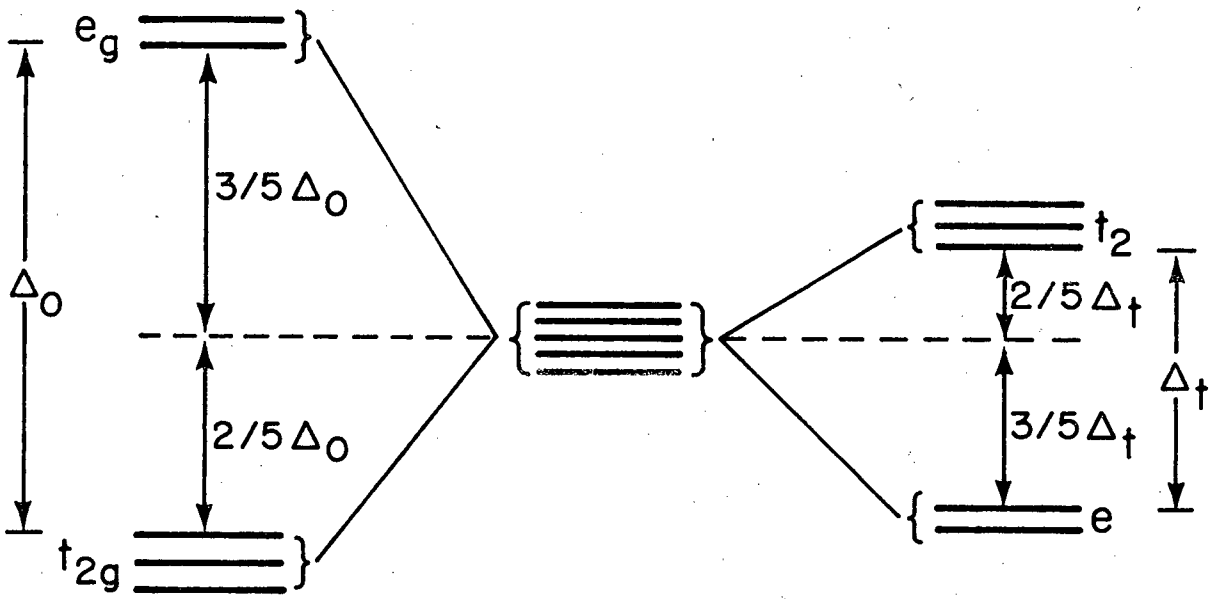

XBL 794-9343

Fig. 3. Energy-level diagrams showing the splitting of a set of d orbitals by octahedral and tetrahedral electrostatic crystal fields (C7).

A metal that requires four ligands to attain the inert gas configuration is likely to take on a tetrahedral configuration. From Fig. 4 it can bee seen that the spacial orientations of the first two orbitals of Fig. 2 fall between the ligand-metal bonding directions in a tetrahedral complex. The nonequivalence of the d-orbital energy levels, denoted by Δ_t in Fig. 3, is related to the octahedral energy splitting by $\Delta_t = 4/9\ \Delta_o$. The actual magnitude of the energy-level splitting caused by ligand addition to form the metal complex can be deduced from visible-ultraviolet spectroscopy. The series for common ligands in order of increased splitting is $I^- < Br^- < Cl^- < F^- < OH^- < NH_3 <$ bipyridine $< CN^-$.

Hydride stabilization in coordination compounds has been explained by Chatt and Shaw (C5,C6) to be a consequence of ligand-field stabilization energies (Δ) of both the original catalyst and the hydride complex formed after hydrogen scission.

According to Chatt and Shaw, the energy separation between the highest occupied bonding or non-bonding levels and the lowest vacant antibonding levels must be greater than some critical value in order for the hydride to be stable. As an example, for octahedral aqueous transition-metal ions, especially in the first series, the separation (Δ) between levels t_{2g} and $e_g(\sigma^*)$ is not enough to achieve stability (see Fig. 5). The hydrogen atom dissociates because the bonding electrons in the H-M σ-bond are easily promoted through the t_{2g} level to the vacant antibonding $e_g(\sigma^*)$.

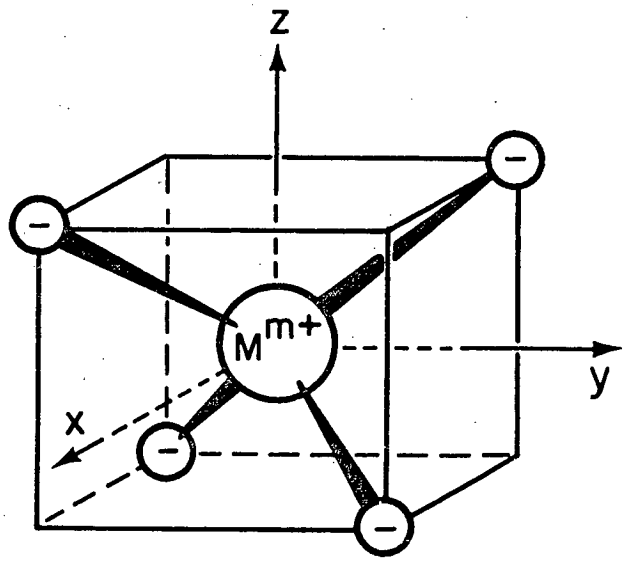

XBL 794-9342

Fig. 4. Sketch showing the tetrahedral arrangement of four negative charges around a cation, M^{m+}, with respect to coordinate axes that may be used in identifying the d orbitals (C7).

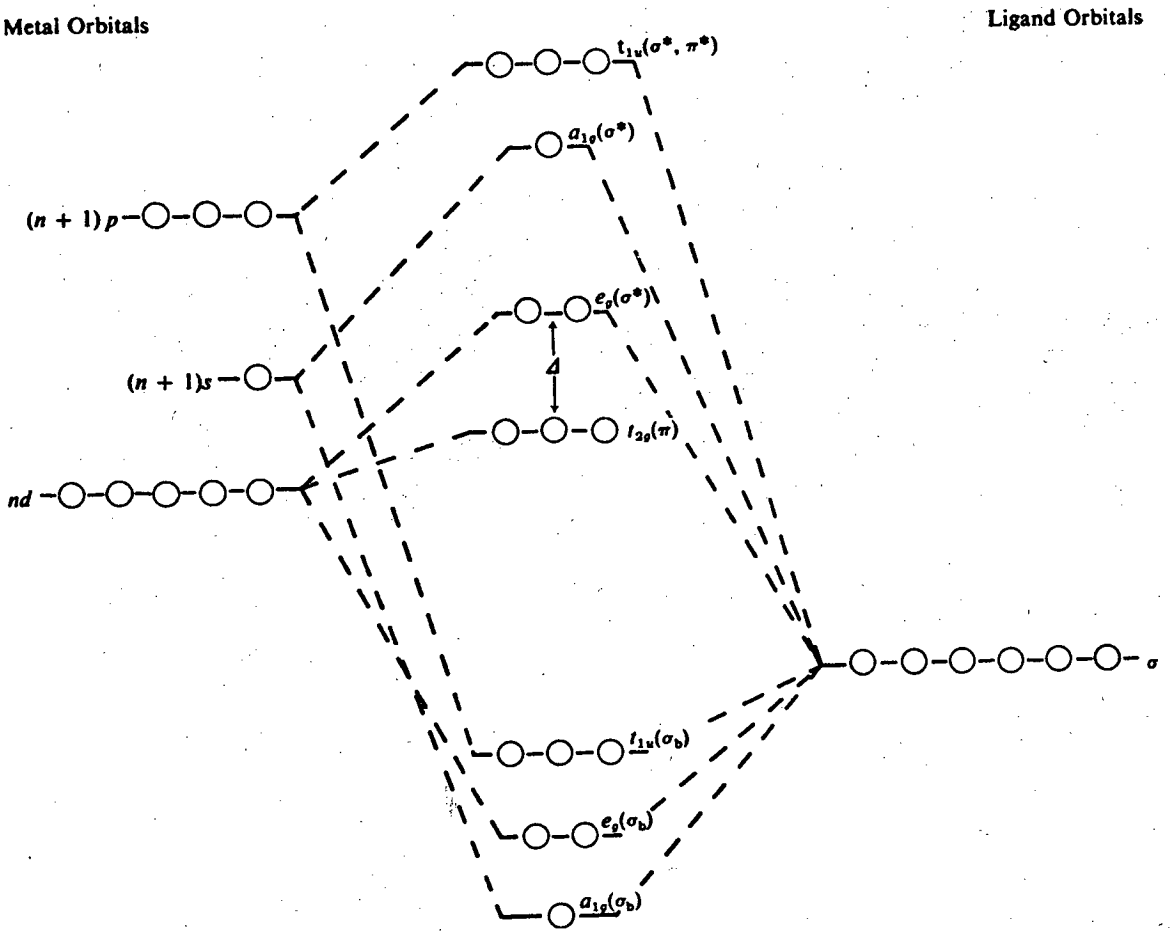

Fig. 5. Molecular orbital diagram for an octahedral complex with only σ-bond contributions from the ligands. Asterisk indicates antibonding; b, bonding (Kl).

Certain π-bonding ligands such as tertiary phosphines and carbon monoxide have back-bonding interaction of metal t_{2g} orbitals with the ligand π and π* orbitals, resulting in the lower of the t_{2g} level to yield a greater separation (Δ) (see Fig. 6). The separation of energy-level splitting Δ also increases with atomic number of the metal. Consequently osmium forms a more stable complex than iron, measured by both decomposition temperature and H-M bond strength, as shown in Table 2.

From the preceding analysis, hydrogen complexes of the 3d transition metals (V, Cr, Mn, etc.) are apparently unstable if they contain only ligands with low field-splitting energies (i.e., H_2O, OH^-, Cl^-). Hydrogen complexes with high field-splitting ligands (CO, CN^-, etc.) do exist; their structures have been unequivocally characterized, but they are oxygen and moisture sensitive.

The hydrido-metal carbonyls are only slightly soluble in water, but they behave as acids (C7) and will ionize to give carbonylate ions. The relative acid strength is listed after the hydrido formation reaction. Strong acidity of carbonyl hydrides indicates a labile hydrogen atom, and consequently a less stable but more reactive species.

The formation of hydrido carbonyls may occur by two mechanisms. The dinuclear carbonyls probably split homolytically:

$$Co_2(CO)_8 + H_2 \rightleftharpoons 2\ HCo(CO)_4 \qquad pK \sim 2.5$$

$$Mn_2(CO)_{10} + H_2 \rightleftharpoons 2\ HMn(CO)_5 \qquad pK \sim 7$$

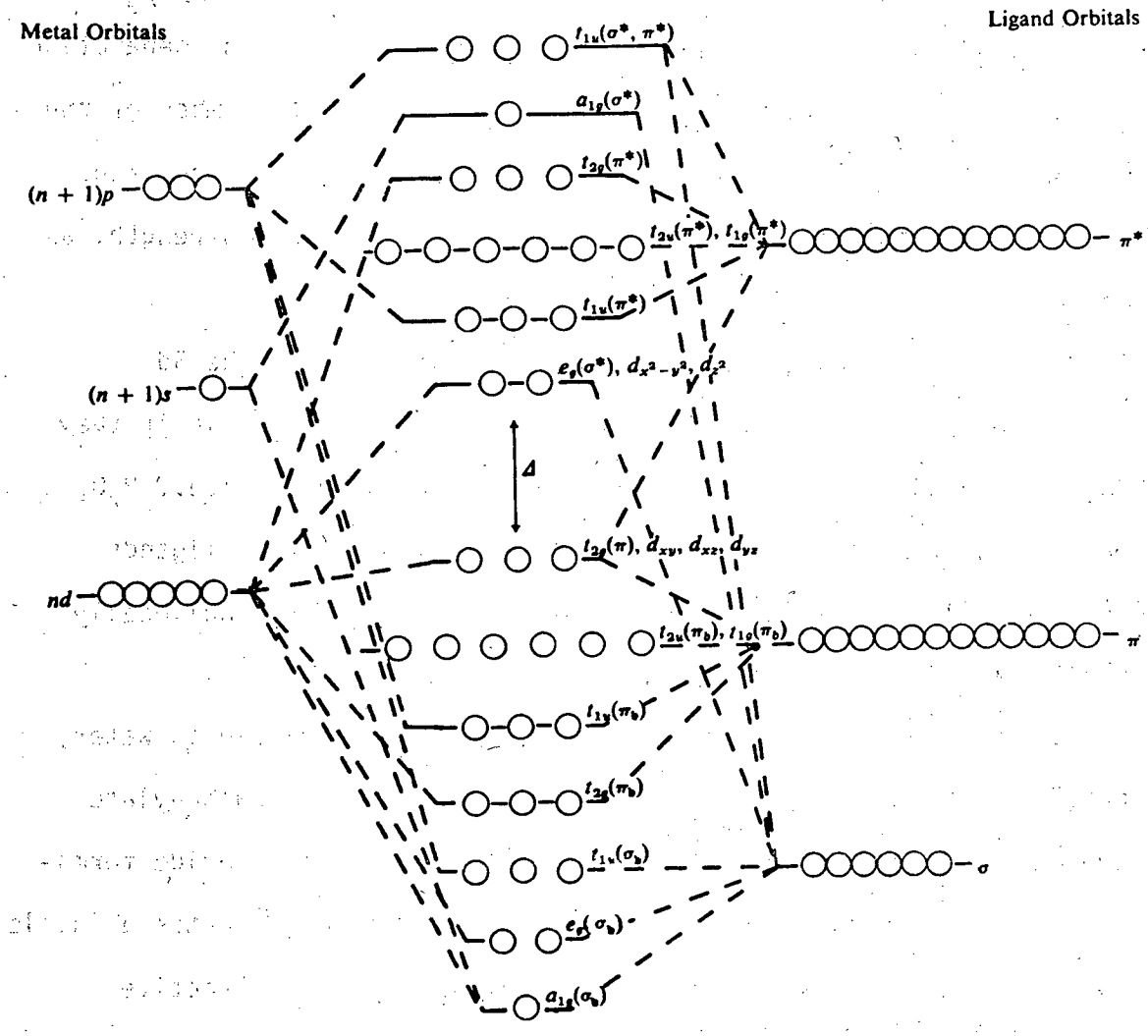

Fig. 6. Molecular orbital diagram for an octahedral complex with contributions from π-bonding and antibonding orbitals of the ligands (K1).

Table 2. Metal-hydrogen stretch frequencies and decomposition points of iron-group hydrido complexes (C5).

Metal	CO cm^{-1}	Decomp Pt ^oC	Melting Pt ^oC
Fe	1849	155	155
Ru	1938	310	175
Os	2039	315	171

Homolytic splitting is less likely for the heavier transition metals, since the d-bonding to d-antibonding orbitals energy separation is greater there. The mononuclear or heavier carbonyls $M(CO)_x$ may form hydrides by an initial CO dissociation step (B1). For iron,

$$Fe(CO)_5 \rightleftharpoons Fe(CO)_4 + CO$$

$$H_2 + Fe(CO)_4 \rightleftharpoons H_2Fe(CO)_4 \qquad pK \sim 4$$

Evidence for this mechanism comes from the apparent energy of activation of 60 kcal/mole for hydrogen activation, which is large compared with 14 kcal/g-mole and 20-24 kcal/g-mole respectively for homolytic and heterolytic splitting by metal ions (K1).

The hydrogen atom may even be anionic, especially in complexes containing tertiary phosphines such as $PtHBr(Et_3P)_2$. Here again the hydrogen ion occupies a full coordination site in a square-planar arrangement.

Hydrogen anion (hydride) in transition metal complexes has a very large ligand-field strength (Δ). Thus, hydrogen complexes are much paler than the corresponding dichloro complexes because the d-to-d electron trnasitions are shifted to the ultraviolet region. The shift with hydrogen may be as strong as that with cyanide, which has the greatest field strength of all the common ligands.

Hydrogen anion also has one of the highest trans-effects; that is, it destabilizes the ligand trans to itself. The rate of substitution

of the trans ligand may be increased a million-fold. The trans effect is also reflected back to the hydrogen and makes it very sensitive to substitution of its opposing ligand. Ligands with high trans-effects weaken the H-M bond as evidenced by going along the trans-effect spectrum from a weak NO_3^- to strong CN^- (C5).

2. Substrate Activation by Metal Carbonyls

Substrate activation by metal complexes has been reviewed with emphasis on reaction types (K1) and similarities with heterogeneous systems (C12). Deuterium-exchange reactions for aromatics with both homogeneous and heterogeneous catalysts have been reviewed (G3), as well as the activation of C-H bonds on aromatics (P2).

The directionality of d-orbitals is of fundamental importance in hydrogenation catalysis. The central metal ion can assemble the reactants (hydrogen and substrate) sequentially, and bring them into the spacial orientation that will easily produce a transition state.

Interaction of a transition metal and a substrate (say, alkene) usually occurs through formation of π-complexes. According to the Dewar-Chatt-Duncanson theory (D1,C8) an alkene is bound to a d^8 metal ion with the longitudinal axis of the olefinic carbons perpendicular to the metal-alkene bond, as in Fig. 7a. Bonding is mechanistically illustrated in Fig. 7b. A σ-bond is formed by donation of a pair of electrons from the bonding π-orbital of the alkene to a suitable hybrid orbital (such as dsp^2) of the d^8 metal ion. Concurrently the metal donates electrons from its filled pd orbitals to empty antibonding π^* orbitals on the alkene. The resultant π-bonding in many instances overshadows the weaker σ-bond.

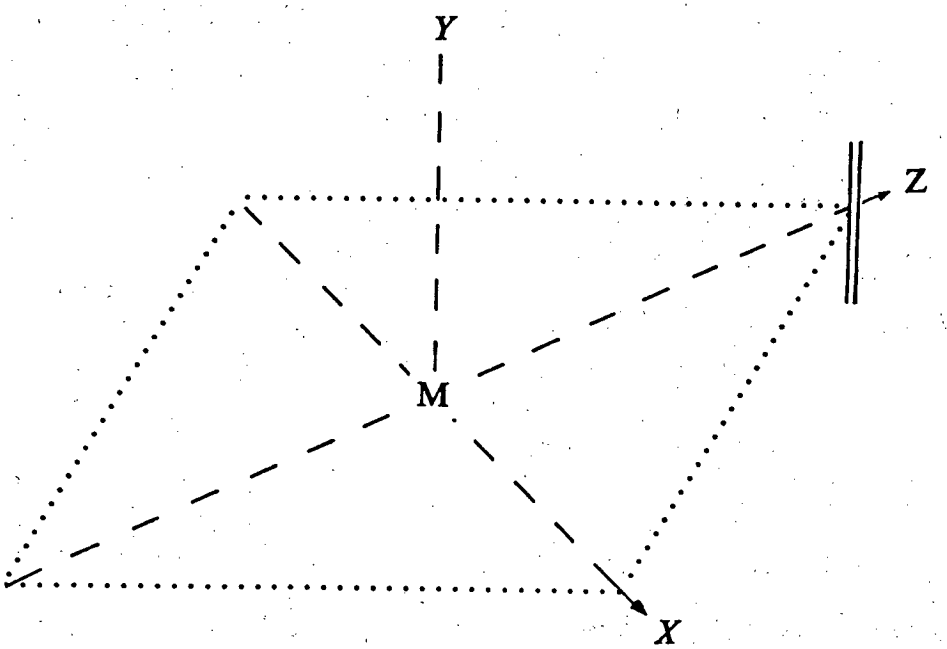

(a)

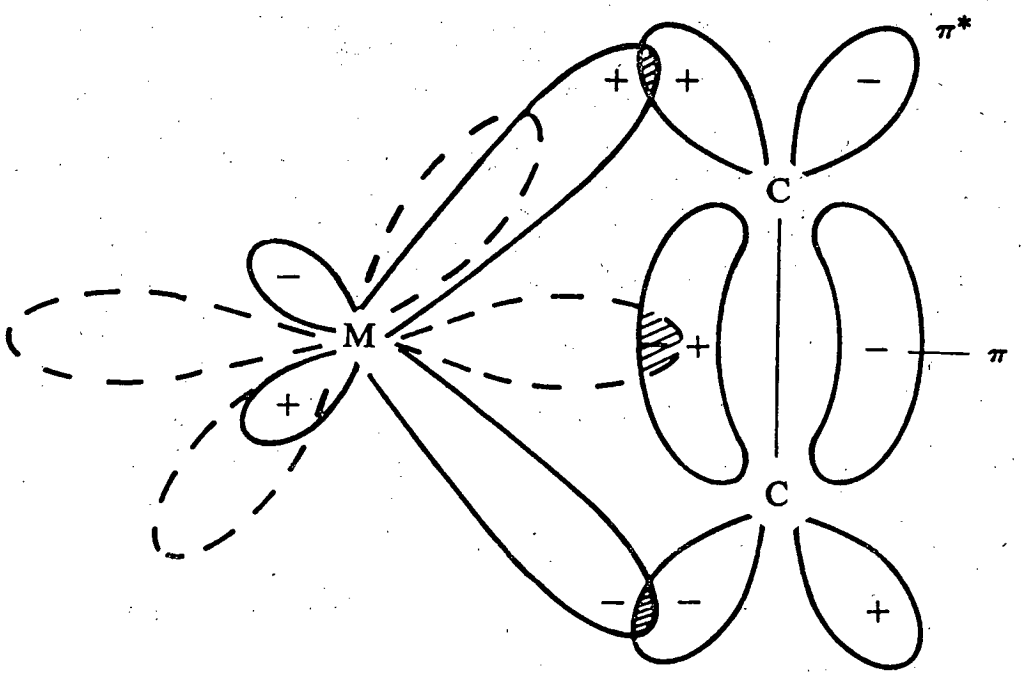

(b)

Fig. 7. Bonding in square-planar d^8 metal-olefin complexes (K1).

The molecular-orbital energy level diagram in Fig. 8 also applies to the metal olefin complex under discussion. The ordering of the d electronic levels becomes $d_z^2 > d_{x,z} > d_{x^2-y^2} > d_{xy} > d_{yz}$ (H5). Just as for hydride complexes, the stability of the olefin complexes is determined by Δ, the energy difference between the highest filled and lowest empty molecular orbitals. This separation increases in the order Ni(II) < Pd(II) < pt(II) for d^8 square-planar complexes; that is, the heaviest element in a group forms the most stable complex (C6). For $PtCl_4^{2-}$ and $PdCl_4^{2-}$, Δ has been measured as 23,450 cm^{-1} and 19,150 cm^{-1} respectively (G4). Such determinations have not been made for olefin complexes because charge-transfer contributions combine with d-d transitions and complicate absorption band assignments.

Octahedral complexes, having a coordination number of 6, are less able to form stable metal alkene complexes. The high oxidation states of the metal limit the effective back-donation of electrons to the π^* orbital of the alkene, thus forming a weaker π-bond between the metal and olefin. This weakening is especially pronounced in metal ions having few electrons in the t_{2g} levels (d-orbitals positioned between the x, y, or z axes of Figs. 1 and 2) that are potentially able to overlap with the olefin π^* orbitals. Hence Ti(III), V(III), V(II), and Cr(III) form labile olefin complexes which participate quickly in subsequent catalytic reactions such as Ziegler-Natta polymerizations.

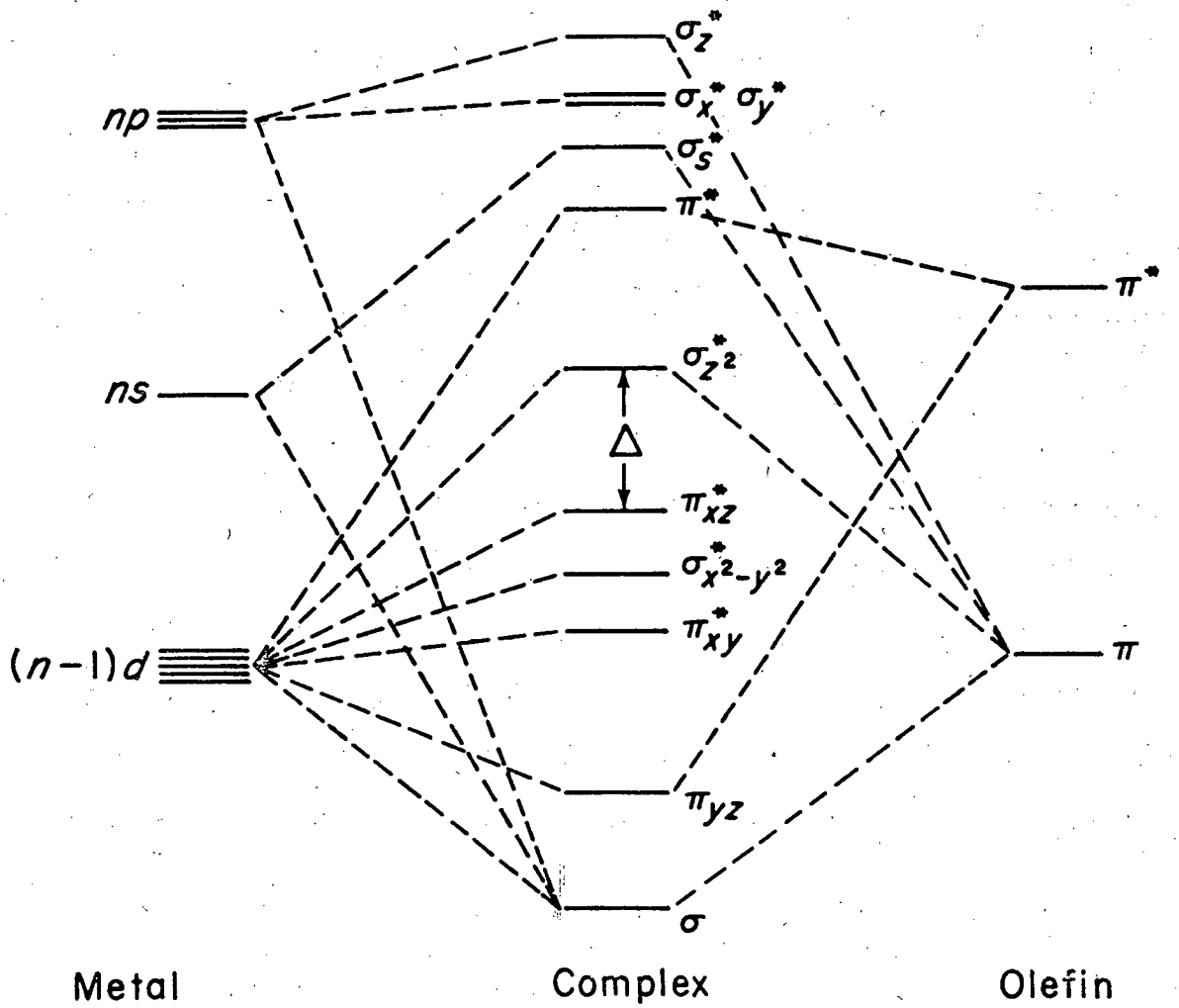

Fig. 8. Molecular orbital diagram for the metal-olefin complex of a d^8 square-planar metal ion (K1).

Iron carbonyls provide numerous examples of π-bonded-complex intermediates, starting especially from Fe(CO), Fe(CO), and $Fe(CO)_5$. In all cases one carbonyl group is displaced from iron (or other metal) for each π-bond formed with an alkene. Manuel (M3) has reported the isomerization of a series of mono-olefins by iron pentacarbonyl, which yielded an equilibrium distribution of products among the geometric isomers, with the trans form predominating. The order of reactivity of the various olefins is terminal (α-) olefin > cis-internal olefin > trans-internal olefin > trisubstututed olefin. Polar substances if present increase the rate of isomerization, apparently because they enhance disporportionation of iron carbonyl to hydrido complexes. The hydrido-iron π-complex rearranges to an iron alkyl complex which can rotate to establish an equilibrium mixture of isomers. An alternate mechanism for rearrangement involves the transfer of a hydrogen form the olefin complex to form an allylic compound in which the original double bond loses its identity. The replacement of the hydrogen to form olefin can produce the equilibrium mixture. the major difference between the two mechanisms is the source of the hydrogen ion to form hydrido-carbonyl. The hydrogen in the π-complex comes from the polar co-catalysts, whereas in the alkyl complex it comes from the olefin. For the purposes of hydrogenation the former mechanism would have to operate. The latter mechanism is supported by Sternberg's work (S2) on isomerization of 1-hexene with $[H_2Fe_2(CO)_8]^{2-}$.

For cobalt carbonyl, insight into substrate activation is given mainly by work on hydroformylation (H2,K2,J2). Olefin activation leading to hydrogenation occurs through π-complexation with $HCo(CO)_4$ to form $RCo(CO)_4$, an alkyl carbonyl (M5). Loss of a CO gives a species $RCo(CO)_3$, which quickly takes up H_2 to yield RH and $HCo(CO)_3$. The hydrogenolysis to RH may be accomplished with $HCo(CO)_4$ for styrene, heptene, and conjugated-diene hydrogenations (J1).

Activation of aromatics is similar to that of olefins. The π-electrons of the carbon ring donate charge to the metal to form a π-complex. The aromatic may complex all of its double bonds with a metal, if open coordination sites are available as in the case of "sandwich compounds" like ferrocene.

For the purposes of hydrogenation, aromatics are activated by metal complexation due to the disruption of the π-electrons in the aromatic ring. This lowering of the resonance energy opens a pathway for reduction of the double bonds as shown by the reversible reduction of benzene-manganese tricarbonyl (W5)

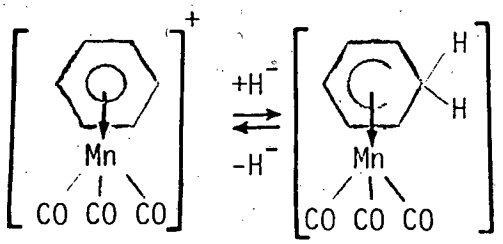

In summary, substrate activation viewed in the quantitative terms of crystal field or molecular-orbital theory becomes manageable with

the application of spectroscopic methods. The activity of transition metal complexes is governed mainly by the metals' electronic configuration. The knowledge of how the two are related provides the tool for designing metal complexes for catalytic requirements.

3. The Effect of Varying Ligands

Ligands of a catalytically active transition metal complex may be changed to enhance certain aspects of the reaction. The activity of transition metal complexes is governed, mainly by the metal's electronic configuration. It is expected that if one metal in a triad catalyzes a certain reaction, the others will also be effective but at different rates. The metal determines the possibility of a reaction, but its environment may be adjusted to promote or diminish that possibility. the environment of the metal center is primarily dictated by the surrounding ligands. The most important parameters usually considered in varying ligands are reaction rate and selectivity. often these two results are in conflict, and the optimum conditions indicate a slower rate in order to increase the yield.

The simplest ligands encountered in transition metal complexes are monatomic units bound to the metal by having donated a pair of electrons to form a σ-bond. These ligands are bound in the "classical" sense; the metal has a well-defined oxidation number, there being no electron back-donation (π-bond) to the ligand.

Not only halogens, but also water and ammonia, are among the most important classical ligands. A metal usually complexes with as many ligands as are required for it to attain the electronic structure of the next inert gas.

Purely classical complexes are usually inactive catalytically, due to an insufficient energy separation Δ that fails to stabilize olefin and hydride intermediates. The classical ligands can alter catalysis of active species, due usually to a inductive effect transmitted along the σ-bond. Although $RhX(Ph_3P)_3$ is not strictly a classical complex, due to π-interaction between the metal and triphenylphosphine, it clearly shows the effect of ligand (X = Cl, Br, or I) on the rate of reaction (01). The rate of hydrogenation of cyclohexene correlates inversely with the electronegativity of the ligand, indicating electronic effects upon the rate limiting transition state (see Fig. 9).

Ligand effects for nonclassical ligands, both σ- and π-bonding, are rarely correlated by simple electronic effects such as electronegativity or linear free-energy relationships. Simple examples of ligand effects with nonclassical complexes are the observed hydrogenation-rate increases for substituted butadiene-iron carbonyl complexes, $CH_3CH{=}CH - CH{=}CHR \cdot Fe(CO)_3$. The activity of R varies with order $COCH_3 \sim CHO > CONH_2 \sim COOCH_3 > CH_3 > CH_2OH >$ COOH, where electron-withdrawing substituents produce higher activity (F2), mainly by weakening the π-bond with the diene. The same effect on rate has been observed for methyl sorbate hydrogenation to methyl 3-hexenoate with arene-chromium carbonyl complexes. The arene ligands (benzene, toluene, ethylbenzene) increase the rate as their electron-withdrawing ability increases (C9).

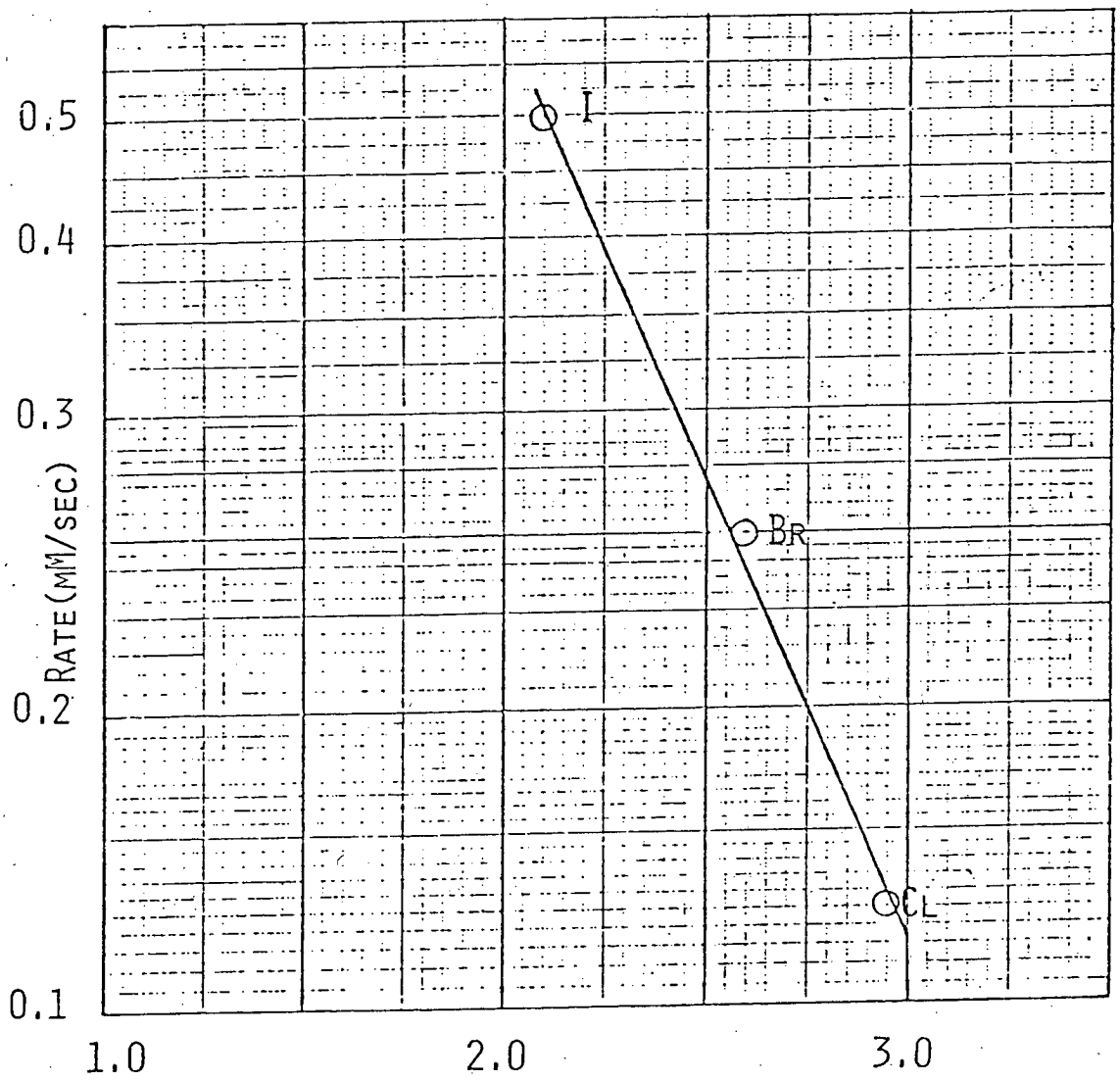

Figure 9. Effect of anion X on rate of cyclohexene hydrogenation by Rh x $(PPh_3)_3$.

Hydride formation by transition metals in low-valence states is known to be stabilized by π-acceptors, such as carbon monoxide and phosphines. Dihydride formation is favored by even more basic phosphine ligands. This may be viewed as an interaction of a Lewis-base metal center with a Lewis-acid hydrogen molecule. Increasing π-acceptor property in ligands decreases the ease of dihydride formation. In monohydride systems, introduction of ligands that are stronger σ-donors and weaker π-acceptors reduces the acidity of the metal hydride, and gives increased hydrogenation activity for certain carbonyl phosphine systems (S3).

Hydrogen and olefin complexed to a metal have similar ligand properties, and this can lead to speculation about the formation of a hydrogenation reaction transition state. Both hydride and organo-ligands cause high ligand-field splitting much like CN^-, CO and R_3P. Not only does, say, trialkylphosphine stabilize the M-C or M-H; bond but the introduction of H or C groups strengthens the M-P bond, and an overall tightening of the complex is observed. The excessive stabilization of either hydride or olefin complex can hinder the subsequent addition of the second reactant, and few hydride-olefin complexes are known. Hence, for catalysis in general, the energy needs to bring olefin and hydrogen into the close proximity required for reaction must be provided by complex tightening that results from the presence of these two ligands of high field strength.

In summary, the ligands surrounding a metal have a large influence on hydrogen- and olefin-complex stability. The stability of both

types of complexes is increased by π-bonding ligands which cause large energy separations (due to high field strength) between orbitals. To promote catalytic activity of the lighter transition metals,, where the d energy levels are closely spaced, ligands of high field strength should be used. Aquo-complexes of cobalt are inactive whereas dicobalt octacarbonyl and pentacyano-cobalt are good hydrogenation catalysts. For the heavier metals, with larger energy separations, a ligand with moderate field strength is sufficient. Too high an energy spacing reduces the reactivity of the intermediates by making them too stable and may thus hinders catalytic activity. Proper choice of ligands may make previously inactive metals active or enhance the activity of a ineffective catalyst.

II. STATEMENT OF THE PROBLEM

A. Adapting Homogeneous Hydrogenation Catalysts to Coal Liquefaction

The present project is part of an extensive study aimed at developing basic information about low-temperature low-pressure conditions for liquefying coal. The study focuses on using massive amounts of the Lewis acid, zinc chloride, as both a catalyst for depolymerization of coal and a vehicle for transporting the reactants and the solid and liquid products.

Although zinc chloride has good bond-breaking ability to achieve reactive structures in coal, it appears unable to activate molecular hydrogen adequately. Coal-derived reactive fragments that are activated but not hydrogenated may either incorporate a hydrocarbon radical or repolymerize to a refractory structure. For treatment with zinc chloride melts, selective hydrogenation is a major concern. Liquefaction consumes hydrogen but economics dictate using only the minimum hydrogen to achieve fully the desired reactions--that is, obtaining the most liquefaction from the least input of hydrogen.

Insufficient hydrogenating ability of zinc chloride may perhaps be enhanced by the use of co-catalysts. The liquid state of the melt is ideally suited for the addition of homogeneous hydrogenation catalysts. Transition-metal carbonyls can themselves form acid hydrido complexes, and may prove to be stable in an acidic environment such as a zinc chloride melt. The stability of pure metal carbonyls at higher temperatures requires a substantial CO pressure, and for practical pruposes a way must be found to prevent catalyst

decomposition at lower CO pressures. Concurrently the presence of CO may aid liquefaction by its incorporation into the coal. From an economic standpoint, liquefaction with a mixture of H_2 and CO is desirable because a hydrogen purification step can be eliminated.

1. Instability of Metal Carbonyls

A major problem in regard to use of transition-metal complexes as hydrogenation catalysts for coal has been their lack of stability at temperatures above 200°C. The metal complexes can decompose to finely dispersed metal which sometimes acts as a heterogeneous rather than homogeneous catalyst. Numerous proven homogeneous catalysts were tried by Holy et al. (H3) for hydrogenating coal at temperatures below 175°C; all were inactive and also were incorporated into the coal. Among these trial catalysts were rhodium, iridium, or palladium complexes, none of them carbonyls.

2. Compatibility of Metal Carbonyls in Zinc Chloride Metals

A further criterion for a homogeneous catalyst is its compatibility in catalytic melts. Zinc chloride is a strong Lewis acid, having a high affinity for electrons under reaction conditions. zinc chloride requires two more electron pairs to complete its octet; consequently it competes for any free electron-donating ligands in the melt. A hydrogenation co-catalyst that reacts by way of a ligand dissociation step, such as $RhCl(Ph_3P)_3$, will have its dissociated ligand complexed by zinc chloride and unavailable for reassociation for catalyst regeneration. Decomposition or dimerization of the co-catalyst will occur, leading to a loss of hydrogenation activity.

Use of metal carbonyl with a Lewis acid catalytic melt has the advantage of being stabilized by excess CO. The objective is to find a form of complex which accommodates hydrogenation, and readily completes the cycle by discharging the hydrogenated product.

3. Hydrogenation of Model Compounds of Coal with Homogeneous Catalysts

The chemical structure of coal is incompletely defined, due to its complex biological and geological origin, amorphous structure, and solid state. Furthermore, as a solid, it is not amenable to several analytical techniques which might otherwise elucidate its chemistry with regard to liquefaction. Therefore model compounds which simulate structures which are believed present in coal, are utilized to reduce the complexity of the test system.

Polynuclear aromatic structures are believed to be predominant in coal, and have been chosen as the primary models for testing hydrogenation behavior. These structures tend to contain three or four fused rings connected to similar structures by bridging carbons, ether oxygens, or thioether sulfurs, to form a three-dimensional matrix. Several poly-nuclear aromatics containing heteroatoms were hydrogenated to determine if coal heteroatoms would have adverse effects on metal-carbonyl catalysis. Cyclohexene hydrogenation by $RhCl(Ph_3P)_3$ was also studied to draw comparison between the hydrogenation mechanisms for noble-metal catalysts and metal carbonyls.

No kinetic work on hydrogenation of polynuclear aromatics with metal carbonyls is known to have been reported previously. Therefore, to understand more fully the behavior of the catalyst-substrate

system, a kinetic study was undertaken with a phosphine-substituted manganese carbonyl catalyst. The effects of catalyst composition and concentration, hydrogen, carbon monoxide pressures, and substrate concentration were determined.

4. The Effect of Zinc Chloride and Metal Carbonyls on Coal

The final phase of this study integrated the various tasks by determining the hydrogenation activity of the metal carbonyls in conjunction with the depolymerization ability of the zinc chloride. A low-sulfur western subbituminous coal (Wyodak) was used for the study. The conversion of coal to preasphaltenes was measured.

III. SUBSTITUTION OF METAL CARBONYLS WITH π-ELECTRON DONOR LIGANDS

A. Basic Considerations

Transition-metal carbonyls are catalytically active for hydroformylation at 175°C and 1000-3000 psi. Among them, cobalt carbonyl has been found to catalyze hydrogenation of polynuclear aromatics such as those found in coal liquids. Conditions of 135 to 200°C and about 5000 psi pressure with equimolar hydrogen and carbon monoxide were used by Friedman and co-workers (F1), who suggested that $Co_2(CO)_8$ adds hydrogen to coal. Subsequent efforts to hydrogenate coal with proven homogeneous transition metal catalysts have failed (H3) the catalysts decomposing and not being recovered. If any catalytic activity was noted, it presumably came from the result of decomposition of the complex to a catalytically active heterogeneous form.

Thus the foremost task in adapting a homogeneous hydrogenation catalysts to coal liquefaction is to stabilize the complex to withstand the reaction environment. Their conditions of successful use without coal to approach the range (200-250°C and 100 psi) of a non-pyrolytic coal-liquefaction process. Since the carbonyl catalysts require substantial pressures of CO to remain homogeneous, this drawback is the first factor to consider here.

It is possible in principle to alter the ligand composition of a coordinated complex so as to alter its reactivity for some reactions and not for others. This principle has been applied successfully in masking reactions (J7) and isomer synthesis (B6).

Because pure transition metal carbonyls are highly symmetrical (usually octahedral or tetrahedral), several equivalent orientations of the moledule will be present which will perform the same catalytic function. Consequently, one part of a molecule may be altered by ligand substitution while the rest retains a catalytically active configuration. A judicious choice of the replacement ligand could well provide enhanced stability without adversely affecting the catalytic activity. The electronic influence of the substituting ligand should cause the remaining CO moiteies to be more tightly bound thus requiring a smaller CO pressure to prevent decomposition. To insure stability, the substituting ligand must be bound even more tightly, since, in contrast to CO, a reserve supply of that ligand species will not be present during use of the complex.

Slaugh and Mullineaux (S3) have provided evidence for the practicality of substitution in cobalt carbonyl, finding improved selectivity in hydroformylation when phosphine ligands are substituted. Tucci (T3,T4) studied this system further, and showed that selectivity is a function of the basicity of the substituted ligand. A partial pressure of 200 to 300 psi of carbon monoxide was adequate to prevent catalyst decomposition.

In regard to ligand bonding, certain theoretical consideration will now be reviewed in order to emphasize the effect of substitution on complex stability. This review is a consolidation of ligand bonding theory presented by Cotton and Wilkinson (C7) and Basolo and Pearson (B5). The bonding of carbon monoxide to a transition metal

has been explained convincingly in terms of molecular orbital theory. Bonding of CO to a metal corresponds to interaction between the metal d electrons and carbon σ electrons. Since the d electrons have specific orientations, the attached carbon monoxides are localized about the metal in a specific geometry.

The bonding occurs in two simultaneous steps, illustrated by Fig. 11. The carbon donates its lone pair of electrons to form a σ-bond with the metal. Concurrently the metal donates electrons in its $d\pi$-orbitals to the carbon's empty $p\pi$-antibonding orbital, to establish a π-bond. This mechanism allows concurrent σ- and π-bond formation to mutually reinforce each other. Although the bonding mechanism of CO to a metal forms a double bond the bond strength is not high enough to prevent dissociation, and ultimately decomposition occurs. Other ligands generally display stronger σ-bonding and weaker π-bonding than CO. In systems containing other ligands, the more negative metal will form stronger π-bonds with the remaining CO molecules (Fig. 12), so as to render the substituted metal carbonyl more stable.

Based on extensive spectroscopic data for substituted metal carbonyls, force-constant calculations indicate that the order of decreasing π-bonding tending (or π-acidity) of some common ligands (C7) is

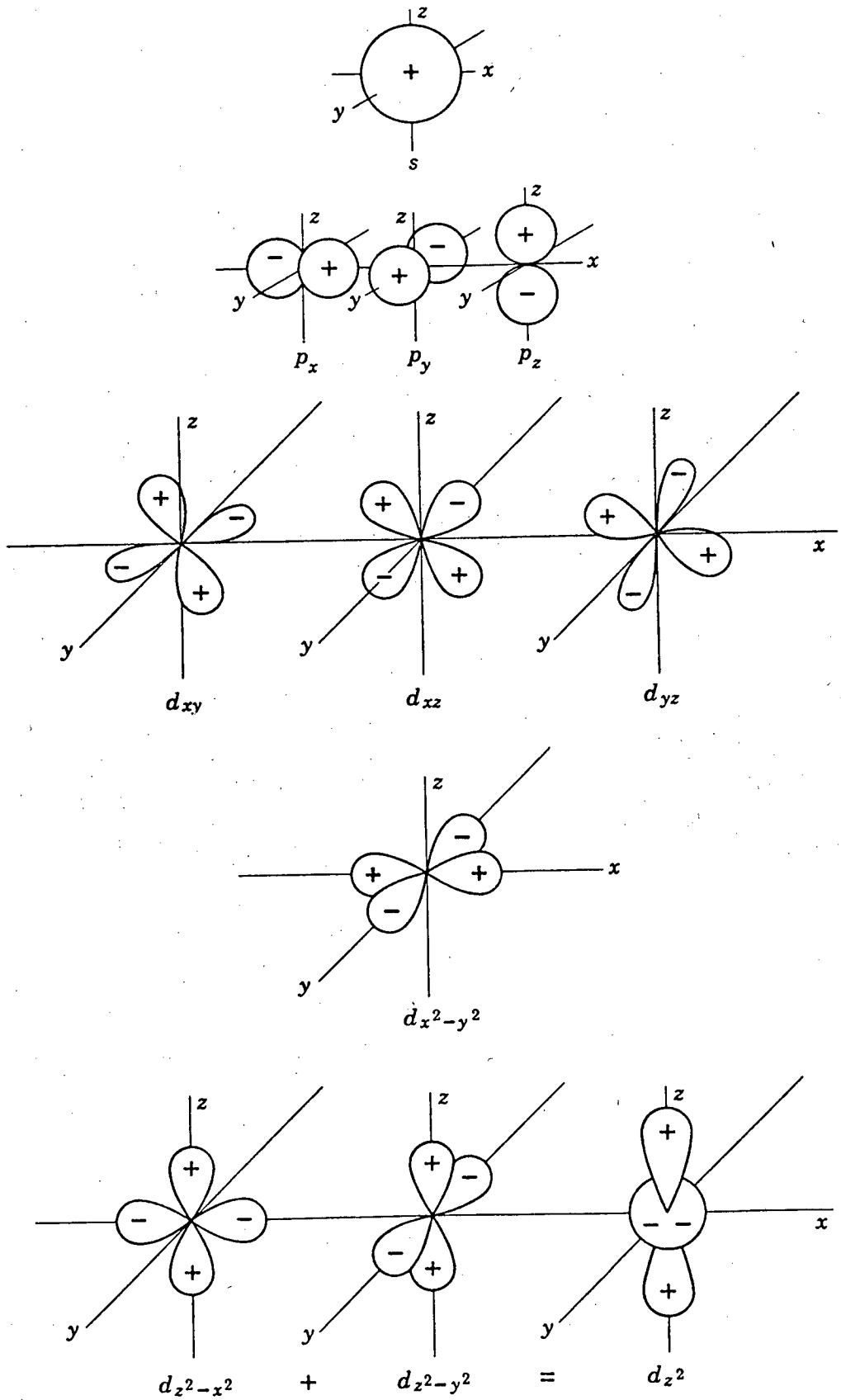

Fig. 10. Atomic orbitals (B5).

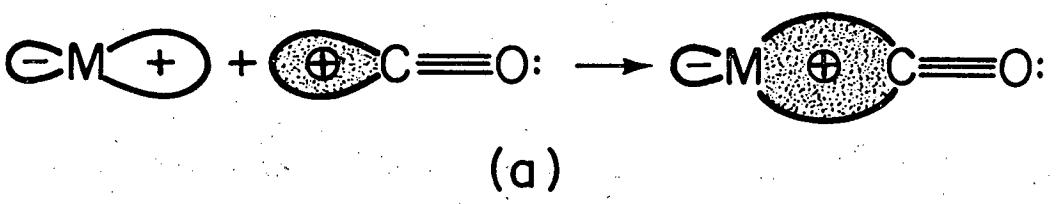

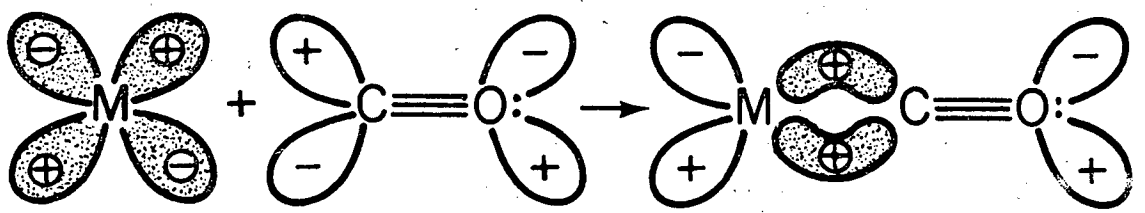

XBL 794-9341

Fig. 11. Representation of M-C bonding in metal carbonyls by molecular orbital theory. Shaded orbitals contain electron; open orbitals are empty. The σ-bonding is represented by (a), π - bonding by (b).

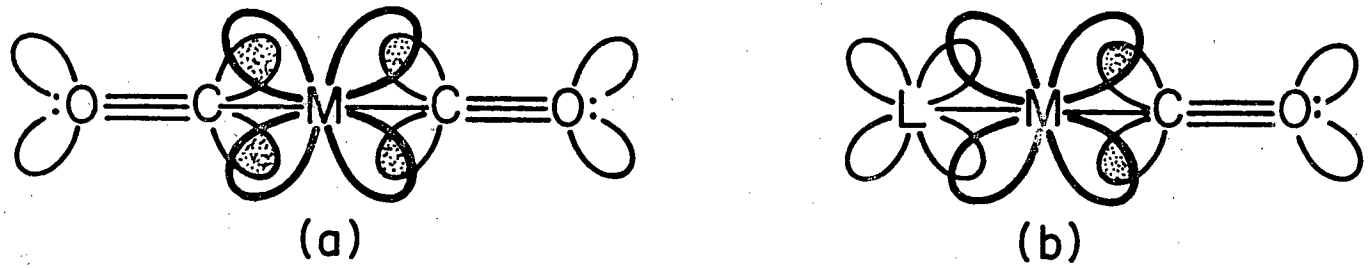

XBL 794-9340

Fig. 12. Competition for π-bonding in metal carbonyl derivatives such as $M(CO)_5L$. (a) the π-bonding of CO molecules cis to L but trans to CO. (b) The π-bonding of CO trans to weak π-bonding ligand L.

$$CO \sim PF_3 > PCl_3 \sim AsCl_3 \sim SbCl_3 > PCl_2(OR) > PCl_2R$$

$$> PCl(OR)_2 > PClR_2 \sim P(OR)_3 > PR_3 \sim AsR_3 \sim SbR_3$$

$$\sim SR_2 > RCN > NR_3 \sim OR_2 \sim RCH > H_2NOR$$

a ranking of mixed ligands of the types PX'X"X"" has been reported by Tolman (T2). The best π–bonding ligands are PF_3, CO, and NO, whereas amines which cannot π–bond are at the end of the series.

A good prospect of suitable ligands would be among the phosphines; although they possess limited π–bonding ability, they can form strong σ–bonds with the metal due to an available lone pair of electrons.

In selecting a ligand, some consideration also must be given to its size and shape. For highly substituted metal atoms, such as $Ni(PX)_4$, steric effects are superimposed on the electronic effects, in controlling the rates of ligand dissociation and exchange, and catalytic activity. Tolman (T2) has correlated steric effects with the cone one angle of the ligand, the conic surface having its apex at the metal atom and lying tangent to van de Waals surface of the entire ligand group atoms. The smaller the cone angle is, the less the steric hindrence. PPh_3 has one of the largest cone angles (184^o) while $P(OCH_3)_3$ has one of the smallest (107^o).

The size of the ligand is not of concern in stability considerations, but may limit a catalyst's activity by restricting its access to the pore structure of coal, or to reactive sites in the exposed surfaces.

The work on hydroformylation, cited earlier, reinforces theoretical arguments that a substituted metal carbonyl may provide sustained catalytic activity with improved stability. Until now, no similar study has been available for hydrogenation, thus justifying the present investigation on the effects of ligand substitution on hydrogenation activity and complex stability.

B. Experiments

The metal carbonyls, $Co_2(CO)_8$, $Ni(CO)_4$, $V(CO)_6$, $W(CO)_6$, $Mo(CO)_6$, $Fe(CO)_5$, $Fe_2(CO)_9$, $Mn_2(CO)_{10}$, and $CH_3C_5H_4Mn(CO)_3$ were purchased from Alfa Inorganics, Inc. and used without further purification.

Phosphines and phosphites used for ligand substitution reactions were obtained from Aldrich Chemical Co., with the exception of tri-p-toyl phosphite, diethylphenyl phosphines, and tri-isopropyl phosphine which were purchased from Pfalz and Bauer, Inc. Phenyl methyl sulfide and dibutyl sulfide were purchased from Eastman Chemicals.

The solvent for most experiments was technical grade 95+% normal decane, nonane, or octane purchased from Phillips Petroleum. Decalin (95+%) and anthracene (95%) were obtained from Eastman Chemicals, and 9,10-dimethylanthracene (95+%) from Aldrich.

The nitrogen and hydrogen (99.999%) used in the experiments were supplied by Lawrence Berkeley Laboratories and contained less than 1.5 ppm water or oxygen. The hydrogen was passed through a Matheson

catalytic deoxygenator before use. Carbon monoxide was obtained as "Matheson purity" 99.999% min. NO was also supplied by Matheson as "Chemically Pure" 99.0+%.

Substitution reactions and hydrogenations were conducted in a 600 ml autoclave purchased from Parr Instruments, Co. The autoclave internals consisted of a stirrer, cooling loop, thermocouple well, sample tube, and a glass liner. The bomb was fitted for gas inlet and sampling, liquid sampling, and liquid injection (Fig. 13). Reactor temperature was automatically controlled by alternately energizing the heating mantle, or a solenoid valve which admits cooling water to the cooling loop. Reaction temperature was recorded on a 10 mv strip chart recorder attached to the thermocouple, and showed that the reaction temperature varied $\pm 1^{o}C$ during a run. Reactor heat-up to $200^{o}C$ was typically accomplished in 15 min. Pressure was indicated by a gauge reading either 0 to 1000 psi or 0 to 2000 psi, calibrated to ±10 psi. The autoclave was protected by an Inconel rupture disc, rated at 2000 psi at $72^{o}C$.

Substitution reactions were normally followed by screening the resulting compound for hydrogenation activity. In the typical procedures, 10 millimoles anthracene and 1 millimole metal carbonyl, based on metal, were weighed out and placed in the glass liner. One hundred milliliter decane was added, and 1 millimole substituting ligand was either weighed in or added by pipette. The glass linear was placed in the reactor and the reactor sealed. The appropriate support lines were connected, and a vacuum line was attached to the gas outlet.

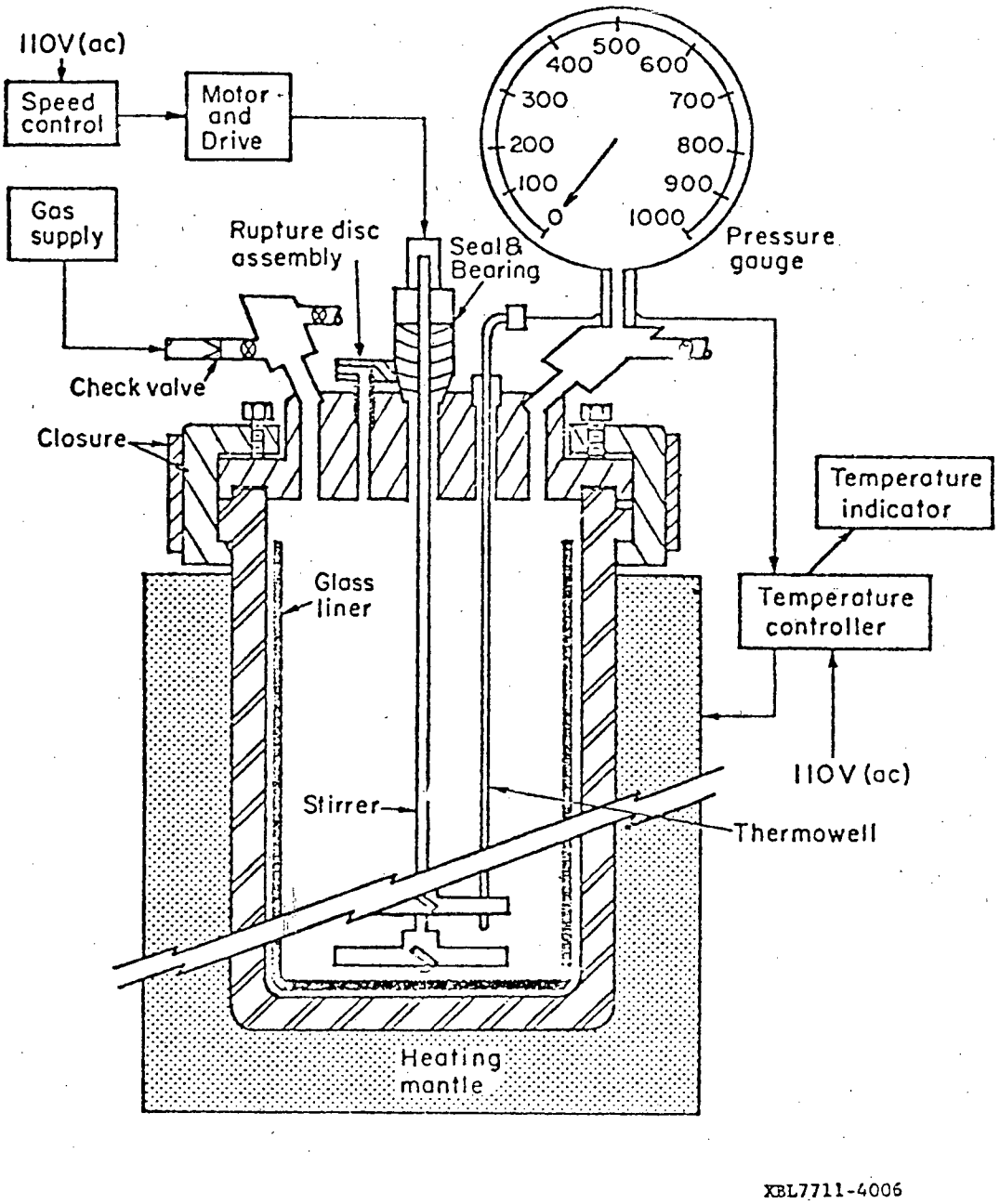

Fig. 13. Parr Autoclave

The reactor was purged by alternately drawing a vacuum and pressurizing the reactor to 300 psi with either hydrogen, carbon monoxide, or a 1:1 mixture of the two. The reactor was then pressurized to the initial condition, and heating commenced; reaction was conducted for the heat-up time plus 1 hr. During the run liquid samples were taken for later analysis by gas chromatography.

The stability of the complex could be determined visually by inspecting for clarity and color. Decomposition and hence loss of catalytic activity could easily be seen in all cases. Upon decomposition, the metal precipitates and clouds the solution. Also the characteristic brilliant color of the solution vanishes. The stability measurements were started with an initial pressure of 300 psi of synthesis gas, that is, an equimolar mixture of hydrogen and carbon monoxide. After heat-up, the pressure was 495 psi at which more synthesis gas was added to 600 psi. A sample was taken after an hour. After sampling the temperature was raised in increments of $25^{o}C$. At each new temperature the pressure was noted, and another sample taken. The temperature and pressure recorded before the conditions at which the complex decomposed are given in the Results sections.

Hydrogenation activity was screened in these reactions to determine which compounds warranted further study. The samples taken after 1 hr of reaction time were analyzed by gas chromatography.

The chromatography used in this study was a Varian Aerograph, model A-90-P, with a 1/8 in. x 10 ft column containing 4% Dexsil

300 GC on Chromasorb H. P. (100 to 120 mesh) operated isothermally at 200°C. Injector, detector, and collector temperatures were 280°, 295°, and 290°C respectively. These conditions can separate decane, dihydroanthracene, and anthracene sharply, eluted in that order. Increasing the column temperature by 15°C separates pyrene and dihydropyrene on the same time scale. Anthracene is not completely soluble at room temperatures in decane at these levels. Dihydroanthracene was referenced to the solvent, decane, which was used an an internal standard for concentration calculations. Since only one hydrogenated produce 9,10-dihydroanthracane is produced, the amount of anthracene can be calculated by difference.

C. Results and Discussion

1. Substitution Reactions

The results of the stability studies of substituted metal carbonyls are given in Table 3. Notably all the metal carbonyls can be stabilized by ligand substitution. The initial conditions, 200°C and 600 psi synthesis gas are severe enough to decompose all the unsubstituted carbonyls listed. Most sensitive is cobalt carbonyl, which decomposes at 150° below 410 psi CO. After substitution it is only moderately stabilized to 210°C and 730 psi synthesis gas. The other carbonyls are more stable, preserving the integrity of the complex at 300 to 350°C under only slightly higher total pressures, part of which is the partial pressure of the solvent, decane. Decane has a 20 psi vapor pressure at the initial temperature of 200°C. the initial stability of the metal carbonyl seems unrelated to the

Table 3. Stability of substituted metal carbonyls.

Carbonyl	Ligand	Decomposition Temperature °C	Decomposition Total Pressure (psi) (H_2/CO=1/1)
$Co_2(CO)_8$	$(Bu)_3P$	210	730
	$(Et)_3P$	200	720
	$(Ph)_3P$	200	720
	diphos*	375	900
	bipy*	325	840
	en*	<200	decomposed
$Mn_2(CO)_{10}$	$(Bu)_3P$	300	800
	$(Et)_3P$	300	800
	$(Ph)_3P$	350	700
	Ph_2ClP	300	800
	$(BuO)_3P$	350	800
	$(ClCH_2O)_3P$	300	720
	(Et_2PhP)	300	720
$Fe_2(CO)_9$	$(Bu)_3P$	300	720
$Fe(CO)_5$	$(Bu)_3P$	300	800
	Ph_2ClP	350	800
	(PhMe)S	250	650
$V(CO)_6$	$(Bu)_3P$	300	800
$Cr(CO)_6$	$(Bu)_3P$	350	700
$Mo(CO)_6$	$(Bu)_3P$	300	800
$W(CO)_6$	$(Bu)_3P$	300	800
$Ni(CO)_4$	$(Bu)_3P$	300	1200**

*Bidentate ligands (see Fig. 14).

**Higher initial pressure.

stability of the substituted compound; while dicobalt octacarbonyl is relatively stable in air, substitution does not impart as much stability to it as to vanadium hexacarbonyl. Vanadium hexacarbonyl is so reactive that it may flash when exposed to air; but upon substitution it is stable to 300°C.

The electronic nature of the ligand greatly affects stability. As mentioned earlier, the σ- vs π-bonding ability has a pronounced effect, typically by the behavior of phosphines vs sulfides. The sulfide is less π-acidic so it should stabilize the carbonyls more than phosphine; however, the σ-bond between sulfur and metal is weaker, and allows dissociation to take place through the substituted ligand. Decomposition of the complex is the result.

Substitution of metal carbonyls with polydentate ligands was also investigated. It can be seen from Table 3 that the polydenate ligands greatly improve stability, through their chelating action (see also Fig. 14). As an example ethylenediamine (en) complexes with nickel in solution (C10).

$$Ni^{2+}_{(aq)} + 6\ NH_{3(aq)} \rightleftharpoons [Ni(NH_3)_6]^{2+}_{(aq)} \quad \log K = 8.61$$

$$Ni^{2+}_{(aq)} + 3\ en(aq) \rightleftharpoons [Ni(en)_3]^{2+}_{(aq)} \quad \log K = 18.28$$

The system $[Nien_3]^{2+}$ contains three chelate rings and is 10^{10} times more stable than the case where no ring is formed. This can be understood from thermodynamic relationships:

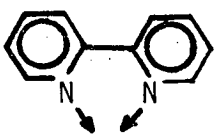

2,2 bipyridine
(bipy)

$H_2NH_2C=CH_2NH_2$

ethylenediamine
(en)

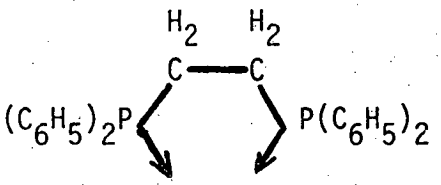

1,2-bis (diphenylphosphino)ethane)

(diphos)

Figure 14. Polydentate ligands.

$$\Delta G^{O} = \Delta H^{O} - T\Delta S^{O} = -RT \ln K$$

From thermodynamic data it can be shown that stability due to chelation arises entirely from an entropy effect (to make ΔG^{O} more negative). Bonding three en molecules is easier than bonding six NH_3; that is once one side of the en molecule is bound, the nearness of the other end gives a high probability of its being bound also.

This reasoning also explains the decrease in chelation with increasing ring size. In reviewing Table 3, both diphos and bipyridine stabilize cobalt carbonyl, since they are planar with their donor atoms in close proximity. On the other hand, ethylenediamine is a longer chain, and should have less of a chelation effect (as is the case). All chelation vanishes if the molecule bridges two carbonyls which is possible with ethylenediamine but less so with the other two ligands. The stability of the diphos is greater, as expected, since phosphorous compounds have greater metal π-bonding ability than nitrogen. the bipyridine complex rivals it, due to an extensive π-structure in the aromatic rings to which the metal may donate a high degree of electron density. The delocalization of electrons in the aromatic π-structure facilitates more than usual donation of the nitrogen to form a strong σ-bond resulting in a very stable complex.

2. Activity of Substituted Carbonyl Complexes

An important part of this study of metal carbonyl substitution was the measurement of the resulting catalytic activities as revealed by the results in Tables 4, 5 and 6.

The substituted cobalt carbonyls, Table 4, showed the highest hydrogenation activity of the metal carbonyls studied. The most active compound tested was triethylphosphine substituted cobalt carbonyl which completely hydrogenated anthracene to dihydroanthracene in less than 1 hr at 175°C. The other phosphines had satisfactory activity with the exception of triphenylphosphine which failed to catalyze hydrogenation probably due to its bulkiness. The polydentate ligands that are required to stabilize cobalt carbonyl to higher temperatures by chelation also showed good activity for hydrogenation with the exception of ethylenediamine. The iron carbonyl complexes in Table 5 were not as active as the cobalt carbonyls. Interestingly methylphenylsulfide gave the best activity at 200°C showing that sulfur is not a potential catalyst poison.

Several runs were made with PPh_2Cl to further study this catalyst but the activity is irreproducible ranging from 0 to 21 conversion. Unless this variability can be avoided the potential advantages of the iron carbonyls cannot be fully utilized.

The hexacarbonyls of Cr, Mo, W and V showed little hydrogenation activity as shown in Table 6. Only manganese carbonyl has sufficient activity for further study. Although it is not effective for hydrogenating phenanthrene it is not poisoned by nitrogen heterocyclics such as quinoline and has activity greater than iron and approaching the more unstable cobalt carbonyls.

Table 4. Hydrogenation with $Co_2(CO)_8$.

Substituting Ligand	Temp. °C	Press. Bars	Time min	Substrate	Solvent n-C_x	Product Percent
Et_3P	175*	35	1:15	A	8	92
Et_3P	175	30	0:58	A	10	99
Ph_3P	250**	51	2:45	A	9	none
Bu_3P+Ph_3P	175	29	0:49	A	10	93
$(EtO)_3P$	200	39	1:02	A	9	73
Bu_3P	200	38	1:40	P	8	none
Et_3P	200	36	2:20	P	10	6
Ph_3P	200	43	0:55	P	10	none
Ph_3P+Bu_3P	175	30	0:30	P	10	1
Bu_3P	175	34	0:55	N	9	1
bipy	200	41	0:45	A	10	54
en	200	41	1:00	A	10	none (decomp.)
diphos	200	41	1:00	A	10	40
diphos	200	41	1:00	Py	10	<1
bipy	250	68	1:00	Py	10	<1

Key to Substrates:
A = anthracene
P = phenanthrene
N = naphthalene
Py = pyrene

Table 5. Hydrogenation with $Fe(CO)_5$.

Substituting Ligand	Temp. °C	Total Press Bars	Time Min.	Substrate*	Solvents*	Product Percent
Bu_3P	225	36	2:30	A	10	4
Bu_3P	200	41	1:34	A	4	none
Et_3P	250	44	4:00	A	10	35
Ph_3P	200	39	2:10	A	10	none
$(EtO)_3P$	200	38	4:05	A	10	none
Ph_2ClP	300	51	2:00	A	10	21
NO	200	43	1:45	A	10	none
$MePh_5$	200	37	1:00	A	9	15
Bu_3S	200	43	4:30	A	9	2
Bu_3P	225	43	2:46	P	10	1

*Key to solvents: 2, dioxane; 4, decalin; 6, benzene; 8, n-octane; 9, n-nonane; 10, n-decane.
Key to substrates: A, Anthracene; P, phenanthrene.

Table 6. Hydrogenation with miscellaneous carbonyls.

Carbonyl	Substituting Ligand	Temp. °C	Press. Bars	Time Min.	Substrate	Solvent*	Product Percent
$Fe_2(CO)_9$	Bu_3P	200	41	1:00	A	10	10
$Ni(CO)_4$	Bu_3P	200	78	1:00	A	10	trace
	Bu_3P	200	41	1:31	A	9	1
$V(CO)_6$	Bu_3P	200	43	1:05	A	10	1
$Mo(CO)_6$	Bu_3P	250	58	1:30	A	6	none
$Mo(CO)_6$	Bu_3P	200	41	0:45	A	6	none
	Bu_3P	200	44	3:15	A	2	none
	Bu_3P+Et_3P	200	40	2:35	A	10	1
$W(CO)_6$	Bu_3P	200	39	1:00	A	10	none
$Mn_2(CO)_{10}$	Bu_3P	200	41	1:00	A	10	32
$Mn_2(CO)_{10}$	Bu_3P	200	41	1:00	Q	10	86
$Mn_2(CO)_{10}$	Bu_3P	200	41	1:00	P	10	none

*Key to substrates: A, anthracene; Q, quinoline; P, phenanthrene.
Key to solvents: 2, dioxane; 4, decalin; 6, benzene; 8, n-octane; 9, n-nonane; 10, n-decane.

Three additional polynuclear aromatic hydrocarbons were studied for their relative susceptibilities to hydrogenation. The reactions with phenanthrene pyrene, and naphthalene were very slow compared to anthracene. This has been attributed (F5) to their inability to stabilize free radical intermediates of the form:

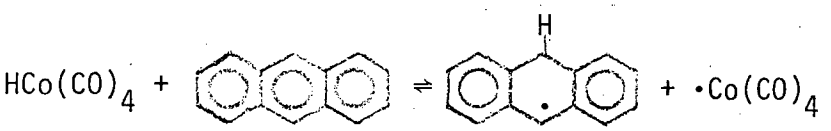

In summary, the dinuclear metal carbonyls $Co_2(CO)_8$, $Fe_2(CO)_9$, and $Mn_2(CO)_{10}$ are more active hydrogenation catalysts than the mononuclear carbonyls. This may be due to the ease of metal-metal bond cleavage to form hydrides. The mononuclear carbonyls must first dissociate CO to become coordinately unsaturate prior to hydrogen activation. This requires more energy than homolytic or heterolytic splitting.

The practical considerations pertaining to catalysts for coal liquefaction serve to determine which type of catalyst should be investigated further and point to a compromise between the opposing factors of stability and activity. The experiments made suggest that manganese carbonyl derivatives are the catalysts with greatest potential. Based on the success of these substitution studies which have drawn upon the fundamental properties of transition metal bonding, a study was conducted of the mechanism of homogeneous hydrogenation at elevated temperatures and pressures, to be described in Chapter IV.

3. Additives to Improve Catalytic Activity of Substituted Metal Carbonyls

The substitution reactions of metal carbonyls are accelerated in two-phase systems such as benzene/50% aqueous sodium hydroxide in the presence of phase-transfer catalysts, quaternary ammonium salts such as tetra-n-butyl-ammonium iodide (H9). Reaction proceeds slowly, or not at all, in the absence of the phase-transfer catalyst. The phase-transfer catalyst function is to shuttle hydroxyl groups from the aqueous to the organic phase. The presence of hydroxyl groups are known to promote water-gas shift with iron carbonyl (W2). Since both ligand substitution to form hydrides and water-gas shift are advantageous to metal carbonyl catalyzed hydrogenations, three commercially used phase-transfer catalysts were investigated in conjunction with $Fe(CO)_5$.

Table 7 lists the additives tried with $Fe(CO)_4Bu_3P$. the presence of sodium hydroxide improves the hydrogenation ability of the catalyst; this may result by forming the hydride $NaHFe(CO)_3Bu_3P$ (C7) or promoting water-gas shift (W2). Dramatic improvement in hydrogenation rate is noted when the reaction is conducted in ethanol instead of decane. Only trace amounts of the anthracene remained unreacted. It appears that ethanol provides a liquid phase to dissolve the NaOH. The phase transfer catalyst, trimethyl-benzylammonium chloride increases the effectiveness of the basic medium to accelerate a substitution step of the metal carbonyl-probably by hydride formation.

Table 7. Phase transfer catalysts added to $Fe(CO)_4Bu_3P$ catalyzed hydrogenation of anthracene.

Temp. = 200°C; 1mM $Fe(CO)_4$ Bu_3P; 100 ml solvent; P = 55 bars; $H_2/\overline{CO}$ = 1.0

Additive	Amount gm	Solvent	Conversion Percent
None		C_{10}	4
NaOH, H_2O	0.36,5	C_{10}	9
NaOH,H_2O,Triton B*	0.36,1,0.4	C_{10}	12
NaOH,H_2O,TBAC*	0.5,10,1	EtOH	99+
NaOH,H_2O,TBAC	1.26,1,0.2	C_{10}	0
H_2O,TEA	10,1	EtOH	(decomp.) 0

Triton B = 40 percent benzyltrimethylammonium hydroxide in MeOH.
TBAC = trimethylbenzylammonium chloride.
TEA = triethylamine.

IV. CATALYTIC KINETICS OF ANTHRACENE HYDROGENATION WITH SUBSTITUTED DIMANGANESE DECACARBONYL

The exploratory studies, just described, for thermal stability and homogeneous catalytic activity for a group of substituted metal carbonyls have shown that dimanganese decacarbonyl is a promising starting material for further investigation of hydrogenation catalysis in nonpyrolytic coal liquefaction. Anthracene was chosen as a model reactant because of its prevalence in coal derivatives, its ease of hydrogenation to 9,10-dihydroanthracene, and the absence of resulting by-products. Kinetic experiments have been carried out to determine the mechanism by which manganese complexes catalyze the hydrogenation of anthracene. A substantial number of ligands were used to substitute one or two of the carbonyls on dimanganese decacarbonyl, leading to new conclusions about ligand basicity and substituent effects.

Although manganese complexes have been found to be homogeneous catalysts for hydrogenation, previous work at elevated temperature and pressures is extremely limited. Two unpublished studies have been cited by James (J3). 1-Octene has been hydrogenated by $Mn_2(CO)_{10}$ at 80 to 150°C under 200 bars of hydrogen; also unsaturated fatty esters have been saturated, the conditions not being specified. A later study confirmed the hydrogenation of octenes and also of cyclohexene. At higher temperatures (200-235°C) hydroformylation products were observed (W6). In none of the cases were kinetics reported.

The most relevant study to manganese carbonyl hydrogenation of aromatics is a report of the existence of aromatic complex cations of the type $ArMn(CO)_3^+$, Ar being benzene, methyl substituted benzenes and naphthalene (W5). The presence of hydride from, say, sodium borohydride promotes the reaction,

$$ArMn(CO)_3^+ \underset{-H^-}{\overset{+H^-}{\rightleftharpoons}} (ArH)\ Mn(CO)_3$$

to form a partially hydrogenated complex which is stable at 160^o for Ar = benzene. The hydride-aromatic complex is very reactive and attacks carbon tetrachloride to produce chloroform and the original cation.

Some analogies for manganese carbonyl catalysis can be drawn from other metal carbonyl systems, especially hydroformylation catalyzed by cobalt carbonyl which forms aldehydes from olefins. This reaction is accompanied by competitive hydrogenation of the olefin to paraffin and of the product aldehyde to alcohol, both unwanted in the case of hydroformylation.

In studies of the hydrogenation of 1,3-cyclooctadiene with phosphine substituted cobalt carbonyl, Ogata and Misono (O2) reported that $HCo(CO)_3PR_3$ (with R = butyl) appears to be the true catalyst which can complex with the substrate R' to give $(R'H)\ Co(CO)_3PR_3$; this intermediate may then react with another hydride or with molecular hydrogen to form cyclooctene.

$$(R'H)\ Co(CO)_3Bu_3P + HCo(CO)_3Bu_3P$$
$$\rightarrow R'H_2 + [Co(CO)_3Bu_3P]_2$$

Under hydrogen atmosphere the final hydrogenolysis step could involve

$$(R'H)\ Co(CO)_3Bu_3P + H_2 \rightarrow R'H_2 + HCo(CO)_3Bu_3P$$

The complete mechanism with hydrogen involves an allylic(I) and a dihydride(II) form

$$-CH{=}CH{=}CH{=}CH- + HML_n \rightarrow$$

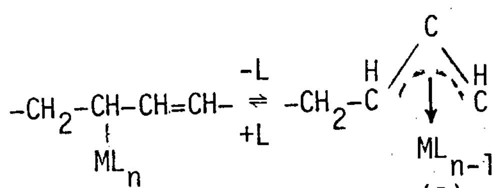

(I)

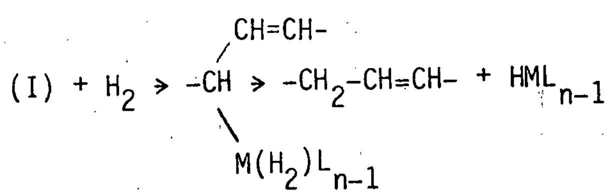

(II)

Several features of this system will be found analogous to catalysis with manganese complexes.

A. Experiments

Apparatus and procedures for the hydrogenation reactions has been described in the previous section, so only the particular modification pertaining to each group of experiments will be discussed here.

1. Substrate Dependence

The autoclave liner was charged with substrate, solvent, and catalyst. After sealing, the reactor was purged, pressurized with CO, and heated to a reaction temperature of 200°C. The pressure was noted and hydrogen was added to start the reaction. Samples were taken for analysis at various times.

2. Catalyst Concentration Dependence

Rate studies at various catalyst were carried out, the amount of catalyst being varied over a 60-fold range. The carbon monoxide pressure was kept constant at 20 bars; two hydrogen pressures were used, 20 and 52 bars. Samples were analyzed after 1 hr of reaction time except for cases where large amounts of catalysts were used and shorter reaction times were dictated.

3. Carbon Monoxide Dependence

The effect of carbon monoxide on rate was established by initially charging the reactor with a 1:1 mixture of hydrogen and carbon monoxide to 21 bars, heating the reactor to reaction temperature, and then admitting CO to maintain the desired partial pressure. The initial CO pressure was required to prevent catalyst decomposition during heat-up. Samples were withdrawn after 1 hr and analyzed.

4. Hydrogen Dependence

The reactor was charged with substrate, catalyst, and solvent, then purged and pressurized to 14 bars with CO. After heat-up, the pressure was 34 bars at 200°C. At 200°C the solvent n-decane contributes 1.3 bars to the total pressure. Hydrogen was added to the

desired pressure (up to 74 bars) and samples were taken after 1 hr. In all kinetic experiments the hydrogen consumed was less than 3% of the initial charge of hydrogen, so that the hydrogen concentration could be assumed to be constant.

5. Ligand Effects

The influence of ligand type and quantity on the rate of reaction was studied. Dimanganese decacarbonyl was substituted with phosphines and phosphites. Ligand quantity was varied only for tri-n-butylphosphine. In all studies with other ligands, a 1:1 ratio of metal atom to phosphorus was maintained.

6. Temperature Effects

To measure accurately the effect temperature, both heatup and total pressure had to be standardized. The reactor was charged with substrate, catalyst, and solvent; after purging, synthesis gas (1:1, H_2:CO) was used to pressure the reactor to 21 bars. After heatup to 200^{o}, synthesis gas was added to increase the pressure from 34 to 41 bars. The reactor was then cooled or heated to the desired temperature, in less than 2 min. After 1 hr, samples were taken.

Reaction was conducted above the normal boiling point ($175^{o}C$) of the solvent (n-decane) and different amounts of solvent would flash during sampling at different temperatures. Because decane was used as an internal standard in the gas-chromatagraphic analysis, it was imperative that a uniform amount of solvent be withdrawn with the sample. This was achieved by pressurizing the sample from the reactor into an evacuated 70 ml stainless-steel sampling bomb, which was quenched and depressurized before analysis.

7. Product Analysis by Infrared Spectroscopy

For measurements at ambient conditions, samples withdrawn from the reactor were allowed to cool and injected into 0.1 ml NaCl infrared cells. Spectra were recorded on a Perkin-Elmer 137 spectrophotometer or a Digilab FTS-10 Fourier transform spectraphotometer. Spectra were recorded with n-decane in a matched reference cell. Polystyrene was used for calibration of the spectra.

For measurements at reaction conditions, solutions were measured in a thermostatted, high-pressure infrared cell at 200°C, designed by Tinker and Morris (T5). The windows were made of calcium fluoride with a path length of 1.0 mm.

The cell was connected to the reactor sample outlet with a heated line. during the course of the reaction, samples could be admitted to the cell and spectra recorded on a FTS-10 spectrophotometer. Normally the cell was flushed between scans with excess sample. The spectra were referenced to n-decane under about 7 bars CO pressure and calibrated with polystyrene film.

B. Results and Discussion

1. Effect of Anthracene Concentration on Rate

For $Mn_2(CO)_{10}$ substituted with tri-n-butylphosphine at constant partial pressures of H_2 and CO and constant temperature plots of the logarithm of the normalized concentration on a linear time scale yields a straight line (e.g., Figs. 15 and 16) indicating first-order dependence on anthracene. 9,10-dihydroanthracene was the sole product; no by-products such as tetrahydro-or

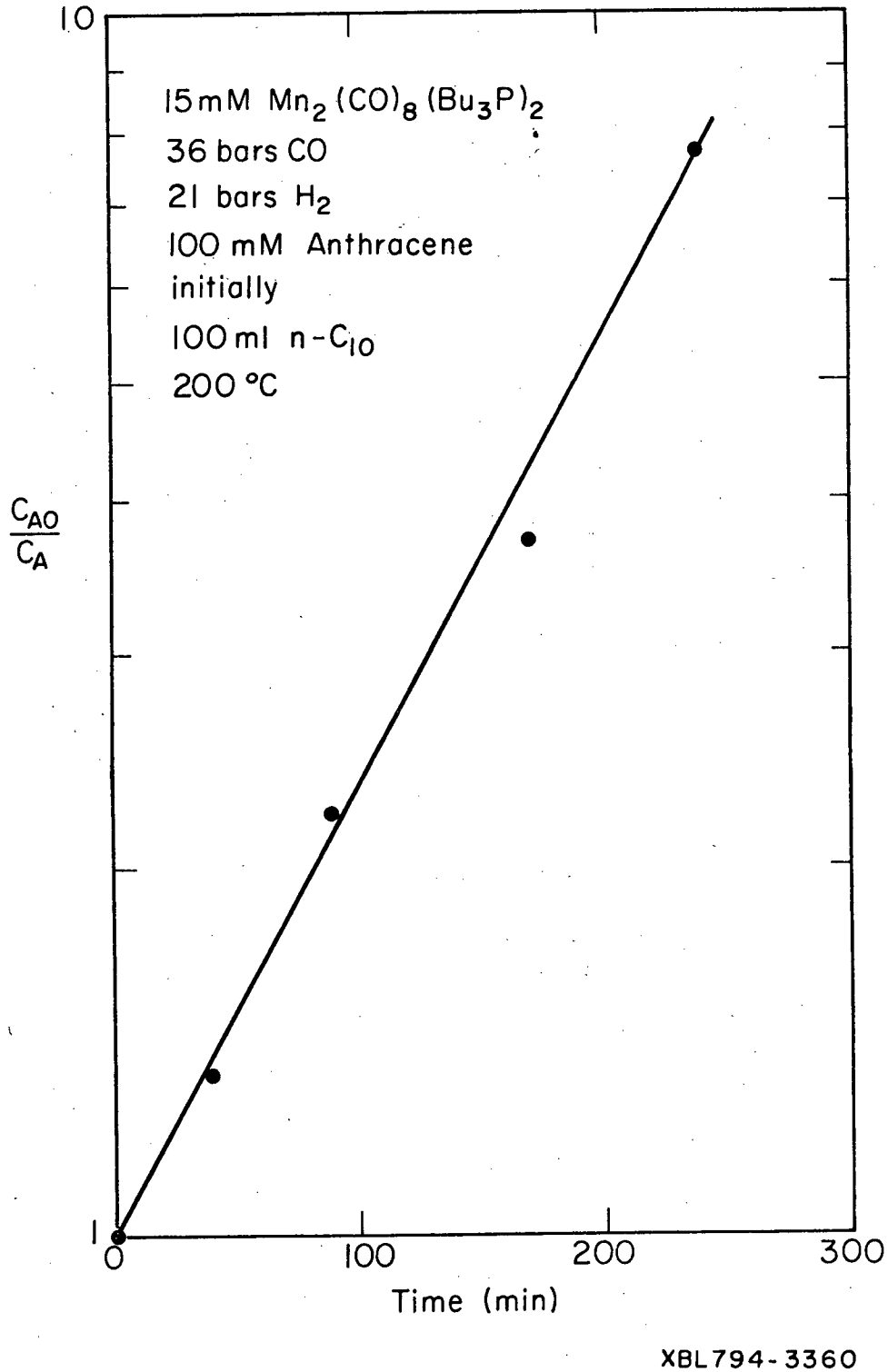

Fig. 15. Hydrogenation of anthracene with $Mn_2(CO)_8(Bu_3P)_2$.

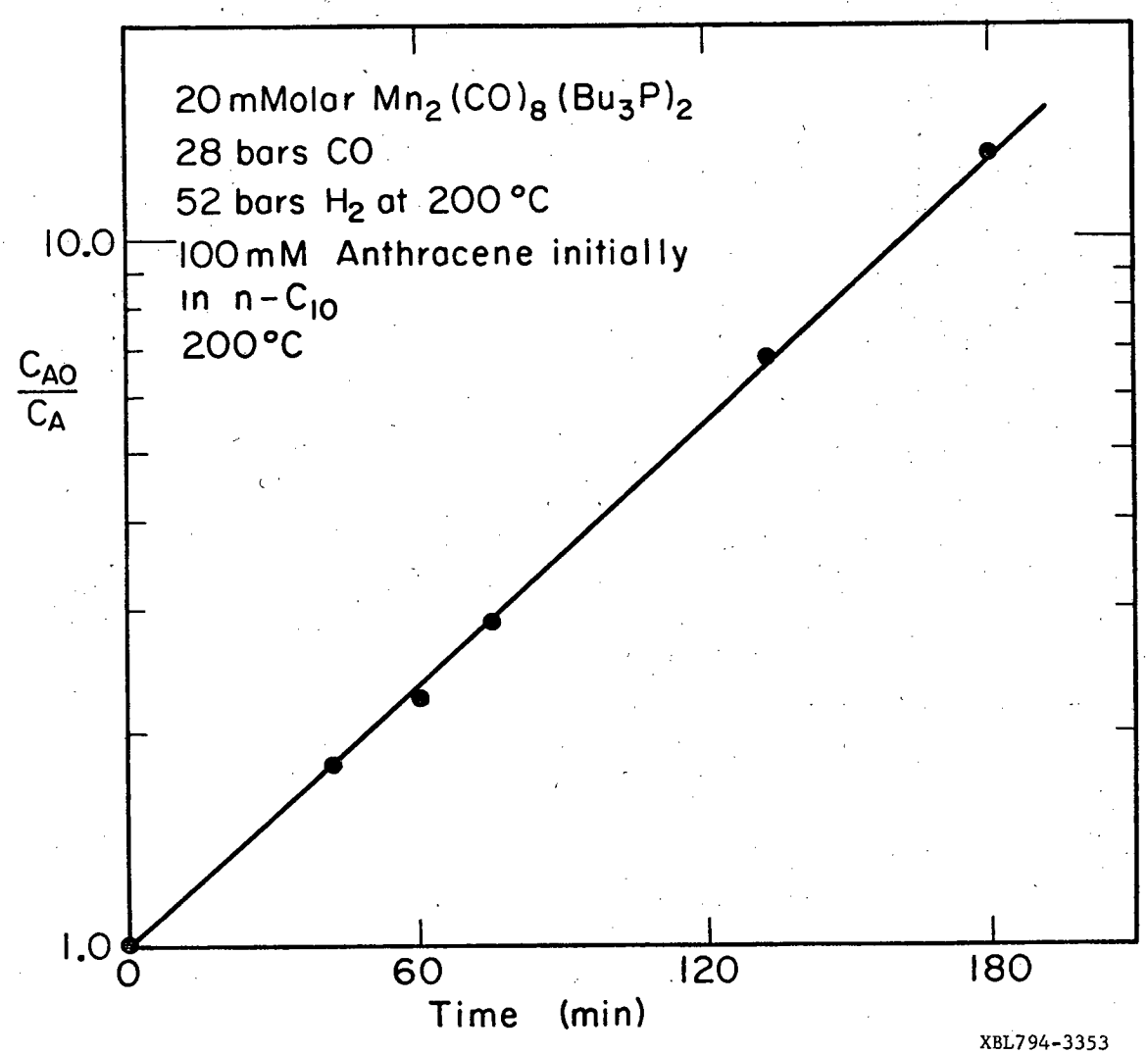

Fig. 16. Hydrogenation of anthracene with $Mn_2(CO)_8(Bu_3P)_2$.

octahydro-anthracene were detected by gas chromatography and subsequent mass spectrometry. The hydrogenation of anthracene proceeds to completion (>99.5% by G. C.) and has been treated as an irreversible reaction.

One experiment was conducted with dicobalt octacarbonyl. The same first order dependence was borne out but the reaction rate is 13.3 times faster for the same catalyst concentration (Fig. 17).

2. Rate Dependence on Catalyst Concentration

The knowledge that the rate of reaction is a function of the anthracene concentration to the first power yields the integrated form of the generalized rate equation.

$$\frac{-dC_A}{dt} = kC_A C_o^n$$

$$\ln \frac{C_{Ao}}{C_A} = kC_o^n t$$

where C_{Ao} is the initial concentration of anthracene, C_A the concentration of anthracene at time, t and C_o the concentration of catalyst charged to the reactor. The exponent of C_o, n, may be determined by taking the logrithm of both sides of the equation.

$$\ln \ln \frac{CA_o}{C_A} = \ln kt + n \ln C_o$$

A log-log plot of $\ln(CA_o/C_A)$ vs C_o has the slope n. such plots appear in Figs. 18 and 19.

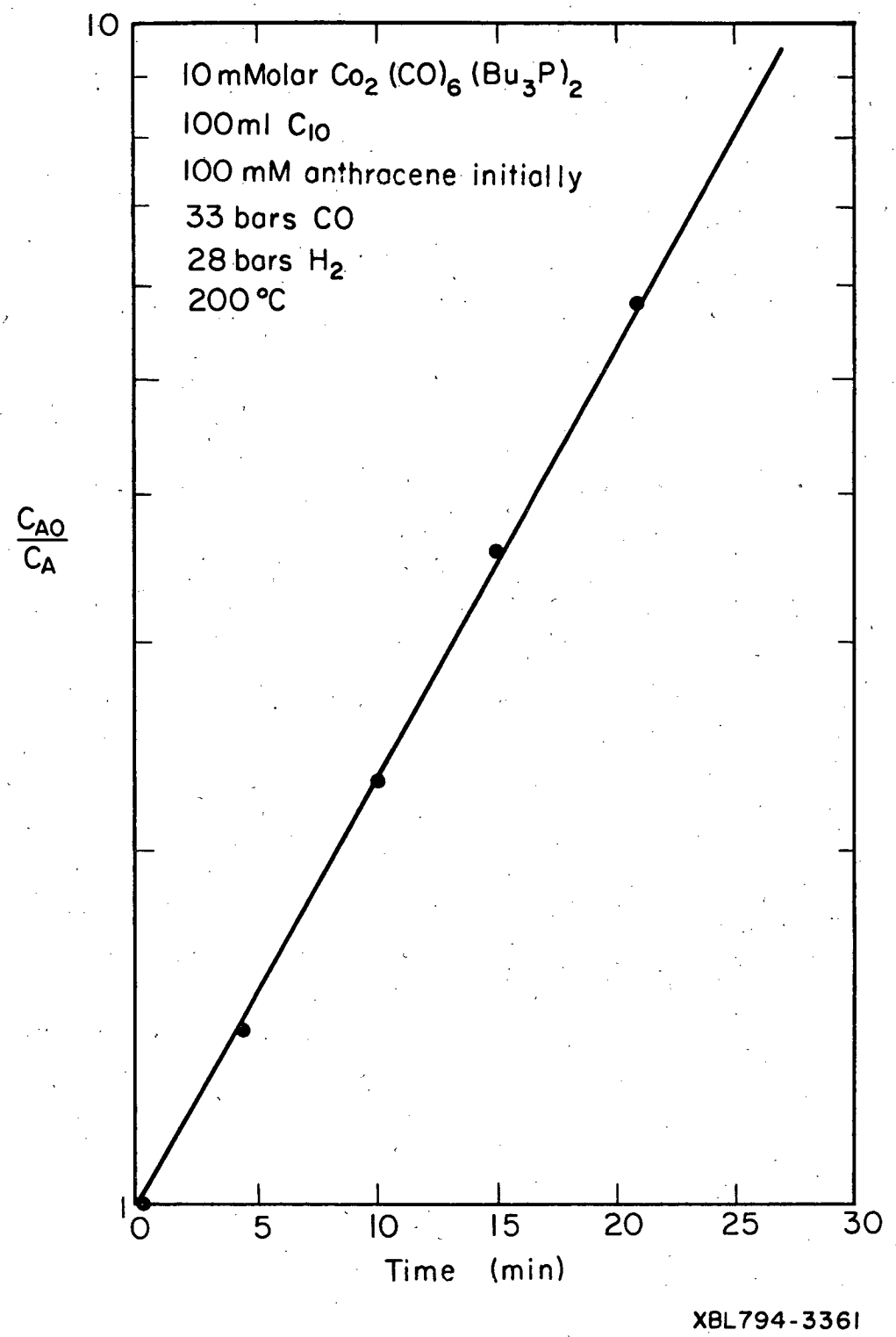

Fig. 17. Hydrogenation of anthracene with $Co_2(CO)_8$.

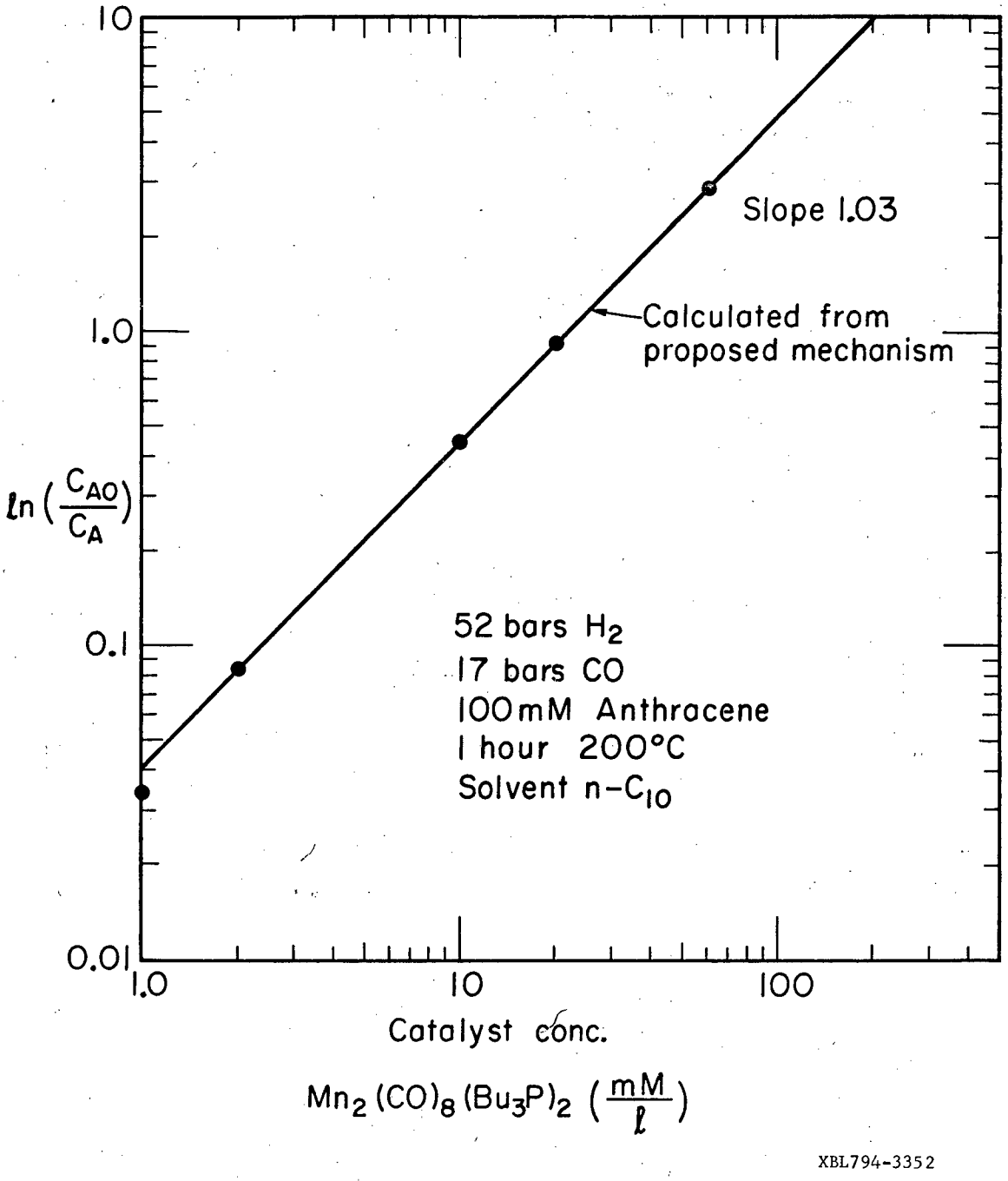

Fig. 18. Rate dependence on catalyst concentration.

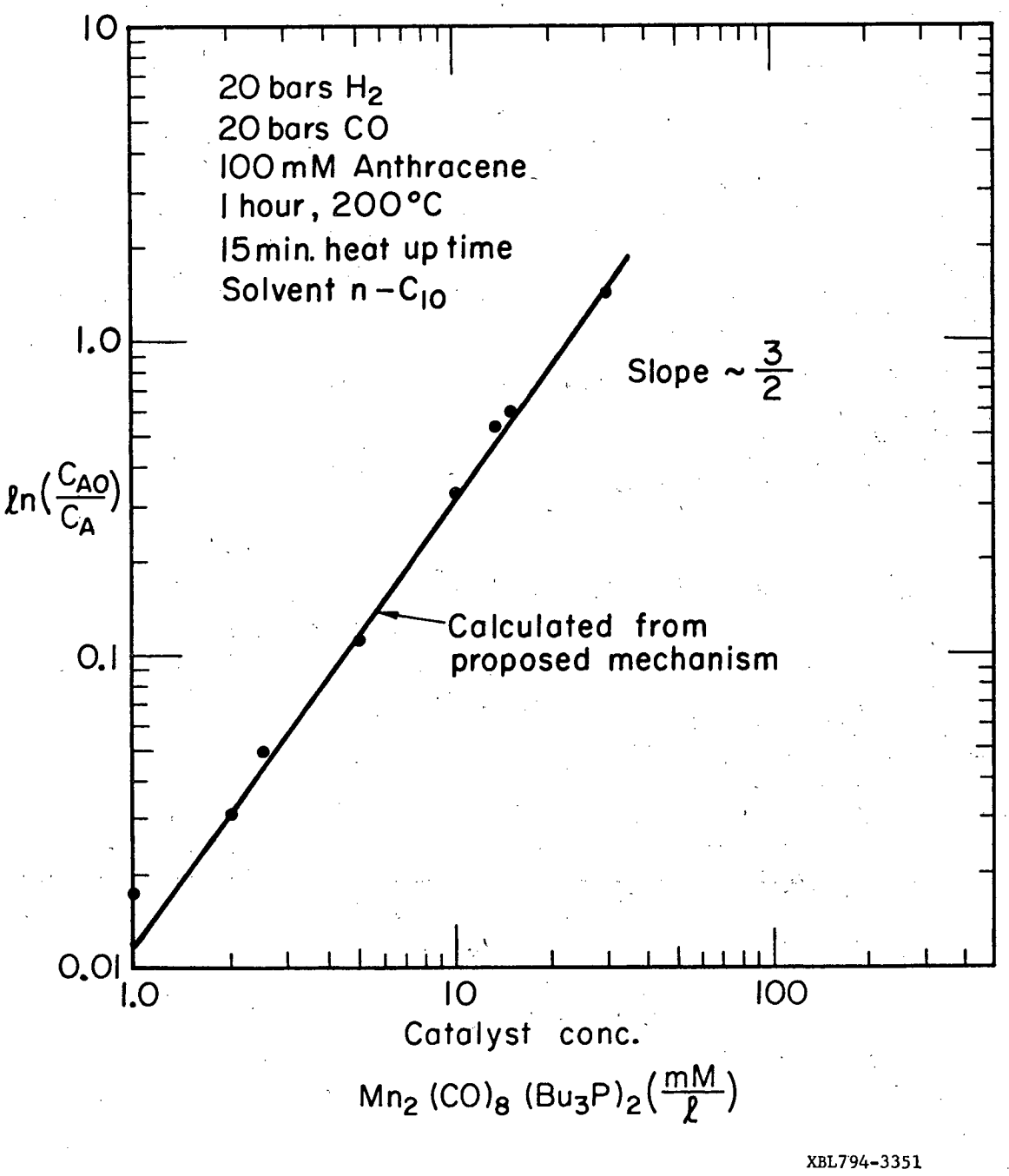

Fig. 19. Rate dependence on catalyst concentration.

The value for n at a hydrogen pressure of 17 bars indicates close to a 1.5-order catalyst dependence while at higher hydrogen pressure of 52 bars the order drops to nearly 1.0. The inverse dependence of catalyst order on hydrogen pressure suggests a transition from a rate determining step that involves two molecules of catalyst to a step containing only one molecule of catalyst.

3. Effect of Hydrogen Pressure on Rate

By again applying the method used in the previous section, the order of hydrogen pressure was determined.

$$\ln \ln \frac{CA_o}{C_A} = \ln kt + m \ln P_{H_2}$$

where m is the order of the dependence of the rate on hydrogen pressure p_{H2}.

From Fig. 20 it is evident that the rate of hydrogenation goes from a first-order dependence at low pressure to a region where the rate is independent of hydrogen pressure. As the hydrogen pressure increases, the relative increase in rate falls off, so that the rate tends to become independent of hydrogen; a further increase in hydrogen may even decrease the rate. The reduction in reaction order with increasing pressure suggests retardation by adsorbtion which would be represented by a hydrogen term in the demoninator of the rate equation.

4. Rate Dependence on Carbon Monoxide Pressure

Figure 21 demonstrates the effect of increasing the partial pressure of carbon monoxide on the rate of anthracene hydrogenation.

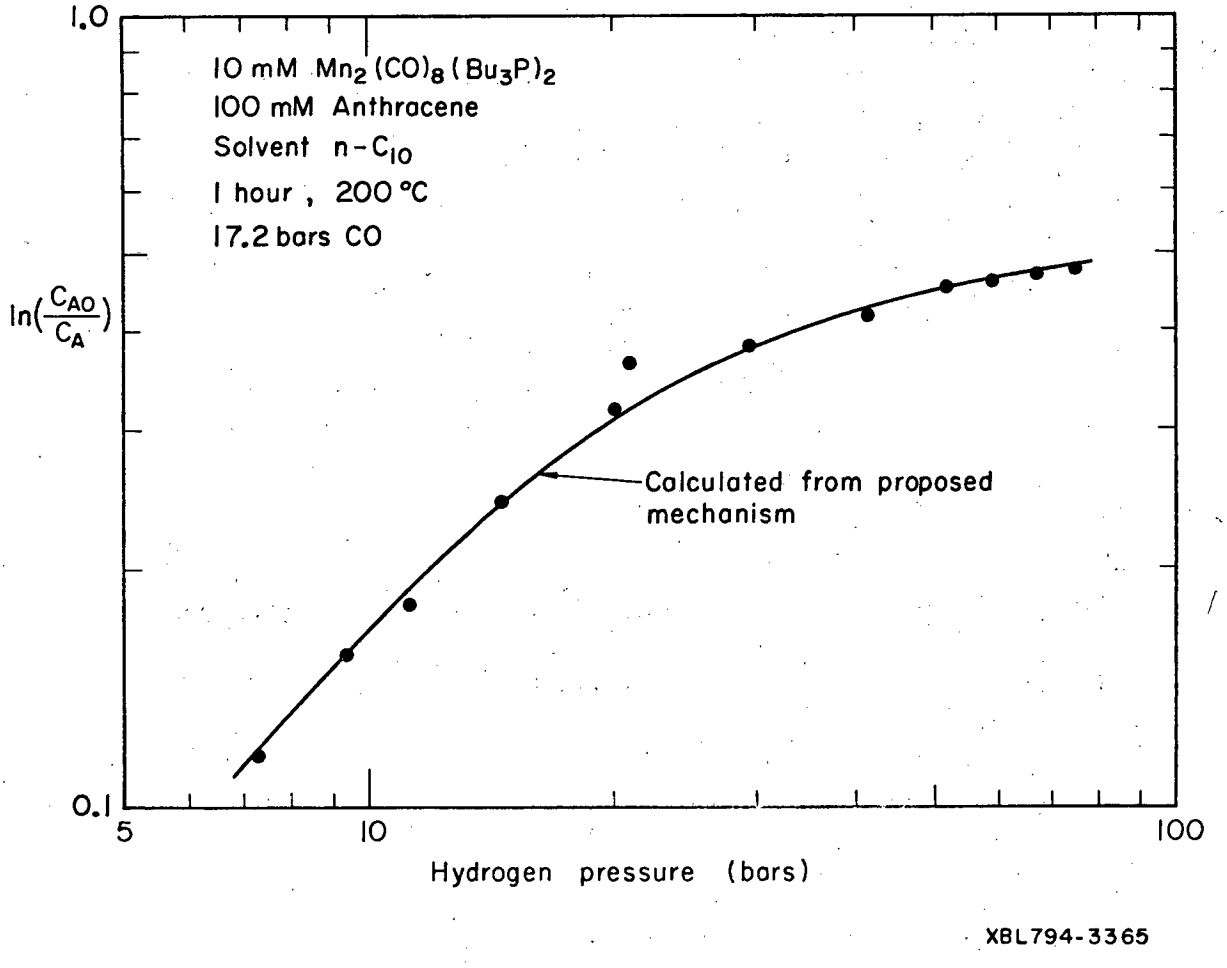

Fig. 20. Rate dependence on hydrogen pressure.

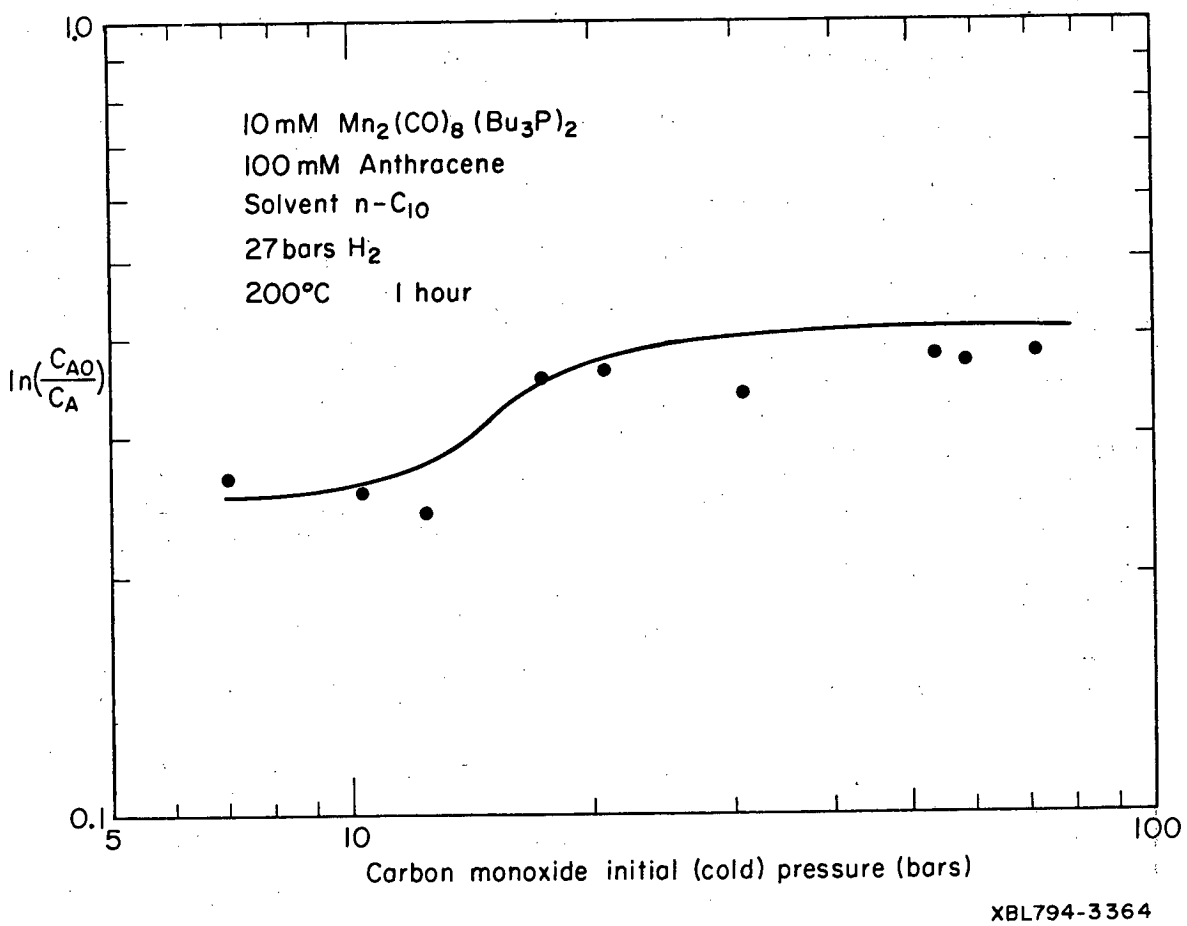

Fig. 21. Rate dependence on carbon monoxide pressure.

At pressures less than about 17 bars catalyst decomposition occurs over the course of the reaction. Above 17 bars initial CO pressure the rate of hydrogenation is almost independent of CO pressure. The weak dependence of rate on pressure rules out a CO dissociative mechanism in the rate determining step. This is analogous to anthracene hydrogenation by $Co_2(CO)_8$, but in contrast to the observed inverse CO dependence in hydroformylation.

Figure 21 also helps explain another factor in the irreproducibility of the hydrogen dependence data. The data for the hydrogen dependence was taken at 14 bars initial CO pressure which is between the decomposition and the stable regime of the catalyst. Small errors in the initial charge of CO may have led to the erratic behavior of the system. An arbitrary curve has been drawn between the two regions in Fig. 21 but the curve may be much steeper and the decomposition effect more pronounced.

5. Temperature Effect on Rate

The effect of temperature on the rate of anthracene hydrogenation is shown as an Arrhenius plot of Fig. 22. The straightness of the line suggest that the mechanism of hydrogenation is not changing in the rate of 175 to 230°C. From the slope of the line on apparent activation energy of 24.0 kcal/mole may be calculated. This activation energy is in accord with the value 22.9 kcal/mole reported by Osborn et al. (010) for the hydrogenation of cyclohexene with tristriphenylphosphine rhodium chloride.

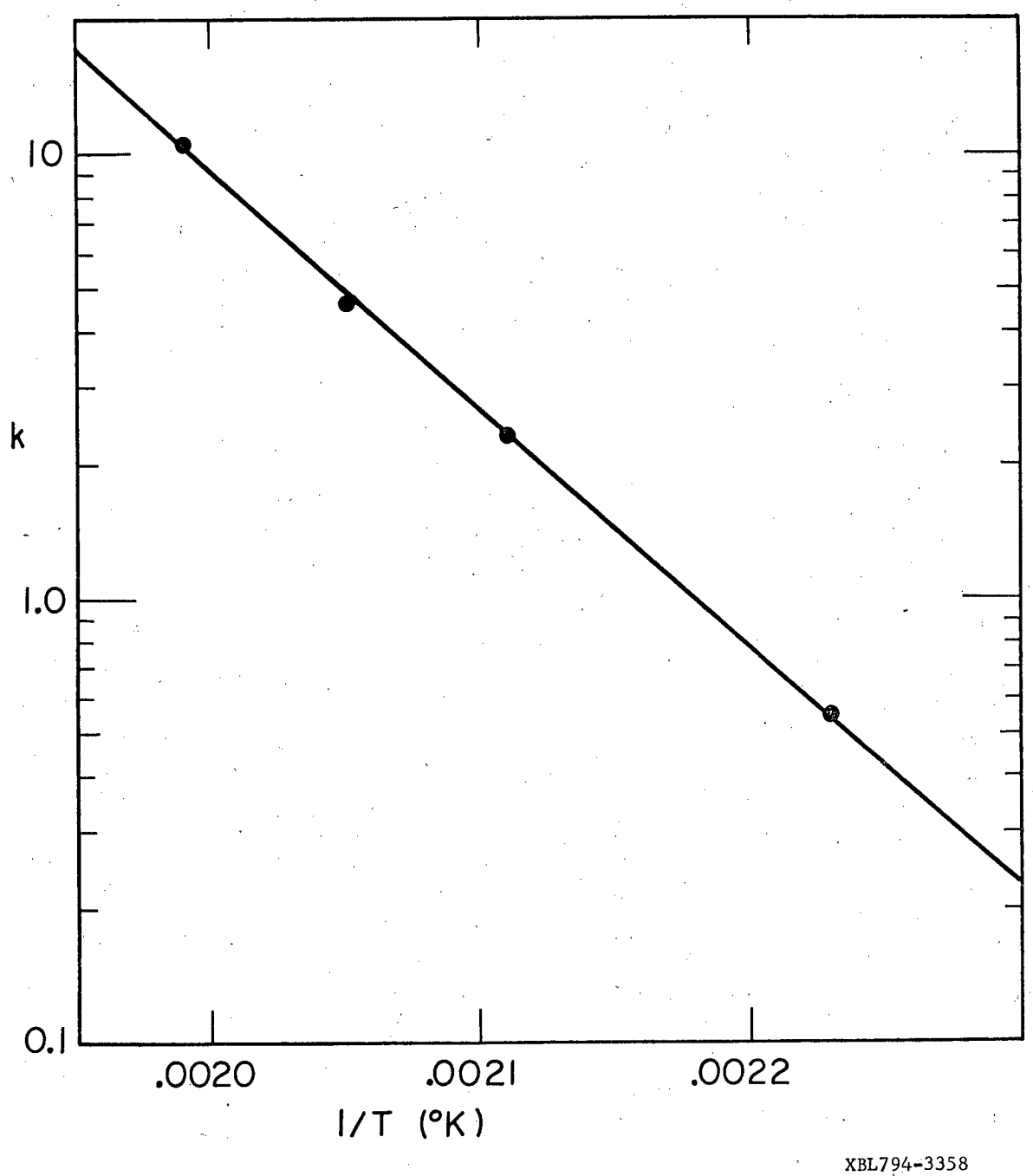

Fig. 22. Arrhenius plot of anthracene hydrogenation.

6. Proposed Mechanism for Hydrogenation of Anthracene with Tri-n-Butylphosphine Substituted Dimanganse Decacarbonyl

Homogeneous hydrogenation by manganese carbonyl has been limited to the two systems previously mentioned and no reports on kinetics or mechanisms have been found in the literature. The kinetic information gained on anthracene hydrogenation has been consolidated by a mechanism that predicts quantitatively all the trends observed. Due to the complexity of the problem a computer program was written to correlate the data and ascertain the validity of several proposed mechanisms.

The general procedure for arriving at the proposed mechanism was composed of three stages. First a mechanism was chosen that seemed to reflect the desired trends, first order dependence on anthracene and a decrease in order of catalyst and hydrogen dependence on increasing hydrogen pressure. Then a rate equation was formulated from the trial mechanism. Normally the rate equation contained several unknown constants, and was more complex than could be determined graphically. The second stage of the analysis was the computer determination of the constants to provide for the lowest standard deviation fit of the data. Finally, the computer generated output was compared graphically to the experimental data. This strategy provided a means to converge on the true mechanism. General trends seen from incorrect guesses, indicated how the mechanism failed and where corrections should be made. This method afforded the opportunity of systemizing somewhat the elucidation of the mechanism, often a new intuitive process.

a. Proposed Mechanism for Anthracene Hydrogenation by $Mn_2(CO)_8(Bu_3P)_2$. The following mechanism has been found to most accurately describe the mechanism of anthracene hydrogenation by tri-n-butylphosphine substituted dimanganese decacarbonyl.

$$Mn_2(CO)_{10} + 2L \overset{K_1}{\rightleftharpoons} Mn_2(CO)_8L_2 + 2\ CO \quad (1)$$

$$H_2 + Mn_2(CO)_8L_2 \overset{K_2}{\rightleftharpoons} 2\ HMn(CO)_4L \quad (2)$$

$$Mn_2(CO)_8L_2 \overset{K_3}{\rightleftharpoons} 2\ Mn(CO)_4L \quad (3)$$

$$HMn(CO)_4L + H_2 \overset{K_4}{\rightleftharpoons} H_3Mn(CO)_3L + CO \quad (4)$$

$$Mn(CO)_4L + A \overset{K_5}{\rightleftharpoons} Mn(CO)_4A + L \quad (5)$$

$$Mn(CO)_4L + H_2 \overset{K_6}{\rightleftharpoons} H_2Mn(CO)_3L + CO \quad (6)$$

$$H_2 + Mn(CO)_4A \underset{k_7^+}{\overset{k_7}{\rightleftharpoons}} HMn(CO)_4AH \quad (7)$$

$$H_3Mn(CO)_3L + HMn(CO)_4AH \overset{k_8}{\rightarrow} H_2A + H_2Mn(CO)_3L + HMn(CO)_4 \quad (8)$$

L is tri-n-butylphosphine, A anthracene, and H_2A 9,10-dihydroanthracene.

Steps 1 through 6 are assumed to be in equilibrium. The combination of steps 7 and 8 as competing rate determining steps require that $R_7 = R_8$ so:

$$k_7(Mn(CO)_4LA)(H_2) - k_7^+(HMn(CO)_4AH) = k_8(H_3Mn(CO)_3L)(HMn(CO)_4AH)$$

which gives

$$(HMn(CO)_4AH) = \frac{k_7(Mn(CO)_4A)(H_2)}{k_7^+ + k_8(H_3Mn(CO)_3L)}$$

The overall rate of reaction is given by

$$\frac{-d(A)}{dt} = k_8(H_3Mn(CO)_3L)(HMn(CO)_4AH)$$

$$= \frac{k_7k_8(H_3Mn(CO)_3L)(H_2)(Mn(CO)_4A)}{k_7^+ + k_8(H_3Mn(CO)_3L}$$

The manganese carbonyl charged to the reactor as $Mn_2(CO)_{10}$ is distributed into various substituted species and very little of it is left as $Mn_2(CO)_{10}$. The mass balance for the initial manganese carbonyl charged, C_o, is a summation of all the forms of the catalyst.

$$C_o = HMn(CO)_4L + H_3Mn(CO)_3L + Mn(CO)_4A + Mn_2(CO)_{10}$$

$$+ H_2Mn(CO)_3L + HMn(CO)_4AH + Mn_2(CO)_8L_2$$

$$+ Mn(CO)_4L$$

The assumption that these species are at equilibrium allows the overall rate equation to be solved as a quadratic function of C_o. The equation is unweildy but can be simplified if only monomeric species of manganese are used in the mass balance. Only the first three species contribute significantly to amount of the catalyst present at reaction conditions so the mass balance can be further simplified:

$$C_o = HMn(CO)_4L + H_3Mn(CO)_3L + Mn(CO)_4A$$

$$C_o=(HMn(CO)_4L)(1 + K_4(H_2)/(CO)$$

$$+ K_3^{1/2}K_5K_2^{-1/2}(L)(A)/(H_2)^{1/2})$$

$$C_o = (HMn(CO)_4L)(D)$$

The overall rate expression as a function of $Mn_2(CO)_{10}$ charged to the reactor becomes:

$$R = \frac{-d(A)}{dt} = \frac{k_7k_8K_2^{-1/2}K_4K_5(C_o)^2(H_2)^{1/2}(A)}{D^2(k_7^+(CO)/(H_2) + k_8K_4(C_o)/D)}$$

The computer program, included in Appendix I, was able to iterate on only four constants. This required some constants in the rate expression to be combined. The combinations are given for the simplified rate equation consistent with the computer program.

$$\frac{R}{(A)} = \frac{OK_2(C_o)^2(H_2)^{1/2}}{((CO)/(H_2) + OK_3(C_o)/V)V^2}$$

$$V = 1 + DEL_2(H_2)/(CO) + DEL_3(A)(L)/(H_2)^{1/2}$$

Thus

$$OK_2 = k_8K_7K_4K_5K_2^{-1/2}K_3^{1/2} = 0.085$$

$$OK_3 = k_8K_4/k_7^+ = 1.9$$

$$DEL_2 = K_4 = 0.35$$

$$DEL_3 = K_5K_3^{1/2} = 0.16$$

By substitution and from the results of the computer program

$$K_4 = 0.35$$

$$K_8/k_7^+ = 5.4$$

$$K_5K_3^{1/2}/k_2^{1/2} = 0.16 \text{ mM}^{-2} \text{ psi}^{1/2}$$

$$k_7 = 0.028 \text{ mM}^{-1}\text{psi}^{-1}\text{hr}^{-1}$$

The computer program correlation with the above constants fits the data with a standard deviation of 10.9%. The fit of the data is shown graphically in Figs. 18 through 21 as the calculated curves. It can

be seen that the mechanism predicts quite well all the trends indicated by the experimental points.

Several features of the above mechanism should be discussed. The first six steps of the proposed mechanism consist of reactions which proceed faster than the rate determining steps and are considered to be in equilibrium. The substitution of $Mn_2(CO)_{10}$ with Bu_3P forms $Mn_2(CO)_8(Bu_3P)_2$ and the reported kinetics indicate the reaction is completed in less than 15 min., which is the heatup time for the reactor used in these studies (W4). Substitution may also proceed via an initial $HMn(CO)_5$ formation by thermal homolytic Mn–Mn bond rupture with coordinative addition of hydrogen. the hydride formed reacts quickly with phosphine even at room temperature to give $HMn(CO)_4L$. The reaction is complete in less than 5 min (B2). Probably the ligand substitution and hydride formation are competing pathways. In any event equilibrium is assured and most of the original $Mn_2(CO)_{10}$ charged to the reactor converts to $HMn(CO)_4L$. For L = Bu_3P essentially all the manganese is in the form $HMn(CO)_4Bu_3P$ (B2).

The mechanism for hydrogenation of anthracene postulates a free radical intermediate, $Mn(CO)_4Bu_3P$. The long metal-metal bond length in conjunction with a measurement of 19 kcal/mole for the bond strength in $Mn_2(CO)_{10}$ has led to the hypothesis that many reactions of $Mn_2(CO)_{10}$ occur through initial homolytic fission (H6). Homolytic fission produces $Mn(CO)_5$ radicals which can participate in recombination, decomposition, or substitution (F4).

The concept of homolytic fission has been shown to be valid for other dinuclear carbonyls. ($Te_2(CO)_{10}$, $Re_2(CO)_{10}$, and $MnRe(CO)_{10}$) (J5).

Direct proof of the existence of substituted manganese carbonyl radicals has been provided by electron spin resonance (K5). Extended photolysis of $Mn_2(CO)_3(Bu_3P)_2$ in the presence of Bu_3P in heptane resulted in the formation of a paramagnetic species. The species had an esr signal consistent with $Mn(CO)_3(Bu_3P)_2$ having a square pyramid structure with mutually trans Bu_3P groups in basal positions. The radicals are moderately stable since recombination is impeded by steric repulsion caused by the phosphines. The substituting phosphine has a large effect on homolytic fission leading to radical stabilization. CO dissociation studies indicate for the 16-electron, 5-coordinate $M(CO)_4L$, the ligands which are weak π-acceptors or poor σ-donors tend to occupy basal positions (A4). Extended to 17-electron species, L = Bu_3P would tend to occupy basal positions more than L = $(EtO)_3P$ and indeed the $Mn(CO)_3L_2$ radical is more stable when L = Bu_3P. Since the phosphine in $Mn(CO)_4L$ occupies a basal position, a rearrangement to axial positions must take place before two radicals can recombine to form $Mn_2(CO)_8L_2$. As a consequence phosphine substituted manganese carbonyls are more stable than $Mn(CO)_5$.

The postulated free radical intermediate, $Mn(CO)_4Bu_3P$ was not isolated but is a plausible compound in view of the detection of its homologue $Mn(CO)_3(Bu_3P)_2$. Ten other less well characterized

manganese carbonyl free redicals have been reported (K5) including $Mn(CO)_4(Et_3P)$ and $Mn(CO)_4(Ph_3P)$ which were formed thermally at 120^oC in xylene. It should be noted that manganese carbonyl radicals will quickly abstract hydrogen from solvents to form hydrides so $Mn(CO)_4Bu_3P$ is not expected to be in appreciable concentrations in the catalyst mass balance (M12).

The activation of the aromatic substrate, anthracene, may occur through a free radical mechanism initiated by homolytic fission. the substituted manganese carbonyl radical complexes with anthracene to form a stable intermediate. The interaction is analogous to the reaction of CH_3 or CCl_3 with aromatics; in that aromatics can greatly stabilize free radicals (S6). Free radical mechanisms have been suggested for aromatic hydrogenation with $Co_2(CO)_8$ under Oxo conditions (F5). The evidence which supports a free radical mechanism is the linear function of the log of the relative reactivity of the aromatic with the localization energy for the formation of the resulting free radical. The $Co_2(CO)_8$ catalyzed hydrogenation rate of an aromatic is a direct consequence of its ability to stabilize aromatics. The hydrogenation of aromatic compound by $Mn_2(CO)_8(Bu_3P)_2$ has the same trend; that is, the ease of hydrogenation is given by anthracene > phenanthrene ~ naphthalene > benzene (Chapter III).

The sharp inhibition of the reaction by hydrogen pressure was only evident in trial rate equations which contained both a trihydride and a hydrogen deficient species in the catalyst mass balance. Dihydride

complexes do not have adequate hydrogen dependence to match the hydrogen inhibition curve. Four hydrogen deficient monomeric manganese intermediates can be postulated $Mn(CO)_5$, $Mn(CO)_4Bu_3P$, $Mn(CO)_4A$, and $Mn(CO)_3(Bu_3P)A$. The high reactivity toward hydrogen substraction by the free radicals $Mn(CO)_5$ and $Mn(CO)_4Bu_3P$ warrants their exclusion from the mass balance leaving $Mn(CO)_4A$ and $Mn(CO)_3(Bu_3P)A$ as the principle hydrogen deficient species.

Whether phosphine or CO dissociates upon anthracene complexation with $Mn(CO)_4Bu_3P$ (step 5 in the mechanism) can be determined from the rate dependence on excess phosphine and CO pressure (Figs. 29 and 12). The near independence of rate on CO pressure rules out the CO dissociation reaction, whereas the high inhibiting effect of excess phosphine suggests the phosphine dissociation step to be operating. The computer fit of the case of CO dissociation gave a poor fit of the data (20% standard deviation). Alternatively the phosphine dissociation step gave essentially the same fit of the data (10.9%) as when no excess phosphine rate data was included (10.7%). This reinforces the hypothesis that ligand dissociation is inhibited at high phosphine concentrations and not the appearance of an inactive di- or triphosphine complex. The good fit of the data shows it is necessary to include only $Mn(CO)_4A$ as the hydrogen deficient species in the mass balance. This anthracene complex is analogous to the naphthalene-manganese tricarbonyl complex discovered by Winkhaus, Pratt and Wilkinson (W5) at atmospheric CO pressure; the higher coordination of

the anthracene complex is due to the greater CO partial pressure (>20 bars).

The final step of the mechanism proceeds via a partially hydrogenated form of the anthracene-manganese complex $HMn(CO)_4AH$. This is a six-coordinate complex similar to naphtalene-manganese tricarbonyl $Mn(CO)_3ArH$ treated with a hydride donor (W5). The high hydrogen and CO pressure account for the higher coordination of the anthracene compound. The monohydride $Mn(CO)_4AH$ is also a plausible intermediate but does not give good fit of the experimental data (22 standard deviation) as does the dihydride $HMn(CO)_4AH$ (10.7). The high reactivity of $HMn(CO)_4AH$ with $H_3Mn(CO)_3Bu_3P$ precludes it from being at significant concentrations to be included in the mass balance or detection by spectroscopy.

7. Infrared Spectroscopy

Infrared spectroscopy was used to verify the existence of a higher hydride form of manganese carbonyl postulated in the reaction scheme. The first phase of the spectroscopy work entailed assigning carbonyl stretching frequencies to manganese carbonyls known to be present. Once these frequencies are known they can be subtracted from more complicated spectra of mixtures and the remaining peaks can then be assigned to the intermediate species.

$Mn_2(CO)_{10}$ dissolved in normal decane gave three absorbtion peaks in the range, of CO stretch from 1700 to 2200 cm^{-1}, Fig. 23. The values of Table 8 agree with the literature (F3). Slight discrepancies are due to solvent effects.

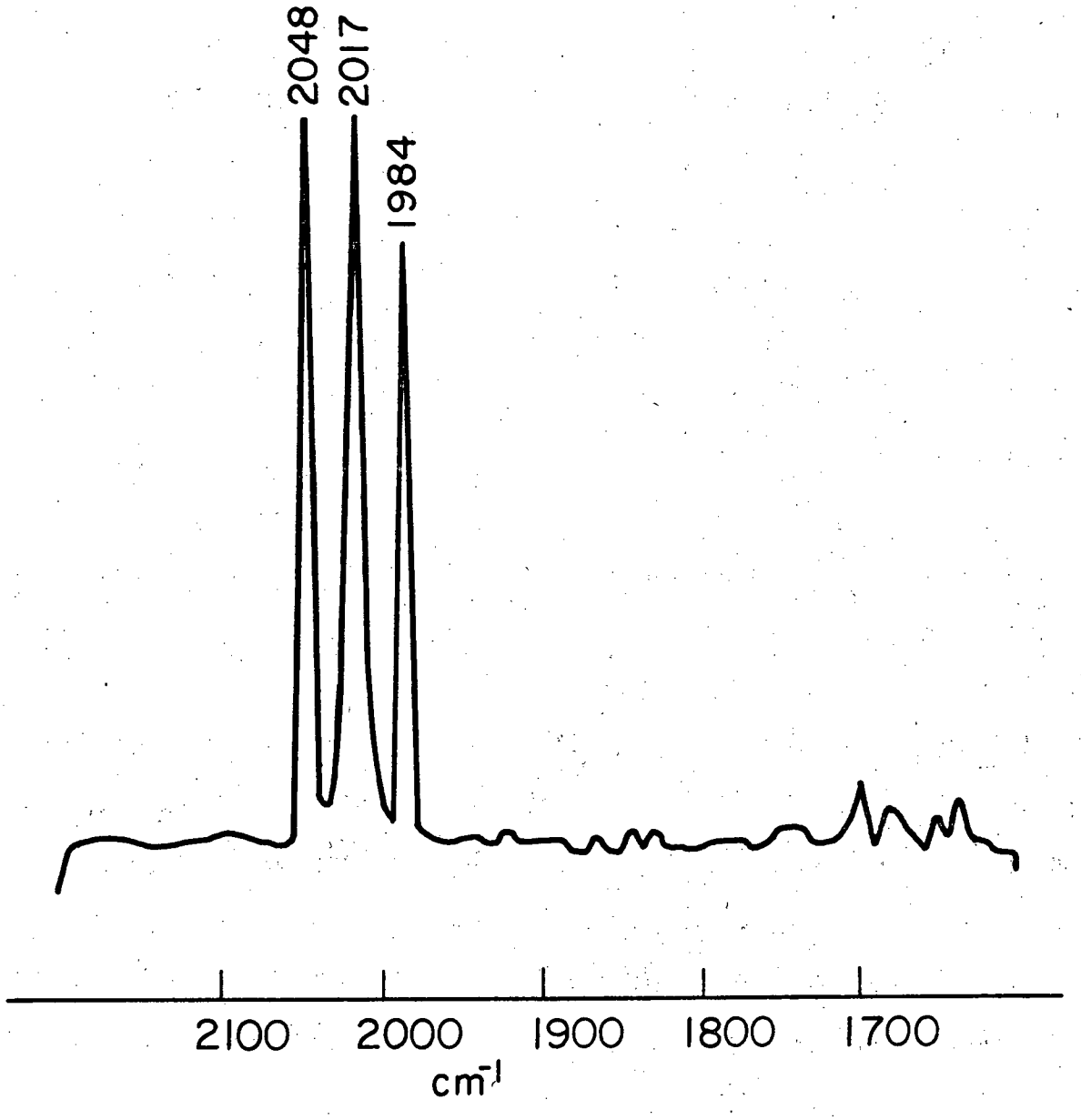

Fig. 23. Infrared spectrum of 1 mM $Mn_2(CO)_{10}$ in n-C_{10} 0.1 mm path length.

Table 8. Infrared spectra of substituted manganese carbonyls.

Compound	Frequencies (cm^{-1})					Author
$Mn_2(CO)_{10}$	1984s 1983m	2017s 2013vs	2048s 2044m			F3
$Mn_2(CO)_2(Bu_3P)$	1933s	1971sh	1993vs	2009s		W4
$Mn_2(CO)_8(Bu_3P)_2$	1904vw	1949vs 2949vs	1964sh	1973m 1974w	2048w	L3 W4
$HMn(CO)_3(Bu_3P)_2$	1896					
$HMn(CO)_4(Bu_3P)$	1947vw 1950 A_1	1960vs 1960 B_2	1979m 1979 B_1	2057w 2057 A_1		experimental calculated assigned CK bond

Abbreviations: s, strong; w, weak; v, very; m, medium; sh, shoulder.

An equimolar solution (based on metal atom) of $Mn_2(CO)_{10}$ and Bu_3P heated to 200°C under 41 bars CO pressure gives the spectrum in Fig. 24 which is probably a mixture of $Mn_2(CO)_{10}$, $Mn_2(CO)_9Bu_3P$, $Mn_2(CO)_8Bu_3P$ and $HMn(CO)_4Bu_3P$ (L3,W4). The large number of peaks is reduced to a simplified spectrum if hydrogen is present during the reaction and a small excess (<30%) Bu_3P is added. The new spectrum Fig. 25a was postulated to be that of $HMn(CO)_4Bu_3P$ but no reference spectrum could be found in the literature to confirm this. A theoretical recourse for establishing the structure of a substituted metal hexacarbonyl from its ir spectra is provided by Cotton and Kraihanzel (C13).

The method of Cotton and Kraihanzel (CK) uses symmetry arguments to predict the relative intensity and number of infrared and Raman vibrational modes of substituted hexacarbonyls of transition metals. Experimental data are fitted to the equations under guidelines provided by the CK method and supplemented by Orgel (O4). Proper fit of the equations gives good assurance of the structure of the compound and yields force constants for the carbonyl stretching frequencies. The experimental spectrum listed in Table 8 has four absorbtion frequencies for $HMn(CO)_4Bu_3P$ indicating a cis structure to be correct. Three of the frequencies (2057 as A, 1979 as B_1, 1969 as B_2) were used to solve the secular equations. The fourth frequency was then calculated to see if a good fit was obtained. The calculated value of 1947 is a close enough match to the experimental value of

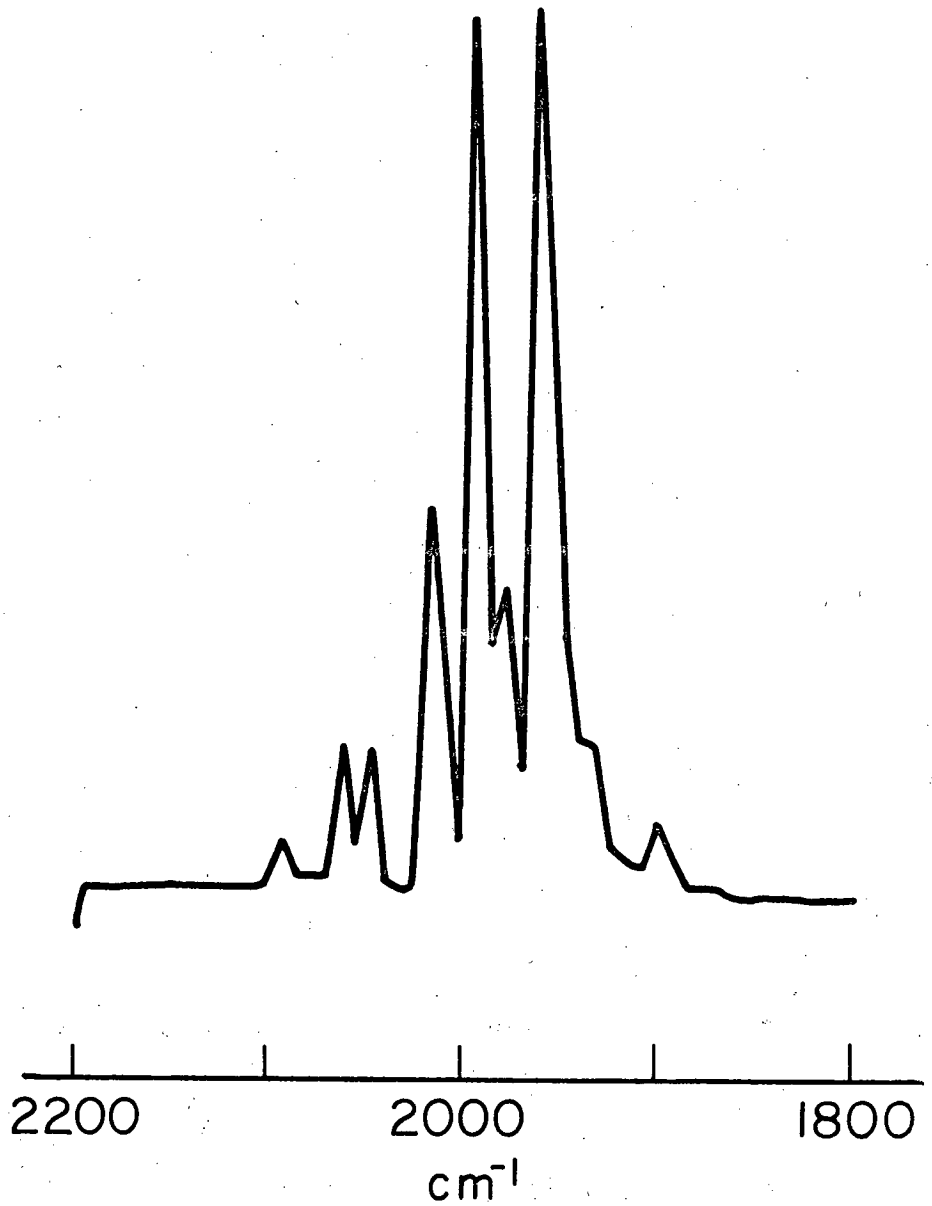

XBL794-3355

Fig. 24. Infrared spectrum of 1 mM $Mn_2(CO)_{10}$ and Bu_3P in n-C_{10}, 0.1 mm path length.

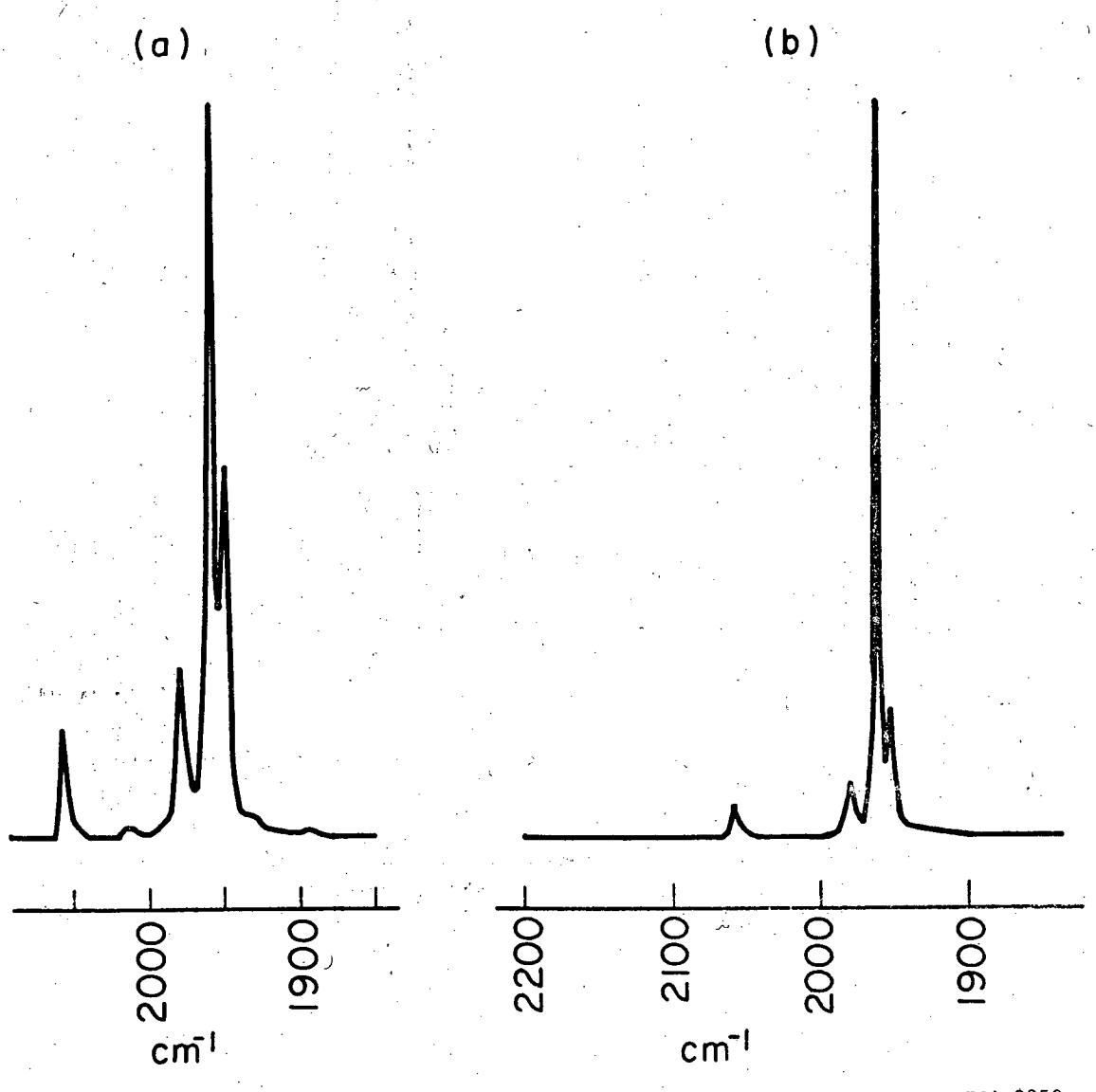

Fig. 25. Infrared spectra of $HMn(CO)_4Bu_3P$ in $n\text{-}C_{10}$ (a) under low hydrogen pressure (b) under high hydrogen pressure. Path length of 0.1 mm.

1950 to give assurance that the spectrum is indeed caused by cis-$HMn(CO)_4Bu_3P$. The force constants calculated are in CK terminology. These are comparable

K_1 = 15.79 millidynes/A

K_2 = 16.35

K_i = 0.27

to values calculated for other substituted hexacarbonyls of Mo, Cr, and Mn (C13,F3,C14).

The effect of hydrogen pressure on substituted manganese carbonyl was investigated. $Mn_2(CO)_{10}$ is completely substituted to $Mn_2(CO)_8(Bu_3P)_2$ during the heat-up time of the reactor. Monohydride formation of the resulting substituted complex occurs readily in the presence of molecular hydrogen or a hydrogen donating solvent such as ethanol. Indeed from the spectra of $HMn(CO)_4Bu_3P$ no unreacted $Mn_2(CO)_{10}$ or $Mn_2(CO)_8(Bu_3P)_2$ could be detected.

Upon increase of hydrogen pressure, the absorbance of the cis-$HMn(CO)_4Bu_3P$ spectrum increases slightly at three frequencies (1950, 1979, and 2057 cm^{-1}) while at the fourth (1960) it increases inordinately (see Fig. 25b). After relieving the hydrogen pressure to vacuum, the compound reverts to the monohydride form in Fig. 26. The appearance of the increased absorbance at 1960 cm^{-1} indicates that another species is present at increased hydrogen pressures.

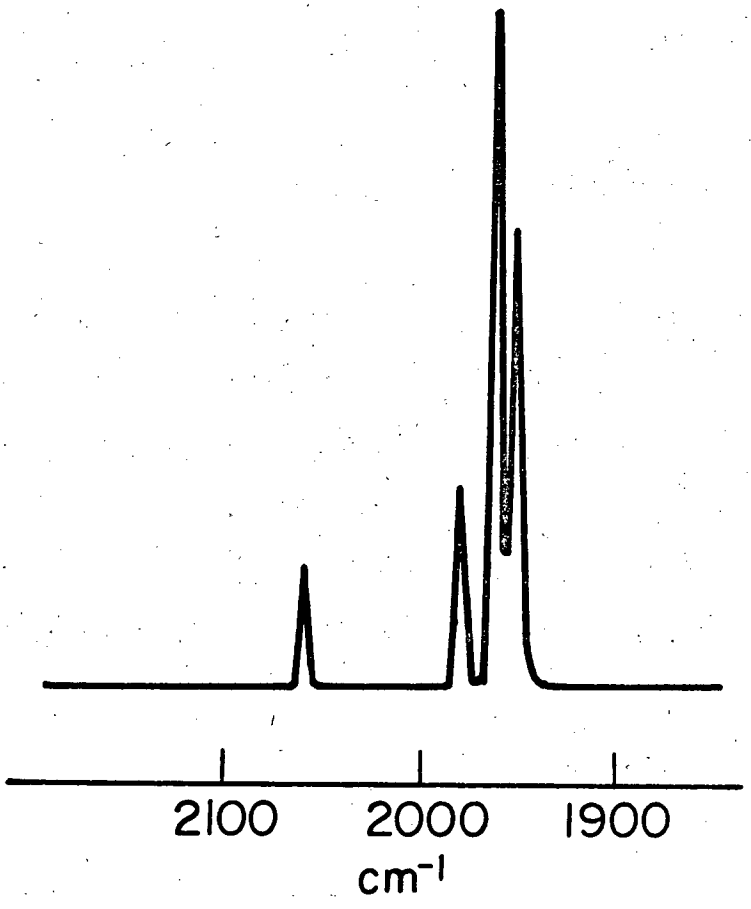

XBL794-3354

Fig. 26. Infrared spectrum of 1 mM $HMn(CO)_4Bu_3P$ in $n\text{-}C_{10}$ after hydrogen depressurization 0.1 mm path length.

Evidence that this is a hydride form can be obtained from H-M stretching frequencies. Figure 27 shows the full useful spectra obtained in n-C_{10}. Cotton, Down, and Wilkinson (C15) have reported the hydrogen stretch frequency for $HMn(CO)_5$ is 1783 cm^{-1} which upon deuteration shifts to 1290 cm^{-1}, the ratio of frequencies being 1.38 as expected. The spectra for $HMn(CO)_4Bu_3P$ shows a peak at 1653 cm^{-1}, upon increasing hydrogen pressure a second peak appears at 1636 cm^{-1}, Good spectra could not be obtained for $H_3Mn(CO)_3Bu_3P$ in these sets of runs because the CaF_2 windows cracked from thermal shock when cool solvent was inadvertently admitted to the cell. The cell did not leak liquid but gas integrity was not assured and the effective hydrogen pressure was not sufficient to stabilize large amounts of the trihydride.

The same experiment was carried out with deuterium instead of hydrogen. The spectrum in the carbonyl stretching range, 1900 to 2200 cm^{-1}, was unchanged but the peaks at 1636 and 1653 were absent. Upon addition of hydrogen to the reactor both peaks appeared. The D-M stretch frequency could not be determined since n-C_{10} absorbs strongly in that range. Nevertheless the appearance of a second hydride peak with increased hydrogen requires only small distortions in the octahedral arrangement to accommodate seven ligands. Four possible geometries of seven coordinate complexes are possible D_{5h}, C_{2V}, C_{3V} and C_5 but only the latter, tetragonal base-trigonal base has been proven rigorously for metal complexes (M10). This structure is most favorable for molecules of the formula

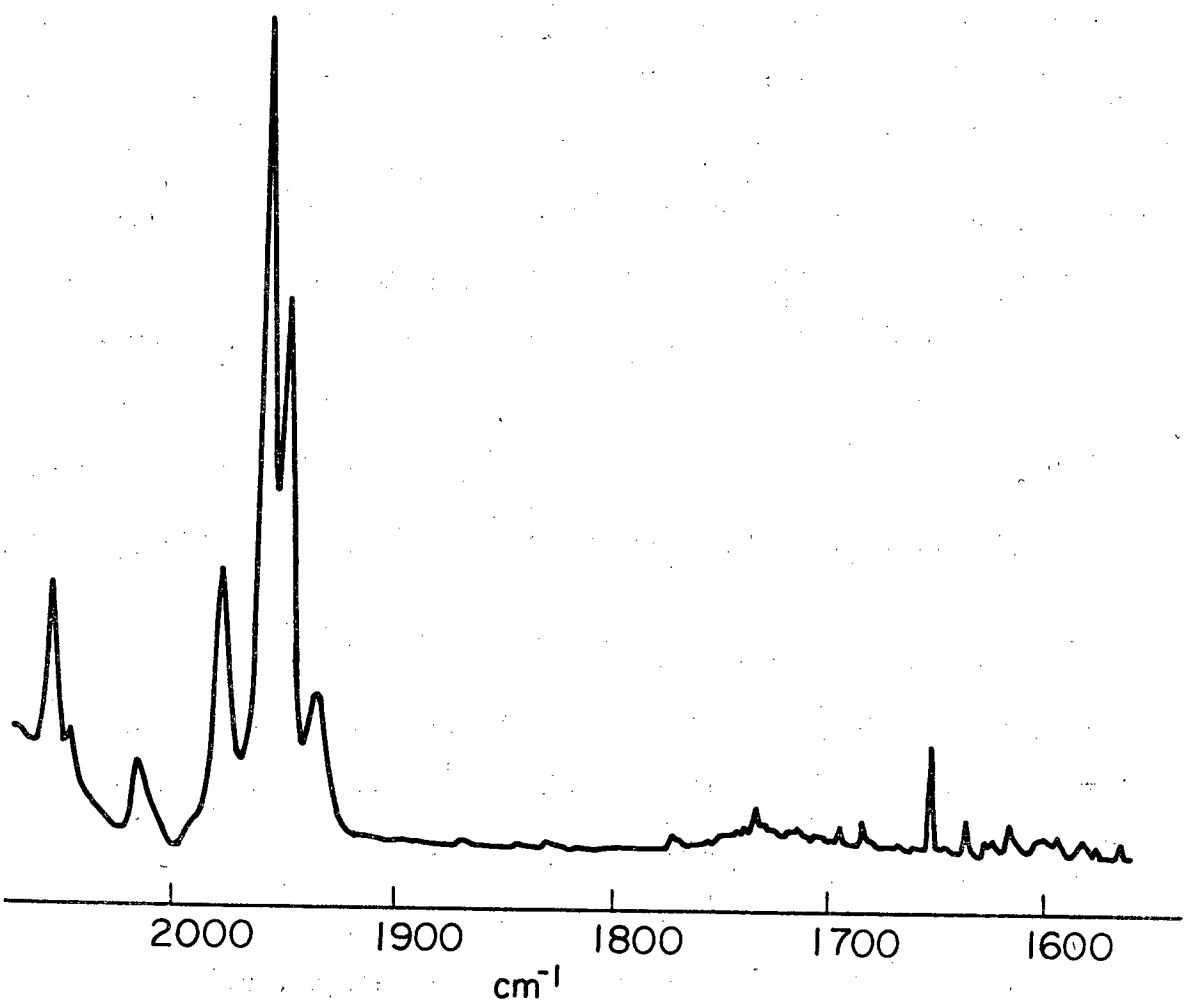

XBL794-3356

Fig. 27. Infrared spectrum of 1 mM $HMn(CO)_4Bu_3P$ in $n\text{-}C_{10}$ showing H-Mn stretch (*) 1 mm path length 200°C.

MX_4Y_3 particularly if X and Y differ greatly in steric or electronic properties. This is especially true in $H_3Mn(CO)_3Bu_3P$, where the hydrogen ligands are much smaller and have different configureations from mutually similar CO and PBu_3. Figure 28 shows that this structure has a certain degree of symmetry that may give only one CO absorbance that coincidentially occurs at the major absorbance of cis-$HMn(CO)_4Bu_3P$.

8. Hydrogen of 9,10-Dimethylanthracene

9,10-dimethylanthracene was hydrogenated under the same conditions as used for the catalyst screening program. The amount of conversion to hydrogenated product was less (21.8%) than with anthracene as the substrate (33%). Both cis and trans 9,10-dihydro-dimethyl-anthracene were present at a ratio of 1.35.

The presence of both isomers of 9,10-dihydro-dimethylanthracene at about equal ratios indicates that hydrogenation is not taking place on just one manganese atom which would give exclusively the cis form. Isomerization of cis to trans has not been found for $Co_2(CO)_8$ hydrogenation of cis, 9,10-dihydrodimethylanthracene under Oxo conditions but the cobalt catalyzed reaction favors the trans product slightly (T7). Cis isomer would be favored for the $H_3Mn(CO)_3L$ acting as an attacking group on metal on a partially hydrogenated cis-$HMn(CO)_4LAH$ where the fully hydrogenated H_2A is the leaving group. The trans isomer is formed if $H_3Mn(CO)_3L$ attacks the M-C bond in the complex.

9. Conclusions

The mechanism for hydrogenation of anthracene by $Mn_2(CO)_8(Bu_3P)_2$ is governed by two competing rate determining steps; the formation of

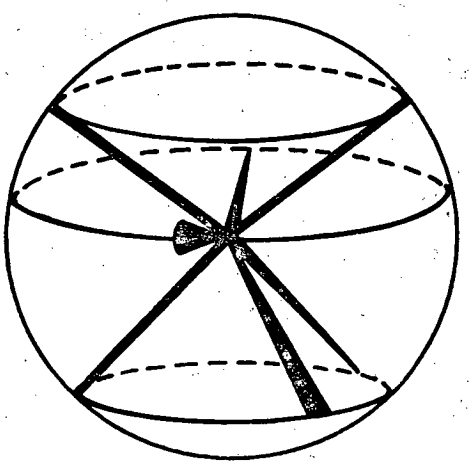

XBL 794-6112

Fig. 28. C_s-3:2:2 model for seven-coordinate complexes as idealized in a "points on a sphere model" (M12).

a manganese–anthracene complex and the reaction of this complex with a trihydride manganese complex. The rate equation derived from this mechanism accounts for all the data and is consistent with observations made about similar reactions involving dicobalt octacarbonyl. The trihydride intermediate, detected by infrared spectroscopy, is also indicated by the hydrogenation of dimethylanthracene giving both cis and trans isomers; steric effects caused by the methyl groups on anthracene do not hinder the reaction greatly further indicating that two manganese complexes are involved.

V. EFFECTS OF THE SUBSTITUTING LIGAND ON REACTION RATES

A. Effect of the Degree of Substitution on Activity

The degree of substitution, that is the number of sites on a metal carbonyl that are replaced by substituting ligands affects the catalytic activity. This is demonstrated in Fig. 29. For the standard conditions given a metal to phosphine ratio of 1.0 is the most effective for hydrogenating anthracene. At ratios of less than one, catalyst decomposition has a deleterious effect on rate. At ratios greater than one the higher degree of substitution retards the rate presumably because higher substituted compounds are less active than the monosubstituted ones. This may be due to reduced ability to form hydrogen or olefin complexes. Such tendencies have been noted for hydroformylation by substituted $Co_2(CO)_8$ (T3) in that selectivity to normal from branched products reaches a maximum at ligand to metal ratio of 1.

B. The Effect of the Substituting Ligand on Rate

Table 9 lists the ligands that were used as substituting agents on dimanganese decacarbonyl and the resulting effects on the reaction rate. The highest rates were achieved with PPh_2Et and diphos while PPh_3 and PPh_2Cl gave poor results. Steric effects seem to be unimportant since PCy_3 the ligand with the largest cone angle (T2) and diphos a polydentate ligand both had good activity.

1. Reaction Rate Dependence on Ligand Acidity

The effect of ligand acidity in altering the hydroformylation reaction has clearly been shown (T4). When hydroformylating with

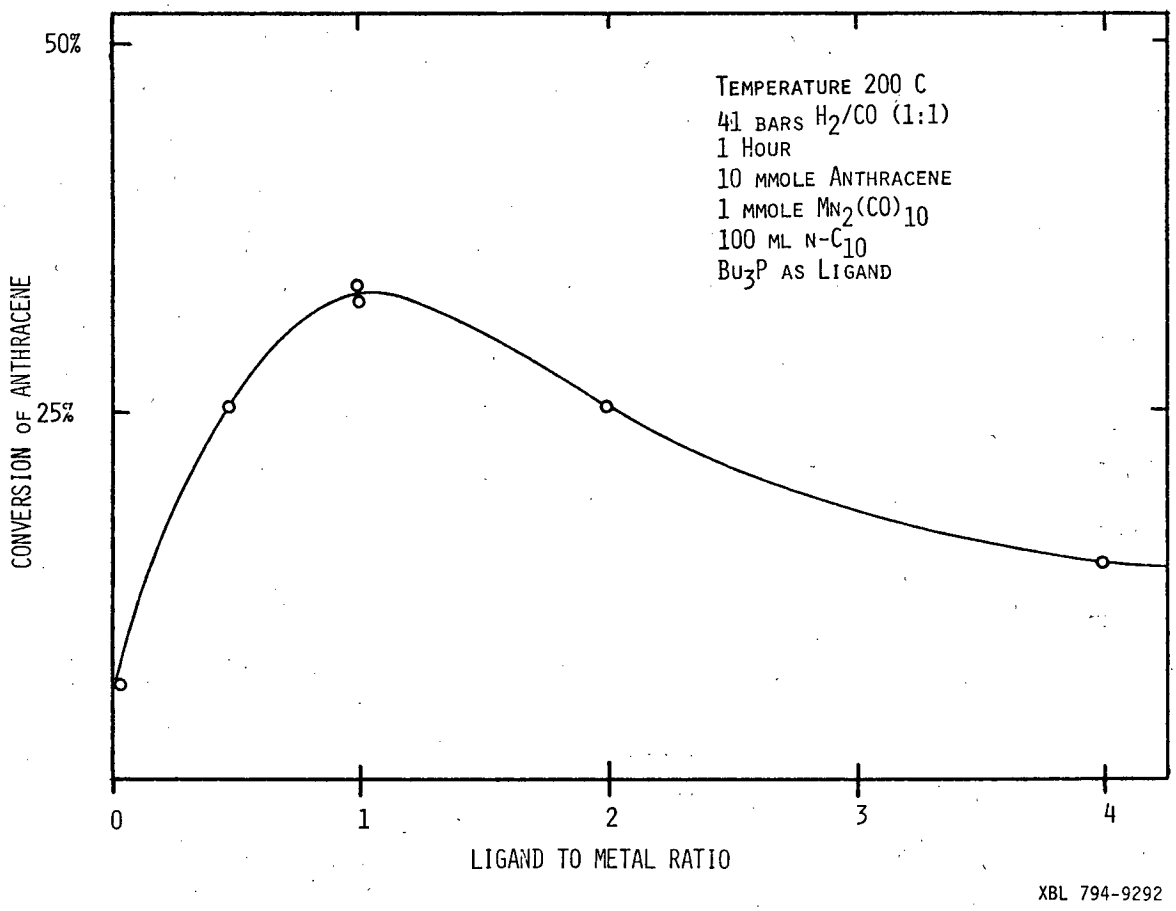

Fig. 29. Effect of the degree of substitution on catalytic activity.

Table 9. Effect of varying ligand on rate of anthracene hydrogenation with $Mn_2(CO)_8L_2$.

Ligand	k ($mM\ hr^{-1}$)	cone angle (degrees)
PBu_3	0.39	130
PEt_3	0.27	132
$PPhEt_2$	0.38	136
PPh_2Et	0.48	140
PPh_3	0.08	145
PPh_2Cl	0.02	138
PCy_3	0.14	179
$P(n\text{-}C_8)_3$	0.32	130
PPr^i_3	0.13	160
diphos	0.47	121
$P(OMe)_3$	0.21	107
$P(OEt)_3$	0.25	109
$P(OEt)_3$	0.25	~110
$P(OPh)_3$	0.13	121
$P(Oo\text{-}tol)_3$	0.15	128
$P(OP^i_r)_3$	0.23	130

phosphine substituted $Co_2(CO)_8$, an increase in ligand acidity is accompanied by a increase in the reaction rate constant. This linear relationship was interpreted as a function of σ-donor effects of the ligand which effected the equilibrium

$$HCo(CO)_3L \rightleftharpoons HCo(CO)_3 + L$$

The acidic ligands, L, increase the dissociation to form more $HCo(CO)_3$ which is a faster reacting species than $HCo(CO)_3L$. Concurrent to hydroformylation, unwanted olefin hydrogenation occurs. Studies of the effect of the ligand on the unwanted reaction revealed that the rate of hydrogenation is insensitive to the ligand. This indicates that hydrogenation occurs by a different mechanism than hydroformylation, that is, the rate determining step probably does not contain a ligand dissociation of the type given in the previous equation. This applies to $Mn_2(CO)_8(Bu_3P)_2$ catalyzed anthracene hydrogenation since no correlation between rate and ligand acidity (H4) was found.

2. Linear Free-Energy Correlations

Kabachnik (K3,K4) has measured the ionization constants (pK and pK_2) of organic phosphorous acids of the general formula

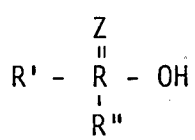

where R', R" can be alkyl, aryl, alkO or H. Z is sulfur or oxygen. The Hammett formula was found to be applicable to ionization constants of phosphorous acids. By assigning numeric values (σ) to each R, the equation $pK = pK_o - \rho\Sigma\sigma$ gives a straight line. The σ values tabulated by Kabachnik are a measure of the electronic effect of the organic group (R',R") on the dissociation of H^+. This is in effect a measure of the acidity of each individual R' or R" attached to a phosphorous. Since the Hammett relation holds, the sum of the s's ($\Sigma\sigma$) is an indication of the total acidity of the tertiary substituted phosphorous.

Figure 30 is a linear free-energy plot of the rate of hydrogenation of anthracene with respect to Kabachnik's parameter. Two parallel lines may be drawn through the data representing the families of phosphines and phosphites. If the linear free energy relationship were valid the lines would be coincidental and the scatter would be much less than what is observed. The poor fit of the data shows that the hydrogenation activity of substituted dimanganese decacarbonyl is influenced by more than simple inductive electronic effects transmitted through σ-bonds.

C. ^{31}P NMR Correlations of Ligand Effects

The failure of the linear free energy relations and the Hammett-type parameters in correlating the effect of ligand on rate shows that the mechanism of hydrogenation is influenced by more than inductive electronic effects along intermolecular axes. It may be

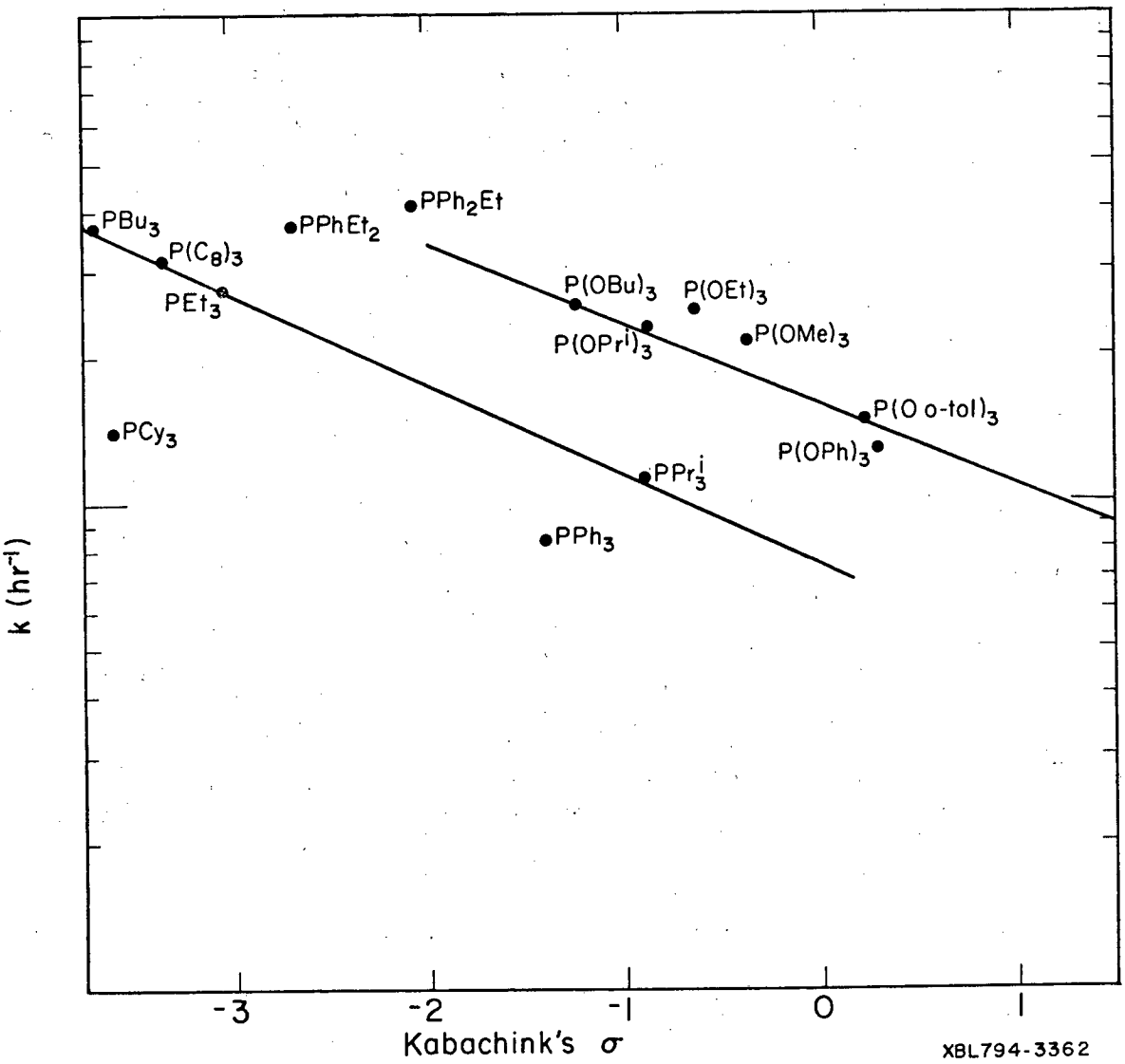

Fig. 30. Linear free-energy relationship of $Mn_2(CO)_8(Bu_3P)_2$ catalyzed hydrogenation of anthracene.

surmized that when both σ- and π-bonding are present, as in the case of substituted metal complexes, a simple electronic effect along only the σ-bond will not adequately describe the system.

The synergistic effects of π-back-donation on bond strength was, in the past, an area of controversy. ^{31}P NMR provided much of the evidence to prove that π-bonding in metal complexes exists and further indicated that proposed linear correlations will show curvature unless π-bonding is taken into account (C11).

The literature revealed that several investigators have had limited success in correlating NMR shift with metal-ligand complexation data (G1,G2,M6,M7,M8). The best correlations have been made relating the chemical shift of the free ligand with the charge due to complexation (M7). Grim (G1) obtained a linear fit for data on chemical shift of $(PPh_2R)M(CO)_5$ by varying R as alkyl groups. He obtained three parallel lines for Mo, V, and W although the trend does not hold for a wide variety of ligands such as PR_3.

Correlations attempted between a free ligand and a complexed one cannot be expected to be as simple as a Taft or Hammett relation due to the structure differences between the complexed and uncomplexed P atom. A crucial difference becomes evident when the nature of the uncomplexed phosphine is reviewed. The free phosphine possesses a lone-pair of electrons which are donated to the metal to form the complex and become localized in the P-M bond. The free ligand, on the other hand, allows the lone-pair to adapt to molecular geometry ranging from pure p^3, uncomplexed, to sp_3 hybrid where the

unshared pair of electrons acts as a dative bond. The free ligand easily rehybridizes to release sterically induced stresses and thereby alters the magnetic environment of the phosphorus nucleus. Small deviations in bond angles (1-2^{o}) causes by steric repulsion give rise to significant changes in chemical shift (C11). Complexed ligands are less prone to this effect.

On the basis that free ligands are too susceptible to sterically induced chemical shifts compared to the complexed analogs, little correlations between phosphine chemical shifts and complexation behavior should be expected. In fact no correlation was found between free ligand chemical shift and rate of anthracene hydrogenation. Complex behavior would correlate better with the chemical shift of the ligands where the lone-pair is localized as, in another complex or a chemical bond. This accounts for the good fit of Grim's data (G1) where group contribution effects were noted in complexed ligands.

1. Correlation of Phosphorus Ligand Substituted $Mn_2(CO)_{10}$ Activity with Chemical Shift

The study of one complex to predict the chemistry of another can certainly be useful but a more convenient method was sought. If localization of the phosphorous lone-pair is the key criterion then localization by bond formation should yield good correlations. The class of compounds found which had the lone pair firmly bound and had sufficient NMR data available where the phosphine oxides, OPR_3, see Table 10. Figure 32 shows that reaction rate constant of anthracene hydrogenation is dependent on the chemical shift of the ligand oxide.

Table 10. ^{31}P NMR chemical shifts of phosphine and phosphite oxides.

No.	Compound PR_3	δ of the Oxide (ppm)	Refs.
1	PMe_3	48	M9
2	PEt_3	48	C11
3	$Pi\text{-}Pr_3$	55	F10
4	PBu_3	43	E1
5	$Pt\text{-}Bu_3$	41	C11
6	$P(cyclo\text{-}C_5)_3$	68	F10
7	PCy_3	50	C11
8	PPh_3	27	F10
9	$P(n\text{-}C_8)_3$	47	F10
10	$PPhMe_2$	33	A11
11	PPh_2Me	29	A11
12	$PPhEt_2$	42	C11
13	PPh_2Et	33	A11
14	$PHCy_2$	46	C11
15	PH_2Cy	22	C11
16	$PHBu_2$	29	C11
17	$PH(n\text{-}C_8)_2$	28	C11
18	$PH_2(n\text{-}C_8)_2$	10	C11
19	$PHPh_2$	26	F9
20	$P(CH_2CH_2CN)_3$	37	C11
21	$PPh_2(t\text{-}Bu)$	39	A11
22	PI_3	-273	K6
23	PBr_3	-103	C11
24	PCl_3	2	C11
25	PF_3	-36	E1,C11
26	PPh_2Cl	43	C11
27	$PPhCl_2$	35	C11
28	$P(m\text{-}C_6H_4F)_3$	21	D3
29	$P(p\text{-}C_6H_4Cl)_3$	22	D3
30	$P(OMe)_3$	2	M9,E1
31	$P(OEt)_3$	-1	E1
32	$P(Oi\text{-}Pr)_3$	-6	F10
33	$P(OBu)_3$	1	F10
34	$P(Ot\text{-}Bu)_3$	-14	E1
35	$P(On\text{-}C_5)_3$	-4	F10
36	$P(OPh)_3$	-18	F10,E1
37	P(Op-tol)	-16	C11
38	$PPh(OMe)_2$	19	M9
39	$PPh_2(OMe)$	33	M9
40	$P(OC)_3CCH_3$	8	V1
41	$PPh_2(iPr)$	36	A11
42	$PPh(Bu)_2$	45	F10

Table 10. Continued.

No.	Compound PR_3	δ of the Oxide (ppm)	Refs.
43	$P(NMe_2)_3$	23	F10,E1
44	$PPh_2(OEt)$	31	M9
45	$P(p\text{-}C_6H_4F)_3$	22	D3
46	diphos	36	M9
47	P(Oo-tol)	-17	C11
48	$P(OCH_2CCl_3)_3$	-9	C11
49	$PPh(OEt)_2$	17	C11
50	$PPh(OPh)_2$	12	C11
51	$P(p\text{-tol})_3$	33	*

Key to abbreviations: Ph, phenyl; Cy, cyclohexyl; tol, tolyl; diphos, bis 1,2-diphenylphosphino ethane.

*Estimated from carbonyl stretch frequency of $Ni(CO)_3(P\text{-tol})_3$ using Fig. 35.

The ^{31}P chemical shifts reflect several interdependent chemical phenomena called asymmetric loading (C11); a summation of (1) the total occupation of the d orbitals of P (2) the unbalance of the σ-bonds as determined by the difference in electronegativities of the various substituents on P as well as the "bond" nature of the unshared pair, and (3) the deviations from geometric symmetry. Since deviations from geometric symmetry are minimized in the tetrahedral structure of OPR_3, the two relevant electronic effents are the ligand acidity due to electronegativity and the σ to π-bonding ratios. Ligand acidity and π-bonding increase from the phosphines to the phosphites.

The maximum in the curve can thus be attributed to a mechanism of anthracene hydrogenation that has two rate determining steps one favored by high ligand acidity and the other by low acidity; a compromise is met at the maximum. Another possibility may be the formation of an intermediate complex that is most favored with ligands of intermediate σ and π-bonded ligands.

2. Relationship Between Ligand Acidity and Chemical Shift

Checks of the validity of using the chemical shifts of ligand oxides as an indicator of electronic effects is required to ascertain if the plot of Fig. 31 is justified.

The pKa of alkyl and aryl phosphines R_3P, reported by Henderson and Streuli (H4) can be correlated with δ of OPR_3 as shown in Fig. 32. The δ correlation greatly improves the fit of the data compared to the Taft σ* parameter originally proposed. Deviations

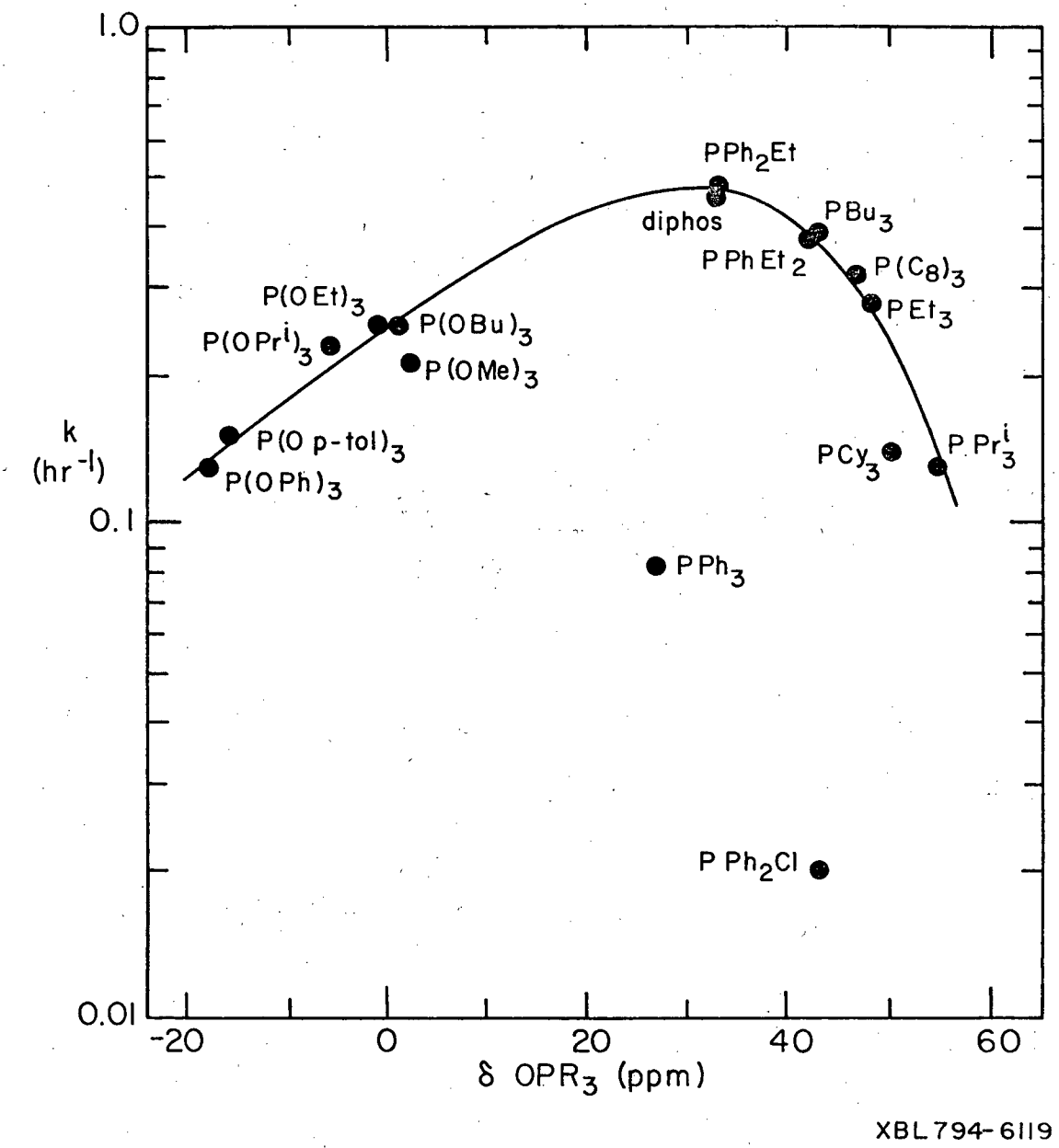

Fig. 31. Rate of anthracene hydrogenation by $Mn_2(CO)_8(Bu_3P)$ in decane at 200°C with 41.3 bars H_2/CO (1:1).

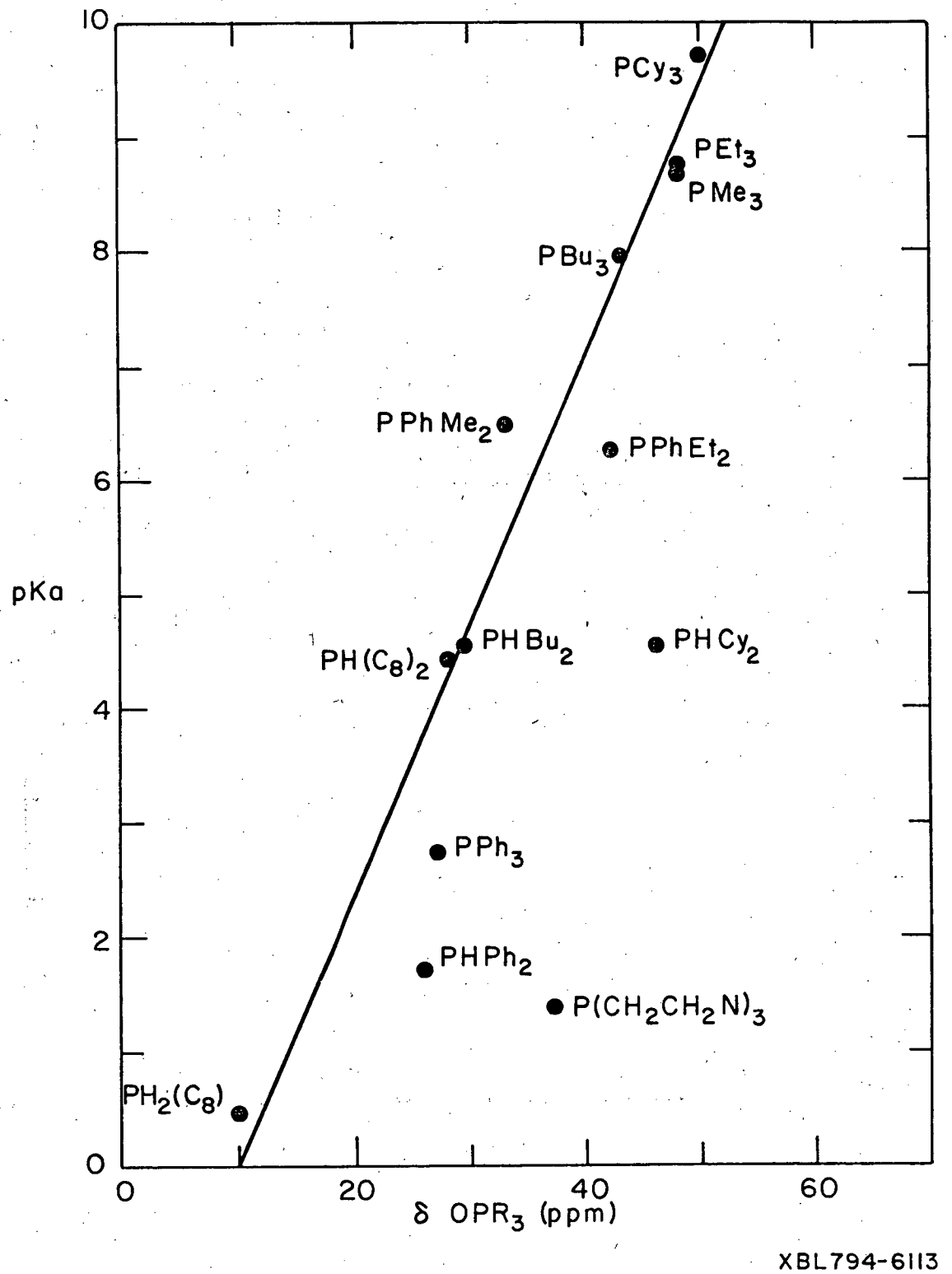

Fig. 32. Relationship between phosphine basicity and the ^{31}P NMR chemical shift of the corresponding oxide.

from the correlation are in the same direction as observed by Henderson and Streuli, in that phenyl phosphines seem to fall below the line. They conclude that this is probably due to the steric effect of solvation of the product phosphonium ion (H4).

The effect of structure on the reactivity of phosphines was described by Henderson and Buckler (H11). The nucleophilicity of phosphines by S_N2 attack of alkyl halides in the reaction,

$$R_1R_2R_3P + C_2H_5I \rightleftharpoons R_1R_2R_3C_2H_5P^+ + I^- \qquad (1)$$

gave a linear free-energy relationship with the Taft σ^* parameter that was adequate for the tertiary phosphines. Inclusion of primary and secondary phosphines gave appreciable scatter since their basicities were not well described by σ^* probably because σ^* was derived for carbon not for phosphorous. Figure 33 demonstrates a linear free-energy relationship between the nucleophilicity of the phosphine and the chemical shift of the corresponding oxide. The fit of Henderson and Buckler's data is greatly improved. Chemical shift data was not available for all the compounds, nontheless, all the types of phosphines are represented. The fit of the data reinforces the premise that once deviations from geometric symmetry are minimized inductive effects can be predicted by chemical shift. The major advantage of using chemical shift over σ is the availability and ease of compiling chemical shift data.

The previous correlations are valid not only for phosphines but may be extended to phosphites since they have also been correlated

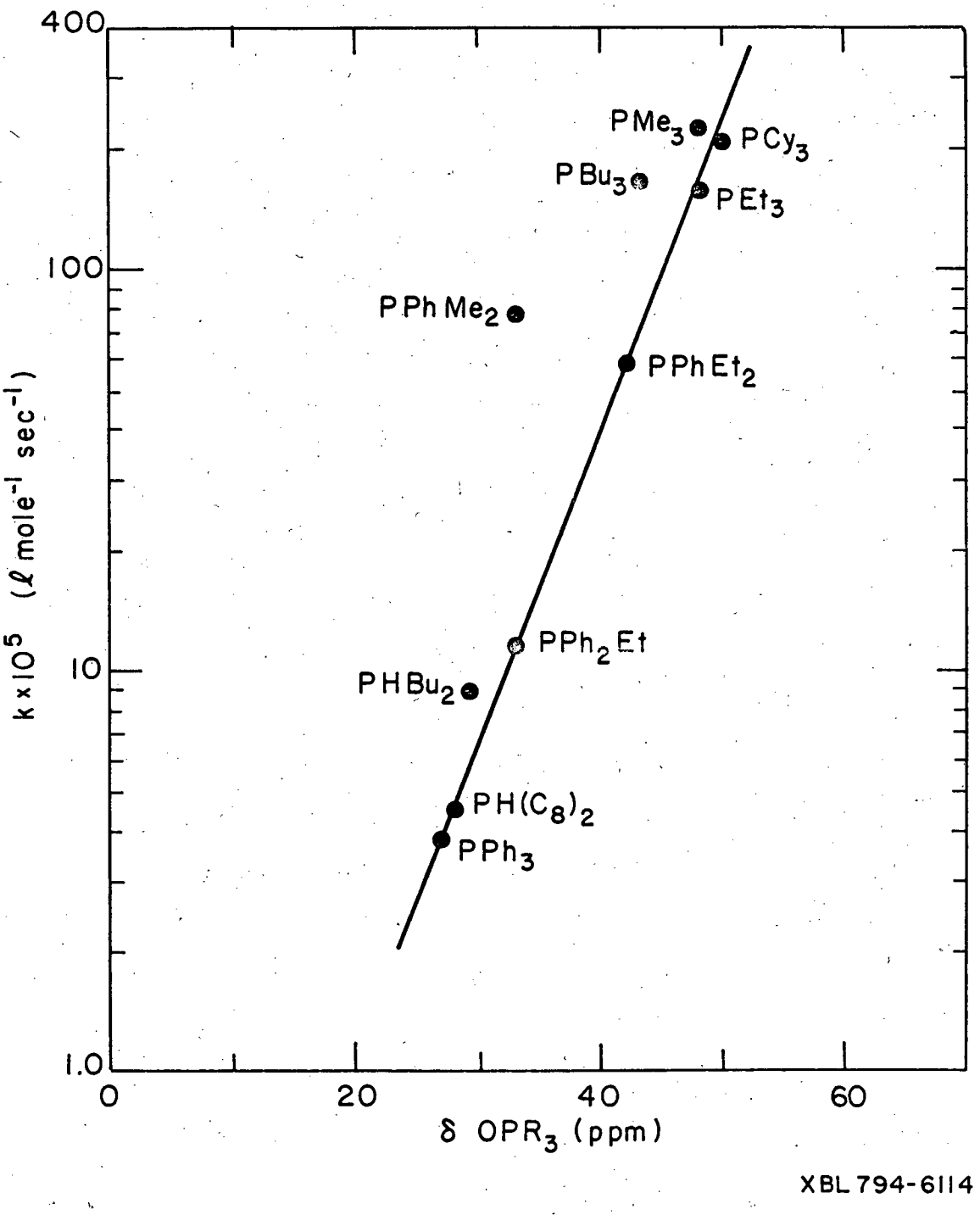

Fig. 33. Linear free-energy relationship for secondary and tertiary phosphines with ethyliodide in acetone at 35°C.

with σ parameters (K3,K4). A study by Streuli (S10) that gives a measure of relative proton basicities of both phosphines and phosphites was performed by determining their half neutralization potentials ΔHNP relative to N, N'-diphenyl quanidine as a standard for titrations with perchloric acid in nitromethane. Figure 34 is a plot of the half neutralization potential vs OPR_3 chemical shift. The nonlinearity of ΔHNP reflects the polarizability of the compound (B6, p. 573) in addition to its nucleophelicity.

3. Correlation of Carbonyl Stretch Frequency of Metal Complexes with Chemical Shift

The infrared spectra of metal carbonyl complexes correlated with ligand basicity and Hammett parameters have been cited as evidence for inductive effects and π-bonding (T2,E1,A10). The correlations are linear for aryl and alkyl phosphines and phosphites but fail to encompass the halogen substituted compounds, notably PF_3 and PCl_3 (T2,E1). The deviation of the halogen phosphines has been attributed to π-bonding between the metal and phosphorous induced by the highly electronegative halogens.

The concept of the σ phosphorous-metal bond predominating in alkyl and aryl phosphine metal complexes is reinforced when ^{31}P NMR data is viewed in conjunction with infrared measurements of metal carbonyl complexes containing phosphine ligands. Tolman reported the measurement of the A_1 carbonyl stretching frequency for $Ni(CO)_3L$ (T2). Data for 70 monodentate phoephorous ligands could be correlated by assigning each substituent a contribution effect X_i such that for any $Ni(CO)_3PR_1R_2R_3$, the stretch frequency ν_{CO} in cm^{-1} is:

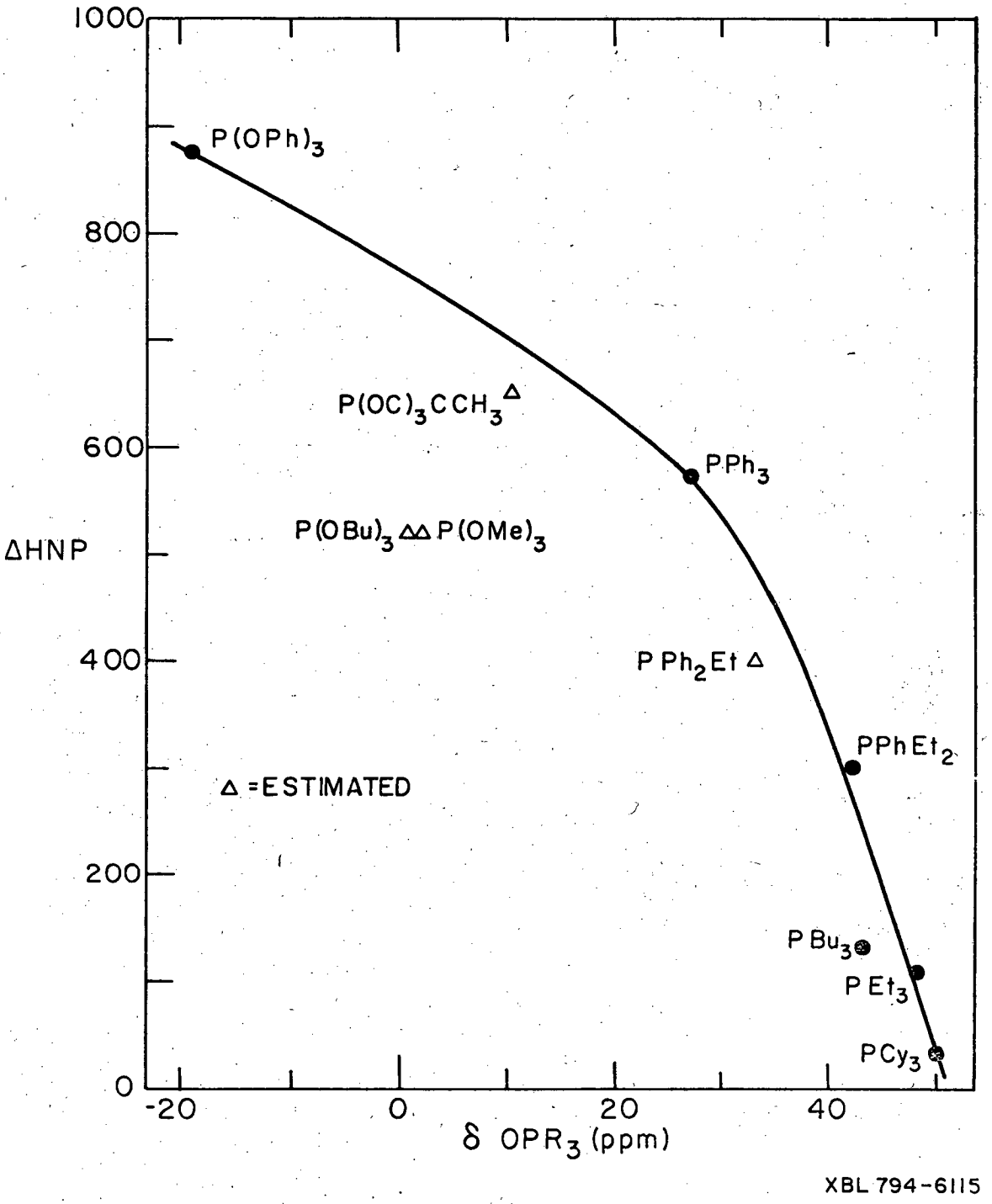

Fig. 34. Half neutralization potential of phosphine compounds.

$$\nu_{CO} = 2056.1 + \sum_{i=1}^{3} X_i$$

The substituent contribution parameter X_i is useful in showing that inductive effects determine ν_{CO}. Comparison of X_i with Kabachnik's σ gives a nonlinear relation showing that electronic effects are indeed transmitted through the P-M-C σ-bond but the nonlinearity suggests that other factors, perhaps reduced σ-donation or enhanced π-acceptor behavior are present in the complexes.

Tolman had no success in correlating the infrared data with the ^{31}P NMR chemical shift of the ligand (T2). This may again be attributed to the ease of rehybridizations of the phosphines. In Fig. 35, Tolman's data are correlated with the ^{31}P NMR chemical shift of the oxide of the substituting ligand. For aryl and alkyl phosphines and phosphites slight deviations from the line are noted for the bulkier ligands having a cone angle above 145^{o} (T8). For the alkyl and aryl phosphines and phosphites the carbonyl stretch frequency can be predicted by

$$\nu_{CO} = 2078.25 - 0.35(\delta_{OPR_3})$$

The major deviations from the correlation with ν_{CO} depicted in Fig. 35 are due to phosphines having halogen substituents. These are divided into two classes, easily polarizable Br and I having

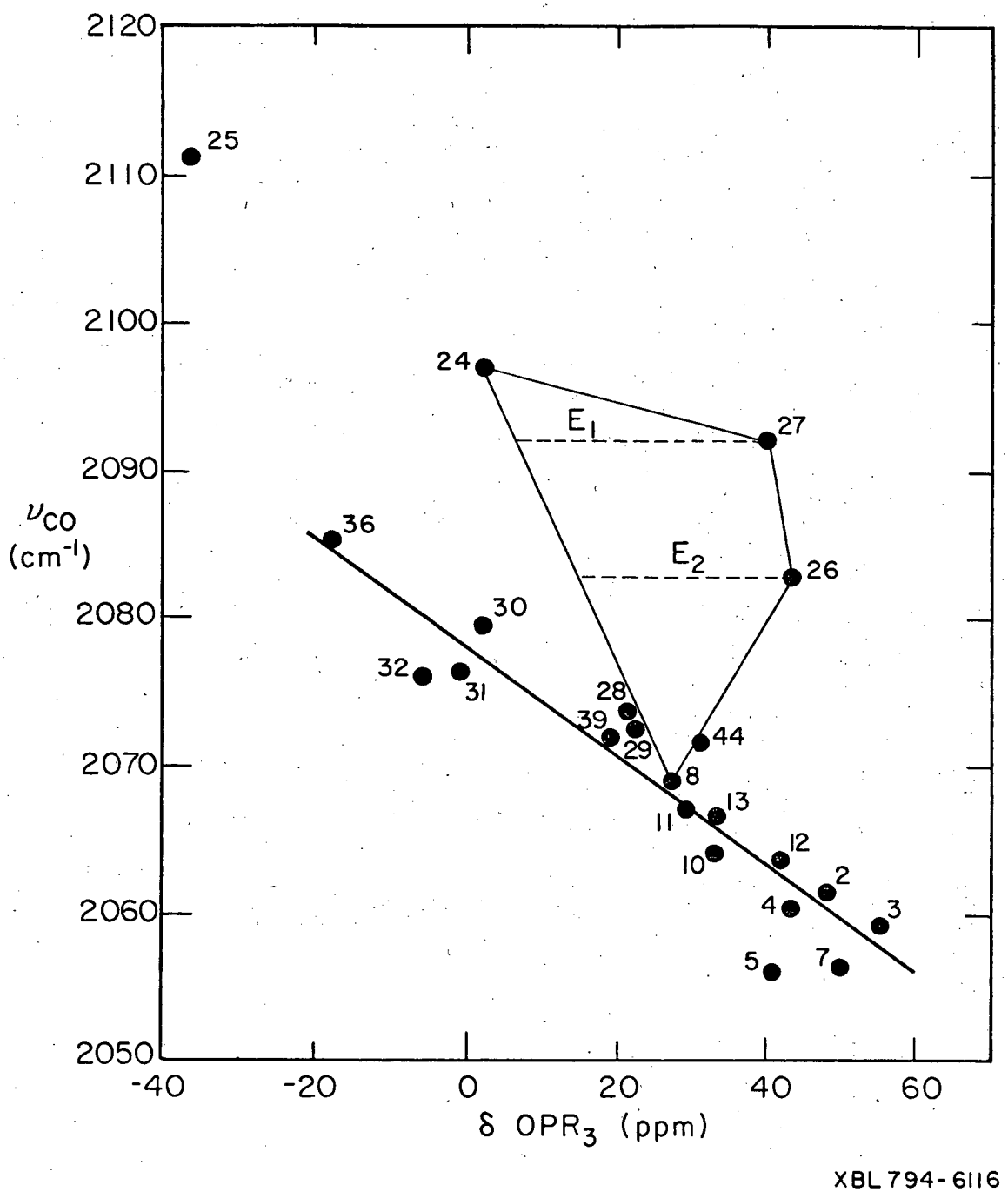

Fig. 35. Carbonyl stretch frequency of $Ni(CO)_3PR_3$ correlated with ^{31}P NMR chemical shift of OPR_3.

d-orbitals or non-polarizable Cl and F. The fluorine and chlorine compound are electro-negative enough compared to phosphorous to shrink, the phosphorus 3d orbit to form a π-bond with nickel. The decrease in electron density in the metal d-orbitals by back donation to phosphorus leaves less of the electron density to be donated into the M-C π-bond of the carbon trans to the phosphorus. Less metal-to-carbon back donation gives a weaker M-C bond and a stronger C-O bond with a correspondingly higher C-O stretch frequency (C7, p. 685). The large increase in ν_{CO} is more than is expected from inductive effects operating via a σ-bond systems.

Empirical findings show additivity rules govern the chemical shift of similar substituents. For instance $OPEt_3$ (2) $OPPhEt_2$ (12) $OPPh_2Et$ (13), and $OPPh_3$ (8) in Fig. 35 fall on the same line. It is recognized that large deviations in chemical shift can be observed for mixed phosphoryl compounds OPRR'R" in which the R's have greatly differing electronegativities (C11).

Correlations of carbonyl stretch frequency with chemical shift of OPR_3 for octahedral complexes can be successful provided, of course that steric effects are not significant. As an example, the E_1 mode of ν_{CO} for $W(CO)_5(PR)_3$ is correlated by σ_{OPR_3} in Fig. 36. Some scatter of data is evident since ν_{CO} was recorded in several solvents (A9,F7,G5,A10,M6,S11-13). A line has been drawn through the data corresponding to the compounds that are not expected to π-bond, that is, the phosphines and alkylphosphites. The compounds that π-bond show deviation to the right of the curve increasing with stronger π-bonding.

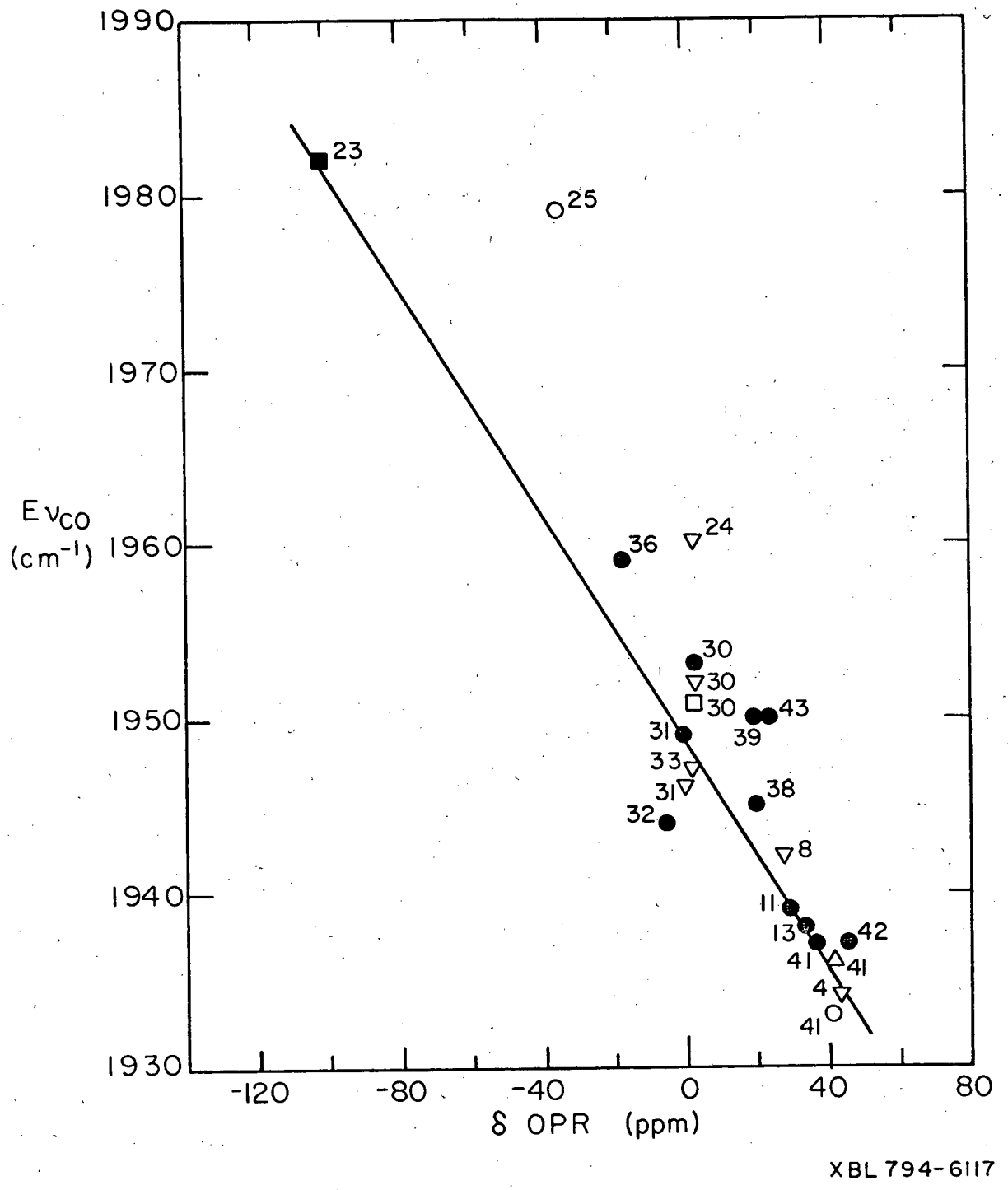

Fig. 36. E_1 mode carbonyl stretch frequency of $W(CO)_5PR_3$ correlated with chemical shift of OPR_3.

4. Correlation of Catalytic Activity with Chemical Shift

The correlation of the rates of $Mn_2(CO)_8(Bu_3P)_2$ catalyzed anthracene hydrogenation by δ of OPR_3 suggests that other reactions may be amenable to such treatment.

An important step in homogeneous hydrogenation by metal complexes is oxidative addition of hydrogen to square planar complexes to form a cis-dihydrogen octahedral complex. This is exemplified by:

$$\text{trans} - Ir^{I}X(CO)L_2 + H_2 \rightarrow Ir^{III}H_2X(CO)L_2 \qquad (2)$$

(X = halogen, L = tertiary phosphine or phosphite). The rate depends on the ligands X and L. Figure 37 shows the rate data of Strohmeier and Onoda (S14) as a function of the chemical shift of the ligand oxide. The three curves one for each halogen go through maximum as was observed for anthracene hydrogenation.

The reverse of oxidative addition of hydrogen, reductive elimination is also influenced by ligand sbustitution. Mays, Simpson, and Stefanini (M14) studied the reverse of reaction 2 by displacing the hydrogen ligand by trimethylphosphite. The rate data in Fig. 38 can be correlated by Kabachniks σ but a better fit is obtained if the chemical shift of the ligand oxide is used. Whether the correlation remains linear when extended to phosphites cannot be determined without more data.

The ligand dependence of oxidative addition and reductive elimination are clearly a function of the ligand bacisity. Correlation with the chemical shift provides a method of determining the

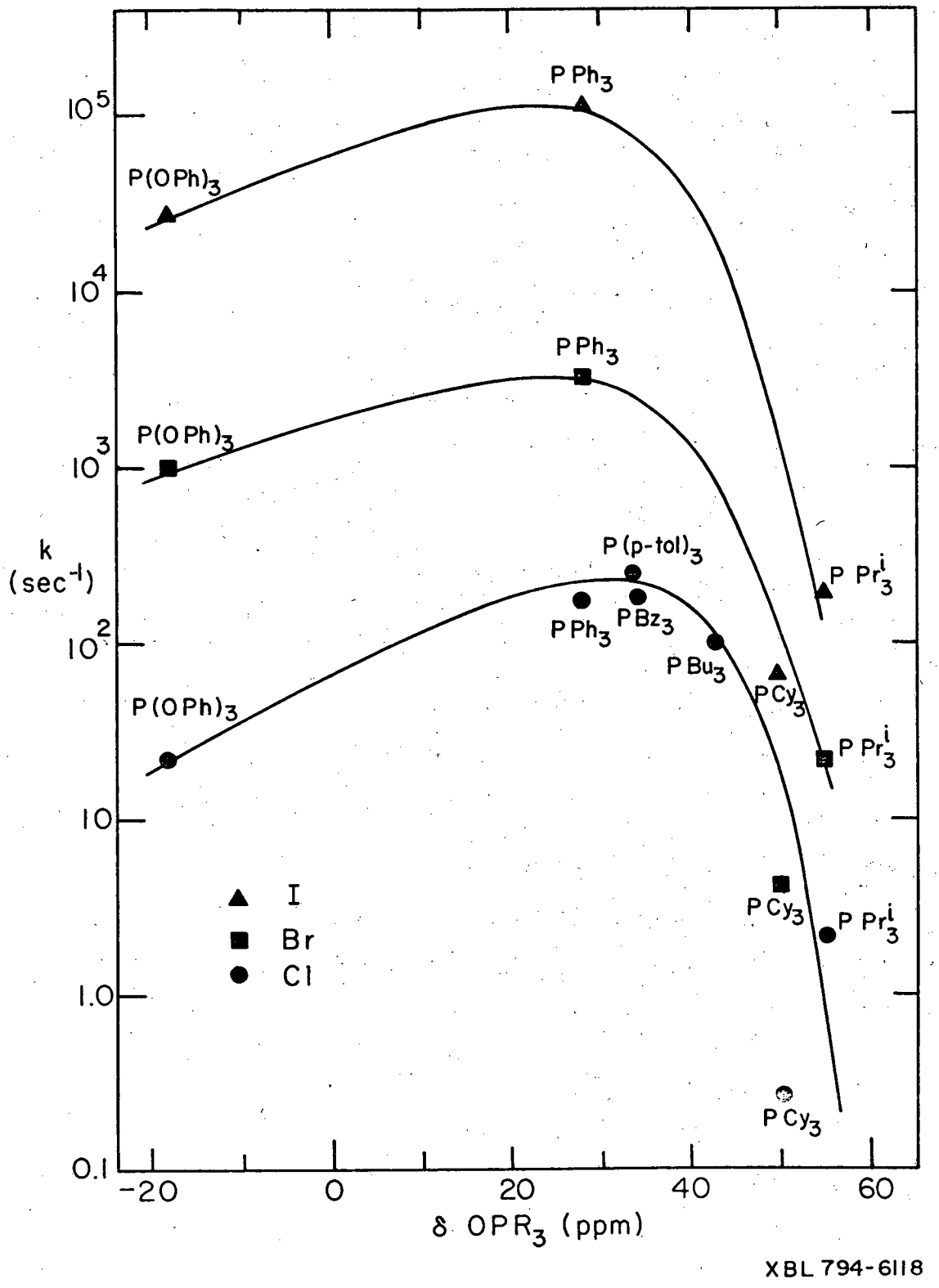

Fig. 37. Ligand influence on rate of oxidative addition of hydrogen to $IrX(CO)L_2$ to form $IrX(CO)L_2H_2$ at 30°C in toluene.

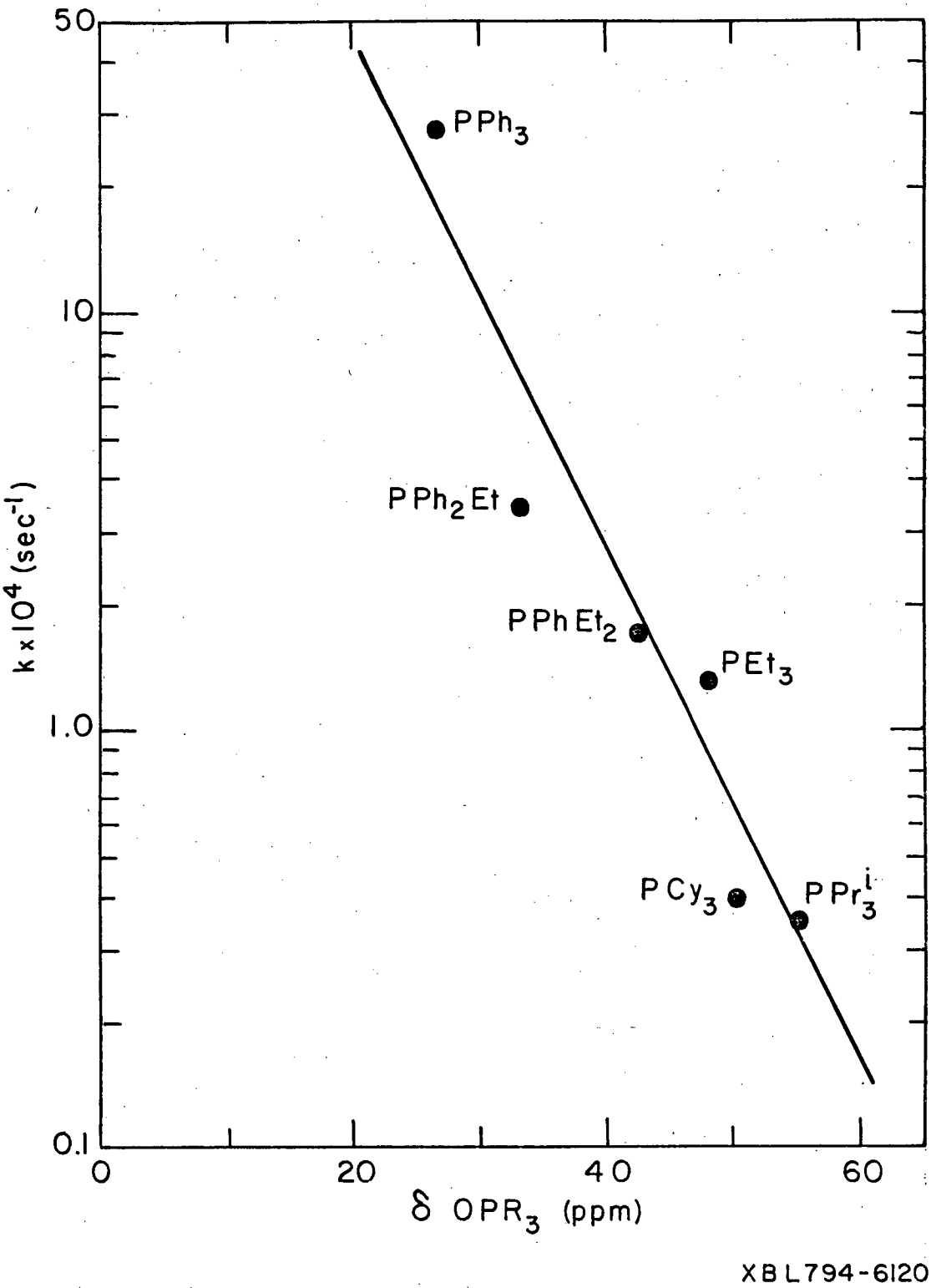

Fig. 38. Rate of reductive elimination of hydrogen by $P(OMe)_3$ from $Ir(CO)L_2H_2$ at 25°C in $CHCl_3$.

optimum ligand from a reaction rate standpoint. The curvature of the correlation may be indicative of certain mechanistic aspects of the reaction whereby the possibility arises that oxidative addition reactions show characteristic curvature not found with reductive elimination. Such knowledge may be useful in identifying rate limiting steps in complex mechanisms.

Since chemical shift is directly related to basicity and in effect Kabachnik's σ, a correlation of reaction rate with chemical shifts is a linear free energy relationship. The nonlinear nature of rate with chemical shift implies a change in mechanism. If this is so the oxidate addition of hydrogen to $Ir(CO)_2L_2$ may proceed by competing mechanisms each being differently effected by ligand basicity. This could concievably occur in the example cited if solvent interaction plays a significant role in complexation. Solvent effects can account for large changes in a transition state leading to non-linear free energy relationships (J2). Hydrogenation of anthracene by $Mn(CO)_5L$ exhibits a maxima perhaps because of the necessity of two intermediates of manganese, one a hydride the other and aryl complex, to complete a second order reaction--the stability of each being dependent to different extents on the basicity of the substituting ligands.

The basicity of ligards as described by chemical shift of the oxide can be used to predict other types of reactions. Hydroformylation by $HCo(CO)_4L$ (T3,T8) is linearly dependent on ligand basicity and consequently on OPR_3 chemical shift Fig. 39. Cis-trans

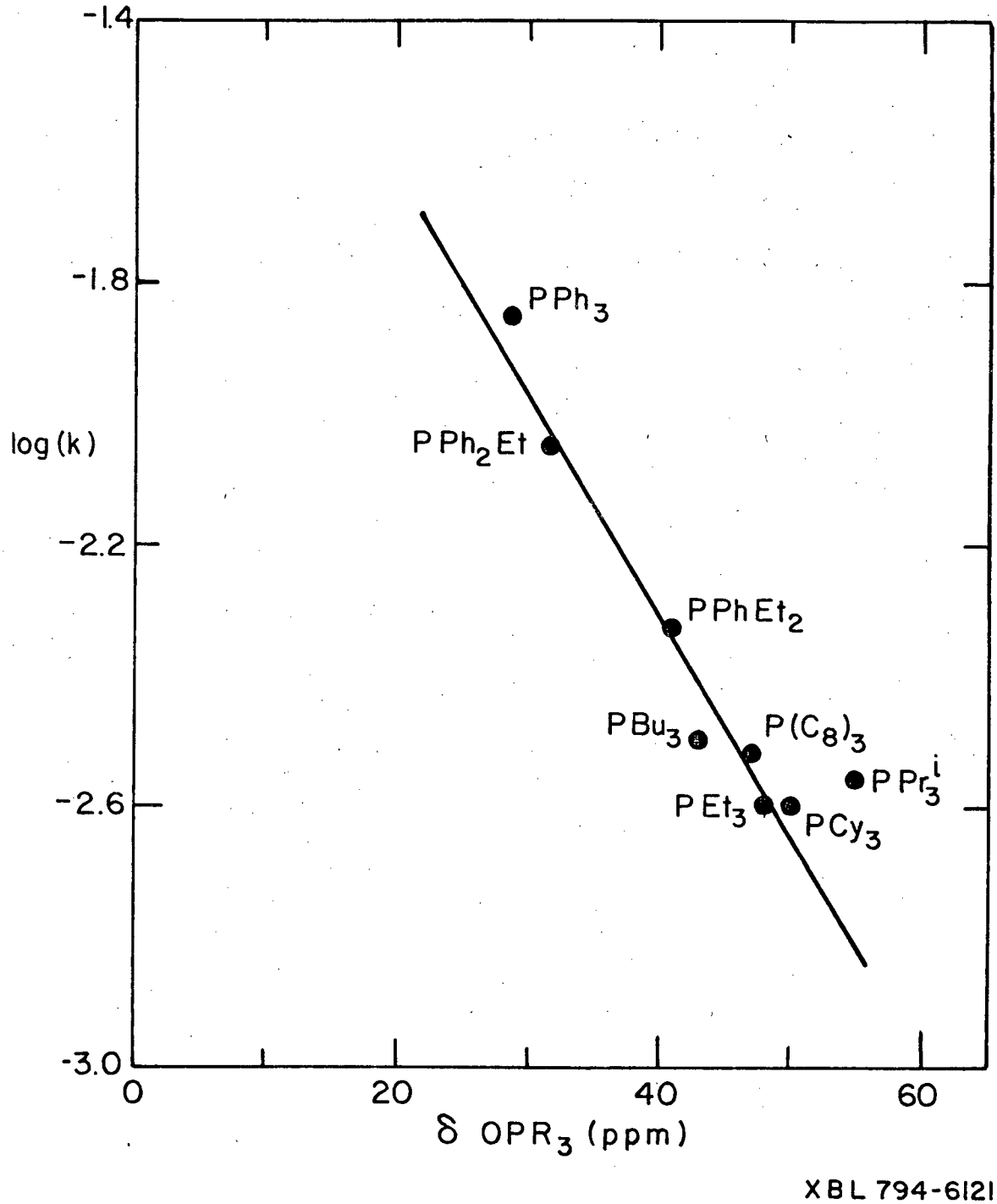

Fig. 39. Rate of hydroformylation of 1-hexene in benzene with $HCo(CO)_4PR_3$ at 160°C and 1000 psi $H_2/CO(1.2/1)$.

isomerication equilibria of octahedral complexes behave in a predictable manner for (carbene)$Cr(CO)_4L$ (F7), as shown in Fig. 40.

The effect of ligands on the cis-trans equilibrium constant, K has been incorrectly attributed to steric effects (T8). There is a relation between the bulkiness of the ligand and the chemical shift caused by the effect of bond angles on the magnetic shielding of the P nucleus. For quadrupally connected phosphorus however, this effect is minimal owing to the near tetrahedral structure (C11) and determination of the importance of steric effects can only be deduced if a large range of ligand sizes and basicities are studied.

Substitution reactions, where one phosphorus ligand, L', was used to displace another on NiL_4 to form NiL_3L' gives a semi-quantitative measure of relative ligand binding ability (T2). The data did not correlate with the carbonyl strech frequency of the related $Ni(CO)_3L$ compounds and it was judged that steric effects dominate the electronic effects for NiL_4 ligand exchange. This is not entirely the case. Figure 41 is a correlation of the semi-quantitative binding ability observed as a function of OPR_3 chemical shift. The electronic effects are evident and severe steric effects are only noted for the bulkiest of ligands such as $P(t\text{-}Bu)_3$(5).

The apparent lack of similarity with $Ni(CO)_3L$ were perhaps due to the difference between the high π-bonding ability of CO compared to phosphines and phosphites.

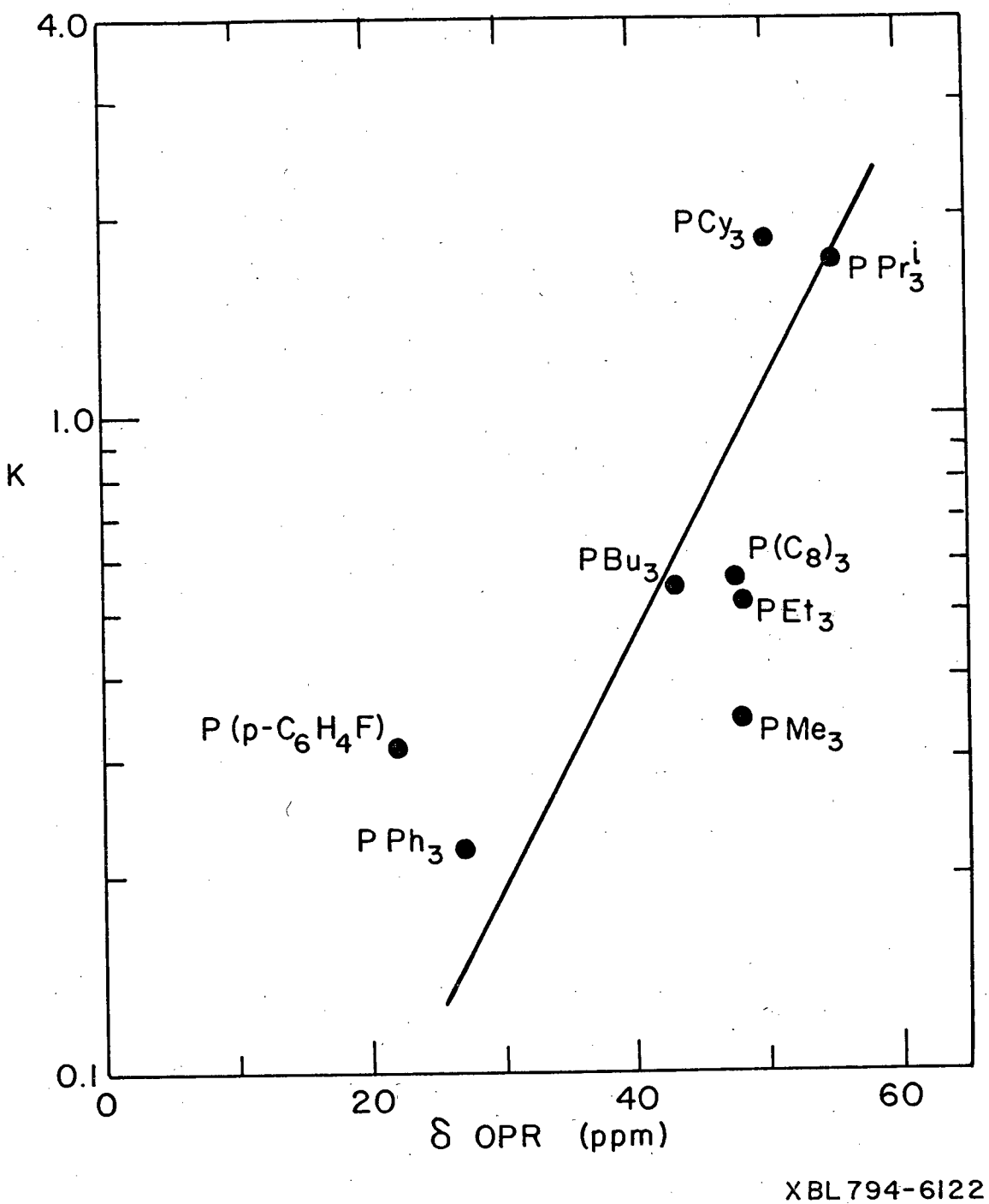

Fig. 40. Effect of varying ligands on the cis-trans equilibrium of (carbene) $Cr(CO)_4L$ in toluene-d_8 at 60°C.

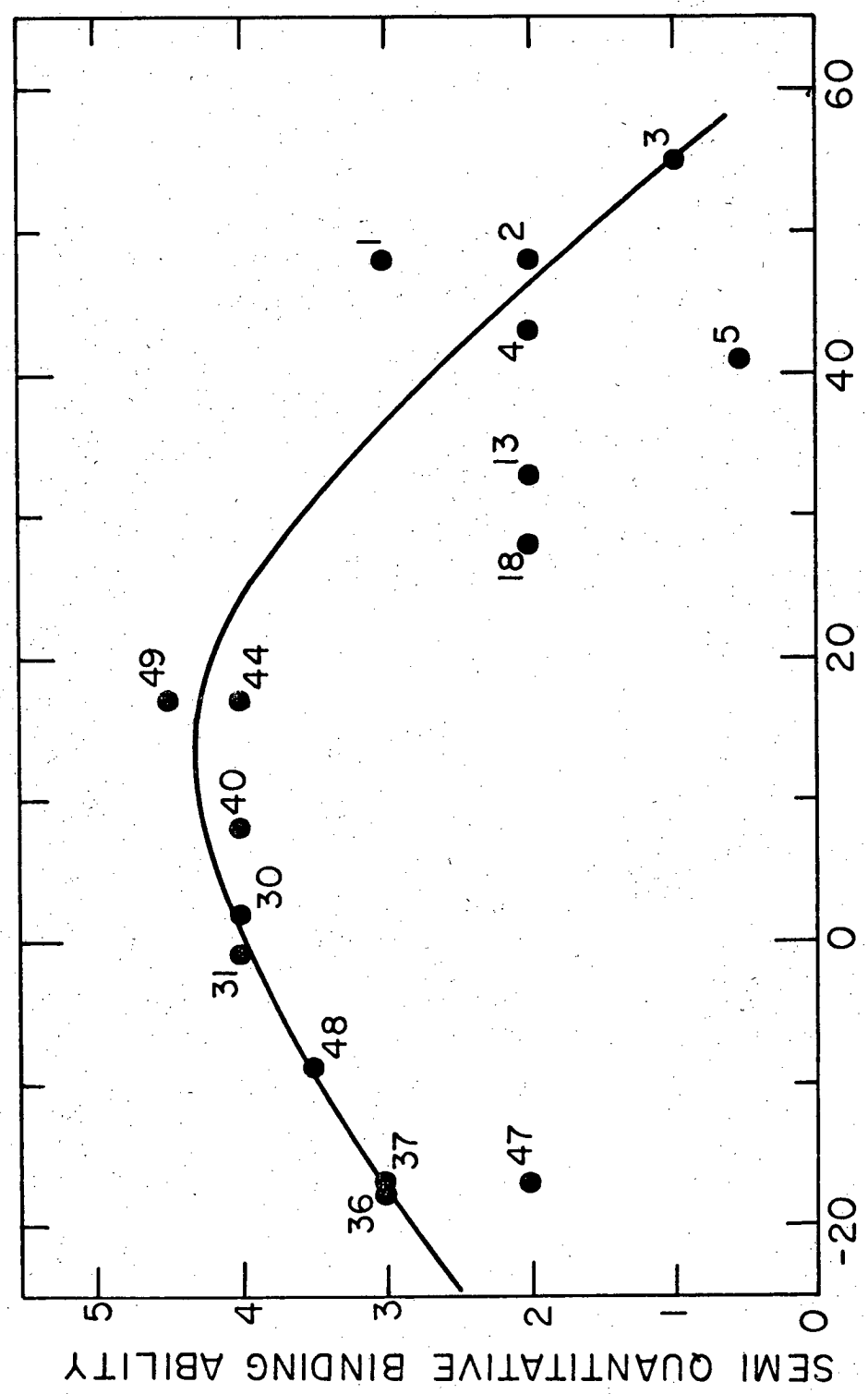

XBL794-6123

Fig. 41. Steric and electronic effects in $Ni(PR_3)_4$.

A noteworthy aspect of Fig. 41 is that the maxima does not occur at the alkyl phosphites which have the smallest cone angle (i.e., $P(MeO)_3$(30) 107° or $P(EtO)_3$(31) 109°) but at $PPh(EtO)_2$(49) with a cone angle of 116°(17). The binding ability of ligands determined by ligand exchange in NiL_4 appears to be an electronic effect if unencubered by steric hinderence; the two being in close competition for some ligands.

5. Correlation of Spin-Spin Coupling Constants with Chemical Shift

Phosphorus-31 nuclear magnetic resonance studies of compounds containing other magnetically active nuclei can yield information from mutual interactions in the form of spin-spin coupling constants. This can be especially fruitful for metal-phosphorus ligand complexes where the metal is also active, such as, Rh, W, Pt, etc. Grim et al. (G5) found a rather unsatisfactory correlation between the carbonyl stretch frequency of $W(CO)_5L$ and the phosphorus-tungsten coupling constant, J_{W-P}. Two crossing lines were drawn through the data one for phosphines the other for phosphites. The fit of the data is somewhat better if the stretch frequency is graphed as a function of chemical shift of the corresponding phosphoryl as was done in Fig. 36. More importantly, it can be seen from Fig. 42 that the chemical shift of OPR_3 is directly related to the coupling constant. More recent data has been included (F8,A9,M17).

Coupling constants have been here related to Hammett parameters here (S15,B6,M18) as have chemical shifts for closely related compounds (i.e., PH_2ArX, OPF_2ArX) so the relationship between J_{W-P}

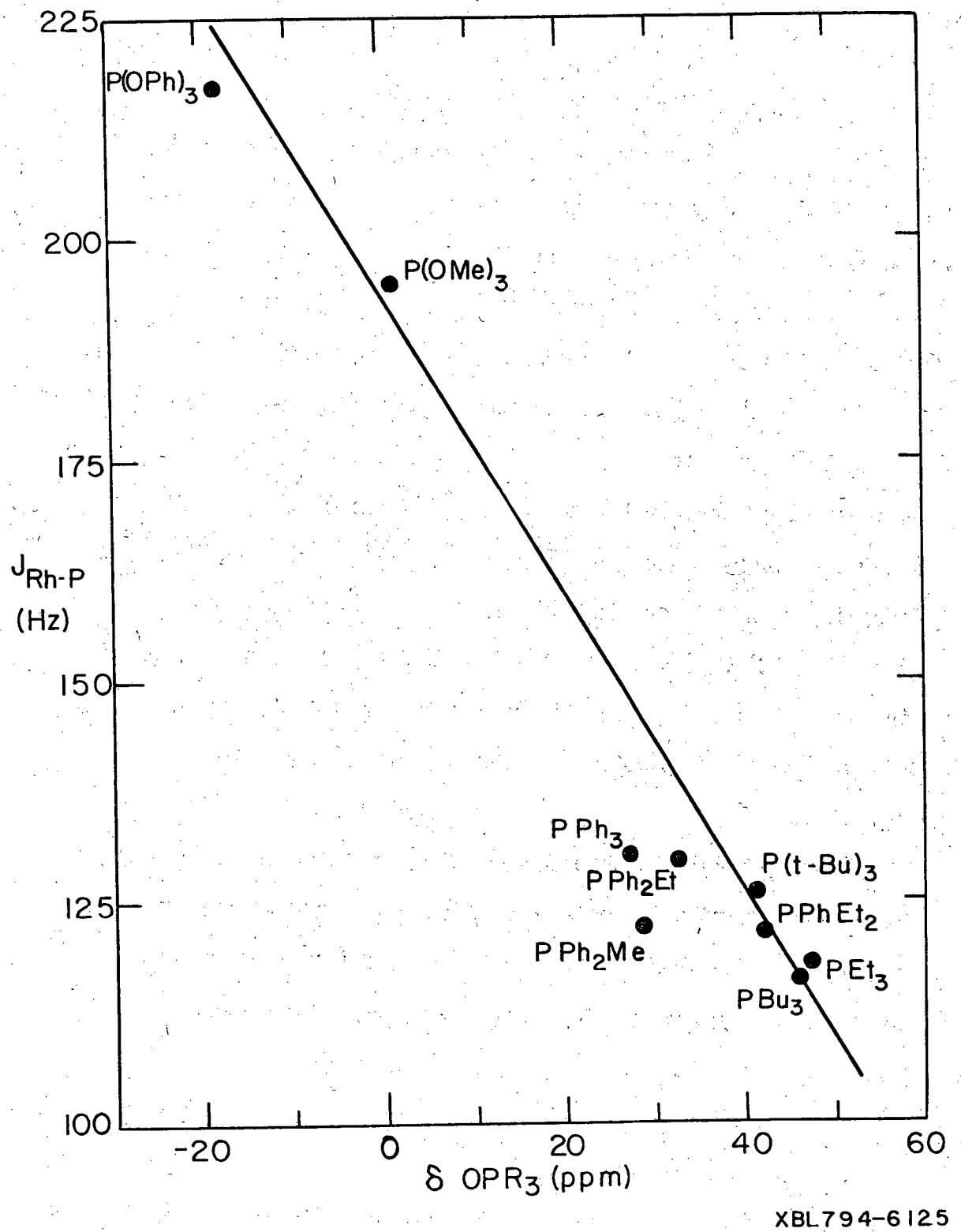

Fig. 43. Relationship between rhodium-phosphorus coupling constant and chemical shift of OPR_3 for trans-$RhCl(CO)(PR_3)_2$.

A direct relationship between Tolman's infrared measurements (T2) and ^{13}C NMR chemical shift of $Ni(CO)_3PR_3$ was found by Bodner (B6) and just as for ν_{CO} a group contribution equation was formulated to predict ^{13}C NMR shift. He concluded that ^{13}C shift is a measure of ratio of electron donor-acceptor character of PR_3. The ^{13}C chemical shifts are correlated with ^{31}P chemical shifts of OPR_3 in Fig. 44. The major deviation is again from a halogen species, PCl_3 which was in line in the ν_{CO} - ^{13}C correlation. The different behavior of PCl_3(24) in the two systems is a result of the inability of ^{13}C NMR to differentiate between σ and π-effects in the M-P bond because they have been transmitted through the metal.

^{31}P NMR shifts of metal complexes such as $Ni(CO)_3PR_3$ (M8) and $M(CO)_5Pr_3$ M=Mo, W, Cr (G1) are only roughly correlated in the chemical shift of the complexed and uncomplexed ligand.

6. Conclusions About Chemical Shift Correlations

In summary, ^{31}P chemical shift of phosphoryls, OPR_3, is a good measure of the basicity and reactivity of the parent phosphines PR_3 because the bond angle component of the chemical shift is minimized by localizing the phosphine lone-pair electrons in the O-P bond. The remaining electronic component causing chemical shift are determined by the electronegativity of the substituents, R, attached to the phosphorus. Correlations of reaction rate constants with OPR_3 chemical shift are, in a manner, like linear free energy relationships which at this time only lack of experience limits their utility. With

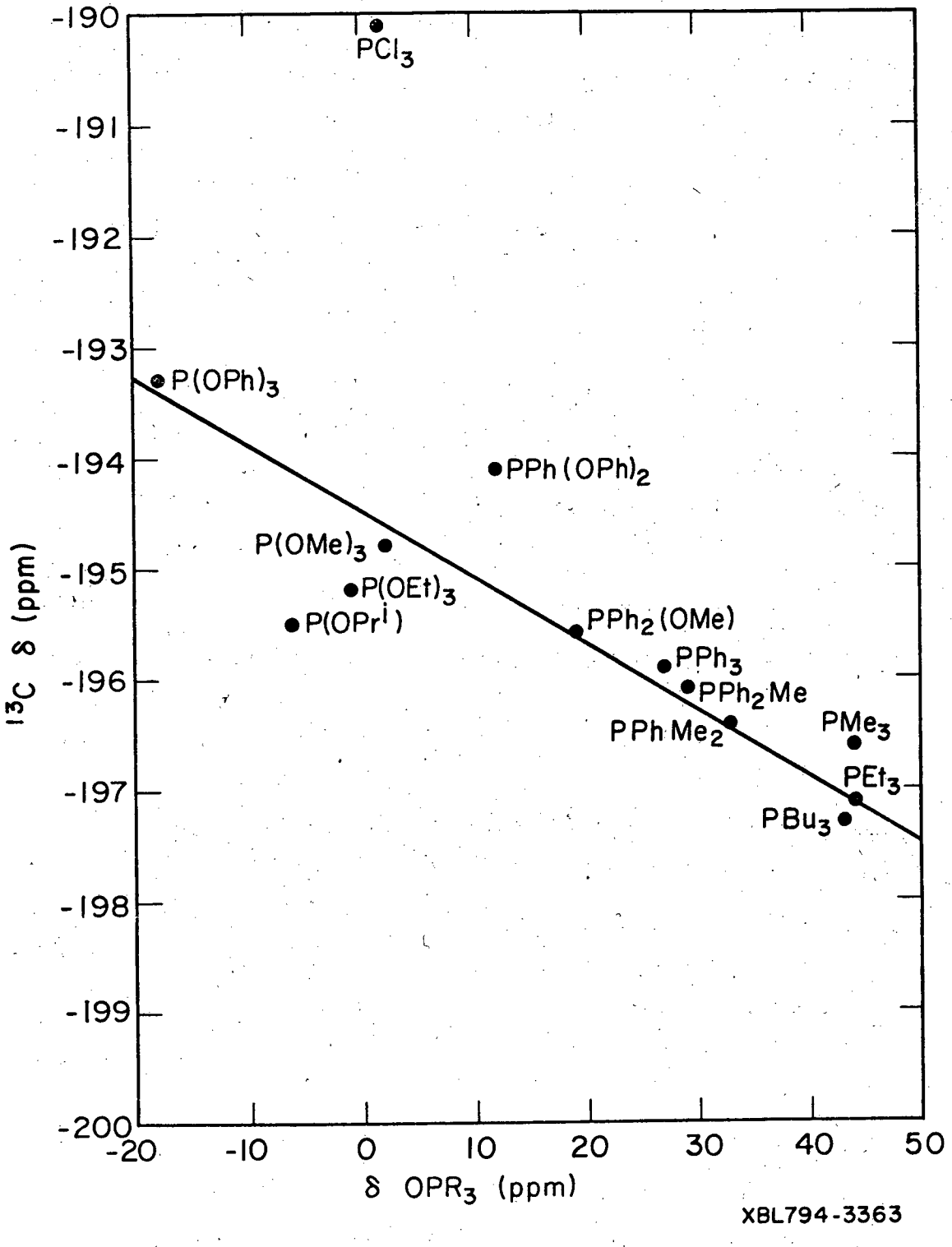

Fig. 44. Relationship between ^{13}C NMR shift and ^{31}P NMR shift of OPR_3 in $Ni(CO)_3(R_3P)$.

time, such correlations have the potential to reliably predict mechanistic aspects of metal-phosphorus ligand complexes and in turn homogeneous catalysis activity.

VI. HYDROGENATION OF CYCLOHEXENE WITH $RhCl(Ph_3P)_3$

$RhCl(Ph_3P)_3$ is probably the most useful hydrogenation catalyst that has resulted from stabilization of a metal coordination complex by ligand substitution. The replacement of pyridine by excess triphenyl phosphine (Ph_3P) in 1,2,6-$Rhpy_3Cl_3$, formed a complex with much greater catalytic action and versatility than shown by the parent compound for hydrogenating double and triple bonds at room temperature and atmospheric pressure (O1). $RhCl(PPh_3)_3$, known as Wilkinson's catalyst, has been used extensively for many different reactions (J6,M4,A5,M13,O5,S7,S8).

Despite extensive study of $RhCl(Ph_3P)_3$, several aspects of the mechanism of hydrogenation by it are unclear, and mutually contradictory models have been proposed. Siegel and Ohrt have presented a mechanism which supposes a rhodium complex with both hydrogen and olefin, which provides a pathway for isomerization and deuterium exchange as well as hydrogenation (S9). They assumed the rate-determining step to be the conversion of the complex to alkane and $RhCl(Ph_3P)_2$; all other reactions being at equilibrium. However, the existence of this olefin hydrogen intermediate was not demonstrated leaving open the question as to whether the formation of the complex or its rearrangement and decomposition is the rate-limiting step. This aspect of the mechanism could not be verified because they were unable to determine numerical values for the equilibrium constants K_L, K_O, K_{OL}, and K_H in Fig. 47.

A modified version of Siegel and Ohrt's mechanism is given in Fig. 45. This mechanism shows that the rate determining transition state will involve a rhodium-olefin-hydrogen complex if any one of steps 4-7 is controlling. If a significant amount of $RhCl(Ph_3P)_2(H)_2(Ol)$ is present in the reaction mixture, it becomes likely that its decomposition (step 6 or 7) controls. If not, it is likely that complex formation is rate-limiting (step 4 or 5).

The rate equation derived from Fig. 45 is

$$\text{Rate} = k(H_2)(Ol)(Rh)_o(B)/D \quad .$$

where

$$D = (L) + K_L(B) + K_HK_L(H_2) + K_OK_L(Ol) + K_{HL}(H_2)(L) + K_{OL}(L) + K_{OH}(H_2)(Ol)$$

(Ol) = olefin concentration (M)

(L) = free PPh_3 concentration (M)

$(Rh)_o$ = total Rh concentration (M)

(H_2) = hydrogen concentration (M)

(B) = benzene concentration (M)

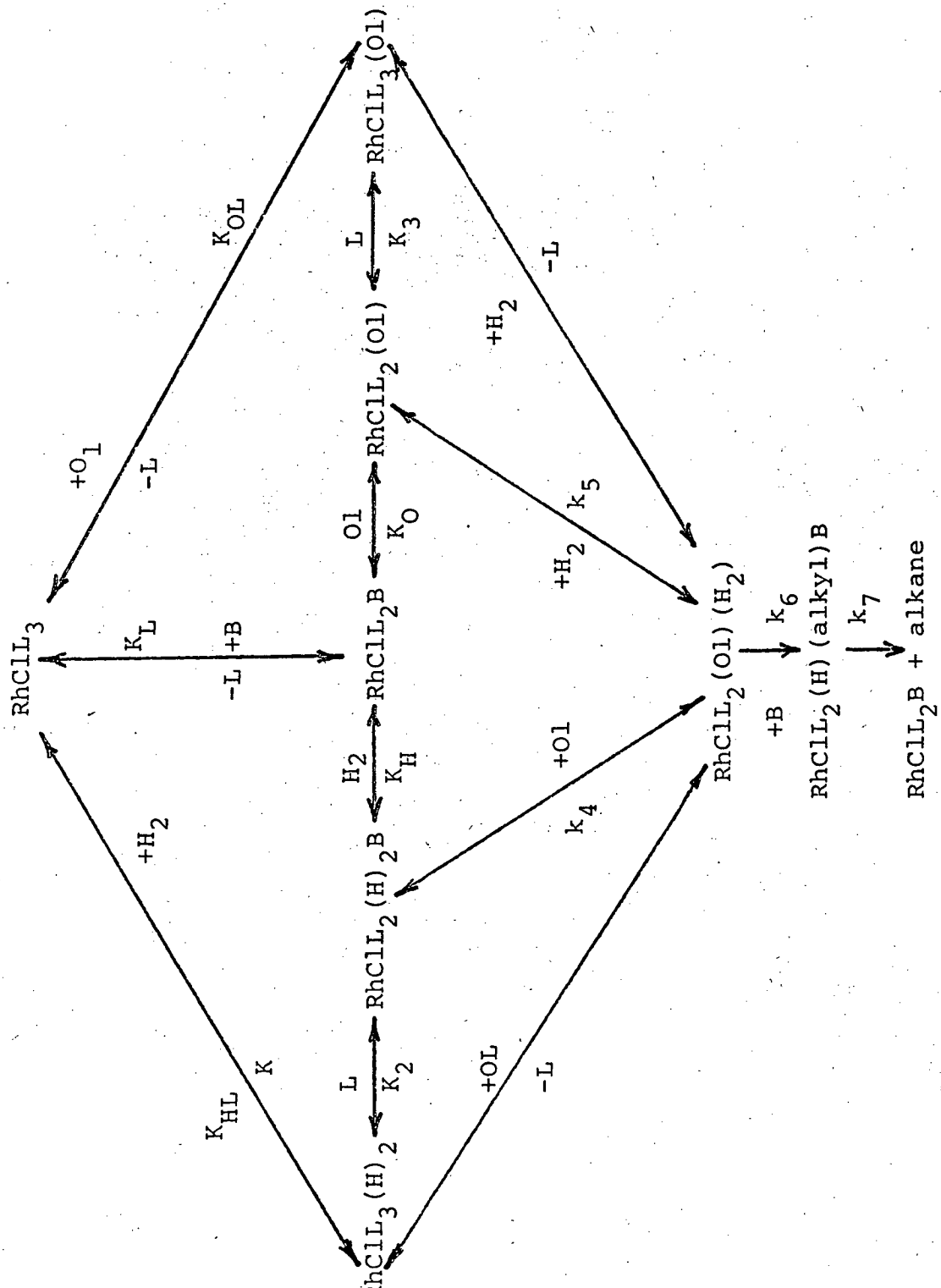

Fig. 45. Mechanism of cyclohexene hydrogenation by $RhCl(PPh_3)_3$.

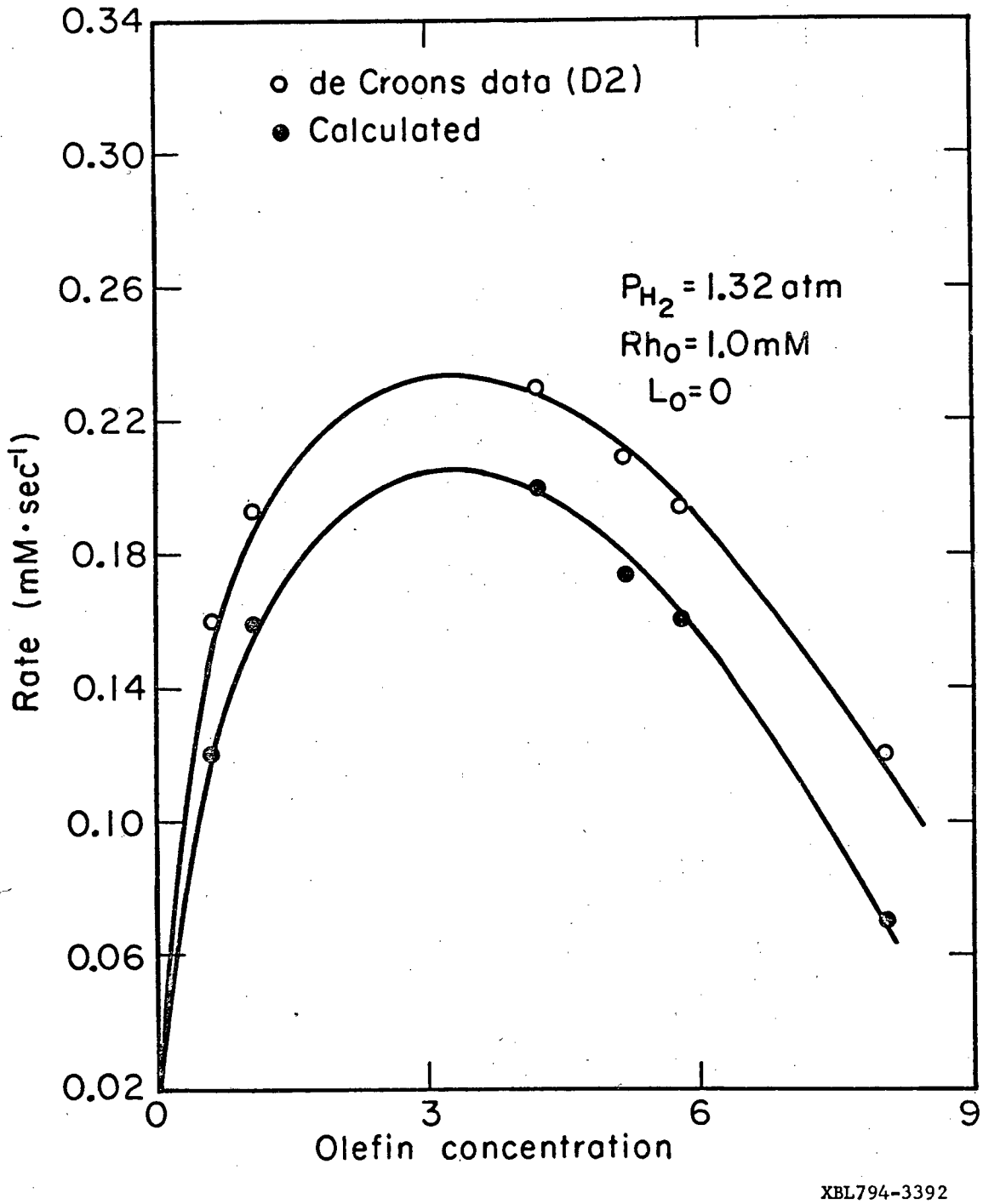

Fig. 46. Effect of olefin concentration on hydrogenation rate.

The concentration of free ligand is:

$$(L) = \frac{-b + (b^2 + 4\ ac)^{1/2}}{2a}$$

where

$$a = 1 + K_{HL}(H_2) + K_{OL}(Ol)$$

$$b = K_L(B) + K_{OH}(H_2)(Ol) + K_0K_L(Ol) + K_HK_L(H_2 - a(L)_o)$$

$$c = (Rh)_o + (L)_oK_L + K_{HO}(H_2)(Ol) + K_0K_L(Ol) + K_HK_L(H_2)$$

The apparent rate constant, k, is defined for the possible rate-limiting steps:

Step 4: (reaction of H complex)

$$K_{HL}K_2k_4 = K_LK_Hk_4 = k$$

Step 5: (reaction of Ol complex)

$$K_{OL}K_3k_5 = K_LK_0k_5 = k$$

Step 6: (rearrangement)

$$(K_{HL}K_2K_4)\ k_6 = (K_{OL}K_3K_5)\ k_6 = k$$

Step 7: (decomposition)

$$(K_{HL}K_2K_4)\ K_6k_7 = (K_{OL}K_3K_5)\ K_6k_7 = k$$

Because the mechanism for hydrogenation by $RhCl(Ph_3P)_3$ contains so many equilibrium constants, it is virtually impossible to determine all their values from kinetic data alone. If one reaction step is identified as rate-determining, the other reactions will be faster and can be assumed to maintain equilibrium with the reactants. Then the rate constant can be evaluated easily if the equilibrium constants are measured independently.

Electronic spectroscopy in the visible range was used by Howell (H7) to measure equilibrium constants K_L, K_H, K_{HL}, and also K_{OH} during the course of reactions. Unmeasured were K_O and K_{OL} which were examined at an insensitive wavelength. The present study has been directed toward completing these measurements.

A. Experimental

1. Reagents

$RhCl(PPh_3)_3$ was purchased from Aldrich Chemical Company. Its elemental analysis indicated 99+ purity. The shelf life of a once-opened bottle is limited to one or two weeks, due to

decomposition of PPh_3 to form $OPPh_3$. Solutions made from old bottles of $RhCl(PPh_3)_3$ were turbid, probably from insufficient ligand concentration which could allow insoluble dimer, $[RhCl(Ph_3P)_2]_2$, to form. Care was taken to use only fresh $RhCl(Ph_3P)_3$ for this study. Eastman reagent grade PPh_3 was recrystallized twice from 1:1 benzene-ethanol solution. Mass spectrometry showed less than 0.1 $OPPh_3$ in the recrystallized batch.

Matheson-Coleman-Baker spectroquality benzene was distilled with sodium metal-benzophenone complex under a positive pressure of nitrogen. Reagent-grade cyclohexene, from the same supplier was refluxed over CaH_2 under a positive pressure of nitrogen for 72 hr or more. The distillate was degassed by alternate freezing and thawing with liquid nitrogen under vacuum. Gas chromatography indicated both benzene and cyclohexene to be 99.5+% pure, the impurity in the benzene probably being cyclohexene.

Nitrogen was of 99.999 purity, conforming to Lawrence Berkeley Laboratory specifications and certified to contain less than 1.5 ppm oxygen or water.

2. Procedure

Benzene solutions of $RhCl(PPh_3)_3$ were prepared for optical absorbance measurements. $RhCl(PPh_3)_3$ and PPh_3 (if required) were accurately weighed and placed in a calibrated 100 ml round bottom flask. The flask was connected directly to the benzene still. A Teflon-coated magnetic stirring bar was inserted through a sidearm of the flask, and the sidearm was sealed with a rubber septum. The flask

was purged for air by alternately drawing a 40 micron vacuum and filling with nitrogen for five cycles. Benzene was then admitted to the flask, and the volume noted. The solution was then stirred to bring about complete dissolution. Turbide solutions resulted only when old $RhCl(PPh_3)_3$ was used, or when oxygen was inadvertently admitted to the flask; such turbide solutions were discarded.

Cyclohexene was added to the solution by connecting a buret barrel between the solvent stills with Teflon tubing, terminating with stainless steel syringe needles, inserted in the rubber septums of the calibrated flask, the cyclohexene storage flask, and the top and bottom of the buret barrel. The buret and tubing were purged with N_2. The buret was filled with cyclohexene to a certain mark and drained into the $RhCl(PPh_3)_3$-benzene solution. This method eliminated the need for syringes which are prone to oxygen contamination.

A 1 cm path length quartz spectrophotometer flow cell was connected to the septum of the mixing flask with Teflon tubing. The cell was purged with a positive pressure of nitrogen above the solvent level, after which the syringe needle was pushed into the solvent. Nitrogen under pressure then forced the solution into the cell. After about 50 ml of solution had passed through the cell, the tubing was clamped and cut above the clamp, and the sealed cell was taken for optical absorbance measurements.

A Cary 129 Spectrophotometer was used to record the visible spectra of the solutions. At least two superimposed scans were taken of each sample to assure that settling of precipitates or decomposition of the solution was not occurring. Absorbance measurements were recorded from 410 to 490 nm. Benzene, cyclohexene, and PPh_3 do not absorb above 306 nm.

3. Spectroscopic Measurements for Ligand Dissociation of $RhCl(PPh_3)_3$

To determine K_0 and K_{0L} in the proposed mechanism, the ratio of $RhClL_3$ to its dissociated species $RhClL_2B$ and their extinction coefficients must be known. Two studies (A8,H7) have reported differing values, and spectroscopic measurements were carried out to obtain an independent value.

The dissociation equilibrium

$$RhCl(PPh_3)_3 + B \rightleftharpoons RhCl(PPh_3)_2B + PPh_3$$

gives the following equation for the absorbance of $RhCl(PPh_3)_3$ solutions.

$$A = (Rh)_o\varepsilon_L - \frac{(\varepsilon_L - \varepsilon)}{2}\left[-(L_o + K_L) + [(L_o + K_L)^2 + 4(Rh)_oK_L]^{1/2}\right] \quad (2)$$

where

$(Rh)_o$ = initial concentration of $RhCl(PPh_3)_3$

= total Rh concentration (mM)

L_o = excess ligand concentration (mM)

ϵ = extinction coefficient of $RhCl(PPh_3)_2$ $(mM\ cm)_{-1}$

ϵ_L = extinction coefficient of $RhCl(PPh_3)_3$ $(mM\ cm)_{-1}$

K_L = dissociation equilibrium constant.

The values for absorbance and concentration for pairs of solutions (with and without excess ligand) were substituted into Eq. (2) to give the extinction coefficients at various wavelengths. Howell's (H7) value of $K'_L = 1.4 \times 10^{-3}$ M was adopted over Arai and Halpern's much smaller value (A8) because of Howell;s wider range and greater number of data points (106 vs 6). The pertinent extinction coefficients are given in Table 11. The agreement with Howell's values at 425 nm are good but poor with Arai and Halpern's at 410 nm.

4. Spectroscopic Measurements of $RhCl(Ph_3P)_2(Ol)$

The olefin-rhodium complexes in the proposed mechanism are considered to be in equilibrium.

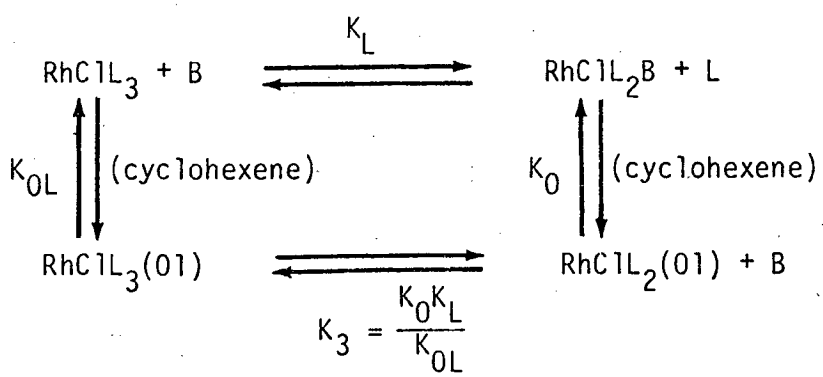

Table 11. Extinction coefficients for $RhClL_3$ and $RhClL_2$ and dissociation constant for $RhClL_3$ at 25°C.

K_L' (mM)	ϵ ($cm\ mM)^{-1}$	ϵ_L ($cm\ mM)^{-1}$	λ nm	Author
1.4	770	1496	425	(H7)
0.14	420	1420	410	(A8)
1.4	882	1434	410	This Work
1.4	816	1582	425	
1.4	883	1557	440	
1.4	913	1461	450	
1.4	862	1176	470	
1.4	740	896	490	

$$K_L = \frac{K_L'}{(B)} = \frac{(RhL_2B)(L)}{(RhL_3)(B)} \quad , \quad \text{with } (B) = 11.25\ M \ .$$

This equilibrium scheme yields the following equations for the absorbance of cyclohexene-$RhCl(PPh_3)_3$ solutions:

$$\frac{A}{(Rh)_o} = \varepsilon_L - \frac{(\varepsilon_L - \varepsilon_{OL})\, K_{OL}(Ol)}{1 + K_{OL}(Ol)} + \left[\frac{(\varepsilon_L - \varepsilon_O)(K_{OL}Ol)(1 + K_O Ol/B)}{1 + K_{OL}(Ol)} - (\varepsilon_L - \varepsilon_O)\, K_O \frac{Ol}{B} - (\varepsilon_L - \varepsilon)\right] \theta \qquad (5)$$

Here θ = fraction of Rh existing as $RhCl(PPh_3)_2$, given by

$$\theta = \frac{N}{2(Rh)_o(1 + K_O Ol/B)(1 + K_{OL}/B))} \qquad (6)$$

where

$$N = -(L_o + K_L B + K_O K_L Ol + L_o K_{OL} OlB + [(L_o + K_L + K_O K_L Ol + L_o K_{OL} OlB)^2 + 4K_L(Rh)B_o(1 + K_O Ol)(1 + K_{OL} Ol)]^{1/2}$$

ε_{OL} = extinction coefficient for $RhCl(PPH_3)_3(Ol)$ $(cm\ M)_{-1}$

ε_O = extinction coefficient for $RhCl(PPh_3)_2(Ol)$ $(cm\ M)_{-1}$

$$K_O = \frac{(RhCl(Ph_3P)_2 Ol)(B)}{(RhCl(PH_3P(B)(Ol)} = K'_O(B)$$

Solutions of $RhCl(PPh_3)_3$, excess ligand, and cylohexene were made in benzene and absorbance measurements were made at each wavelength (410, 425, 440, 450, 470 and 490). Using the extinction coefficients in Table 11 with K'_L = 1.4 mM, the absorbance data were fit by an iterative computer program that varied K_0, K_{OL}, ϵ_0 so as to converge on the minimum sum of the squares of the errors by a relaxation technique.

At all wavelengths the calculated extinction coefficient for the $RhClL_3$-olefin complex was inordinately large, leading led to the conclusion that the concentration of $RhClL_3(Ol)$ was negligible. To test this hypothesis, the computer program was rerun floating only K_0 and ϵ_0 with K_{OL} and ϵ_{OL} set to zero. The fit of the data was not changed significantly, with the standard deviation changing from about 2 to 3%. The results of the computer fit are given in Table 12. (The computer program used is given in the Appendix.)

The value for K'_0 at different wavelengths showed a variation from 1.42 to 2.04. The lower wavelengths (410 and 425 nm) are less reliable due to the presence of an isobestic point ($\epsilon = \epsilon_0$) at about 425 nm; experimental errors which result in small differences in the measured absorbance can give very different values of the dissociation constant in this region. The computer fit of the data to K'_0 is not sensitive as shown by the two computer fits where K'_0 was kept constant at 2.0. Neither the percent standard deviation nor ϵ_0 changed appreciably, indicating that the program is converging on a

Table 12. Extinction coefficients and dissociation constant for $RhCl(PPh_3)_2(Ol)$.

$K_{OL} = 0$	Solvent	Benzene	(B = 11.25M)
$K_L' = 1.4$ mM	Temperature	25°C	
	$K_O = K_O'(B)$		

λ (nm)	K_O' M^{-1}	ε_O $(cm\ mM)^{-1}$	Percent Std Dev (absorbance)
410	1.42	1054	1.5
425	1.77	821	2.2
440	1.95	709	3.0
450	2.02	652	3.2
470	2.04	540	3.6
490	2.04	411	3.7
410	2.0*	1070	1.7
425	2.0*	742	2.3

*K_O was kept constant and only ε_O was allowed to vary in these determinations.

shallow minimum. An average value for K'_0 of 2.0 M^{-1} was adopted from the four highest wavelengths for the kinetic correlations.

B. Correlation of Kinetic Data for Cyclohexene Hydrogenation Catalyzed by $RhCl(Ph_3P)_3$

The value for K'_0 obtained from the present spectroscopic study, and for K_{HL} and K_{HO} reported by Howell (H7), with K_{OL} and K_H neglected in accordance with experimental findings, were used to recorrelate available data for $RhCl(PPh_3)_3$ catalyzed hydrogenation of cyclohexene (Table 13). Fifty rate values reported by Ohrt (O6) and ninety-nine by Howell (H7) were used in the computer fit to determine k_{app}. Osborne's data (O1) were not used in this fit because his solvent composition was not indicated. The contribution of Osborne's result assuming the solvent was benzene is included along with data by de Croon et al. (D2) in the final correlation of all the available differential rate data (310 points).

Table 13 shows the resulting fit to the rate data using equilibrium constants obtained from spectroscopy. Due to uncertainty over the value for the ligand (PPh_3) dissociation constant K'_L, a set of ten representative rate data was first correlated at several values of K_L (0.0007, 0.2, 0.7, 1.2, 1.4, 1.6, and 2.1) with K_{HO} and k_{app} allowed to float. The lowest standard deviation was observed at K'_L = 1.4 mM, hence this value, the same as reported by Howell and sustained independently in the present study, was used in further correlations.

Table 13. Determination of k_{app} from kinetic data.

$K_H = 0$ $K_{HL} = 14{,}400$

$K_{OL} = 0$ $K'_L = 0.0014$ M

Run	K'_O (M^{-1})	K_{HO} (M^{-1})	k_{app} $(M\text{-sec})^{-1}$	Percent % Std. Dev.	Number of Data
1	2.0	0.858*	0.100*	9.4	149
2	2.0	0	0.86*	14.7	149
3	2.0	0	0.86*	17.6	149
4	2.0	0.85	0.10*	14.5	310
5	2.0	0.85	0.10*	13.4	295**

*Values floated in computer fit of 149 rate data for the rate equation derived from Fig. 45.

**Computer fit without de Croon and co-workers' data (D2).

The first computer fit of the 149 rate data allowed both K_{HO} and k_{app} to vary. Table 13 shows there is an excellent match between the value of K_{HO} from the kinetic fit (0.858 M^{-1}) and that reported by Howell (H7) from spectroscopy (0.851 M^{-1}). The standard deviation was understandably higher (9.4) than for the same data correlated by Howell where K_{HO}, k_{app}, and K_O' were floated (7.6%). Considering that the spectroscopic value of K_{HO} could have been used without floating, only one effective variable (k_{app}), was floated here, as compared to two effective variables, in Howell's work. A rounded-off value of K_{HO} = 0.85 M^{-1} was adopted for further correlations. The fit obtained over such a wide range of variables and such a large group of data from two different laboratories provides compelling evidence for the validity of this reaction model. It appears likely that a large part of the standard deviation is of experimental origin, with additional contributions from the uncertainties of the spectroscopic K's and from neglected equilibria such as K_H and K_{OL}.

In the first computer fit, Siegel and Ohrt's hypothesis of a hydrogen olefin complex intermediate was assumed correct and in fact the convergence of K_{HO} to a non-zero value supports that hypothesis. The second computer fit, made to determine the effect of neglecting K_{HO} in the rate equation, gave a significantly larger standard deviation (14.7% compared with the previous 9.4). The improvement obtained by including K_{HO} is larger than would result from inserting an additional purely empirical adjustable parameter,

which could be expected to produce only about 2% reduction relative to the 14.7 standard deviation.

The report by de Croon et al. (D2) shows a rate inhibition at olefin concentrations greater than 3M. This has been incorporated into the proposed mechanism by permitting competition between benzene and olefin for the coordinately unsaturated species, $RhCl(Ph_3P)_2$, produced by ligand dissociation. Run 3 tested the fit of the data, to the mechanism without benzene coordination (i.e., using K'_L; see Table 11) and without the cross term K_{HO}. A standard deviation of 17.6% (compared to 14.7% when K'_L is used) supports de Croon's concept. Thus, both benzene coordination and K_{HO} are required to permit a true representation of the kinetics.

The inhibiting effect of olefin is illustrated in Fig. 46. Discrepancy exists between de Croon et al. (D2) and other studies (H7,O6,O1) in that de Croon's rate data is always porportionately higher, causing a higher standard deviation (14.5%) when all the rate data are correlated (H7,O6,O1,D2). Nevertheless the trends are consistent, and the shapes of the curves calculated from the mechanism in Fig. 46 accurately predict olefin inhibition.

At high concentrations, the olefin complexes most of the rhodium and decreases $RhCl(Ph_3P)_3(H)_2$ formation. This makes it improbable that the reacting complex $RhCl(Ph_3P)_3(H)_2(Ol)$ is formed via a hydrogen complex. Concurrently the low benzene concentration reduces the rate at which the hydrogen-olefin complex $RhCl(Ph_3P)_2(H)_2(Ol)$ decomposes to reaction product. The

complexing strength of benzene appears to be much greater than that of cyclohexene ($K_{OL} \sim 0$).

In summary, the values for the thermodynamic and kinetic constants for the mechanism presented in Fig. 45 are:

$K_{app} = 0.10 \pm 0.01\ M^{-2}\ sec^{-1}$ (0.086 in second fit)

$K'_L = 1.40 \pm 0.02 \times 10^{-3}\ M$

$K_L = 1.24 \pm 0.17 \times 10^{-4}$

$K_H \leq 600\ M^{-1}$

$K'_O = 14{,}400 \pm 200\ M_{-1}$

$K_O = 22.5 \pm 0.5$

$K_{OL} \leq 2.5 \times 10^{-2}\ M^{-1}$

$K_{HO} = 0.85 \pm 0.01\ M^{-1}$

The combined constants can be calculated from the relationships

$K_2 = K_L K_H / K_{HL}$

$K_3 = K_O K_L / K_{OL}$

$K_4 = K^{OH} / K_2 K_{HL}$

$K_5 = K_{HO} / K_3 K_{OL}$

$K_{HO} = K_3 K_5 K_{OL} = K_2 K_4 K_{HL}$

$K_L = K'_L(B) \qquad K_O = K'_O(B)$

A Henry's law constant of 26200 cm Hg/M was used for hydrogen solubility in benzene (C16).

A graphic comparison of the rate equation with and without the denominator cross term K_{HO} is given in Figs. 47 and 48. The fit of the calculated rate equation is significantly better for $K_{HO} = 0.85\ M^{-1}$. The difference in fit is more pronounced than in Howell's

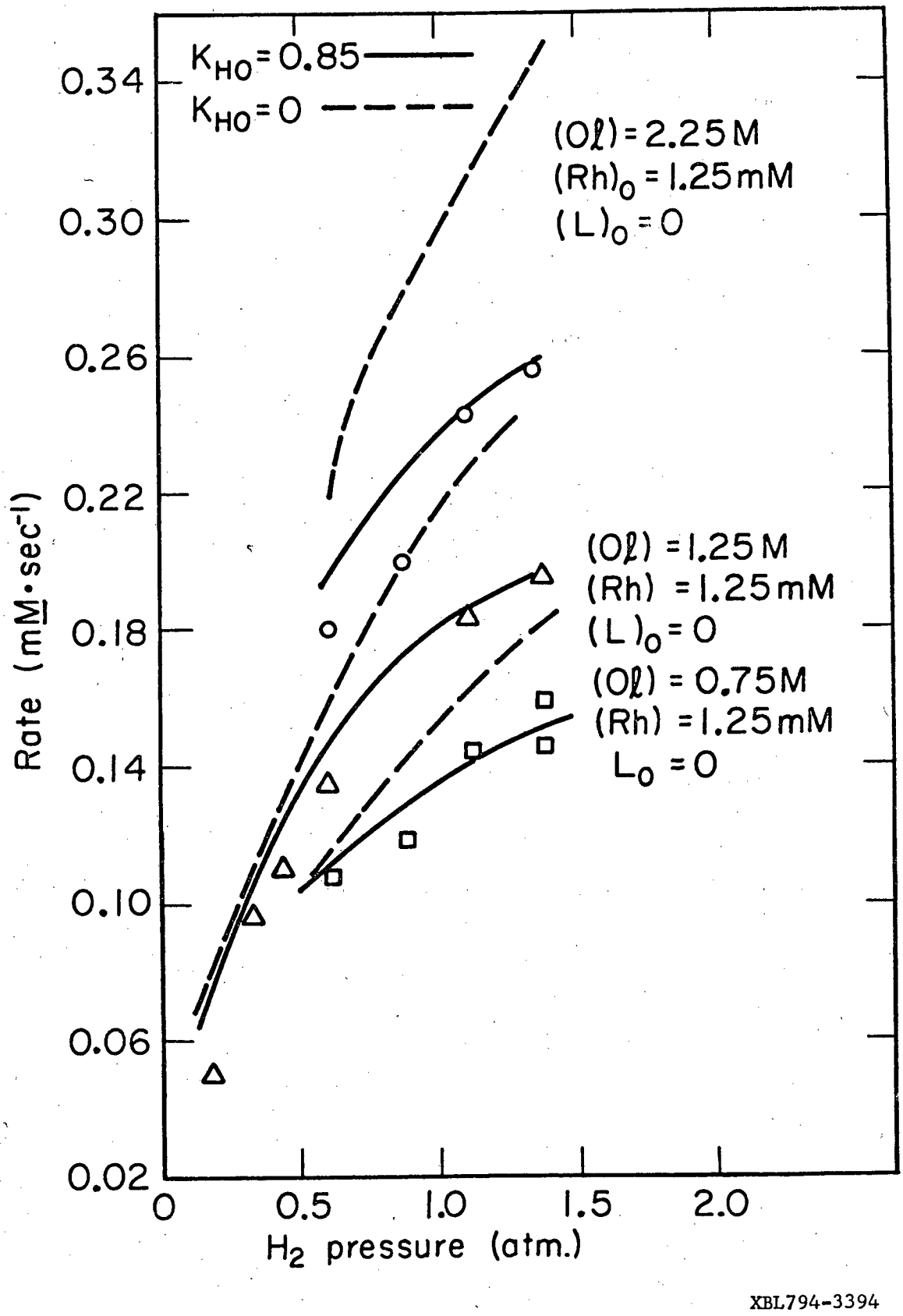

Fig. 47. Effect of hydrogen on cyclohexene hydrogenation rate.

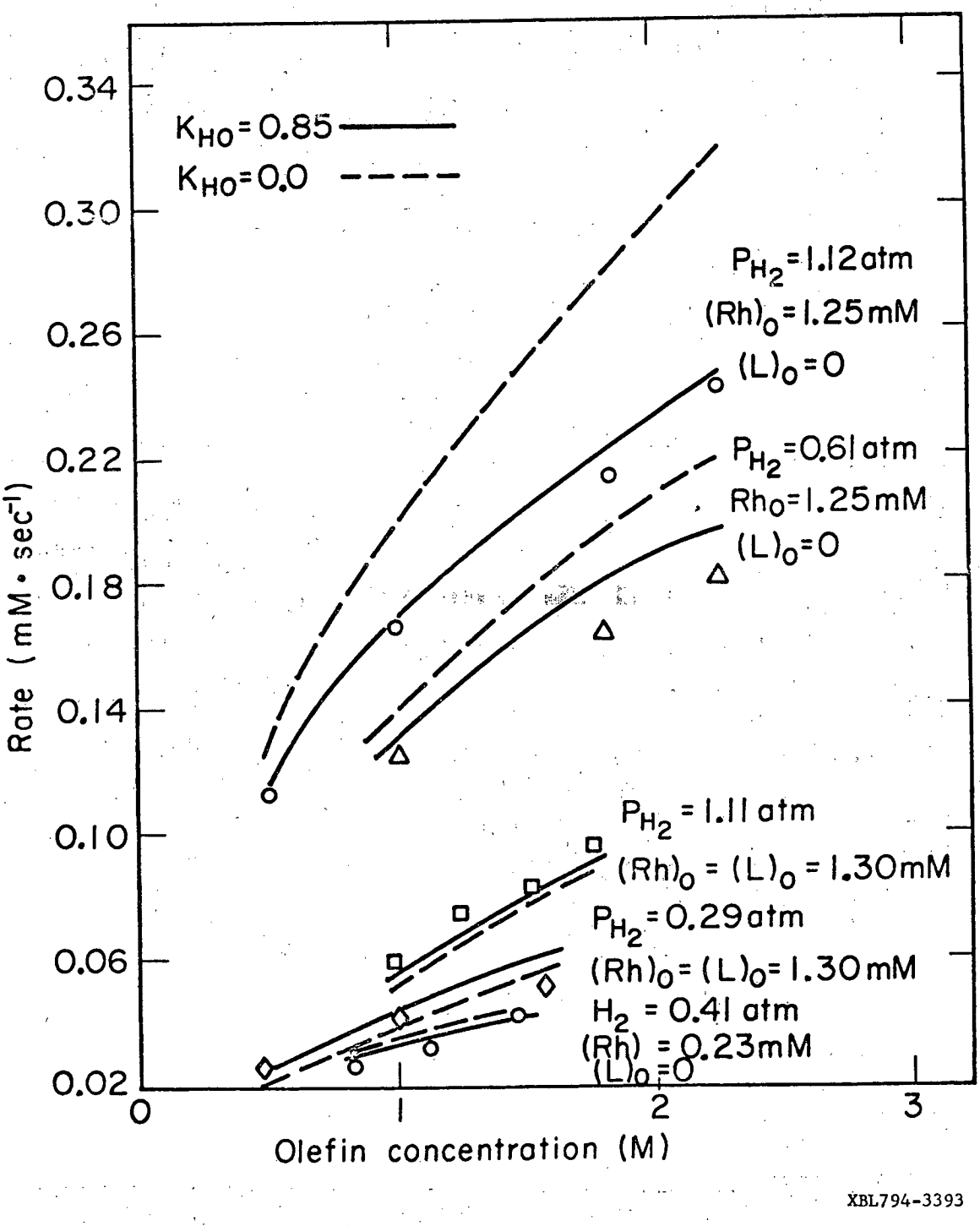

Fig. 48. Effect of olefin or cyclohexene hydrogenation rate.

work, because of the absence of K_{OL} as an adjustable parameter that could compensate for the error with the $K_{HO} = 0$ model.

Figure 49 shows the distribution of the initially added $RhCl(PPh_3)_3$ at three reaction conditions. The most hydrogen-olefin complex is present at high hydrogen and olefin concentrations as expected. Since there is little or no RhL_3Ol and RhL_2H_2, the sensitivity of the rate equation to the value of K_L is low due to a compensating effect by RhL_3H_2 and RhL_2Ol to form RhL_2OlH_2.

C. Discussion

Recently several studies have been published regarding the mechanism of cyclohexene hydrogenation by $RhCl(Ph_3P)_3$. Halpern, Okamoto, and Zachariev (H8) reported the kinetics of hydrogenation of cyclohexene with $Rh(Cl(H)_2(PPH_3)_3$ and excess PPh_3. They concluded that the mechanism is:

$$RhClL_3(H)_2 + Ol \overset{K}{\rightleftharpoons} RhClL_2(H)_2(Ol) + L$$

$$RhClL_2(H)_2(Ol) \overset{k}{\rightarrow} [X] \underset{\text{fast}}{\overset{L}{\rightarrow}} RhClL_3 + \text{alkane}$$

The values for $k = 0.2 \pm 0.04$ sec^{-1} and $K = 3.4 \pm 0.6 \times 10^{-4}$. [X] is a coordinatively unsaturated (or solvent containing) bisphosphine complex. The values for the equilibrium constants found by spectroscopy and kinetics may be compared to their measurements for formation of $RhClL_2(H)_2(Ol)$ since $K = K_{HO}/H_{HL}$. The value

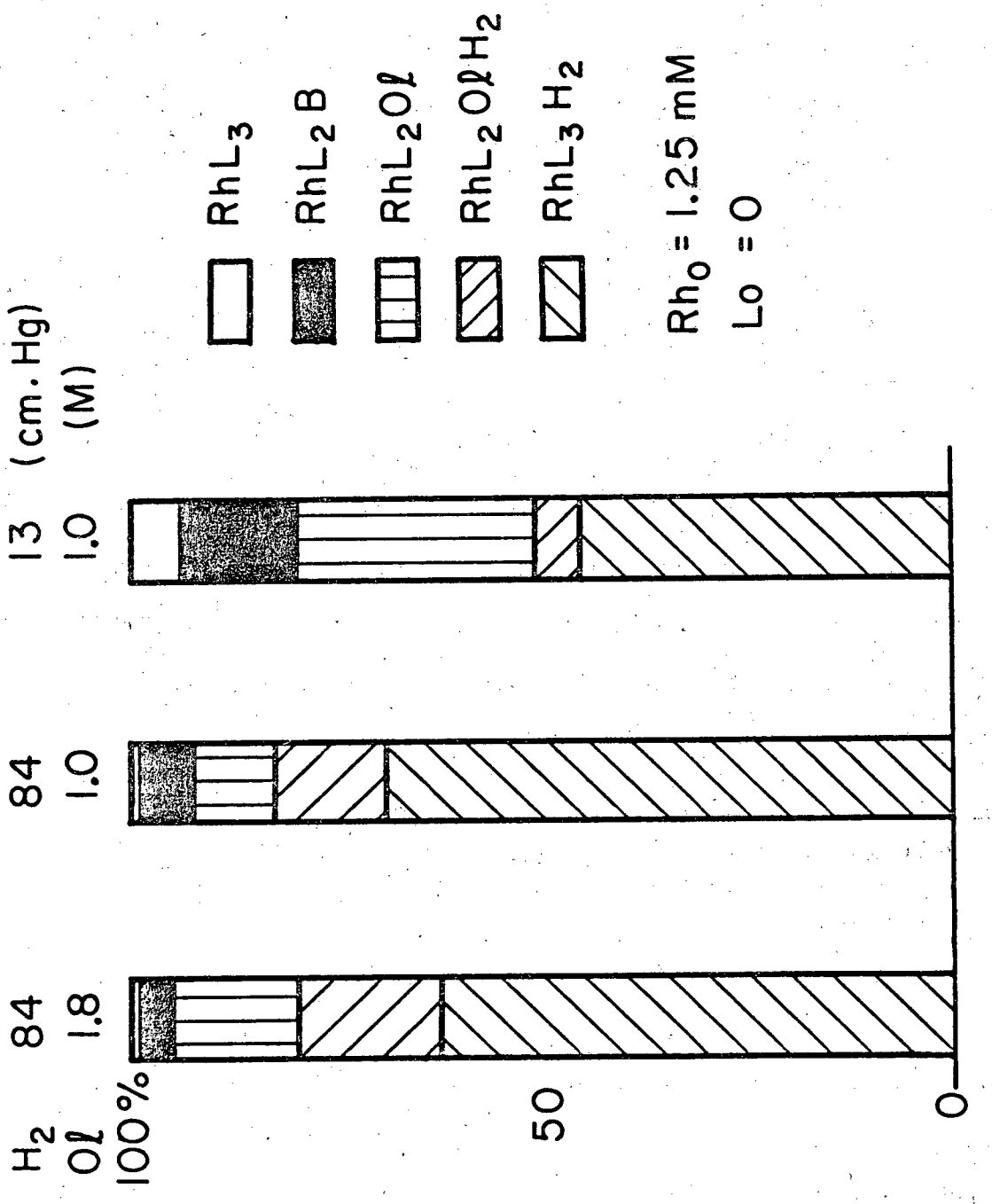

Fig. 49. Distribution of various Rh complexes during cyclohexene hydrogenation.

obtained in this study $K = 0.6 \times 10^{-4}$ is somewhat different. The discrepancy can be reconciled if Halpern's method to determine K is reviewed. The rate data were fit by the pseudo-first-order kinetic equation:

$$-d/dt(RhClL_3H_2) = k_{OBS}(RhClL_3H_2)$$

and from their mechanism presented in section

$$\frac{1}{k_{OBS}} = \frac{1}{k} + \frac{(L)}{Kk(Ol)}$$

The values for k and K may be obtained from the slope and intercept of a linear plot of $1/K_{OBS}$ vs (L)/(Ol).

The greatest error in calculating k and K comex from determining the intercept (1/k) from their graphical solution. The values of the ordinate range from 0 to 1100 for $1/k_{OBS}$ and 5.0 is reported for the intercept. If the line through the data is drawn slightly differently a value of 1.0 for the intercept still gives excellent fit of the data and is in coordinance with the value reported in this work of

$K = K_{HO}/K_{HL} = 0.6 \times 10^{-4}$ and $k = K_{app}(B) \sim 1.0$.

The agreement of the values of $K(= K_{HO}/K_{HL})$ and $k = k_{app}$) is good considering independent methods and laboratories arrived at the same conclusion. Both works support the existence of a hydrogen-olefin-complex and its decomposition being the rate limiting step. The values for the equilibrium constants found it this study are deemed more accurate because they fit the data for the overall

mechanism instead of just one possible path studied as a stoichiometric reaction.

Two other reports (R2,D2) proposed new mechanisms for cyclohexene hydrogenation by $RhCl(Ph_3P)_3$, wherein the equilibrium and rate constants were determined by computer programs. De Croon and co-workers' (D2) report a mechanism containing two competing rate determining steps to account for their data, the two competing steps being required to conform to the maxima in the rate dependence on olefin concentration. They conclude that the rate limiting steps are the formation of $RhClL_2(H)_2(Ol)$. If this was the case none of this complex would be detected in solution, contrary to Howell's work (H7), because its decomposition must be faster than its formation. This is also inconsistent with Halpern's et al. (H8) stoichiometric studies just mentioned. Since de Croon et al. computer fit their data by floating all the equilibrium constants and the rate constant without the aid of physical measurements, less certainty can be given to their values and understandably do not agree with other studies (H8,H7, and this work).

A second mechanism proposed by Rousseau, Evrard, and Petit (R2) asserts that a coordinately unsaturate species $RhClL_2H_2$ is the active catalyst. This mechanism also neglects the existence of the hydrogen-olefin complex $RhClL_2(H))_2(Ol)$ but assumes the rate limiting step to be the reaction of $RhClL_2H_2$ with olefin to form the product cyclohexane. The major drawback of this mechanism is its inability to account for rate inhibition at high olefin

concentrations. Again all the kinetic and equilibrium constants were calculated by a computer program and are in disagreement with those found in this study.

D. Summary

In conclusion, Figs. 47 and 48 illustrate definitive evidence that a substantial amount of a complex of the composition $RhCl(H)_2(OL)(PPh_3)_2$ is present under reaction conditions. The olefin may be complexed in π-bonded form or as an equilibrium mixture of that form and an alkyl form. Correspondingly, the rate-determining step may be either formation of the alkyl complex (followed by rapid conversion to cyclohexane), or a slow conversion of the alkyl to cyclohexane. However, the consistent results in evaluating ϵ_{HO} and K_{HO} suggest that there is only one rate-determining step; hence, that K_{HO} is either $K_2K_4K_{HO}$ or $K_2K_4K_{HL}(1 + K_6)$, and ϵ_{HO} is either ϵ_{olefin} alone or a weighted average of ϵ_{olefin} and ϵ_{alkyl}. In either event, the conclusion can be drawn that the rate-determining step involves an H-atom transfer.

VII. APPLICATION OF SUBSTITUTED METAL CARBONYLS TO COAL AND MODEL COMPOUNDS OF COAL

The application of metal carbonyls to catalyze hydrogenation of coal was suggested by two factors, the relative stability of metal carbonyl complexes at higher temperatures, and the frequently favorable action of H_2–CO and H_2O–CO mixtures (compared with hydrogen) in liquefying coal. Investigations by Fischer (F6) in 1921, demonstrated that the yields of ether-soluble material recovered (13 to 35%) from coal hydrogenation with water and carbon monoxide were higher than those obtained with hydrogen. Interest in coal liquefaction utilizing the water-gas shift reaction prompted a series of studies in the U. S. Bureau of Mines (A1-3,A6,A7,A9), with encouraging results. Freshly powered lignite with appropriate solvents showed 90% conversion to low-sulfur oil after reaction for 10 min at 380°C, under 4,500 psi pressure of CO–H_2O mixture or of synthesis gas (1:1 CO/H_2).

The role of carbon monoxide in coal liquefaction is to inhibit cross-linking of the coal during liquefaction (A1). The carbon monoxide combines with alkaline materials in coal ash to make formates, which then donate hydrogen to double-bonded oxygen (i.e., carbonyl groups) in coal.

$$M^+ + OH^- + CO \rightarrow HC(=O)O^-M^+$$

$$C{=}O + H{:}\overset{O}{\overset{\|}{C}} - O^{-}M^{+} \rightarrow - \overset{H}{\overset{|}{C}} - O^{-}M^{+} + CO_2$$

$$- \overset{H}{\overset{|}{C}} - O^{-}M^{+} + H_2O \rightarrow H - \overset{|}{C} - OH + OH^{-} + M^{+}$$

In addition, carbon monoxide hydrogenates olefins and easily reduced aromatic rings; the rate is lower than with hydrogen (A3), making the use of synthesis gas preferable to use of H_2O and CO.

The reactivity of carbon monoxide with coal is a function of the carbonates in coal ash. A composition of the mineral matter in the coal used in this study is shown in Table 14. A large portion of the ash is composed of alkali metals which form the carbonates in the base catalyzed reaction with CO.

The conditions of liquefaction with synthesis gas also provide the possibility of transition metal carbonyl formation from components of coal ash. Although transition metals are not in great abundance, they may be more catalytically active than the alkali carbonates. The predominant transition metal suitable for carbonyl formation is iron. The iron is usually in the form of pyrite which readily forms iron carbonyl under CO pressure. Iron carbonyl has been shown to catalyze the water-gas shift reaction (W2) and may form hydrogen is situ in the coal matrix. Thus under CO pressure metal carbonyl catalysis may be a competing reaction with alkali metals.

The applicability of metal carbonyls as co-catalysts to zinc chloride was investigated in two phases, first with model compounds containing heteroatoms and second with coal.

Table 14. X-ray fluorescence analysis of dried Wyodak coal.

Element	Amount In Raw Coal	Possible Impurity to Ash
Mg	wt% 0.5 ± ---	0.88
Al	1.41 ± 0.21	2.66
Si	1.83 ± 0.27	3.92
S	0.98 ± 0.15	
Cl	0.01 ±	
K	0.07 ± 0.01	0.08
Ca	0.85 ± 0.06	1.02
Ti	0.12 ± 0.02	0.20
Fe	0.20 ± 0.01	0.26
V	ppm 120	
Cr	27 ± 7	
Mn	73 ± 6	
Ni	12 ± 1	
Cu	51 ± 2	
Zn	22 ± 2	
Ga	6 ± 1	
As	1.0 ± 0.6	
Se	2.3 ± 0.5	
Br	1.4 ± 0.5	
Rb	9 ± 1	
Sr	208 ± 8	
Hg	7 ± 1	
Pb	10 ± 2	
		9.02%

Analysis by Robert Giauque and associates, LBL (10-9-74).

A. Reactions of Metal Carbonyls and Zinc Chloride with Model Compounds Containing Heteroatoms

Single bonds between carbon and heteroatoms S, N, and O provide weak links (compared with double bonds and C-C) in the organic matrix of coal. In particular, ethers R-O-R and thioethers R-S-R are relatively susceptible to bond breaking. Thus, reduction in the effective molecular weight of coal is most easily accomplished by removal of heteroatoms. Such removal also eliminates polar interactions between adjacent structures.

These two effects combine to depolymerize coal and make it more liquid-like. Since heteroatom removal is important for both liquefaction and product quality the effect os zinc chloride with metal carbonyls was investigated on model compounds of coal containing heteroatoms.

1. Reaction of Dibenzyl Ether with Zinc Chloride and $Co_2(CO)_6(Bu_3P)_2$

The organic oxygen content of subbituminous coal, 15 to 20%, is composed of about half ether groups (C-O-C) (B5). Thus the breaking of ether bonds can be a major factor in a liquefaction process. The effect of the combined hydrogenation and cracking ability of cobalt carbonyls and zinc chloride was tested on a model compound, dibenzyl ether.

Earlier experiments by Mobley and Bell (M16) showed that when dibenzyl ether in cyclohexane was heated in the presence of zinc chloride a tar or polymer was formed. The polymerization appeared to

result from Friedel-Crafts alkylation of $C_6H_5CH_2^+$ fragments (formed by C-O-C cleavage) onto the aromatic rings of other ethers or fragments. When the reaction was conducted in an aromatic solvent (benzene) instead of an alkane (cyclohexane) the reactive fragments of the cleaved ether alkylated onto the aromatic solvent. The product formed by having benzene as solvent is diphenylmethane. In neither experiment was any toluene detected, indicating that no hydrogenation by zinc chloride takes place at these conditions.

Substituted metal carbonyl hydrogenation activity was tested by reacting 5 ml of dibenzyl in 20 ml of cyclohexane with 0.7 gm $ZnCl_2$ and 1.0 gm $Co_2(CO)_6(Bu_3P)_2$ under 760 psi 1:1 H_2/CO for 1 hr at 175°C in the Parr autoclave. The usual purge and heat-up procedures were followed as described earlier for the substitution studies. Samples taken after 1 hr were cooled and analyzed by gas chromatography (also previously described) with the Dexsil column operated at 110°C. The eluted peaks were identified by comparison to the pure compounds.

Mobley and Bell found no toluene in their experiments run at similar conditions without carbonyls. With the presence of $Co_2(CO)_6(Bu_3P)_2$ as a co-catalyst, the sample from the reactor contained about 1% toluene (5% with respect to dibenzyl ether) the rest of the dibenzyl ether was either unreacted (70%) or formed soluble and insoluble polymers. A summary of the experiments are given in Fig. 50.

175 C, 1 Hour, 600 psi H_2/CO

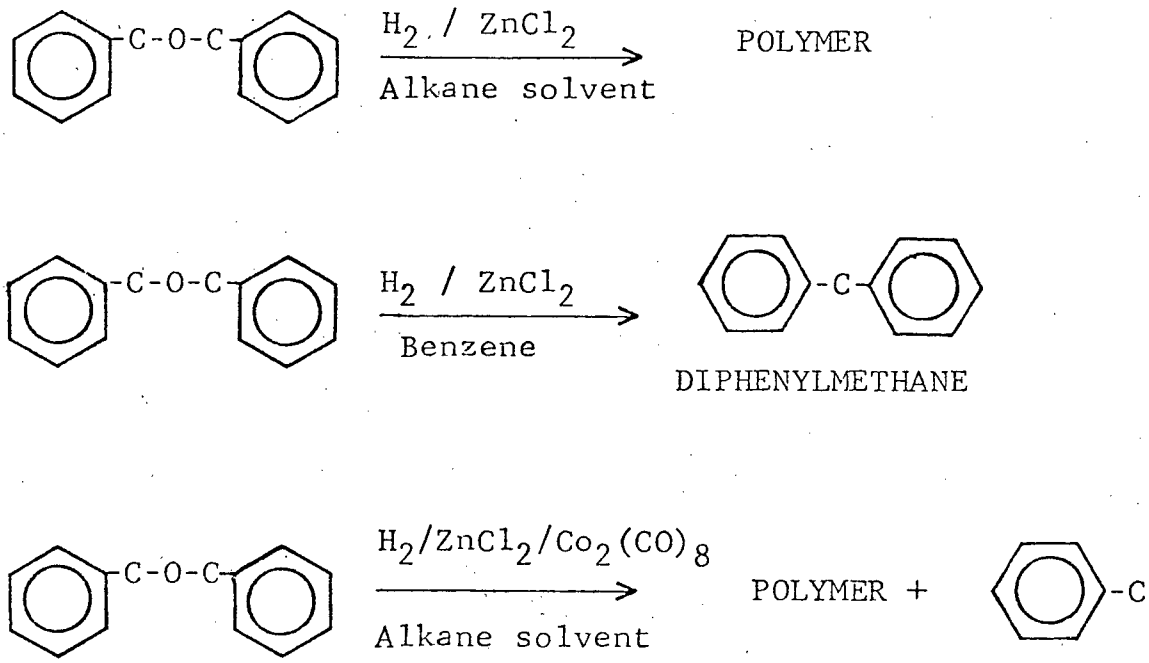

Fig. 50. Dibenzyl ether studies.

The low yield of toluene was probably due to the inability of $HCo(CO)_3Bu_3P$ to donate its acidic hydrogen H^+ to the carbonium ion formed by the zinc chloride ($C_6H_5CH_2^+$). The ability of $Mn_2(CO)_8(Bu_3P)_2$ to catalyze water-gas shift was discovered after the dibenzyl studies (see Section 3 of this chapter). Analogously, $Co_2(CO)_6(Bu_3P)_2$ catalyzed water-gas shift may have been responsible for the formation of toluene from dibenzyl ether, since water is the product of deoxygenation by a zinc chloride treatment.

In conclusion, several useful pieces of information can be gleaned from the dibenzyl ether experiments. The runs where only zinc chloride in either alkane or aromatic solvents shows that zinc chloride is effective in cleaving very reactive ether bonds and forming reactive fragments (presumably carbonium ions) which readily polymerize. The absence of toluene as a product shows that zinc chloride alone at 175°C is unable to activate molecular hydrogen and is inactive as a hydrogenating catalyst. When $Co_2(CO)_6(Bu_3P)_2$ is used in conjunction with zinc chloride toluene is found in the product showing that hydrogenation (probably via $(HCo(CO)_4Bu_3P)$ of the reactive fragments has occurred. The substituted metal carbonyls appear to be viable hydrogen-transfer agents, activating molecular hydrogen and capping off the reactive fragments.

2. Reaction of Quinoline with $Mn_2(CO)_8(Bu_3P)_2$

Nitrogen compounds in coal may pose an environmental and chemical problem in its combustion through the oxidation of the nitrogen to unwanted nitrogen oxides. The removal of nitrogen is also needed as an aid to liquefaction, because acid-base complexing of the nitrogen increases the effective molecular weight of the converted coal. Usually the nitrogen is multiply bonded so the first step in its removal is to convert the multiple bonds to single bonds by hydrogenation. Since a large fraction of nitrogen in coal is in aromatic structures, quinoline was chosen as a model structure for hydrogenation with $Mn_2(CO)_8(Bu_3P)_2$.

Hydrogenation of quinoline was carried out with $Mn_2(CO)_{10}$ and Bu_3P under the same conditions as for anthracene hydrogenation (200^oC, 600 psi synthesis gas). For 10 millimoles quinoline charged to the reactor, 86% was converted to 1,2,3,4-tetrahydroquinoline, as analyzed by gas chromatography. The peak coincided with an authentic sample (Aldrich 95%) and since no unidentified peak or shoulders were observed it appears that only the ring containing the heteroatom is hydrogenated. This is not unexpected in view of the fact that the nitrogen is able to complex to the manganese thus making the ring with heteroatom more accessible for hydrogenation.

The sample from the reactor although having the characteristic yellow of the active catalyst was slightly cloudy probably from metallic manganese resulting from catalyst decomposition. This could

have occurred in the initial substitution reaction where quinoline may have competed with Bu_3P for the $Mn_2(CO)_{10}$.

3. Water-gas Shift Catalyzed by $Mn_2(CO)_8(Bu_3P)_2$

During investigation of hydrogenation of anthracene by $Mn_2(CO)_8(Bu_3P)_2$, one run was made without hydrogen. Analysis of the reaction product showed mostly anthracene, and unexpectedly a trace amount of 9,10-dihydroanthracene. The hydrogen for the reaction could have been abstracted from the solvent, normal decane (a slow but possible reaction (K5)), from water picked up by hygroscopic $Mn_2(CO)_{10}$, or from moisture initially in the reactor.

Since it is more likely that the hydrogen came from water, an experiment was conducted with water as a possible source of hydrogen. The reactor was charged and purged as for a hydrogen-dependence study, but 10 ml of water was substituted. After 1 hr reaction at 200°C, 10% of the anthracene was converted to dihydroanthracene. This amounts to 30% of the conversion that takes place under 300 psi H_2. Analysis of the gas in the reactor by gas chromatography showed about 3% H_2 and 1% CO_2. A similar experiment without anthracene present gave the same gas analysis. Further analysis of reaction-product gases showed the presence of trace amounts of methane, ethane, propane, and butanes (<0.002%). The hydrocarbons may be a product of synthesis reaction in conjunction with the water-gas shift, but more probably they are a product of hydrocracking.

B. Reactions of Metal Carbonyls in Zinc Chloride with Coal

Two sets of experiments were carried out with coal. An experiment run with catalytic amounts of zinc chloride (1 to 2%) focused on the hydrogenation ability of the metal carbonyls. Studies with massive amounts of zinc chloride as the liquid medium for the reaction were made to test the ability of the carbonyl to function as a co-catalyst.

1. Combined Use of Minimal Zinc Chloride with Metal Carbonyls

a. Procedure. The effects of substituted metal carbonyls in conjunction with catalytic amounts of zinc chloride were studied in the same manner as was used in anthracene hydrogenation. One hundred milliliters of n-C_{10} was placed into the reactor glass liner with 20 gms each of zinc chloride and undried coal (-28 to +100 mesh). The appropriate metal carbonyl was weighed and added. The liner was placed in the reactor, and the reactor sealed and purged. Six hundred pounds per square inch H_2/CO (1:1) was added, and the reactor was heated in 15 min time to reaction temperature. After 1 hr the reactor was cooled to room temperature (within 2 min) by quenching under running tap water.

The reactor was depressurized, and the contents were filtered in a Buchner funnel. After washing with 6 liters of hot water and 40 ml cyclohexane to remove $ZnCl_2$ and decane, the reacted coal as dried overnight in a vacuum oven at 105°C.

The oven-dried coal was extracted in a Soxhlet apparatus first with toluene and then pyridine. The percent extracted is reported on a dry ash-free basis.

Three experiments were conducted at a temperature (200°C) where no thermal decomposition would occur with a monodentate ligand (Bu_3P). One blank run was made with no zinc chloride or metal carbonyl. The other two tested the effect of $Co_2(CO)_6(Bu_3P)_2$ with and without added zinc chloride. The experiments were repeated with a polydentate ligand (1,2-bis diphenylphosphino)ethane) which establizes $Co_2(CO)_8$ to a higher temperature (350°C).

The elemental analysis of the coal used in this study is given in Table 15. Undried coal contains 24 wt% moisture.

b. Results. Table 16 gives the results of reacting Wyodak subbituminous coal with zinc chloride and cobalt carbonyl. Cobalt carbonyl was used because it has the greatest hydrogenation activity. Cobalt carbonyl substituted by a polydentate ligand, such as 1,2-bis (diphenylphosphino)ethane (diphos) is stable enough to be used at high temperatures. After every experiment, the catalyst could be recovered from the reacted coal as a filtrate, indicating that neither the zinc chloride nor the coal caused decomposition.

The three experiments conducted at 200°C were at too low temperature to give a good indication of the effects of the zinc chloride and carbonyl. The reduction in toluene solubles upon addition of zinc chloride may be a result of a small reactive fraction of asphaltenes being broken down by zinc chloride to cyclohexane soluble oils. The decrease of both asphaltenes and preasphaltenes in the reaction with $Co_2(CO)_6(Bu_3P)_2$ alone may be due to the production of oils but since the reaction is run in decane there is no simple way of determining the amount of oils produced.

Table 15. Composition of Roland top-seam Wyodak sub-bituminous coal.

	Raw Coal
Carbon	59.85
Hydrogen	4.91
Nitrogen	0.98
Sulfur	0.56
Chlorine	<0.05
Ash	13.7
Oxygen (by difference)	19.95
	100.00

Analysis performed by U. C. Microlab.

Table 16. Reaction of Wyodak coal with metal carbonyls and zinc chloride.

100 ml C_{10} — Time 1 hr
20 gm $ZnCl_2$
20 gm Coal (-28 to +100 mesh)
Pressure H_2/CO (1:1) — 1030 psi at 200°, 1150 psi at 250°

Catalyst	Amount (gms)	Temperature °C	% Extracted Toluene	Pyrdine
none*		200	2.3	6.6
$Co_2(CO)_6(Bu_3P)_2$*	1.0	200	1.4	5.4
$Co_2(CO)_6(Bu_3P)_2$	1.0	200	0.5	6.2
none*		250	0.1	5.3
$Co_2(CO)_8$+diphos*	0.05,1.15	250	1.3	10.0
$Co_2(CO)_8$+diphos	0.05,1.15	250	3.6	19.5

*No $ZnCl_2$.

The experiments at 250°C are much more informative. The blank run with coal showed less than 0.1% asphaltenes and 5.3% preasphaltenes. Addition of $Co_2(CO)_8$ and diphos to the reaction mixture doubled the amount of preasphaltenes, indicating that hydrogenation of the coal structure was taking place. The zinc chloride--$CO_2(CO)_8$--diphos combination provided very effective in that the preasphaltene content of the treated coal was increased four-fold compared to the blank run. The asphaltene content was tripled. The increase in solubilities indicates that bond-breaking and hydrogenation are taking place concurrently.

2. Use of Metal Carbonyls in Zinc Chloride--Methanol Melt

a. Procedure. The procedure given in the previous section, for reacting coal in massive amounts of zinc chloride was modified by a catalyst-pretreatment step which substituted the phosphine ligand onto the metal carbonly before exposing it to zinc chloride. The high Lewis acidity of the zinc chloride would allow it to compete with the metal carbonyl for the free phosphine, if the substitution step were carried out in the melt.

Substitution of phosphine into the carbonyl was carried out in 50 ml methanol at 165°C under 750 psi H_2/CO (1:1) pressure for 1/2 hr. After cooling the bomb was opened and 50 gms Wyodak coal and 273 gms. $ZnCl_2$ were added. The bomb was sealed, purged, and pressurized to 300 psi CO and 300 psi H_2. After heating to 250°C, a pressure of 1350 psi was reached. The reaction was run for 1 hr, after which the bomb was quenched in cold water.

During quenching the bomb was slowly depressurized to limit foaming. The contents of the bomb were washed with 6 liters of hot water and filtered in a Buchner funnel. After vacuum oven-drying a 105°C, the melt-treated coal was extracted in a solvent apparatus with toluene and pyridine.

b. Results. The effect of metal carbonyl additives in melt-treatment of coal was evaluated on the basis of the amount of asphaltenes and preasphaltenes obtained compared to a blank run where no additives were used. Treatment with a combination of iron and manganese carbonyls had negligible effect on the extractability of the treated coal. There was a slight increase in solubility for the cobalt carbonyl treatment probably because of its greater hydrogenating activity.

The concentrations of substituted metal carbonyls (2 to 6% in $ZnCl_2$) did not give significant hydrogenation of the coal at these conditions it appears the major effect comes from the action of the zinc chloride-methanol alkylation and the benefits of the added carbonyl are overshadowed.

The cobalt run reported last in Table 17 shows an effect of short reaction time at higher temperature coal conversion. In this particular run the controller failed to shut off the heating mantel at 250°C and the reactor temperature shot to 300°C for 2 to 3 min before it could be cooled. The rest of the reaction was conducted in the usual manner. The temperature overshoot had a dramatic effect on solubility--86% of the original coal became pyridine soluble.

Table 17. Reaction of coal in $ZnCl_2$--Methanol melt containing metal carbonyls.

273 gm $ZnCl_2$ 50 gm MeOH 1 hour		50 gm Wyodak Coal (-28 to +100 mesh) Temp. 250° Pres. 34.3 bars H_2; 20.6 bars CO	
Additive	Amount gms	Percent % Extracted (daf) Toluene	Pyridine
none		11.8	21.1
$Fe(CO)_5$ + Bu_3P	4.6 ,12.83	11.0	24.2
$Mn_2(CO)_{10}$	5.0		
$Co_2(CO)_8$+diphos	1.71,3.98	15.6	27.3
$Co_2(CO)_8$+diphos*	1.71,3.98	29.1	57.0

*Temp. overshoot to 300°C for 2-3 min at start.

3. ESCA Analysis of Zinc Chloride Treated Coal

Raw Wyodak and zinc chloride treated Wyodak coal were analyzed by ESCA for surface composition. The treated coal was reacted in zinc chloride at 250°C for 1 hr without hydrogen. The product was extracted with cyclohexane, benzene, and pyridine. Total extraction was 15 on a moisture- and ash-free basis.

Table 18 shows the relative abundance of elements found on the surface of the extracted melt-treated coal compared to raw coal. Zinc, chlorine and nitrogen were increased from residues of treatment. An unexpected rise in surface carbon content is noted. The treated coal surface also contains less oxygen than raw coal. The oxygen in raw coal may be a product of air oxidation or ether and hydroxyl groups. The concentration of the latter should be lower for an extracted coal. All the metals contributing to coal ash have been reduced with the exception of cobalt. An especially encouraging observation is the absence of surface sulfur in the melt treated coal. The removal of sulfur may be mass transfer rather than kinetically limited.

4. Summary

In summary, several useful characteristics of metal carbonyl catalysis were demonstrated by the experiments with compounds containing heteroatoms. The substituted carbonyls are not poisoned by nitrogen, sulfur, oxygen compounds or water. The carbonyls are catalytically active for promoting water-gas shift thus being able to utilize hydrogen from water split out from ethers or moisture present

Table 18. Elements detected by ESCA on the surface of melt-treated-coal.

	Raw Coal	Melt Treated Coal
C	*	+
N	*	+
O	*	–
Na	*	0
Al	*	–
Si	*	–
S	*	0
Cl	*	+
K	*	–
Ca	*	–
Mn	*	–
Fe	*	–
Co	0	+
Ni	*	–
Zn	0	+

* detected.
\+ more than in raw coal.
– less than in raw coal.
0 not detected.

in undried coal. Finally, it is apparent that the substituted metal carbonyls are stable in both acidic and basic media even at elevated temperatures under only moderate CO pressure.

The ability of substituted metal carbonyls to form hydrides from molecular hydrogen is perhaps the most useful property for coal liquefaction. Unfortunately, the hydrides formed are acidic and are slow to add to the carbonium ions formed by Lewis acid bond cleavage by zinc chloride. The acidic environment also inhibits the base catalyzed formate mechanism of CO. Preliminary indications taken from the increase in hydrogenation activity by $Fe(CO)_4Bu_3P$ in the presence of NaOH show that a basic medium may be a more appropriate vehicle for carbonyl catalysis. Nontheless the experiments conducted with coal in the presence of zinc chloride and substituted metal carbonyls showed that hydrogenation is taking place and substituted metal carbonyls can act as co-catalysts in a zinc chloride melt.

ACKNOWLEDGEMENTS

This work has been performed under the auspices of the U. S. Department of Energy under contract No. W-7405-ENG-48, Office of Basic Energy Sciences, Division of Chemical Sciences, B&R No. KC0302O1, which support is gratefully acknowledged.

APPENDIX

The rate equations formulated for the kinetics of hydrogenation by $Mn_2(CO)_8(Bu_3P)_2$ and $RhCl(PPH_3)_3$ involve the determination of several equilibrium and rate constants. The forms of the equations were not amenable to graphical techniques or limiting condition analysis to find the values for all the constants E evaluation of the constants was done by a computer program which iterated values for the constants until a fit of the data gave a minimum standard deviation.

The strategy of the program was based on a converging matrix. Figure 51 depicts such a matrix for three constants k_{app}, K_0, and K_{HO}, for the rhodium kinetics computer program. Initial guesses for the three constants are expanded to form a 6x6x6 matrix with initial increments of k_{app}, K_0, and K_{HO}. The program searches each of the 216 values to find the best fit of the data to the kinetic equation as determined by the minimum in the sub of the deviations of the predicted rates from the measured rates. If the best fit was contained within the core of the matrix the increment size was halved and the search repeated. A minimum standard deviation on an edge of face of the matrix caused the matrix to double to encompass the value and repeat the search. The matrix, in both cases corrected itself to place the new found minimum in its center.

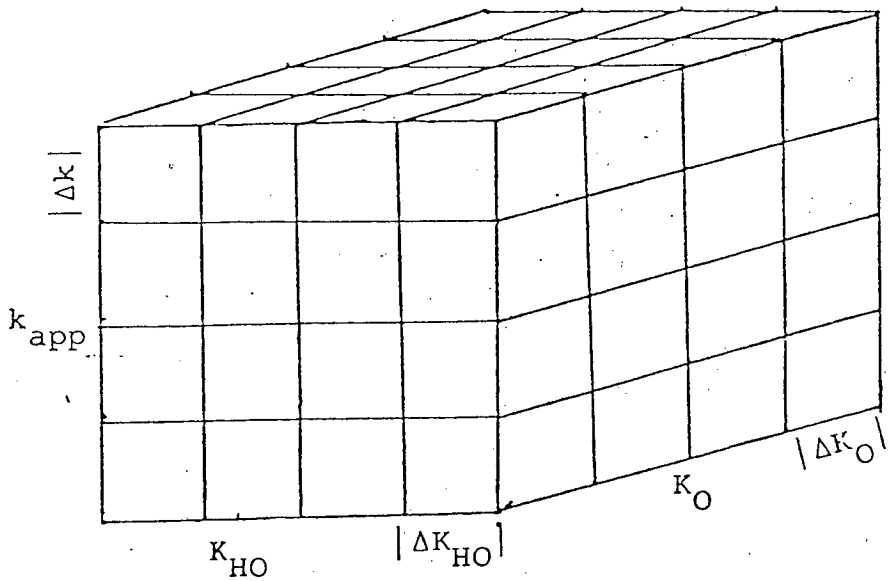

Fig. 51. Grid for fitting kinetic constants.

1. Program Olefin 2

This program was used to fit the extinction coefficients for the rhodium-olefin complex, and exemplifies the calculation procedure used to fit the other absorbance data. The results are given for a typical set of absorbance data taken at 440 nm.

```
                PROGRAM OLEFIN2 (INPUT,OUTPUT)
              C     THIS PROGRAM FITS THE ABSORBANCE DATA FOR THE OLEFIN SOLUTIONS
              C     TO THE EQUILIBRIUM SCHEME ALLOWING OLEFIN ADDITION TO EITHER
              C     ASSOCIATED OR DISSOCIATED CATALYST SPECIES. MOLAR EXTINCTION
              C     FOR THE OLEFIN COMPLEXES ARE ALLOWED TO FLOAT. EQUILB CONSTANTS
              C     HAVE UNITS OF LITERS/MOLE.
000003          DIMENSION OK2(6),OK3(6),DEL2(6),DEL3(6),A(100),C(100),EL(100),COL
               1(100),AMAX(100),O(100),P(100),Q(100),R(100),S(100),VAR(6,6,6),
               2AM(100),AC(100)
000003          READ 1000,LAMDA
000011       1000 FORMAT(I3)
000011          NDATA=8
000012          M=1
000013          MMIN=2
000014          DO 10 I=1,NDATA
000016          READ 2,C(I),EL(I),COL(I),A(I)
000031        2 FORMAT (4F10.5)
000031       10 CONTINUE
000034          READ 14,PK, EPS, DEL1
000045       14 FORMAT (3F10.5)
000045          DO 11 I=1,NDATA
000047          BZ=1.-COL(I )/9.87
000052          PK=.0014*BZ
000054          AMAX(I)=EPS*C(I)
000057          O(I)=C(I)*COL(I)
000061          P(I)=EL(I)+PK
000063          Q(I)=PK*COL(I)
000065          R(I)=EL(I)*COL(I)
000067          S(I)=4.*C(I)*PK
000072       11 CONTINUE
000074          READ 17,OK2(1),OK2SIZ,OK3(1),OK3SIZ,DEL2(1),DEL2SIZ,DEL3(1),DEL3SI
               1Z
000120          PRINT17,OK2(1),OK2SIZ,OK3(1),OK3SIZ,DEL2(1),DEL2SIZ,DEL3(1),DEL3SI
               1Z
000144       17 FORMAT(8F10.5)
000144          DO 60 III=1,5
000146           PRINT 16,OK2(1),OK2SIZ,OK3(1),OK3SIZ
000161       16 FORMAT(//*OK2 = *,F10.5,*OK1SIZ = *,F10.3,*  OK3 = *,F10.5,
               1* OK3SIZ = *,F10.3)
000161          ITER=0
000162          DO 100 J=1,6
000164          DO 20 L=2,6
000165          DO 20 K=2,6
000166          DO 20 I=2,6
000167          VAR(I,K,L) = 0.0
000175       20 CONTINUE
000203          ITER = ITER +1
000204          IF(ITER-1)6,4,4
000206        4 PRINT 21
000212       21 FORMAT(////*  JJ   DEL2(JJ)      DEL3(JJ)      OK2(JJ)      OK3(JJ)*)
000212        6 DO 30 JJ=2,6
000214          DEL2(JJ)=DEL2(JJ-1)+DEL2SIZ
000217          DEL3(JJ) = DEL3(JJ-1) + DEL3SIZ
000221          OK2(JJ)=OK2(JJ-1)+OK2SIZ
```

```
000224          OK3(JJ)=OK3(JJ-1)+OK3SIZ
000226          IF(ITER-1)30,5,5
000231        5 PRINT 22,JJ,DEL2(JJ),DEL3(JJ),OK2(JJ),OK3(JJ)
000247       22 FORMAT(2X,I2,4F12.5)
000247       30 CONTINUE
000251          DO 40 IT = 1,NDATA
000253          BZ=1.-COL(IT)/9.87
000256          T=1.+OK3(M)*COL(IT)
000261          U=P(IT)+OK3(M)*R(IT)
000264          V=2.*OK3(M)*Q(IT)/T
000270          W=S(IT)*T
000271          X=OK3(M)*COL(IT)/T
000274          DO 40 L=2,6
000275          Y=OK2(L)*COL(IT)     /BZ
000300           Z=1.+Y
000302           B=U+Q(IT)*OK2(L)          /BZ
000307          D=Z*X
000311          E=(-B+SQRT((B*B)+(W*Z)))/(T*Z)
000322          DO 40 K=2,6
000323          F=DEL3(K)*V
000325          G=DEL3(K)*D
000327          DO 40 I = 2,6
000331          H=DEL2(I)*Y+DEL1
000334          APRED=AMAX(IT)-F+(G-H)*E
000342          ERR=(A(IT)-APRED)/APRED
000344          VAR(I,K,L)=ERR*ERR+VAR(I,K,L)
000352       40 CONTINUE
000362          SMALL=VAR(2,2,2)
000364          LMIN=2
000365          KMIN=2
000366          IMIN=2
000367          DO 89 L=2,6
000370          DO 89 K=2,6
000371          DO 89 I=2,6
000372          IF(SMALL-VAR(I,K,L))87,87,88
000401       88 SMALL=VAR(I,K,L)
000407          IMIN=I
000410          KMIN=K
000411          LMIN=L
000412       87 CONTINUE
000412       89 CONTINUE
000420          PRINT 55
000424       55 FORMAT(//*        SDEV     DELTA2(I)    DELTA3(K)      OK2(L)      OK3(
                1M)     I    K    L    M*)
000424          RDELTA2 = 2.*DEL2(IMIN)
000427          RDELTA3 = DEL3(KMIN)*2.
000431          SDEV = SQRT(SMALL/(NDATA-1))
000437          PRINT 56,SDEV,RDELTA2,RDELTA3,OK2(LMIN),OK3(MMIN),IMIN,KMIN,LMIN,
                1MMIN
000464       56 FORMAT(F12.8,4F12.5,4I4)
000464          IF(DEL2SIZ)33,61,33
000465       33 IF(IMIN-2)8,8,58
000470       58 IF(IMIN-6)61,59,59
000473        8 DEL2SIZ=2.*DEL2SIZ
```

```
000475          DEL2(1)=DEL2(IMIN)-3.*DEL2SIZ
000500          IF(DEL2(1)+DEL2SIZ)2001,2001,71
000502     2001 DEL2SIZ=DEL2(IMIN)/5.
000505          DEL2(1)=DEL2(IMIN)/10.
000507          GO TO 71
000507       59 DEL2SIZ=2.*DEL2SIZ
000511          DEL2(1) = DEL2(IMIN)-3.*DEL2SIZ
000514          GO TO 71
000515       61 IF(DEL3SIZ)1,64,1
000516        1 IF(KMIN-2)9,9,3
000521        3 IF(KMIN-6)63,63,64
000524       63 DEL3SIZ = 2.*DEL3SIZ
000526          DEL3(1)=DEL3(KMIN)-3.*DEL3SIZ
000531          GO TO 73
000532        9 DEL3SIZ=2.*DEL3SIZ
000534          DEL3(1)=DEL3(KMIN)-3.*DEL3SIZ
000537          IF(DEL3(1)+DEL3SIZ)2000,2000,73
000541     2000 DEL3SIZ=DEL3(KMIN)/5.
000544          DEL3(1)=DEL3(KMIN)/10.
000546          GO TO 73
000546       64 IF(OK2SIZ)65,77,65
000547       65 IF(LMIN-2)202,202,201
000552      201 IF(LMIN-6)77 ,208,208
000555      202 OK2SIZ=2.*OK2SIZ
000557            OK2(1)=OK2(LMIN)-3.*OK2SIZ
000562          IF(OK2(1)+OK2SIZ)111,111,75
000564      111 CONTINUE
000564          OK2SIZ=OK2(LMIN)/5.
000567          OK2(1)=OK2(LMIN)/10.
000571          GO TO 75
000571      208 CONTINUE
000571          OK2SIZ=OK2SIZ*2.
000573          OK2(1)=OK2(LMIN)
000575          GO TO 75
000575       71 DEL3(1) = DEL3(KMIN)-3.*DEL3SIZ
000601          OK2(1) = OK2(LMIN)-3.*OK2SIZ
000604          IF(DEL3(1)+DEL3SIZ)601,601,600
000607      601 DEL3SIZ=DEL3(KMIN)/5.
000612          DEL3(1)=DEL3(KMIN)/10.
000614          GO TO 600
000614       73 DEL2(1) = DEL2(IMIN)-3.*DEL2SIZ
000620          OK2(1) = OK2(LMIN)-3.*OK2SIZ
000623      600 CONTINUE
000623          IF(OK2(1)+OK2SIZ)731,731,820
000626      731 CONTINUE
000626          OK2SIZ=OK2(LMIN)/5.
000631          OK2(1)=OK2(LMIN)/10.
000633          GO TO 100
000633       75 DEL2(1)=DEL2(IMIN)-3.*DEL2SIZ
000637          DEL3(1)=DEL3(KMIN)-3.*DEL3SIZ
000642      820 CONTINUE
000642      830 CONTINUE
000642          GO TO 100
000643       77 DEL2SIZ=DEL2SIZ/2.
```

```
000645          DEL3SIZ=DEL3SIZ/2.
000646          OK2SIZ=OK2SIZ/2.
000647          DEL2(I) = DEL2(IMIN)-3.*DEL2SIZ
000652          DEL3(I)=DEL3(KMIN)-3.*DEL3SIZ
000656          OK2(I) = OK2(LMIN)-3.*OK2SIZ
000661      100 CONTINUE
000663          PRINT 1001,LAMDA
000671     1001 FORMAT(//*  LAMBDA EQUALS *I3)
000671          PRINT 91,PK,EPS,DEL1
000703       91 FORMAT(////3F15.5)
000703          PRINT 92
000707       92 FORMAT(////*          C        L       COL         E         A
                1ACALC        DEV           AM/CO        AC/CO*)
000707          DO 60 I=1,NDATA
000711          BZ=1.-COL(I )/9.87
000714          T=1.+OK3(MMIN)*COL(I)
000717          U=P(I)*OK3(MMIN)*R(I)
000722          V=2.*OK3(MMIN)*O(I)/T
000726          W=S(I)*T
000727          X=OK3(MMIN)*COL(I)/T
000732          Y=OK2(LMIN)*COL(I)          /BZ
000735          Z=1.+Y
000737          B=U+OK2(LMIN)*O(I)          /BZ
000744          E=(-B+SQRT((B*B)+(W*Z)))/(T*Z)
000755          F=DEL3(KMIN)*V
000757          G=DEL3(KMIN)*Z*X
000762          H=DEL2(IMIN)*Y+DEL1
000765          ACALC=AMAX(I)-F+(G-H)*E
000773          DEV=(A(I)-ACALC)/ACALC
000775          AM(I)=A(I)/(C(I)*1000.)
001000          AC(I)=ACALC/(C(I)*1000.)
001002          BPK=P(I)-EL(I)
001004          PRINT 95,C(I),EL(I),COL(I),E,A(I),ACALC,DEV,AM(I),AC(I)
                1,BPK
001034       95 FORMAT(7F10.5,3F15.5)
001034       60 CONTINUE
001041          STOP
001043          END
```

SDEV	DELTA2(I)	DELTA3(K)	OK2(L)	OK3(M)	I	K	L	M
.02894520	848.32031	0.	1.95039	0.	5	2	2	2

JJ	DEL2(JJ)	DEL3(JJ)	OK2(JJ)	OK3(JJ)
2	424.12109	0.	1.94961	0.
3	424.14062	0.	1.95000	0.
4	424.16016	0.	1.95039	0.
5	424.17969	0.	1.95078	0.
6	424.19922	0.	1.95117	0.

SDEV	DELTA2(I)	DELTA3(K)	OK2(L)	OK3(M)	I	K	L	M
.02894520	848.32031	0.	1.95039	0.	4	2	4	2

JJ	DEL2(JJ)	DEL3(JJ)	OK2(JJ)	OK3(JJ)
2	424.14062	0.	1.95000	0.
3	424.15039	0.	1.95020	0.
4	424.16016	0.	1.95039	0.
5	424.16992	0.	1.95059	0.
6	424.17969	0.	1.95078	0.

SDEV	DELTA2(I)	DELTA3(K)	OK2(L)	OK3(M)	I	K	L	M
.02894520	848.32031	0.	1.95039	0.	4	2	4	2

JJ	DEL2(JJ)	DEL3(JJ)	OK2(JJ)	OK3(JJ)
2	424.15039	0.	1.95020	0.
3	424.15527	0.	1.95029	0.
4	424.16016	0.	1.95039	0.
5	424.16504	0.	1.95049	0.
6	424.16992	0.	1.95059	0.

SDEV	DELTA2(I)	DELTA3(K)	OK2(L)	OK3(M)	I	K	L	M
.02894520	848.33008	0.	1.95039	0.	5	2	4	2

JJ	DEL2(JJ)	DEL3(JJ)	OK2(JJ)	OK3(JJ)
2	424.16016	0.	1.95029	0.
3	424.16260	0.	1.95034	0.
4	424.16504	0.	1.95039	0.
5	424.16748	0.	1.95044	0.
6	424.16992	0.	1.95049	0.

SDEV	DELTA2(I)	DELTA3(K)	OK2(L)	OK3(M)	I	K	L	M
.02894520	848.32520	0.	1.95039	0.	3	2	4	2

JJ	DEL2(JJ)	DEL3(JJ)	OK2(JJ)	OK3(JJ)
2	424.16016	0.	1.95034	0.
3	424.16138	0.	1.95037	0.
4	424.16260	0.	1.95039	0.
5	424.16382	0.	1.95042	0.
6	424.16504	0.	1.95044	0.

SDEV	DELTA2(I)	DELTA3(K)	OK2(L)	OK3(M)	I	K	L	M
.02894520	848.33008	0.	1.95037	0.	6	2	3	2

LAMBDA EQUALS 440

.00134 1557.00000 337.00000

C	L	COL	E	A	ACALC	DEV	AM/CO	AC/CO	
.00101	0.	.59800	.00071	.93500	.95967	-.02571	.92574	.95017	.00132
.00094	.00440	1.00000	.00027	1.06700	1.12611	-.05249	1.13511	1.19799	.00126
.00106	0.	.29900	.00097	1.07000	1.07357	-.00333	1.00943	1.01280	.00136
.00086	.00359	1.28000	.00024	.98100	.96757	.01388	1.14070	1.12508	.00122
.00104	.00330	1.98000	.00022	1.10400	1.08896	.01381	1.06154	1.04707	.00112
.00121	0.	1.79000	.00039	1.03600	1.04176	-.00553	.85620	.86096	.00115
.00097	0.	.99400	.00051	.88700	.87078	.01862	.91443	.89771	.00126
.00095	.00354	.40000	.00040	1.25400	1.20467	.04095	1.32000	1.26807	.00134

2. Program Olefin 2

The object functions of the original Olefin 2 program used for absorbance calculations were replaced by trial rate equation to determine the validity of the assumed mechanism. The best fit given here, was obtained for the mechanism presented in the text. The original program has been modified to float four instead of only three variables. The results contain the data for the $Mn_2(CO)_8(Bu_3P)_2$ catalyzed hydrogenation of anthracene.

```
                PROGRAM OLEFIN2 (INPUT,OUTPUT)
000003          DIMENSION OK2(6),OK3(6),DEL2(6),DEL3(6),A(100),C(100),EL(100),COL
               1(100),AMAX(100),O(100),P(100),        R(100),        VAR(6,6,6),
               2AM(100),AC(100)
               3,VA(6),EIN(6),KIN(6),LIN(6)
               4,SMAL(6),IM(6),LM(6),KM(6),V2(6,6,6),V3(6,6,6),V4(6,6,6),
               5V5(6,6,6),V6(6,6,6)
               6,CO(100)
000003          NDATA=31
000004          DO 10 I=1,NDATA
000006          READ 2,C(I),EL(I),COL(I),A(I),CO(I)
000023        2 FORMAT(5F10.5)
000023       10 CONTINUE
000026          DO 11 I=1,NDATA
000027          COL(I)=EXP(-A(I))
000034          COL(I)=(1.-COL(I))/A(I)
000037          COL(I)=COL(I)*100.
000041       11 CONTINUE
000044          READ 17,OK2(1),OK2SIZ,OK3(1),OK3SIZ,DEL2(1),DEL2SIZ,DEL3(1),DEL3SI
               1Z
000067          PRINT17,OK2(1),OK2SIZ,OK3(1),OK3SIZ,DEL2(1),DEL2SIZ,DEL3(1),DEL3SI
               1Z
000113       17 FORMAT(8F10.5)
000113          DO 60 III=1,5
000115           PRINT 16,OK2(1),OK2SIZ,OK3(1),OK3SIZ
000130       16 FORMAT(//*OK2 = *,F10.5,*OK1SIZ = *,F10.3,*  OK3 = *,F10.5,
               1* OK3SIZ = *,F10.3)
000130          ITER=0
000131          DO 100 J=1,6
000133          DO 20 L=2,6
000134          DO 20 K=2,6
000135          DO 20 I=2,6
000136          V2(I,K,L)=0.0
000143          V3(I,K,L)=0.0
000147          V5(I,K,L)=0.0
000153          V6(I,K,L)=0.0
000157          V4(I,K,L)=0.0
000163          VAR(I,K,L) = 0.0
000167       20 CONTINUE
000175          ITER = ITER +1
000176          IF(ITER-1)6,4,4
000200        4 PRINT 21
000204       21 FORMAT(////*  JJ    DEL2(JJ)      DEL3(JJ)      OK2(JJ)      OK3(JJ)*)
000204        6 DO 30 JJ=2,6
000206          DEL2(JJ)=DEL2(JJ-1)+DEL2SIZ
000211          DEL3(JJ) = DEL3(JJ-1) + DEL3SIZ
000213          OK2(JJ)=OK2(JJ-1)+OK2SIZ
000216          OK3(JJ)=OK3(JJ-1)+OK3SIZ
000220          IF(ITER-1)30,5,5
000223        5 PRINT 22,JJ,DEL2(JJ),DEL3(JJ),OK2(JJ),OK3(JJ)
000241       22 FORMAT(2X,I2,4F12.5)
000241       30 CONTINUE
000243          DO 40 IT = 1,NDATA
000245          DO 40 M=2,6
```

```
000246          DO 40 L=2,6
000247          DO 40 K=2,6
000250          DO 40 I = 2,6
000251          Z=OK2(L)*C(IT)*EL(IT)**.5 *C(IT)
000260          V=1.+       DEL2(I)*EL(IT)/CO(IT)+DEL3(K)*COL(IT)/EL(IT)**.5
000275          D=(CO(IT)    /EL(IT)+OK3(M)*C(IT)/V)*V*V
000303          APRED=Z/D
000305          ERR=(A(IT)-APRED)/APRED
000307          IF(M-2)300,301,300
000311      301 V2(I,K,L)=ERR*ERR+V2(I,K,L)
000320          GO TO 320
000321      300 IF(M-3)303,302,303
000323      302 V3(I,K,L)=ERR*ERR+V3(I,K,L)
000332          GO TO 320
000333      303 IF(M-4)304,305,304
000335      305 V4(I,K,L)=ERR*ERR+V4(I,K,L)
000344          GO TO 320
000345      304 IF(M-5)306,307,306
000347      307 V5(I,K,L)=ERR*ERR+V5(I,K,L)
000356          GO TO 320
000357      306 IF(M-6)320,308,320
000361      308 V6(I,K,L)=ERR*ERR+V6(I,K,L)
000370      320 CONTINUE
000370       40 CONTINUE
000403          SMAL(2)=V2(2,2,2)
000404          SMAL(3)=V3(2,2,2)
000406          SMAL(4)=V4(2,2,2)
000407          SMAL(5)=V5(2,2,2)
000411          SMAL(6)=V6(2,2,2)
000412          DO 316 M=2,6
000414          IM(M)=2
000416          LM(M)=2
000417          KM(M)=2
000421      316 CONTINUE
000422          DO 311 M=2,6
000424          DO 311 L=2,6
000425          DO 311 K=2,6
000426          DO 311 I=2,6
000427          IF(M-2)309,310,309
000431      310 IF(SMAL(M)-V2(I,K,L))311,311,317
000441      317 CONTINUE
000441          IM(M)=I
000443          KM(M)=K
000445          LM(M)=L
000446          SMAL(M)=V2(I,K,L)
000454          GO TO 311
000455      309 IF(M-3)318,324,318
000457      324 IF(SMAL(M)-V3(I,K,L))311,311,319
000467      319 CONTINUE
000467          IM(M)=I
000471          KM(M)=K
000473          LM(M)=L
000474          SMAL(M)=V3(I,K,L)
000502          GO TO 311
```

```
000503      318 IF(M-4)322,323,322
000505      323 IF(SMAL(M)-V4(I,K,L))311,311,321
000515      321 CONTINUE
000515          IM(M)=I
000517          KM(M)=K
000521          LM(M)=L
000522          SMAL(M)=V4(I,K,L)
000530          GO TO 311
000531      322 IF(M-5)325,326,325
000533      326 IF(SMAL(M)-V5(I,K,L))311,311,327
000543      327 CONTINUE
000543          IM(M)=I
000545          KM(M)=K
000547          LM(M)=L
000550          SMAL(M)=V5(I,K,L)
000556          GO TO 311
000557      325 IF(M-6)311,328,311
000561      328 IF(SMAL(M)-V6(I,K,L))311,311,329
000571      329 CONTINUE
000571          IM(M)=I
000573          KM(M)=K
000575          LM(M)=L
000576          SMAL(M)=V6(I,K,L)
000604      311 CONTINUE
000614          SMALL=SMAL(2)
000616          MMIN=2
000617          IMIN=IM(2)
000620          KMIN=KM(2)
000622          LMIN=LM(2)
000623          DO 330 M=2,6
000625          PRINT 340,SMAL(M),M
000634      340 FORMAT(F12.8,I4)
000634          IF(SMALL-SMAL(M))331,331,332
000637      332 SMALL=SMAL(M)
000641          IMIN=IM(M)
000643          KMIN=KM(M)
000644          LMIN=LM(M)
000646          MMIN=M
000647      331 CONTINUE
000647      330 CONTINUE
000651          PRINT 55
000655       55 FORMAT(//*        SDEV     DELTA2(I)    DELTA3(K)      OK2(L)      OK3(
           1M)     I   K   L   M*)
000655          RDELTA2=DEL2(IMIN)
000657          RDELTA3=DEL3(KMIN)
000661          SDEV = SQRT(SMALL/(NDATA-1))
000670          PRINT 56,SDEV,RDELTA2,RDELTA3,OK2(LMIN),OK3(MMIN),IMIN,KMIN,LMIN,
           1MMIN
000715       56 FORMAT(F12.8,4F12.5,4I4)
000715          IF(IMIN-2)59,59,58
000720       58 IF(IMIN-6)61,59,59
000723       59 DEL2SIZ=2.*DEL2SIZ
000725          DEL2(1) = DEL2(IMIN)-3.*DEL2SIZ
000730          IF(DEL2(1)+DEL2SIZ)1,1,71
```

```
000732       1 DEL2SIZ=DEL2(IMIN)/5.
000735         DEL2(1)=DEL2(IMIN)/10.
000737         GO TO 71
000737      61 IF(KMIN-2)63,63,62
000742      62 IF(KMIN-6)64,63,63
000745      63 DEL3SIZ = 2.*DEL3SIZ
000747         DEL3(1)=DEL3(KMIN)-3.*DEL3SIZ
000752         IF(DEL3(1)+DEL3SIZ)7,7,73
000754       7 DEL3SIZ=DEL3(KMIN)/5.
000757         DEL3(1)=DEL3(KMIN)/10.
000761         GO TO 73
000761      64 IF(LMIN-2)202,202,201
000764     201 IF(LMIN-6)203,208,208
000767     203 IF(MMIN-2)205,205,204
000772     204 IF(MMIN-6)77,206,206
000775     202 OK2SIZ=2.*OK2SIZ
000777          OK2(1)=OK2(LMIN)-3.*OK2SIZ
001002         IF(OK2(1)+OK2SIZ)111,111,75
001004     111 CONTINUE
001004         OK2SIZ=OK2(LMIN)/5.
001007         OK2(1)=OK2(LMIN)/10.
001011         GO TO 75
001011     208 CONTINUE
001011         OK2SIZ=OK2SIZ*2.
001013         OK2(1)=OK2(LMIN)
001015         GO TO 75
001015     206 OK3SIZ=OK3SIZ*2.
001017         OK3(1)=OK3(MMIN)
001021         GO TO 200
001021     205 OK3SIZ=OK3SIZ*2.
001023         OK3(1)=OK3(MMIN)-3.*OK3SIZ
001026         IF(OK3(1)+OK3SIZ)112,112,200
001030     112 CONTINUE
001030         OK3SIZ=OK3(MMIN)/5.
001033         OK3(1)=OK3(MMIN)/10.
001035         GO TO 200
001035     200 DEL2(1)=DEL2(IMIN)-3.*DEL2SIZ
001041         DEL3(1)=DEL3(KMIN)-3.*DEL3SIZ
001044         OK2(1)=OK2(LMIN)-3.*OK2SIZ
001050         IF(OK2(1)+OK2SIZ)815,815,100
001052     815 CONTINUE
001052         OK2SIZ=OK2(LMIN)/5.
001055         OK2(1)=OK2(LMIN)/10.
001057         GO TO 100
001057      71 DEL3(1) = DEL3(KMIN)-3.*DEL3SIZ
001063         OK3(1)=OK3(MMIN)-3.*OK3SIZ
001066         OK2(1) = OK2(LMIN)-3.*OK2SIZ
001072         GO TO 600
001072      73 DEL2(1) = DEL2(IMIN)-3.*DEL2SIZ
001076         OK3(1)=OK3(MMIN)-3.*OK3SIZ
001101         OK2(1) = OK2(LMIN)-3.*OK2SIZ
001105     600 CONTINUE
001105         IF(OK2(1)+OK2SIZ)731,731,820
001110     731 CONTINUE
```

```
001110          OK2SIZ=OK2(LMIN)/5.
001113          OK2(1)=OK2(LMIN)/10.
001115      820 IF(OK3(1)+OK3SIZ)821,821,100
001120      821 CONTINUE
001120          OK3SIZ=OK3(MMIN)/5.
001123          OK3(1)=OK3(MMIN)/10.
001125          GO TO 100
001125       75 DEL2(1)=DEL2(IMIN)-3.*DEL2SIZ
001131          DEL3(1)=DEL3(KMIN)-3.*DEL3SIZ
001134          OK3(1)=OK3(MMIN)-3.*OK3SIZ
001140          IF(OK3(1)+OK3SIZ)830,830,100
001142      830 CONTINUE
001142          OK3SIZ=OK3(MMIN)/5.
001145          OK3(1)=OK3(MMIN)/10.
001147          GO TO 100
001147       77 DEL2SIZ=DEL2SIZ/2.
001151          DEL3SIZ=DEL3SIZ/2.
001152          OK2SIZ=OK2SIZ/2.
001153          OK3SIZ = OK3SIZ/2.
001154          DEL2(1) = DEL2(IMIN)-3.*DEL2SIZ
001157          DEL3(1)=DEL3(KMIN)-3.*DEL3SIZ
001163          OK2(1) = OK2(LMIN)-3.*OK2SIZ
001166          OK3(1)= OK3(MMIN)-3.*OK3SIZ
001172      100 CONTINUE
001174          PRINT 92
001200       92 FORMAT(////*    MN2            HYD     ANTH        E         R EXP
                 1R CALC       DEV              CO        AC/CO*)
001200          DO 60 I=1,NDATA
001202          ZZ=OK2(LMIN)*C(I)*EL(I)**.5 *C(I)
001210          V=1.+       DEL2(IMIN)*EL(I)/CO(I)+DEL3(KMIN)*COL(I)/EL(I)**.5
001225          DD=(CO(I)    /EL(I)+OK3(MMIN)*C(I)/V)*V*V
001233          ACALC=ZZ/DD
001235          DEV=(A(I)-ACALC)/ACALC
001237          AM(I)=A(I)/(C(I)*1000.)
001242          AC(I)=ACALC/(C(I)*1000.)
001245          E=X
001246          E=C(I)/V
001250          Q=CO(I)
001252          PRINT 95,C(I),EL(I),COL(I),E,A(I),ACALC,DEV,CO(I),AC(I)
001277       95 FORMAT(7F10.5,2F15.5)
001277       60 CONTINUE
001304          STOP
001306          END
```

JJ	DEL2(JJ)	DEL3(JJ)	OK2(JJ)	OK3(JJ)
2	.61172	.33984	.02275	3.41152
3	.61219	.34008	.02276	3.41191
4	.61266	.34031	.02277	3.41230
5	.61312	.34055	.02278	3.41270
6	.61359	.34078	.02279	3.41309

.34624704	2
.34624779	3
.34624846	4
.34624895	5
.34624988	6

SDEV	DELTA2(I)	DELTA3(K)	OK2(L)	OK3(M)	I	K	L	M
.10743169	.61172	.34008	.02275	3.41152	2	3	2	2

JJ	DEL2(JJ)	DEL3(JJ)	OK2(JJ)	OK3(JJ)
2	.60984	.33961	.02272	3.41074
3	.61078	.33984	.02273	3.41113
4	.61172	.34008	.02275	3.41152
5	.61266	.34031	.02276	3.41191
6	.61359	.34055	.02277	3.41230

.34624504	2
.34624568	3
.34624695	4
.34624779	5
.34624846	6

SDEV	DELTA2(I)	DELTA3(K)	OK2(L)	OK3(M)	I	K	L	M
.10743138	.61172	.33984	.02273	3.41074	4	3	3	2

JJ	DEL2(JJ)	DEL3(JJ)	OK2(JJ)	OK3(JJ)
2	.60984	.33937	.02271	3.40918
3	.61078	.33961	.02272	3.40996
4	.61172	.33984	.02273	3.41074
5	.61266	.34008	.02275	3.41152
6	.61359	.34031	.02276	3.41230

.34624166	2
.34624384	3
.34624504	4
.34624695	5
.34624898	6

SDEV	DELTA2(I)	DELTA3(K)	OK2(L)	OK3(M)	I	K	L	M
.10743086	.61172	.33984	.02272	3.40918	4	4	3	2

JJ	DEL2(JJ)	DEL3(JJ)	CK2(JJ)	CK3(JJ)
2	.60984	.33937	.02270	3.40605
3	.61078	.33961	.02271	3.40762
4	.61172	.33984	.02272	3.40918
5	.61266	.34008	.02273	3.41074
6	.61359	.34031	.02275	3.41230

.34623557	2
.34623924	3
.34624166	4
.34624504	5
.34624903	6

SDEV	DELTA2(I)	DELTA3(K)	OK2(L)	OK3(M)	I	K	L	M
.10742991	.61172	.33961	.02270	3.40605	4	3	2	2

MN2	HYD	ANTH	E	R EXP	R CALC	DEV	CO	AC/CO
1.00000	750.00000	98.31910	.24665	.03400	.03223	.05498	250.00000	.00003
2.00000	750.00000	95.96247	.49687	.08300	.07576	.09552	250.00000	.00004
10.00000	750.00000	80.52708	2.60841	.45000	.45885	-.01928	250.00000	.00005
20.00000	750.00000	65.93670	5.47522	.90000	.98174	-.08326	250.00000	.00005
60.00000	750.00000	32.58541	18.52286	2.90000	3.36286	-.13764	250.00000	.00006
10.00000	105.00000	94.37163	2.28069	.11700	.11921	-.01853	250.00000	.00001
10.00000	135.00000	92.63537	2.47650	.15500	.15724	-.01426	250.00000	.00002
10.00000	160.00000	91.51655	2.59836	.18000	.18617	-.03314	250.00000	.00002
10.00000	210.00000	88.77715	2.78214	.24300	.23870	.01802	250.00000	.00002
10.00000	290.00000	85.57843	2.92719	.32000	.30577	.04654	250.00000	.00003
10.00000	750.00000	80.52708	2.60841	.45000	.45885	-.01928	250.00000	.00005
10.00000	860.00000	80.30398	2.47870	.45600	.46832	-.02630	250.00000	.00005
10.00000	975.00000	79.78675	2.35102	.47000	.47406	-.00855	250.00000	.00005
10.00000	1090.00000	79.60315	2.22919	.47500	.47610	-.00230	250.00000	.00005
10.00000	430.00000	83.11648	2.92964	.38200	.38257	-.00150	250.00000	.00004
10.00000	305.00000	83.97890	2.95915	.36000	.31851	.13027	250.00000	.00003
10.00000	600.00000	81.76956	2.77638	.41700	.43410	-.03939	250.00000	.00004
1.00000	290.00000	99.10538	.27870	.01800	.01540	.16861	290.00000	.00002
2.00000	290.00000	98.41693	.55953	.03200	.04165	-.23166	290.00000	.00002
2.50000	290.00000	97.58953	.70266	.04900	.05624	-.12880	290.00000	.00002
5.00000	290.00000	96.69624	1.42849	.11000	.13448	-.18203	290.00000	.00003
10.00000	290.00000	85.05400	3.02305	.33300	.31272	.06486	290.00000	.00003
13.30000	290.00000	77.26884	4.21866	.54000	.44762	.20637	290.00000	.00003
15.00000	290.00000	75.33368	4.81686	.59600	.51526	.15670	290.00000	.00003
30.00000	290.00000	52.99113	11.24228	1.44000	1.24342	.15810	290.00000	.00004
10.00000	395.00000	83.97880	2.93987	.36000	.36624	-.01704	250.00000	.00004
10.00000	395.00000	83.58532	3.09243	.37000	.38205	-.03154	300.00000	.00004
10.00000	395.00000	84.77343	3.34949	.34000	.40337	-.15709	450.00000	.00004
10.00000	395.00000	83.38953	3.66195	.37500	.41801	-.10288	790.00000	.00004
10.00000	395.00000	83.58532	3.68658	.37000	.41686	-.11240	850.00000	.00004
10.00000	395.00000	83.19437	3.77114	.38000	.41385	-.08179	1050.00000	.00004

K2 = .02263OK1SIZ = .000 OK3 = 3.40137 OK3SIZ = .002

3. Program Kinetic

This program identical in logic to Olefin 2, was used to determine k_{app} and K_{HO} for the rhodium mechanism presented in Fig. 45. Differential rate data from three sources is included (H7,06,01). Two models were tested with K_{HO} allowed to float or set to zero; based on the results of the fit of the data compelling evidence shows that the mechanism of cyclohexene hydrogenation proceeds through a rhodium-olefin-dihydride intermediate.

```
                PROGRAM KINETIC (INPUT,OUTPUT)
000003          DIMENSION OK2(6),OK3(6),DEL2(6),DEL3(6), VAR(6,6,6),
                1A(400),C(400),EL(400),COL(400),AMAX(400),H(400),
                2R(400),C2(400),H2(400),EL2(400)
000003          NDATA=295
000004          M=1
000005          MMIN=2
000006          DO 10 I=1,NDATA
000010          READ 2,C2(I),EL2(I),H2(I),COL(I),R(I)
000025        2 FORMAT(5F10.5)
000025          H(I)=H2(I)/26200.
000030          C(I)=C2(I)/1000.
000032          EL(I)=EL2(I)/1000.
000033          A(I)=R(I)/1000.
000035       10 CONTINUE
000037          READ 2,OLK,OK,EPS,HLK,HK
000055          TK=EPS*HK/HLK
000060          READ 17,OK2(1),OK2SIZ,OK3(1),OK3SIZ,DEL2(1),DEL2SIZ,DEL3(1),DEL3SI
                1Z
000103          PRINT17,OK2(1),OK2SIZ,OK3(1),OK3SIZ,DEL2(1),DEL2SIZ,DEL3(1),DEL3SI
                1Z
000127       17 FORMAT(8F10.5)
000127          DO 60 III=1,5
000131           PRINT 16,OK2(1),OK2SIZ,OK3(1),OK3SIZ
000144       16 FORMAT(//*OK2 = *,F10.5,*OK1SIZ = *,F10.3,*  OK3 = *,F10.5,
                1* OK3SIZ = *,F10.3)
000144          ITER=0
000145          DO 100 J=1,6
000147          DO 20 L=2,6
000150          DO 20 K=2,6
000151          DO 20 I=2,6
000152          VAR(I,K,L) = 0.0
000160       20 CONTINUE
000166          ITER = ITER +1
000167          IF(ITER-1)6,4,4
000171        4 PRINT 21
000175       21 FORMAT(////*  JJ    DEL2(JJ)      DEL3(JJ)      OK2(JJ)      OK3(JJ)*)
000175        6 DO 30 JJ=2,6
000177          DEL2(JJ)=DEL2(JJ-1)+DEL2SIZ
000202          DEL3(JJ) = DEL3(JJ-1) + DEL3SIZ
000204          OK2(JJ)=OK2(JJ-1)+OK2SIZ
000207          OK3(JJ)=OK3(JJ-1)+OK3SIZ
000211          IF(ITER-1)30,5,5
000214        5 PRINT 22,JJ,DEL2(JJ),DEL3(JJ),OK2(JJ),OK3(JJ)
000232       22 FORMAT(2X,I2,4F12.5)
000232       30 CONTINUE
000234          DO 40 IT = 1,NDATA
000236          DO 40 K=2,6
000237          DO 40 L=2,6
000240          DO 40 I = 2,6
000241          BZ=1.-COL(IT)/9.87
000245          EPS=EPS*BZ
000246          OK=OK/BZ
000247          Q=1.+HLK*H(IT)+OLK*COL(IT)
```

```
000255          V=(EPS+EPS*OK*COL(IT)+CK2(L)*H(IT)*COL(IT)       )*(EL(IT)+C(IT))
000266          S= V/(EL(IT)+C(IT))-EL(IT)*0
000273          X=(-S+SQRT(S*S+4.*0*V))/(2.*0)
000305          D=X*EPS+HLK*X*H(IT)+EPS*OK*COL(IT)+
               1OK2(L)*H(IT)*COL(IT)
000317          Z=DEL2(I)*H(IT)*COL(IT)*C(IT)
000323          Z=Z*BZ*11.25
000325          APRED=Z/D
000327          EPS=EPS/BZ
000330          OK=OK*BZ
000331          ERR=(A(IT)-APRED)/APRED
000334          VAR(I,K,L)=ERR*ERR+VAR(I,K,L)
000343       40 CONTINUE
000353          SMALL=VAR(2,2,2)
000355          LMIN=2
000356          KMIN=2
000357          IMIN=2
000360          DO 89 L=2,6
000361          DO 89 K=2,6
000362          DO 89 I=2,6
000363          IF(SMALL-VAR(I,K,L))87,87,88
000372       88 SMALL=VAR(I,K,L)
000400          IMIN=I
000401          KMIN=K
000402          LMIN=L
000403       87 CONTINUE
000403       89 CONTINUE
000411          PRINT 55
000415       55 FORMAT(//*        SDEV     DELTA2(I)    DELTA3(K)      OK2(L)      OK3(
             1M)      I   K   L   M*)
000415          RDELTA2=DEL2(IMIN)
000417          RDELTA3=DEL3(KMIN)
000421          SDEV = SQRT(SMALL/(NDATA-1))
000430          PRINT 56,SDEV,RDELTA2,RDELTA3,OK2(LMIN),OK3(MMIN),IMIN,KMIN,LMIN,
             1MMIN
000455       56 FORMAT(F12.8,4F12.5,4I4)
000455          IF(DEL2SIZ)13,61,13
000456       13 CONTINUE
000456          IF(IMIN-2)8,8,58
000461       58 IF(IMIN-6)61,59,59
000464        8 DEL2SIZ=2.*DEL2SIZ
000466          DEL2(1)=DEL2(IMIN)-3.*DEL2SIZ
000471          IF(DEL2(1)+DEL2SIZ)2001,2001,71
000473     2001 DEL2SIZ=DEL2(IMIN)/5.
000476          DEL2(1)=DEL2(IMIN)/10.
000500          GO TO 71
000500       59 DEL2SIZ=2.*DEL2SIZ
000502          DEL2(1) = DEL2(IMIN)-3.*DEL2SIZ
000505          GO TO 71
000506       61 IF(DEL3SIZ)1,67,1
000507        1 IF(KMIN-2)9,9,3
000512        3 IF(KMIN-6)67,63,63
000515       63 DEL3SIZ = 2.*DEL3SIZ
000517          DEL3(1)=DEL3(KMIN)-3.*DEL3SIZ
```

```
000522          GO TO 73
000523        9 DEL3SIZ=2.*DEL3SIZ
000525          DEL3(1)=DEL3(KMIN)-3.*DEL3SIZ
000530          IF(DEL3(1)+DEL3SIZ)2000,2000,73
000532     2000 DEL3SIZ=DEL3(KMIN)/5.
000535          DEL3(1)=DEL3(KMIN)/10.
000537          GO TO 73
000537       67 IF(OK2SIZ)64,77,64
000540       64 IF(LMIN-2)202,202,201
000543      201 IF(LMIN-6)77 ,208,208
000546      202 OK2SIZ=2.*OK2SIZ
000550           OK2(1)=OK2(LMIN)-3.*OK2SIZ
000553          IF(OK2(1)+OK2SIZ)111,111,75
000555      111 CONTINUE
000555          OK2SIZ=OK2(LMIN)/5.
000560          OK2(1)=OK2(LMIN)/10.
000562          GO TO 75
000562      208 CONTINUE
000562          OK2SIZ=OK2SIZ*2.
000564          OK2(1)=OK2(LMIN)
000566          GO TO 75
000566       71 DEL3(1) = DEL3(KMIN)-3.*DEL3SIZ
000572          OK2(1) = OK2(LMIN)-3.*OK2SIZ
000575          IF(DEL3(1)+DEL3SIZ)601,601,600
000600      601 DEL3SIZ=DEL3(KMIN)/5.
000603          DEL3(1)=DEL3(KMIN)/10.
000605          GO TO 600
000605       73 DEL2(1) = DEL2(IMIN)-3.*DEL2SIZ
000611          OK2(1) = OK2(LMIN)-3.*OK2SIZ
000614      600 CONTINUE
000614          IF(OK2(1)+OK2SIZ)731,731,820
000617      731 CONTINUE
000617          OK2SIZ=OK2(LMIN)/5.
000622          OK2(1)=OK2(LMIN)/10.
000624          GO TO 100
000624       75 DEL2(1)=DEL2(IMIN)-3.*DEL2SIZ
000630          DEL3(1)=DEL3(KMIN)-3.*DEL3SIZ
000633      820 CONTINUE
000633      830 CONTINUE
000633          GO TO 100
000634       77 DEL2SIZ=DEL2SIZ/2.
000636          DEL3SIZ=DEL3SIZ/2.
000637          OK2SIZ=OK2SIZ/2.
000640          DEL2(1) = DEL2(IMIN)-3.*DEL2SIZ
000643          DEL3(1)=DEL3(KMIN)-3.*DEL3SIZ
000647          OK2(1) = OK2(LMIN)-3.*CK2SIZ
000652      100 CONTINUE
000654          PRINT 7
000660        7 FORMAT(////*    KOL         KO          KL          KHL          KH
                1          *)
000660          PRINT 11,OLK,OK,EPS,HLK,HK
000676       11 FORMAT(5E11.4)
000676          PRINT 92
000702       92 FORMAT (////*    RHO      LIGAND      HYD      OLEFIN      R EXP
```

```
C                IF CALC    DEV    FREE LIGAND *)
000702           DO 60 I=1,NDATA
000704           BZ=1.-COL(I )/9.87
000707           EPS=EPS*BZ
000711           OK=OK/BZ
000712           Q=1.+HLK*H(I)+OLK*COL(I)
000717           V=(EPS+EPS*OK*COL(I)+OK2(LMIN)*H(I)*COL(I)       )*(EL(I)+C(I))
000731           S= V/(EL(I)+C(I))-EL(I)*Q
000736           X=(-S+SQRT(S*S+4.*Q*V))/(2.*Q)
000750           DD=X+EPS+HLK*X*H(I)+EPS*OK*COL(I)
                1+OK2(LMIN)*H(I)*COL(I)
000762           ZZ=DEL2(IMIN)*H(I)*COL(I)*C(I)
000766           ZZ=ZZ*BZ*11.25
000770           ACALC=ZZ/DD
000772           EPS=EPS/BZ
000773           OK=OK*BZ
000774           DEV=(A(I)-ACALC)/ACALC
000777           ACALC=ZZ/DD*1000.
001002           X=X*1000.
001003           PRINT 95,C2(I),EL2(I),H2(I),COL(I),R(I),ACALC,DEV,X
001026        95 FORMAT(8F10.5)
001026        60 CONTINUE
001033           STOP
001035           END
```

4. Experimental Rate Data

All the experimental rate data available on cyclohexene hydrogenation is tabulated here. The first 193 rates were obtained in this study. The next 68 rates were obtained from Osborn and associates. The predicted rates were calculated from the constants in Model 1. The units of the data are: Rh-M$\underline{m}$, L_o-m$\underline{M}$, H_2-cmHg, Ol-$\underline{M}$, R and Rpred-m$\underline{M}$/sec.

SDEV	DELTA2(I)	DELTA3(K)	CK2(L)	OK3(M)	I	K	L	M
.13393891	.09954	0.	.85000	0.	5	2	2	2

JJ	DEL2(JJ)	DEL3(JJ)	OK2(JJ)	OK3(JJ)
2	.09954	0.	.85000	0.
3	.09954	0.	.85000	0.
4	.09954	0.	.85000	0.
5	.09954	0.	.85000	0.
6	.09954	0.	.85000	0.

SDEV	DELTA2(I)	DELTA3(K)	OK2(L)	OK3(M)	I	K	L	M
.13393891	.09954	0.	.85000	0.	2	2	2	2

JJ	DEL2(JJ)	DEL3(JJ)	OK2(JJ)	OK3(JJ)
2	.09954	0.	.85000	0.
3	.09954	0.	.85000	0.
4	.09954	0.	.85000	0.
5	.09954	0.	.85000	0.
6	.09954	0.	.85000	0.

SDEV	DELTA2(I)	DELTA3(K)	OK2(L)	OK3(M)	I	K	L	M
.13393891	.09954	0.	.85000	0.	2	2	2	2

KOL	KO	KL	KHL	KH
0.	2.0000	.0014	14400.0000	600.0000

RHO	LIGAND	HYD	OLEFIN	R EXP	R CALC	DEV	FREE LIGAND
.23000	0.	84.00000	1.63000	.06700	.06704	-.00062	.13963
.23000	0.	67.00000	1.57000	.05600	.06034	-.07193	.14342
.23000	0.	51.00000	1.52000	.05000	.05250	-.04753	.14899
.23000	0.	31.00000	1.45000	.04100	.03922	.04531	.16065
.23000	0.	22.00000	1.42000	.03100	.03128	-.00897	.16934
.23000	0.	84.00000	1.32000	.06400	.06398	.00037	.13256
.23000	0.	67.00000	1.25000	.05500	.05714	-.03745	.13599
.23000	0.	51.00000	1.19000	.04700	.04934	-.04741	.14129
.23000	0.	31.00000	1.12000	.03100	.03661	-.15312	.15314
.23000	0.	84.00000	1.02000	.05600	.05922	-.05434	.12428
.23000	0.	67.00000	.93000	.04500	.05190	-.13294	.12680
.23000	0.	31.00000	.80000	.02500	.03235	-.22714	.14384
1.30000	1.30000	84.00000	1.76000	.09600	.08397	.14467	1.47566
1.30000	1.30000	67.00000	1.70000	.08600	.07943	.08276	1.48950

1.30000	1.30000	51.00000	1.65000	.07500	.07432	.00909	1.51131
1.30000	1.30000	31.00000	1.57000	.05900	.06433	-.08292	1.56305
1.30000	1.30000	22.00000	1.54000	.05200	.05742	-.09443	1.60977
1.30000	1.30000	84.00000	1.48000	.08300	.07523	.10323	1.45603
1.30000	1.30000	67.00000	1.42000	.07500	.07093	.05731	1.46833
1.30000	1.30000	51.00000	1.37000	.06600	.06619	-.00289	1.48811
1.30000	1.30000	31.00000	1.29000	.05600	.05711	-.01936	1.53547
1.30000	1.30000	84.00000	1.22000	.07400	.06589	.12312	1.43676
1.30000	1.30000	67.00000	1.16000	.06500	.06171	.05335	1.44746
1.30000	1.30000	22.00000	1.00000	.04100	.04388	-.06561	1.54779
1.30000	1.30000	84.00000	.95000	.05800	.05468	.06073	1.41556
1.30000	1.30000	67.00000	.89000	.05400	.05060	.06727	1.42438
1.30000	1.30000	51.00000	.84000	.05200	.04652	.11780	1.43948
1.30000	1.30000	31.00000	.76000	.04000	.03921	.02027	1.47652
1.30000	1.30000	84.00000	.69000	.05000	.04227	.18286	1.39383
1.30000	1.30000	67.00000	.63000	.04200	.03824	.09844	1.40061
1.30000	1.30000	51.00000	.58000	.03800	.03444	.10342	1.41291
1.30000	1.30000	41.00000	.54000	.03300	.03136	.05231	1.42459
1.30000	1.30000	31.00000	.50000	.02900	.02793	.03825	1.44354
1.30000	1.30000	22.00000	.47000	.02500	.02455	.01816	1.47413
1.33000	1.33000	84.00000	1.60000	.08900	.07947	.11985	1.49534
1.33000	1.33000	67.00000	1.54000	.08300	.07512	.10493	1.50844
1.33000	1.33000	51.00000	1.48000	.07100	.06993	.01530	1.52847
1.33000	1.33000	31.00000	1.40000	.05800	.06049	-.04124	1.57814
1.33000	1.33000	84.00000	1.29000	.07400	.06882	.07528	1.47264
1.33000	1.33000	67.00000	1.23000	.06600	.06461	.02153	1.48387
1.33000	1.33000	51.00000	1.17000	.06200	.05976	.03750	1.50135
1.33000	1.33000	31.00000	1.09000	.05000	.05135	-.02632	1.54559
1.34000	1.34000	31.00000	1.33000	.05400	.05871	-.08020	1.58154
.97000	0.	86.00000	.26000	.07000	.06955	.00650	.21052
.97000	0.	75.00000	.23000	.06300	.06007	.04872	.21449
.97000	0.	60.00000	.17000	.04700	.04310	.09058	.21957
.94000	0.	65.00000	.18000	.05700	.04601	.23886	.21162
.94000	0.	50.00000	.13000	.03500	.03112	.12474	.22207
.94000	0.	40.00000	.10000	.02300	.02212	.03969	.23473
1.32000	0.	86.00000	1.70000	.22500	.21380	.05240	.44072
1.32000	0.	75.00000	1.66000	.21300	.20237	.05251	.45044
1.32000	0.	65.00000	1.62000	.19400	.19040	.01890	.46173
1.32000	0.	60.00000	1.60000	.17700	.18378	-.03690	.46869
1.32000	0.	50.00000	1.56000	.15300	.16897	-.09453	.48626
1.32000	0.	35.00000	1.51000	.11900	.14175	-.16049	.52814
1.32000	0.	75.00000	1.34000	.20400	.18912	.07865	.41891
1.32000	0.	60.00000	1.28000	.16800	.17064	-.01549	.43570
1.32000	0.	50.00000	1.24000	.14600	.15617	-.06511	.45210
1.32000	0.	35.00000	1.19000	.11500	.13021	-.11683	.49195
1.32000	0.	88.00000	1.11000	.19500	.18659	.04508	.37866
1.32000	0.	65.00000	1.02000	.16900	.16098	.04981	.39677
1.32000	0.	60.00000	1.00000	.15900	.15453	.02891	.40264
1.32000	0.	50.00000	.97000	.13600	.14109	-.03607	.41907
1.32000	0.	40.00000	.93000	.12000	.12498	-.03984	.44078
1.32000	0.	35.00000	.91000	.09600	.11596	-.17215	.45533
1.32000	0.	88.00000	.85000	.16300	.16631	-.01990	.34645
1.32000	0.	65.00000	.76000	.11900	.14044	-.15266	.36198
1.32000	0.	65.00000	.43000	.10000	.10210	-.02056	.30828
1.32000	0.	50.00000	.42000	.06500	.08946	-.27345	.33291
1.32000	0.	90.00000	.28000	.08500	.08852	-.03976	.25053

1.32000	0.	60.00000	.17000	.05500	.05120	.07423	.26085
1.32000	0.	50.00000	.14000	.04200	.04003	.04933	.27132
1.32000	0.	35.00000	.08000	.02100	.02048	.02544	.29390
1.32000	0.	91.00000	.07000	.02400	.02993	-.19824	.19852
1.17000	0.	84.00000	1.20000	.21200	.17623	.20297	.36602
1.17000	0.	75.00000	1.17000	.18500	.16748	.10459	.37272
1.17000	0.	65.00000	1.12000	.14800	.15578	-.04997	.38060
1.17000	0.	50.00000	1.06000	.14100	.13640	.03375	.40051
1.25000	0.	101.00000	2.50000	.26700	.23455	.13834	.47261
1.25000	0.	101.00000	1.80000	.23300	.22136	.05257	.42101
1.25000	0.	101.00000	1.00000	.18000	.18146	-.00804	.34309
1.25000	0.	101.00000	.75000	.15900	.15936	-.00225	.31169
1.25000	0.	101.00000	2.10000	.24800	.22882	.08380	.44452
1.25000	0.	101.00000	1.80000	.22900	.22136	.03450	.42101
1.25000	0.	85.00000	2.25000	.24200	.21876	.10622	.47096
1.25000	0.	85.00000	1.80000	.21200	.20913	.01370	.43607
1.25000	0.	85.00000	1.00000	.16600	.17106	-.02960	.35712
1.25000	0.	85.00000	.50000	.11200	.12082	-.07297	.28781
1.25000	0.	67.00000	2.25000	.20000	.20062	-.00310	.49494
1.25000	0.	67.00000	2.10000	.19200	.19830	-.03176	.48367
1.25000	0.	67.00000	1.25000	.15900	.17109	-.07064	.40716
1.25000	0.	67.00000	.50000	.09500	.10980	-.13475	.30824
1.25000	0.	46.00000	2.25000	.18100	.17141	.05594	.53899
1.25000	0.	46.00000	1.80000	.16400	.16385	.00091	.50235
1.25000	0.	46.00000	1.00000	.12500	.13336	-.06266	.41894
1.25000	0.	35.00000	1.50000	.13900	.13670	.01679	.50940
1.25000	0.	25.00000	1.50000	.11200	.11467	-.02326	.55714
1.25000	0.	13.00000	1.50000	.05400	.07751	-.30335	.66022
1.25000	0.	13.00000	1.00000	.04200	.06672	-.37047	.59858
3.50000	0.	119.00000	2.25000	.48300	.44384	.08822	.80719
3.50000	0.	119.00000	1.25000	.39800	.37283	.06752	.64116
3.50000	0.	119.00000	.90000	.34500	.32435	.06368	.56658
3.50000	0.	119.00000	.50000	.25000	.23923	.04501	.46172
3.50000	0.	88.00000	2.25000	.42100	.40669	.03518	.85932
3.50000	0.	88.00000	1.25000	.34900	.34036	.02537	.68732
3.50000	0.	88.00000	.90000	.30400	.29509	.03019	.61025
3.50000	0.	88.00000	.50000	.22200	.21578	.02883	.50239
3.50000	0.	88.00000	.10000	.06400	.06729	-.04896	.35271
3.50000	0.	64.00000	2.25000	.34500	.36508	-.05499	.92605
3.50000	0.	64.00000	1.25000	.28900	.30455	-.05106	.74636
3.50000	0.	64.00000	.90000	.25300	.26319	-.03873	.66595
3.50000	0.	64.00000	.50000	.18700	.19090	-.02043	.55390
3.50000	0.	64.00000	.10000	.05600	.05790	-.03285	.40064
3.50000	0.	38.00000	2.25000	.25400	.29541	-.14018	1.06330
3.50000	0.	38.00000	.90000	.18800	.21151	-.11113	.78046
3.50000	0.	38.00000	.50000	.14000	.15186	-.07808	.65900
3.50000	0.	38.00000	.10000	.04200	.04453	-.05687	.49559
3.50000	.50000	38.00000	.60000	.11000	.12428	-.11487	1.00711
3.50000	.50000	38.00000	.90000	.13500	.16112	-.16213	1.09455
3.50000	1.50000	38.00000	.60000	.06400	.07417	-.13715	1.80266
3.50000	1.50000	38.00000	.90000	.08400	.10128	-.17058	1.87371
3.50000	2.50000	38.00000	.90000	.07100	.07114	-.00190	2.76249
3.50000	3.50000	38.00000	.90000	.05400	.05414	-.00264	3.69979
3.50000	5.00000	38.00000	.60000	.03100	.02770	.11907	5.11304
3.50000	5.00000	38.00000	.90000	.04200	.03956	.06164	5.14598
3.50000	.50000	64.00000	.90000	.15600	.19024	-.17998	.98136

3.50000	1.50000	64.00000	.90000	.09700	.11164	-.13112	1.78247
3.50000	2.50000	64.00000	.60000	.05300	.05393	-.01716	2.64836
3.50000	2.50000	64.00000	.90000	.07400	.07598	-.02612	2.69226
3.50000	3.50000	64.00000	.60000	.04100	.04001	.02471	3.61008
3.50000	3.50000	64.00000	.90000	.05700	.05695	.00080	3.64411
3.50000	5.00000	64.00000	.60000	.03000	.02870	.04527	5.07896
3.50000	5.00000	64.00000	.90000	.04300	.04115	.04501	5.10412
3.50000	.50000	88.00000	.90000	.18200	.20654	-.11882	.92713
3.50000	1.50000	88.00000	.60000	.07900	.08430	-.06283	1.68724
3.50000	1.50000	88.00000	.90000	.10900	.11663	-.06543	1.74119
3.50000	2.50000	88.00000	.90000	.08200	.07816	.04913	2.66163
3.50000	3.50000	88.00000	.60000	.04600	.04077	.12834	3.59056
3.50000	3.50000	88.00000	.90000	.06600	.05817	.13452	3.62030
1.00000	0.	64.00000	.60000	.11000	.10496	.04805	.28875
1.00000	0.	64.00000	.90000	.13400	.12845	.04323	.32501
1.50000	0.	64.00000	.60000	.13300	.13260	.00303	.36479
1.50000	0.	64.00000	.90000	.16300	.16304	-.00022	.41252
2.00000	0.	64.00000	.60000	.15500	.15598	-.00629	.42912
2.00000	0.	64.00000	.90000	.19000	.19233	-.01211	.48664
3.00000	0.	64.00000	.60000	.19000	.19530	-.02714	.53730
3.00000	0.	64.00000	.90000	.23300	.24163	-.03571	.61138
3.50000	0.	64.00000	.60000	.20700	.21249	-.02586	.58460
3.50000	0.	64.00000	.90000	.25300	.26319	-.03873	.66595
.23000	0.	41.00000	1.48000	.04600	.04642	-.00915	.15378
.23000	0.	41.00000	1.16000	.03900	.04356	-.10474	.14635
.23000	0.	22.00000	1.09000	.02400	.02913	-.17613	.16217
.23000	0.	51.00000	.87000	.03700	.04428	-.16439	.13193
.23000	0.	41.00000	.83000	.03100	.03865	-.19798	.13667
.23000	0.	22.00000	.76000	.01700	.02544	-.33173	.15283
1.30000	1.30000	41.00000	1.61000	.06700	.06996	-.04237	1.53176
1.30000	1.30000	41.00000	1.33000	.06200	.06217	-.00280	1.50671
1.30000	1.30000	22.00000	1.26000	.04800	.05105	-.05968	1.57899
1.30000	1.30000	51.00000	1.11000	.06000	.05730	.04713	1.46509
1.30000	1.30000	41.00000	1.07000	.05400	.05361	.00731	1.48174
1.30000	1.30000	31.00000	1.03000	.04800	.04908	-.02210	1.50777
1.30000	1.30000	41.00000	.80000	.04500	.04316	.04270	1.45379
1.33000	1.33000	41.00000	1.44000	.06600	.06578	.00332	1.54802
1.33000	1.33000	22.00000	1.37000	.04300	.05410	-.20514	1.62354
1.33000	1.33000	41.00000	1.13000	.05500	.05600	-.01779	1.51863
1.34000	1.34000	84.00000	1.54000	.09000	.07767	.15876	1.50130
1.34000	1.34000	67.00000	1.47000	.07900	.07302	.08189	1.51331
1.34000	1.34000	51.00000	1.41000	.06800	.06791	.00131	1.53285
1.34000	1.34000	41.00000	1.36000	.06000	.06355	-.05585	1.55105
1.34000	1.34000	22.00000	1.29000	.04200	.05228	-.19667	1.62510
.97000	0.	65.00000	.19000	.05600	.04880	.14743	.21738
.97000	0.	50.00000	.14000	.04000	.03366	.18823	.22819
.97000	0.	40.00000	.10000	.02900	.02252	.28761	.23897
.94000	0.	86.00000	.25000	.07000	.06650	.05267	.20507
.94000	0.	75.00000	.22000	.06500	.05715	.13730	.20890
.94000	0.	60.00000	.16000	.04300	.04037	.06508	.21372
1.32000	0.	40.00000	1.58000	.13300	.15332	-.13251	.51699
1.32000	0.	89.00000	1.39000	.21900	.20346	.07637	.40795
1.32000	0.	65.00000	1.30000	.18200	.17718	.02718	.42926
1.32000	0.	40.00000	1.20000	.13000	.13934	-.06703	.47530
1.32000	0.	25.00000	1.15000	.08700	.10787	-.19350	.53556
1.32000	0.	75.00000	1.06000	.17900	.17289	.03534	.38746

1.32000	0.	75.00000	.90000	.14700	.15237	-.03525	.35389
1.32000	0.	60.00000	.74000	.10800	.13407	-.19443	.36717
1.32000	0.	50.00000	.71000	.08800	.12127	-.27434	.38230
1.32000	0.	40.00000	.67000	.06400	.10601	-.39628	.40217
1.32000	0.	35.00000	.65000	.05200	.09766	-.46752	.41565
1.32000	0.	90.00000	.56000	.12200	.13568	-.10081	.30207
1.32000	0.	75.00000	.51000	.11100	.11998	-.07487	.30931
1.32000	0.	60.00000	.45000	.08500	.10141	-.16185	.31972
1.32000	0.	40.00000	.38000	.05500	.07531	-.26967	.35003
1.32000	0.	35.00000	.36000	.04200	.06789	-.38135	.36187
1.32000	0.	25.00000	.33000	.02800	.05341	-.47574	.39880
1.32000	0.	75.00000	.23000	.07300	.07133	.02335	.25470
1.32000	0.	40.00000	.10000	.02700	.02681	.00723	.28443
1.32000	0.	75.00000	.01000	.00500	.00434	.15297	.19649
1.32000	0.	86.00000	1.63000	.22500	.21131	.06477	.43433
1.32000	0.	75.00000	1.59000	.20400	.19988	.02062	.44388
1.32000	0.	65.00000	1.56000	.19000	.18828	.00914	.45596
1.32000	0.	60.00000	1.54000	.18500	.18167	.01833	.46283
1.32000	0.	50.00000	1.50000	.14300	.16691	-.14328	.48020
1.32000	0.	40.00000	1.46000	.11200	.14955	-.25106	.50455
1.32000	0.	35.00000	1.45000	.11000	.13990	-.21372	.52174
1.32000	0.	89.00000	.86000	.16300	.16788	-.02905	.34681
1.32000	0.	75.00000	.80000	.15700	.15237	.03038	.35389
1.32000	0.	65.00000	.77000	.14100	.14136	-.00251	.36342
1.32000	0.	60.00000	.75000	.12800	.13498	-.05171	.36864
1.32000	0.	50.00000	.71000	.11000	.12127	-.09293	.38230
1.32000	0.	40.00000	.68000	.08600	.10686	-.19521	.40378
1.32000	0.	35.00000	.66000	.06800	.09848	-.30950	.41730
1.17000	0.	60.00000	1.10000	.14500	.14972	-.03152	.38619
1.17000	0.	35.00000	.99000	.11400	.11196	.01819	.43325
1.25000	0.	101.00000	2.25000	.25500	.23148	.10159	.45545
1.25000	0.	101.00000	2.10000	.24500	.22882	.07069	.44452
1.25000	0.	101.00000	1.50000	.21600	.21045	.02639	.39484
1.25000	0.	101.00000	1.25000	.19500	.19797	-.01503	.37047
1.27000	0.	101.00000	2.10000	.25000	.23104	.08205	.44883
1.27000	0.	101.00000	1.80000	.22100	.22348	-.01112	.42504
1.27000	0.	101.00000	1.50000	.20900	.21244	-.01618	.39858
1.27000	0.	101.00000	1.25000	.19100	.19983	-.04417	.37394
3.50000	0.	119.00000	.10000	.07200	.07699	-.06478	.31377
3.50000	0.	38.00000	1.25000	.21400	.24568	-.12895	.86793
3.50000	2.50000	38.00000	.60000	.05400	.05085	.06186	2.70751
3.50000	3.50000	38.00000	.60000	.04000	.03825	.04579	3.65607
3.50000	10.00000	38.00000	.60000	.01700	.01431	.18807	10.05839
3.50000	10.00000	38.00000	.90000	.02300	.02063	.11513	10.07611
3.50000	.50000	84.00000	.60000	.11800	.15685	-.24768	.85895
3.50000	1.50000	64.00000	.60000	.07100	.08104	-.12392	1.72296
3.50000	10.00000	64.00000	.60000	.01700	.01468	.15788	10.04039
3.50000	10.00000	64.00000	.90000	.02400	.02120	.13204	10.05364
3.50000	.50000	88.00000	.60000	.13600	.15858	-.14237	.85224
3.50000	2.50000	88.00000	.60000	.06800	.05528	.23004	2.62280
3.50000	5.00000	88.00000	.60000	.03500	.02912	.20187	5.06469
3.50000	5.00000	88.00000	.90000	.05000	.04182	.19560	5.08648
3.50000	10.00000	88.00000	.60000	.02200	.01484	.48285	10.03296
3.50000	10.00000	88.00000	.90000	.03200	.02144	.49259	10.04434
.50000	0.	64.00000	.60000	.07800	.06924	.12656	.19048
.50000	0.	64.00000	.90000	.09600	.08347	.14463	.21221

1.88000	0.	50.00000	3.33000	.30000	.23441	.27980	.77818
1.88000	0.	50.00000	2.00000	.23800	.22398	.06261	.65463
1.88000	0.	50.00000	1.33000	.20000	.19796	.01029	.57096
1.88000	0.	50.00000	1.00000	.16700	.17604	-.05134	.52068
1.88000	0.	50.00000	.80000	.14600	.15825	-.07738	.48594
1.88000	0.	50.00000	.67000	.12500	.14419	-.13310	.46111
1.88000	0.	50.00000	.50000	.10000	.12184	-.17928	.42524
1.25000	0.	50.00000	3.33000	.23000	.18026	.27591	.59842
1.25000	0.	50.00000	2.00000	.18200	.17417	.04498	.50905
1.25000	0.	50.00000	1.33000	.15400	.15503	-.00667	.44715
1.25000	0.	50.00000	1.00000	.12500	.13843	-.09701	.40944
1.25000	0.	50.00000	.80000	.10500	.12478	-.15854	.38318
1.25000	0.	50.00000	.67000	.09100	.11392	-.20121	.36431
1.25000	0.	50.00000	.50000	.07300	.09653	-.24377	.33689
.63000	0.	50.00000	3.33000	.15400	.11285	.36463	.37463
.63000	0.	50.00000	2.00000	.12100	.11155	.08470	.32604
.63000	0.	50.00000	1.33000	.09500	.10079	-.05742	.29069
.63000	0.	50.00000	1.00000	.08100	.09078	-.10774	.26851
.63000	0.	50.00000	.67000	.05900	.07547	-.21820	.24133
1.25000	0.	67.00000	3.33000	.27800	.20355	.36576	.56344
1.25000	0.	50.00000	3.33000	.22300	.18026	.23708	.59842
1.25000	0.	40.00000	3.33000	.19200	.16255	.18114	.62799
1.25000	0.	33.00000	3.33000	.16900	.14759	.14504	.65527
1.25000	0.	25.00000	3.33000	.13300	.12688	.04825	.69705
1.25000	0.	20.00000	3.33000	.11200	.11125	.00674	.73213
.63000	0.	33.00000	.87000	.06000	.06940	-.13548	.28806
1.25000	0.	33.00000	.87000	.08500	.10664	-.20296	.44263
1.25000	0.	33.00000	1.25000	.11000	.12460	-.11716	.49046
.63000	0.	33.00000	1.25000	.07500	.08017	-.06446	.31557
1.88000	0.	33.00000	1.25000	.14400	.15988	-.09934	.62936
.63000	0.	33.00000	2.50000	.08500	.09251	-.08114	.37671
1.88000	0.	33.00000	2.50000	.18200	.19245	-.05430	.78371
1.27000	0.	101.00000	1.00000	.17100	.18313	-.06626	.34626
1.27000	0.	101.00000	.75000	.14500	.16081	-.09831	.31453
1.25000	0.	101.00000	1.50000	.21000	.21045	-.00212	.39484
1.25000	0.	85.00000	2.10000	.22700	.21624	.04978	.45989
1.25000	0.	85.00000	1.50000	.19600	.19873	-.01373	.40956
1.25000	0.	85.00000	1.25000	.18300	.18683	-.02051	.38486
1.25000	0.	85.00000	.75000	.14400	.14996	-.03974	.32533
1.25000	0.	85.00000	.35000	.09000	.09724	-.07450	.26131
1.25000	0.	67.00000	1.80000	.18300	.19175	-.04561	.45940
1.25000	0.	67.00000	1.50000	.17200	.18212	-.05555	.43236
1.25000	0.	67.00000	1.00000	.14000	.15645	-.10512	.37885
1.25000	0.	67.00000	.75000	.11900	.13684	-.13039	.34643
1.25000	0.	67.00000	.25000	.07500	.06986	.07355	.26112
1.25000	0.	46.00000	2.10000	.17200	.16944	.01508	.52738
1.25000	0.	46.00000	1.50000	.15500	.15557	-.00369	.47439
1.25000	0.	46.00000	1.25000	.13300	.14604	-.08932	.44829
1.25000	0.	46.00000	.75000	.10800	.11633	-.07161	.38532
1.25000	0.	46.00000	.50000	.08800	.09285	-.05226	.34578
1.25000	0.	35.00000	1.80000	.15500	.14395	.07674	.53805
1.25000	0.	35.00000	1.25000	.11000	.12832	-.14274	.48261
1.25000	0.	13.00000	1.80000	.05800	.08132	-.28681	.69059
1.25000	0.	25.00000	1.25000	.09700	.10767	-.09912	.52952
1.25000	0.	13.00000	1.25000	.05000	.07295	-.31464	.63143
1.25000	0.	33.00000	1.25000	.11000	.12460	-.11716	.49046

1.25000	0.	33.00000	2.50000	.14000	.14792	-.05353	.60237

REFERENCES

A1 Appell, H. R., Moroni, E. C., Miller, R. D., Energy Sources 3, 2 163 (1977).

A2 Appell, H. R., Wender, I., Am. Chem. Soc. Div. Fuel Chem. Prepr. 12, 3, 220.

A3 Appell, H. R., Wender, I., Miller, R. D., Am. Chem. Soc. Div. Fuel Chem. Prepr. 3, 4, 39 (1969).

A4 Atwood, J. D., Brown, T. L., JACS, 98, 3160 (1976).

A5 Augustine, R. L. and Van Peppen, J. F., Chem. Comm. 495, 497, 571 (1970).

A6 Appell, H. R., Wender, I., Miller, R. D., U. S. Bureau of Mines Info. Circ. (8543), Proc. of B. of Mines, May 12-13, (1972), p. 32.

A7 Appell, H. R., Wender, I., Miller, R. D., Chem. Ind. (London) 47, 1703 (1969).

A8 Arai, H. and Halpern, J., Chem. Comm., 1572 (1971).

A9 Abd El-Mottaleb, M. S. A., J. Mol. Struct, 32, 203 (1976).

A10 Angelici, R. J. and Malone, M. D., Inorg. Chem. 6, 1731 (1967).

A11 Albright, T. A., Freeman, W. J. and Schweizer, E. E., J. Org. Chem. 40, 3437 (1975).

B1 Bird, C. W., Transition Metal Intermediates in Organic Synthesis, Academic Press, inc., NY (1967).

B2 Byers, B. J., Brown, T. L., J. Orgmet. Chem. 127, 181 (1977).

B3 Brown, T. H., Green, P. J., JACS 92, 2359 (1970).

B4 Brown, T. H., Green, P. J., JACS 91, 3378 (1969).

B5 Blom, L., Edelhausen, L. and Krevelen, D. W., Fuel 36, 135 (1957).

B6 Basolo, F. and Pearson, R. G., Mechanisms of Inorganic Reactions, John Wiley and Sons, Inc., Chapter 2 (1967).

C1 Calvin, M., Trans. Faraday Soc. 34, 1181 (1938).

C2 Chalk, A. J. and Harrod, J. F., Adv. in Organometallic Chemistry, (1967), Vol. 6, p. 120.

C3 Collman, J. C., Roper, W. R., Adv. in Organometallic Chem. (1968), Vol. 7, p. 54.

C4 Chock, P. B. and Halpern, J., JACS 88, 3511 (1966).

C5 Chatt, J., Proc. Chem. Soc., London, 318 (1962).

C6 Chatt, J. and Shaw, B. L., J. Chem. Soc., London, 705 (1959) and 1718 (1960).

C7 Cotton, F. A. and Wilkinson, G., Adv. Inorganic Chemistry, John Wiley and Sons, Inc., NY, 3rd edition, Chapter 20-23 (1972).

C8 Chatt, J. and Duncanson, L. A., J. Chem. Soc., London, 2939 (1953).

C9 Cais, M., Frankel, E. N. and Rejoan, A., Tetrahedron Lett, 1919 (1968).

C10 Cotton, F. A. and Wilkinson, G., Adv. Inorganic Chemistry, John Wiley and Sons, Inc., NY, 3rd edition, p. 650 (1972).

C11 Crutchfield, M. M., et al., Topics in Phos. Chem., Vol. 5 (1967).

C12 Carra, S., Ugo, R., Iorg. Chem. Acta. Rev. 49 (1967).

C13 Cotton, F. A., Kraihanzel, C. S., JACS 84, 4432 (1962).

C14 Cotton, F. A., Inorg. Chem. 3, 5, 702 (1964).

C15 Cotton, F. A., Down, J. L., Wilkinson, G., JCS, 833 (1959).

C16 Cook, M. W., Hanson, D. N. and Alder, B. J., J. Chem. Phys. 26, 748 (1959).

D1 Dewar, M. J. S., Bull. Soc. Chem. Fr. (5) 18C, 79 (1951).

D2 de Croon, M. H. J. M., Van Nisselrooij, P. F. M. T., Kuipers, H. J. A. M. and Coenen, J. W. E., J. Mol. Cat. 4, 325 (1978).

D3 De Ketelaere, R. F. and van der Kelen, G. P., J. Mol. Struct. 27, 363 (1975).

E1 Emsley, J. and Hall, D., The Chemistry of Phosphorus, John Wiley and Sons, Inc., NY, Chapter 5 (1976).

E2 Eaton, D. R. and Stuart, S. R., JACS 90, 4170 (1968).

F1 Friedman, S., Metlin, S., Svendi, A., Wender, I., J. Org. Chem. 24, 1287 (1959).

F2 Frankel, E. N., Maoz, N., Rejoan, A., Cais, M., Proc. 3rd Intern. Conf. Organomet. Chem., Munich, Abst. 210 (1967).

F3 Flintcroft, N., Huggins, D. K., Kaesz, H. D., Inorg. Chem. 3, 8, 1123 (1964).

F4 Fawcett, J. P., Poe, A., Sharma, K. R., JACS 98, 6, 1401 (1976).

F5 Feder, H. M., Halpern, J., JACS 97, 24, 7186 (1975).

F6 Fischer, F., Schrader, H., Brennstopp-Chem. 2, 257 (1921).

F7 Fischer, H. and Fischer, E. O., Chem. Ber. 107, 673 (1967).

F8 Fischer, E. O., Knauss, L., Keiter, R. L. and Verkade, J. G., J. Orgmetall. Chem. 37, 67 (1972).

F9 Fluck, E. and Binder, H., Z. Naturforschg. 226, 805 (1967).

F10 Fluck, E. and Binder, H., Z. Anorg. Allg. Chem. 354, 139 (1967).

G1 Grim, S. O., Wheatland, D. A. and McFarlane, W., JACS 89, 5573 (1967).

G2 Grim, S. O., Weatland, D. A., McAlister, P. R., Inorg. Chem. 7, 1, 1961 (1968).

G3 Garnett, J. L., Cat. Rev. 5, 229 (1971).

G4 Gray, H. B. and Ballhausen, C. J., JACS 85, 260 (1963).

G5 Grim, S. O., McAllister, P. R. and Singer, R. M., Chem. Comm. 38 (1969).

H1 Halpern, J., Adv. in Catalysis 11, 301 (1959).

H2 Heck, R. F. and Breslow, D. S., JACS 83, 4023 (1961).

H3 Holy, N., Nalesnik, T. and McClanahan, S., Fuel 56, 47 (1977).

H4 Henderson, W. A., Steruli, C. A., JACS 82, 5791 (1960).

H5 Hartley, F. R., Chem. Rev. 59, 799 (1969).

H6 Hopgood, D., Poe, J. A., Chem. Comm. 22, 831 (1966).

H7 Howell, R. L., Ph. D. Thesis, University of California, Berkeley, California (1975).

H8 Halpern, J., Okamoto, T., and Zakharien, A., J. Molec. Catal. 2, 65 (1976).

H9 Hui, K. and Shaw, B., J. Orgmet. Chem. 124, 262 (1977).

H10 Halpern, J. and Wong, C. S., Chem. Comm. 629 (1973).

H11 Henderson, W. A. and Buckler, S. A., JACS, 82, 5794 (1960).

J1 James, B. R., Homogeneous Hydrogenation, John Wiley and Sons, Inc., NY, (1973), pp. 167-170.

J2 Johnson, M., JCS (London) 4859 (1963).

J3 James, B. R., ibid., pgs. 63 and 354.

J4 Johnson, C. D., Chem. Rev. 75, 755 (1975).

J5 Jackson, R. A. and Poe, A., Inorg. Chem. 17, 4, 997 (1978).

J6 Jardine, F. H., Osborn, S. A. and Wilkinson, G., JCS(A), 1574 (1967).

J7 Jones, M. S., Ligand Reactivity and Catalysis, Academic Press, Inc. (1968).

K1 Kahn, M. M. T. and Martell, A. E., Homogeneous Catalysis by Metal Complexes, Academic Press, Inc. (1974).

K2 Karapinka, G. L. and Orchin, M. J., Org. Chem. 26, 4187 (1961).

K3 Kabachnik, M. I. and Balueva, G. A., Bull. of the Acad. of Sci. of the USSR Div. of Chem. Sci., α3, 495 (March 1962).

K4 Kabachnik, M. I., Proceed. Acad. of Sci. of USSR, 110:1-6, 577 (1956).

K5 Kidd, D. R., Cheng, C. P. and Brown, T. L., JACS 100, 4103 (1978).

K6 Kostina, V. G., Feschehenko, N. G. and Kirsanov, A. V., Zh. Obschch. Khim. 43, 209 (1973).

L1 Lyons, J. E., Rennick, L. E. and Burneister, J. L., Ind. Eng. Chem. Prod. Res. Develop. 9, 1 (March 1970).

L2 Lacky, J., Szabo, P. and Marko, L., Acta Chim. Acad. Sci. Hung. 46, 247 (1965).

L3 Lewis, J., Manning, A. R., Miller, J. R., JCS(A), 845 (1966).

L4 Lehman, D. D., Shriver, D. F. and Wharf, I., Chem. Comm. 1486 (1970).

M1 Mond, L. C., Langer, C. and Quinke, F., JCS 57, 749 (1890).

M2 Mond, L. C. and Quinke, F., Chem. News 63, 310 (1891).

M3 Manuel, T. A., J. Org. Chem. 27, 3941 (1962).

M4 Montelatici, S., Van der ent, A., Osborn, J. A., Wilkinson, G., JCS(A), 1054 (1968).

M5 Marko, L., Chem. Ind. (London) 260 (1962).

M6 Mathieu, R., Lenzi, J. and Poilblanc, R., Inorg. Chem. 9, 2030 (1970).

M7 Mann, B. E., et al., Inorg. Nucl. Lett. 7, 881 (1971).

M8 Meriwether, L. S. and Leto, J. R., JACS 83, 3192 (1961).

M9 Mooney, E. F. (ed.), Annual Reports on NMR Spec. 5B, Academic Press, Inc., NY (1973).

M10 Meutterties, E. L. and Wright, C. M., Quart. Rev. Chem. Soc. 21, 109 (1967).

M11 Meutterties, E. L., Guggenberger, L. J., JACS 96, 1948 (1974).

M12 Miller, J. R. and Myers, D. H., Inorg. Chim. Acta 5, 215 (1971).

M13 Mague, J. T. and Wilkinson, G., JCS(A), 1936 (1966).

M14 Mays, J. J., Simpson, R. N. F., Stefanini, F. P., JCS(A), 3000 (1970).

M15 Meakin, P., Jesson, J. P. and Tolman, C. A., JACS 94, 3240 (1972).

M16 Mobley, D. P. and Bell, A. T., Univ. of California, Lawrence Berkeley Laboratory Report, LBL-8010 (1978).

M17 Mather, G. G. and Pidcock, A., JCS(A) 1226 (1970).

M18 Maier, L., Phos. 4, 41 (1974).

M19 Mann, B. Masters, C and Shaw, B. JCS(A), 1104 (1971).

N1 Natta, G. and Beati, E., Chem. et Ind. 27, 84-87 (1945).

N2 Natta, G. and Ercoli, Chem. et Ind. 34, 503 (1952).

O1 Osborne, J. A., Jardine, F. H., Young, J. F. and Wilkinson, G. J., JCS(A), 1711 (1966).

O2 Ogata, I., Misono, A., Discuss. Faraday Soc. 46, 72 (1968).

O3 Orchin, M. and Rupiluis, W., Cat. Rev. 6:1, 85 (1972).

O4 Orgel, L. E., Inorg. Chem. 1, 1, 25 (1962).

O5 O'Connor, C. and Wilkinson, G., Tet. Lett. 18, 1375 (1969).

O6 Ohrt, D. W., Ph. D. Thesis, Univ. of Arkansas, Fayetteville, Arkansas, Univ. Microfilm No. 72-10216 (1972).

P1 Pino, P. and Ercoli, R., Ricerca. Sci. 23, 1953 (1953).

P2 Parshall, G. W., Accts. of Chem. Res. 8:4, 113 (1975).

Q1 Quinn, L. D. and Breen, J. J., Org. Mag. Res. 5, 17 (1973).

R1 Roelen, O., U. S. Patent 2,327,066 (1943).

R2 Rousseau, C., Evrard, M. and Petit, F., J. Mol. Cat. 3, 309 (1977/78).

S1 Shaw, J. T. and Ryson, F. T., JACS 78, 2538 (1956).

S2 Sternberg, H. W., Markby, R. and Wender, I., JACS 78, 5705 (1956) and 79, 6166 (1957).

S3 Slaugh, L. H. and Mullineaux, R. D., J. Organ. Mett. Chem. 13, 469 (1968).

S4 Shinn, J. H., Hershkowitz, F., Holten, R., Vermeulen, T. and Grens, E. A., AIChE Natl. Meeting, Miami (Nov. 1978), Symp. on React. Eng. in Coal Proc.

S5 Strohmeier, W., Guttenberger, J. F. and Hellmann, H., Z. Naturforsch. 196, 353 (1964).

S6 Steitwieser, A., Molecular Orbital Theory for Organic Chemists, John Wiley and Sons, Inc., NY (1961), Chapter 13.

S7 Siegel S. and Ohrt, D. W., Chem. Comm. 1527 (1971).

S8 Siegel, S. and Ohrt, D. W., Tet. Lett. 50, 5155 (1972).

S9 Siegel, S. and Ohrt, D. W., Inorg. Nucl. Chem. Lett. 8, 15 (1972).

S10 Streuli, C. A., Anal. Chem. 31, 1652 (1959), 32, 985 (1960).

S11 Schumann, H., Stelzer, O., Kuhlmey, J. and Niederreuther, U., Chem. Ber. 104, 993 (1971).

S12 Strohmeier, W. and Muller, F. J., Chem. Ber. 100, 2812 (1967).

S13 Stelzer, O. and Schmutzler, R., JCS(A) 2867 (1971).

S14 Strohmeier, W. and Onada, T., Z. Naturforschg. 24b, 515 (1969).

S15 Szafraniec, L., Org. Mag. Res. 6, 565 (1974).

T1 Thomas, J. M. and Thomas, J. W., Introduction to Principles of Heterogeneous Catalysis, Academic Press, Inc., NY (1967).

T2 Tolman, C. A., JACS 92, 2953 (1970), and 92, 2956 (1970).

T3 Tucci, E., Ind. and Eng. Chem. Prod. Res. and Dev. 7, 32 (1968).

T4 Tucci, E., Ind. and Eng. Chem. Prod. Res. and Dev. 9, 516 (1970).

T5 Tinker, H. B. and Morris, D. E., Rev. of Sci. Inst. 43, 7, 1024 (1972).

T6 Tolman, C. A., Meakin, P. Z., Lindner, D. L. and Jesson, J. P., JACS 96, 2762 (1974).

T7 Taylor, P. D. and Orchin, M., J. Org. Chem. 37, 3913 (1972).

T8 Tolman, C. A., Chem. Rev. 77, 313 (1977).

V1 Verkade, J. R. and King, R. W., Inorg. Chem. 4, 948 (1962).

W1 Wender, I., et al., JACS 77, 5760 (1955).

W2 Wender, I., Sternberg, H. W., Friedel, R. A. Metlin, S. J. and Markby, R. E., U. S. Bureau of Mines Bulletin 600 (1962).

W3 Wender, I., et al., JACS 74, 4079 (1952).

W4 Wawersik, H. and Basolo, F., Inorg. Chim. Acta 3, 1, 113 (1969).

W5 Winkhaus, G., Pratt, L. and Wilkinson, G., JCS 738, 3807 (1961).

W6 Weil, T. A., Metlin, S. and Wender, I., J. Organomet. Chem. 49, 227 (1973).

Z1 Chem. Engin., 84:26, 109 (Dec. 5, 1977).

This report was done with support from the Department of Energy. Any conclusions or opinions expressed in this report represent solely those of the author(s) and not necessarily those of The Regents of the University of California, the Lawrence Berkeley Laboratory or the Department of Energy.

Reference to a company or product name does not imply approval or recommendation of the product by the University of California or the U.S. Department of Energy to the exclusion of others that may be suitable.

TECHNICAL INFORMATION DEPARTMENT
LAWRENCE BERKELEY LABORATORY
UNIVERSITY OF CALIFORNIA
BERKELEY, CALIFORNIA 94720